Cyprus
University of
Technology

Faculty of
Engineering and
Technology

Doctoral Dissertation

RC-FRAMES INFILLED WITH RC INFILL-WALLS FOR SEISMIC RETROFITTING

Elpida S. Georgiou

Limassol, February 2021

CYPRUS UNIVERSITY OF TECHNOLOGY

FACULTY OF ENGINEERING AND TECHNOLOGY

DEPARTMENT OF CIVIL ENGINEERING AND GEOMATICS

Doctoral Dissertation

RC-FRAMES INFILLED WITH RC INFILL-WALLS FOR SEISMIC RETROFITTING

Elpida S. Georgiou

Limassol, February 2021

Approval Form

Doctoral Dissertation

RC-FRAMES INFILLED WITH RC INFILL-WALLS FOR SEISMIC RETROFITTING

Presented by

Elpida S. Georgiou

Supervisor: Christis Chrysostomou, Professor

Signature _____

Member of the committee: Diofantos G. Hadjimitsis, Professor

Signature _____

Member of the committee: Petros Christou, Associate Professor

Signature _____

Cyprus University of Technology

Limassol, February 2021

Doctoral Dissertation

RC-FRAMES INFILLED WITH RC INFILL-WALLS FOR SEISMIC RETROFITTING

Presented by

Elpida S. Georgiou

Supervising Committee:

Supervisor: Christis Chrysostomou, Professor

Member of the committee: Panagiotis Kotronis, Professor

Member of the committee: Stylianos Yiatros, Assistant Professor

Cyprus University of Technology

Limassol, February 2021

Copyrights

To my husband, George

for his love and faith

Acknowledgements

I would like to express my deepest gratitude and appreciation to my advisor Professor Christis Chrysostomou for the support of my PhD study, for his patience, motivation, and encouragement during the last years. His knowledge and guidance helped me in all the time of research and the preparation of this thesis.

Besides my advisor, I would like to thank the rest of my thesis committee, Professor Diofantos Hadjimitsis and Associate Professor Petros Christou, as well as my supervising committee, Professor Panagiotis Kotronis and Assistant Professor Stylianos Yiatros for their insightful comments, support, and encouragement.

Very special thanks to Lecturer Nicholas Kyriakides for providing guidance, support, and feedback throughout this work and for very helpful suggestions and inspiring conversations regarding the presented work.

I would also like to express my gratitude to my grandmother, my parents, my sister and my brother for their unconditioned love, their encouragement, and for supporting and believing in me.

And my biggest thanks to my husband, George, who has been by my side, living every single minute of it. Your love, support, understanding, patience, and all the sacrifices you went through for me throughout this PhD study are invaluable.

ABSTRACT

The seismic retrofitting of existing multi-storey multi-bay reinforced concrete (RC) frame buildings by the conversion of selected bays into new RC infilled walls is the subject of this research work. The parametric study of the contribution of dowels that connect a new RC infill wall to the surrounding RC frame members was performed through nonlinear dynamic analyses of a numerical finite element (FE) model. The FE model was simulated in DIANA finite element analysis (FEA) software in order to study the effectiveness of the seismic retrofitting of existing structures with the conversion of selected bays into new infilled RC walls for the retrofitting of a multi-storey multi-bay RC frame building. A two-dimensional (2D) frame was modeled, and nonlinear transient analyses were performed to calibrate it using the experimental results obtained from a full-scale experiment found in the literature. The description of the experimental results and of the FE model simulation of the test specimen is provided along with a comparison between the experimental results and the numerical ones. Based on the preliminary results it was concluded that the number of dowels used in the experiment resulted in a monolithic behavior of the RC infilled frame. In order to complement the experimental results and to study the interaction between RC infills and the bounding frame both at the global and local level, numerical simulation experiments were performed by reducing the number of dowels starting from a spacing of 100mm (monolithic) to no dowels. For each scenario, nonlinear response-history analysis was performed and an evaluation of the numerical results of each of these scenarios was subsequently performed. The parametric study of the number of dowels connecting the wall to the bounding frame is presented and conclusions are drawn. The parametric results provide a basis for the development of a general model for the design of RC infills in existing RC frames, particularly regarding the connection details of the new RC infill walls to the existing bounding frame.

Keywords: retrofitting seismic deficient structures, RC infill walls, modeling of dowels, finite element model, nonlinear numerical parametric study

TABLE OF CONTENTS

LIST OF TABLES

LIST OF FIGURES

LIST OF ABBREVIATIONS

2D:	Two dimensional
CFRP:	Carbon Fiber Reinforced Polymer
EC8-3:	Eurocode 8 – Part 3
ELSA:	European Laboratory of Structural Assessment
FE:	Finite Element
FEA:	Finite Element Analysis
ISD:	Inter-Storey Drift
JRC:	Joint Research Center
PsD:	Pseudo-Dynamic
RC:	Reinforced Concrete
SERFIN:	Seismic Retrofitting of RC Frames with RC Infilling

1   Introduction

In recent decades, low and medium rise RC buildings have experienced considerable damage during earthquakes which caused casualties and financial loss. Thereafter, many damaged existing buildings had to be effectively and economically retrofitted. Many different strengthening techniques have been tested and applied in the last decades for the rehabilitation of such existing RC frames. Most of the strengthening techniques disturb the everyday life of occupants, who must vacate the building during the intervention. Nowadays, most of the strengthening strategies are based on global strengthening schemes and the structures are usually strengthened for limiting lateral displacements in order to compensate for the low ductility (Moehle, 2000; Sonuvar, Ozcebe and Ersoy, 2004; Kaplan *et al.*, 2011). Increasing the global stiffness and reducing the seismic deformation expectations of a building for seismic retrofitting purposes may be more cost-effective in comparison with the local intervention of existing components in order to strengthen their capacities (Fardis, 2009).

The strengthening of damaged RC buildings by infilling selected bays in both directions of the frames with RC infill walls, especially on the perimeter, has proved to be one of the most feasible techniques in the seismic strengthening of existing buildings. This is a popular, simple, effective, and economic strengthening method and is preferred when there are too many members to be retrofitted (Ahmet, Ugur and Guney, 2006; Kaplan *et al.*, 2011; Fardis, Schetakis and Strepelias, 2013). According to Chrysostomou and Kyriakides, (2013a) this is the most effective and economic method for retrofitting multi-storey multi-bay RC buildings, especially those with pilotis (soft-storey). This method can be applied to increase the strength, stiffness, and ductility of the building. Also, with the full infill of selected bays of an existing RC frame, the effectiveness of the retrofitting is increased, and the construction cost is reduced. The RC infills as a retrofitting method is commonly applied to guarantee monolithic behavior between the old and the new members to design the new RC walls according to the codes (CEN, 2010; KANEPE, 2017). The monolithic behavior is achieved by the construction of a new thicker web than the beams and the columns of the existing frame panel with the location of the new reinforcement outside the existing members and the details of reinforcement as in a new wall (Fardis, Schetakis and Strepelias, 2013). In this way, the new infill walls are much stronger than what is needed for the strengthening of the structure, and this 'over-strength'

causes additional issues like the weak ending of the foundations of the existing buildings (Fardis, Schetakis and Strepelias, 2013). However, the addition of RC infill walls with the same thickness as the frame members that bound the new wall for the seismic strengthening of RC buildings is relatively a new method.

Even though the RC infills is a common retrofitting method and it is extensively applied to guarantee monolithic behavior between the old and new members, it is not addressed quantitatively by the codes, not even by EC8-3. Specifically, the interaction of new RC infills with the bounding frame, their design, and detailing between the new web and the surrounding frame members need to be regulated. On the other hand, (KANEPE, 2017) refers to the introduction of RC infills within a frame, only in terms of forces, providing tools for calculating their deformations (at yield and failure) and stiffness only if they are integral with the bounding frame. Although for other strengthening methods of existing structures there are guidelines regarding the retrofit design and certain aspects of the seismic response of the retrofitted structure, there are still open issues about the studied retrofit method. For example, their interaction with the bounding frame, their design and detailing between the new web and the surrounding frame members need to be regulated.

The inadequacy of design codes in this respect is due to our poor knowledge of the behavior of walls created by the infilling of a bay of an existing RC frame. Furthermore, regulations do not exist for modeling or evaluation of frame bays converted into RC walls depending on the type and details of the connection. Moreover, the experimental research work that has been performed in the last decades on the use of RC infill walls is not adequate and most of the research has mainly targeted what is feasible: testing of one-to-two storey specimens due to the practical difficulties of testing large specimens with high resistance (Chrysostomou et al., 2016). The tests have been limited to small-scale specimens, possibly owing to the technical limitations of testing walls of very large shear force resistance (Chrysostomou and Kyriakides, 2013a; Fardis, Schetakis and Strepelias, 2013). Another drawback of past investigations is that they did not propose or even follow a quantitative procedure for the design of the connection between the RC infilling and the surrounding frame members. Furthermore, they have not led to, or supported, any procedure for the quantification of the engineering properties of the RC infilled frame which is essential for its analysis and design in the context of modern performance based seismic design, that is the effective stiffness, the moment and shear resistances, the

deformation at yielding and the cyclic deformation capacity (Strepelias *et al.*, 2012). Subsequently, data is lacking for taller full-scale specimens that reflect real applications.

To start filling the gap of knowledge and to study the effectiveness of seismic retrofitting of multi-storey multi-bay RC frame buildings by converting selected bays into new walls through infilling with RC, a full-scale specimen was studied experimentally through (PsD) test within the project "Seismic Retrofitting of RC Frames with RC Infilling" (SERFIN) at the European Laboratory of Structural Assessment (ELSA) facility at the Joint Research Centre (JRC), in Ispra. The purpose was to study the efficiency of the retrofitting method through experimental testing of a full-scale four-storey model with the pseudo-dynamic (PsD) method. The frames of the SERFIN model were designed and detailed for gravity loads only. Different connection details between the infill walls and the bounding frame were used. Further details and information about this research work can be found in (Chrysostomou and Kyriakides, 2013a; Chrysostomou *et al.*, 2014a; Poljansek *et al.*, 2014).

The specimen of the test of the project SERFIN is used in this research to develop a numerical model of the frame that was tested in Ispra. The numerical model is calibrated using the results of the experimental model. The validated model is used to formulate numerical experiments in which the number of dowels is reduced starting at a spacing of 100mm (monolithic response of the test specimen) to no dowels and performing nonlinear response-history analysis for each case. The results of these numerical analyses allow the study of the interaction of RC infill walls with the bounding frames, and of the behavior of this structural system in terms of global and local indices, such as: total base shear, top-storey displacement and energy dissipation, for the former, and dowel behavior, andmoment demand at the base of the wall and the frame elements, for the latter. These results also provide a basis for the development of a general model for the design of RC infills in existing RC frames, particularly regarding the connection details of the new RC infill walls to the existing bounding frame members. To achieve the above, this research was organized in Chapters, as it is stated below.

 In Chapter 1 the problem to be studied is formulated and in Chapter 2 a literature review is presented that collates information from previous research regarding code regulations, behavior of RC infill walls, hysteretic behavior of reinforced concrete and dowel action. In Chapter 3 the experimental results of the SERFIN project, which are used for the

calibration of the numerical models developed in this research are presented. In Chapter 4 the development of the numerical model is presented while in Chapter 5 the calibration of the models that are used for the parametric study is presented. In Chapter 6 the results of the parametric study are reported in the global and local level, along with correlation of the results, and design recommendations. In Chapter 7 the conclusions drawn from this research are stated along with recommendations for future work.

2 Literature review

In recent decades, the aim of building rehabilitation and strengthening gained research attention and numerous techniques have been developed to achieve this. Most strengthening techniques disturb the occupants, who must vacate the building during the renovation. Nowadays, most of the strengthening strategies are based on global strengthening schemes (Moehle, 2000; Kaplan *et al.*, 2011). Also, the structure is usually strengthened to limit lateral displacements in order to compensate for the low ductility (Sonuvar, Ozcebe and Ersoy, 2004; Kaplan *et al.*, 2011). Increasing the global stiffness and reducing the seismic deformation expectations of a building for seismic retrofitting purposes may be more cost-effective in comparison with the local intervention of the existing components, in order to strengthen their capacities (Fardis, 2009). The addition of RC infilled walls in selected bays within existing RC frames, especially on the perimeter, is a simple, effective and cost-effective retrofitting method for multi-storey, multi-bay RC buildings (Kaplan *et al.*, 2011; Fardis, Schetakis and Strepelias, 2013, Chrysostomou & Kyriakides, 2013).

In order to achieve a full monolithic action between the old and the new concrete members according to the code regulations (CEN, 2010; KANEPE, 2017), the usual way to achieve this is through the construction of a new thicker web than the beams and columns of the existing frame panel, encapsulating the latter, at the location of the new wall (Fardis, Schetakis and Strepelias, 2013). In this way, the new walls are much stronger than what is actually needed for the strengthening of the structure, and this 'overstrength' causes additional issues like the weakening of the foundations of the existing buildings (Fardis, Schetakis and Strepelias, 2013). Hence, a significant rotation is expected at the foundation (KANEPE, 2012). However, the design and the construction of the new RC infill walls with the same thickness as the existing beam and columns are not addressed by the codes. Also, (Jirsa, 1988), stated that the new materials must be attached to the existing structure to provide the type of monolithic action generally assumed in the design of the retrofit scheme. A reasonable simple method to make the attachments involves the use of epoxy resins to grout reinforcing bars into the existing concrete elements (Jirsa, 1988).

2.1 Code regulations and guidance

The code regulations and guidance regarding the design and the construction of new RC infill walls with the same thickness as the existing bounding frame members will be discussed in this section.

The design of new RC infill walls and the contribution of the dowels that connect the new infill wall to the existing RC frame are topics that need further study. Even though RC infills is a common retrofitting method and is extensively applied, it is not addressed quantitatively by the codes, not even by Eurocode 8 – Part 3 (EC8-3). There is no quantitative procedure for the design and construction of the new walls. In addition, the contribution of dowels that connect the new infill wall to the surrounding frame members, have not been analyzed adequately yet. The dowels affect the behavior of RC infills and the overall shear resistance capacity of the building. Their action is a complicated mechanism, and the way of designing them is not clear. The only way to design the new RC walls according to EC8-3 is to guarantee monolithic behavior between the old and new concrete. Although for other strengthening methods of existing structures there are guidelines regarding the retrofit design and certain aspects of the seismic response of the retrofitted structure, there are still open issues about the studied retrofit method. For example, their interaction with the bounding frame, as wells as their design and detailing between the new web and the surrounding frame members need to be regulated (CEN, 2010; Fardis, Schetakis and Strepelias, 2013).

According to EC8-3, among other intervention methods, the addition of new structural elements is mentioned (e.g., bracings or infill walls). There are instructions for the design of the structural intervention and the retrofit design procedure. In EC8-3 there are capacity models for the assessment for the existing members of the structure under flexure and capacity models for strengthening with concrete jacketing, with steel jacketing, and with Fibered Reinforced Polymers (FRP) plating and wrapping. For the addition of new RC walls within existing RC frames, there are no models in EC8-3. Furthermore, EC8-3 fully covers retrofitting with FRP or concrete jackets, while it does not address the retrofitting of RC frames with the addition of new walls created by infilling selected bays (CEN, 2010). As mentioned, the only way to design the new RC wall according to EC8-3 is by the full monolithic action between the old and the new members.

On the other hand, KANEPE (2017) refers further to the introduction of RC infills within an existing frame. More specifically, this method is recommended for the installation of RC walls for selected frames for the systematic increase of the stiffness and the seismic capacity of the structure. The new members should be connected properly to the existing frame and must have a safe foundation. During the analysis of the new structure, the rotation of the foundation of the new wall should be considered. The new RC wall can be constructed in situ or can be precast. KANEPE refers to the design of such walls only in terms of forces, providing tools for calculating their deformations at yield, failure, and stiffness only if they are integral with the bounding frame.

American Society of Civil Engineers, 2007 addresses frames with concrete infills with no special provisions for continuity from storey to storey and it considers the concrete of the infill separately from the concrete of the frame. However, American Society of Civil Engineers, 2007, adds that when the frame and the concrete wall are assumed to act as a monolithic wall, flexural strength shall be based on continuity of vertical reinforcement in both the column acting as boundary components and the infill wall, including anchorage of the infill reinforcement in the boundary frame. Nevertheless, it does not provide any guidance for such continuity or anchorage, neither on how to determine key properties of the monolithic wall depending on the connection of the RC infill with the surrounding frame.

It is apparent that the codes and standards for seismic retrofitting of existing RC structures do not provide complete guidance for the design and detailing of the attachment of new walls to existing frames. Furthermore, regulations do not exist for modeling or evaluation of frame bays converted into RC walls depending on the type and details of the connection. Subsequently, further investigation is required regarding their design and construction, and a parametric study of dowels is necessary. Further research should include experimental investigations focused on the behavior of strengthened structures, as well as methods of establishing the connection between the old and newly designed elements (Radomir Folici, 2015). Guidelines have been lacking beyond the epoxy manufacturer's recommendations on details of installing epoxy grouted dowels and design values to use (Loring A. Wyllie, 1988). Frequently, it is necessary to strengthen existing concrete structures for improved seismic performance, either after a damaging earthquake or in preparation for a future event. Epoxy grouted dowels are ideal for this

task due to the strength and ease of installation of epoxy resins to anchor dowels (Loring A. Wyllie, 1988).

2.2 RC infill walls behavior

The approach of subsequent strengthening using RC walls proved to be more advantageous than other methods, and adding RC walls as a global strengthening technique effectively and efficiently resolves the problem of global displacement, capacity, and ductility of the frame structure (Radomir Folici, 2015). It has been mentioned that the simplest and most effective way to improve the behavior of non-ductile RC frames is to provide new walls by infilling strategic bays of the existing frame with RC, especially at the perimeter. Such walls not only increase the lateral stiffness but also relieve the existing non-ductile frames from carrying large lateral forces (Canbay, Ersoy and Ozcebe, 2003). Also, the new walls control the lateral drift and reduce seismic damage to frames and non-structural elements (Dionysis Biskinis, Michael N, Fardis, 2016). Moreover, by adding new RC walls the seismic loss to the frames and the non-structural elements is reduced and the new walls control the seismic lateral drifts (Strepelias *et al.*, 2012). In this section, the behavior of RC infill walls is discussed.

The most important parameters that affect the general behavior of infilled frames were studied and investigated by (Chrysostomou, 1991). Among them, are the effect of the shear connectors, the effect of the number of bays, and the height to length ratio. According to (Chrysostomou, 1991), the models with shear connectors (dowels) have evenly spread cracks, whereas the models without connectors have a few cracks and fail suddenly without any warning. The extensive and numerous cracks spreading over the whole infill have a much higher potential for dissipating energy produced by dynamic loads than the dissipation of energy due to slip and separation between the infills and the frame when connectors are not provided. It was also mentioned that the ultimate load of infilled frames was increased by adding new bays. Moreover, the distribution of forces and the position of plastic hinges are different in the case of multi-bays. Also, it was noted that the influence of the height to length ratio has an important influence on the shear diagonal tension and vertical compression at the center of the infill and had less influence on the compressive stresses at the loaded corners. However, these parameters are better to be investigated in terms of full-scale specimens.

2.2.1 RC infill walls failure modes

In this section, the main failure modes that can occur in RC infills within existing frames as a strengthening method are discussed.

The main failure modes of RC shear walls that were studied by (Benjamin and Williams, 1958) were the tension column failure and the diagonal cracking in the tensile stress region along the compression diagonal. The tension column failure is a sudden failure in tension and shear that comes from the connection between the tension column and the foundation and propagating along the base of the wall towards the compression column (Chrysostomou, 1991). This type of failure is common for walls surrounded by very weak frames. Moreover, the columns designed and built according to older standards can be subject to damage due to seismic loading during earthquakes because of the lack of shear reinforcement and/or insufficient lap-splice length. Such columns may experience brittle failure modes; hence these columns must be retrofitted so as to adhere to current code requirements and survive future earthquakes (Mohamed Mohamed Salah El-Din Darwish, 2006). The diagonal cracking failure mode in the tensile stress region along the compression diagonal is associated with walls surrounded by frames strong enough to withstand tension in the windward column and shear in the leeward column (Chrysostomou, 1991).

Although the addition of walls improved the lateral force resistance of the frames, the capacity of most of the frames was controlled by a tensile failure of the compression splices in the boundary elements (columns) resulting from overturning forces on the walls in Jirsa, 1988. In Jirsa, 1988, it is shown that failure started in the column splices and spread across the wall along the top of the dowels grouted into the foundation beam. In all cases, the grouted dowel performed very well. The dowels along the columns and at the top registered very low strains. At the bottom of the wall, failure occurred at the end of the dowel, not at the interface between the wall and the floor. The tests would indicate that a smaller number of dowels could have been used at the sides and top without significantly changing behavior.

Another failure mode was mentioned according to (Fardis, 2009; Strepelias *et al.*, 2012). Specifically, it is stated that if the new walls take full seismic action, with the existing elements verified like 'secondary' ones in the building, then the new walls are designed

on the basis of forces and detailed as in new buildings. In this way, the flexural plastic hinging will be at the base, and to this end, the plastic hinge zone at the base is provided with boundary elements near the edges of the section, well-confined and detailed for flexure, not for shear, and to develop a flexural plastic hinge at the base.

Moreover, to achieve integral behavior, the new wall should be thick enough to encapsulate the existing beams and columns (Fardis, 2009). For this purpose, the new reinforcement is placed outside the old members, and the wall is detailed as new (Strepelias *et al.*, 2012). According to (Fardis, 2009) in that case, holes and slots should be drilled through the slab, for the vertical bars to pass from one storey to the next and for concrete to be cast from the top. The concrete that fills the slots plays the role of shear keys between the new wall and the slab. For fully integral behavior epoxy-grouted dowels may be placed throughout the interface of the old concrete and the new, at about 0.5m centers. As stated by (Fardis, Schetakis and Strepelias, 2013), for the estimation of the design shear force demand on the dowels around the new web, one should establish what is attained first: a plastic hinge at or near the base of the wall, or the uplift resistance of the wall footing from the ground, alongside plastic hinging at the ends of any tie-beams framing into the footing in the strong direction of the wall.

However, in the case of the full encapsulation and reliance of new reinforcement placed outside the old members and detailed as in a new wall, the frame may end up much stronger than needed for the retrofitting of the building as a whole (Strepelias *et al.*, 2012). This overstrength may not be fully used, if its connections to the floor slabs are weak links (a distinct possibility if the new wall is at the perimeter), or if its foundation cannot transfer the large moment resistance of the wall base to the ground because it uplifts from the ground and rocks during the earthquake. In order to reduce this overstrength and avoid the vertical reinforcement across the floors, the new web may be chosen to be not thicker than the beams and the frame columns (Strepelias *et al.*, 2012).

In the case of a not thicker RC wall than the existing frame beams and columns, the connection of such a new web to the existing frame members is more critical than when these members are fully encapsulated (Strepelias *et al.*, 2012). Even with a very good shear connection, the integral behavior of the old and the new concrete cannot be taken for granted. Also, the force and moment resistance or the deformation capacity of the system cannot be quantified with certainty (Strepelias *et al.*, 2012). Nevertheless, even

when the new wall does not encapsulate the existing beams, it may have to do so for the columns, to provide the lacking confinement reinforcement, especially if the columns have short lap splices (Fardis, 2009).

If the new wall takes up the full bay, it can incorporate the beams and both its columns as boundary elements. Then, only the web of the wall is totally new, and it should be fastened to the existing beams and columns all around the infilled panel through special connectors (dowels). The fastening of these connectors to the existing members and their embedment into the new concrete should be capable of fully transferring the web shear and the tensile capacity of the web reinforcement to the frame members. Poor detailing and lack of proper load-path between the old members and the new parts of the wall may lead to reduced ductility or brittle failure of the web panels. Several types of connections of the infill walls to the surrounding frame were studied in the past like shear keys, dowels, and chemical anchors (Sugano, 1981; Aoyama *et al.*, 1984). Added to that, if there is no integral connection between the existing and the new parts, the seismic behavior is uncertain and the reliability of modeling and verification of the wall as a single, integral element is questionable (Strepelias *et al.*, 2012).

The surveys revealed that these buildings had some common deficiencies in the frame such as low concrete strength, inadequate lateral stiffness, inadequate ductility (ends of members and beam-column joints were not properly confined), inadequate confinement at member ends, 90-degree hooks in column and beam ties and inadequate length of lapped splices in column longitudinal bars made above the floor levels. Test results revealed that both the lateral strength and lateral stiffness increase significantly with the introduction of reinforced concrete infills even when the frame had the deficiencies mentioned above. The deficiency which affected the behavior of infilled frames most adversely was the presence of lap splices in column longitudinal reinforcement. (Ahmet Murat Turk, Ugur Ersoy, 2006)

In conclusion, the simplest and the most effective way of improving the overall behavior of RC buildings, i.e., placing an adequate number of structural walls into strategic bays, eliminates the unsatisfactory seismic behavior due to poor structural system. Such walls not only increase the lateral stiffness significantly but also relieve the existing non-ductile frames from carrying large lateral forces. (Ahmet Murat Turk, Ugur Ersoy, 2006)

2.2.2 RC infill walls disadvantages

The main drawbacks of this retrofitting method that are mentioned in the literature are discussed in this section.

As already mentioned, one of the main problems of the addition of new RC infill walls within existing RC frames is the penalizing of the foundation of the new wall with very high moment demand (Akin, 2005; Fardis, Schetakis and Strepelias, 2013). Usually, the footing of added walls is small and not properly connected to the other footings and as a result, they uplift and rock during the seismic excitation (Fardis, Schetakis and Strepelias, 2013). To avoid this, the new concrete wall should not be thicker than, or surround the old frame members by having just a new web added between the existing columns, without encapsulating them in jackets (Fardis, Schetakis and Strepelias, 2013).

Moreover, studies revealed that the benefit of retrofitting non-ductile RC frames might be limited because of the failure of splices in the existing columns made above the floor level (Valluvan, Kreger and Jirsa, 1993). They have also shown that certain deficiencies in flexure or shear do remain and require supplementary interventions (Fardis, Schetakis and Strepelias, 2013). In order to mitigate that, local FRP jackets are an economic way that can be used at the member ends for the remaining flexural deficiencies (Fardis, Schetakis and Strepelias, 2013). In this way, a quick upgrade of the capacity of the members to the required seismic demand level can be achieved without new analysis of the strengthened structure, since FRP does not change the member effective stiffness or moment resistance (Fardis, Schetakis and Strepelias, 2013).

Furthermore, in real applications, it might be difficult to find places on the perimeter of the building to add new walls that are not prohibited by the architectural function of the building and at the same time help improve its seismic performance (Fardis, Schetakis and Strepelias, 2013).

Another limitation regarding the RC infill walls is that most available test data is on single-storey, single-bay specimens and not in full-scale. However, some conclusions can be drawn from a full-scale test that took place in Ispra (Chrysostomou and Kyriakides, 2013a).

For the analysis, the crucial issue of the building with introduced walls is the distribution of the shear force to the walls and the frame (Canbay, Ersoy and Ozcebe, 2003). Quite a

few issues must be considered, and the most important is the wall and the frame members that were built at different years which have not experienced the same cracking histories. The stiffness of the infilled frame is affected by the type and effectiveness of the connections made between the infill and the frame members (Altin, Ersoy and Tamkut, 1992; Sonuvar, 2001).

2.2.3 Experimental studies for RC infill walls

A lot of experimental work has been done to study the behavior of RC infill walls and their interaction with the surrounding frames (Chrysostomou and Asteris, 2012). Until the beginning of the 1900s, most of the researchers studied the behavior of infilling walls under monotonic or cyclic loading, and only a few subjected model structures to dynamic loads such as (Yanev Bojidar., 1979), as well as (Chrysostomou, 1991). However, even though the behavior of a structure is not the same when exposed to cyclic and dynamic loads, significant data can be taken for the behavior and modes of failure of infilled frames under monotonic loading like the load-displacement relation on which an analytical model is based and is required in dynamic analysis (Chrysostomou, 1991). The experimental studies that were found in the literature regarding the studied retrofitting method are discussed in this section.

Many researchers have focused on the addition of RC infills and found that the construction of RC infills greatly improved lateral load capacity and stiffness of the structure (Jirsa and Kreger, 1989; Altin, Ersoy and Tamkut, 1992; Albanesi *et al.*, 2008; Kaplan *et al.*, 2011). Even in cases of application to damaged buildings, the infill method yields satisfactory results (Canbay, Ersoy and Ozcebe, 2003; Sonuvar, Ozcebe and Ersoy, 2004). A review of the RC infilled frames in the literature indicates that the first published experimental research on this subject is the one reported by (Ersoy and Uzsoy, 1971). The researchers tested nine half-scale, one-storey, one-bay frames with RC infills under monotonic loading and it was concluded that the infill increased the lateral load capacity of the frame and reduced the lateral displacement at failure quite significantly.

Several researchers studied this retrofitting method in Turkey (Altin, Ersoy and Tamkut, 1992; Canbay, Ersoy and Ozcebe, 2003; Sonuvar, Ozcebe and Ersoy, 2004; Kara and Altin, 2006; Altin, 2007; Teymur, Yuksel and Pala, 2008; Baran and Tankut, 2011; Sinan Altin, Ozgur Anil, M. Emin Kara, 2012). The retrofitting of frames by adding RC infills

was first applied after the 1969 Bartin earthquake and after the 1992 Erzincan earthquake, when structural strengthening by RC infills has been used extensively (Canbay, Ersoy and Ozcebe, 2003). In the 1980s, Japan extensively researched the technique (Hayashi, Niwa and Fukuhara, 1980; Higashi, Ohkubo111 and Shimizu, 1980; Ohki and Bessho, 1980; Aoyama *et al.*, 1984; Kato, Katsumata and Aoyama, 1984).

In 1976 (Klingner and Bertero, 1976) a series of RC frames with RC block infill wall was tested taking care of designing their test frames in order to provide sufficient shear capacity to the columns and they connected the infill and the surrounding frame. From their experimental work, they concluded that the infill walls significantly increase the stiffness and the strength of frames and that they change the main behavior of a bare frame. In addition, they noted the concentration of inelastic deformations and the most significant degradation in frame members that were bounding the panels. Finally, they mentioned that the strength of the infill wall is asymptotically approaching the strength of the corresponding bare frame mechanism and load-deflection feature.

Later on, (Higashi, Ohkubo111 and Shimizu, 1980) have experimentally tested one-bay, one-storey RC frames with poor web reinforcement columns strengthened by adding several shear walls using about one-third of the scale specimens. The maximum strength after retrofitting the frames was increased significantly. Moreover, an inelastic frame analytical method was reported that could be useful for the definition of the load-deflection curve on the retrofitted structure. The load-deflection graphs from (Higashi, Ohkubo111 and Shimizu, 1980) tests of a pure frame and of an RC infilled wall case in place are shown for cyclic loading in Figure 2.1(a) and Figure 2.1(b) respectively.
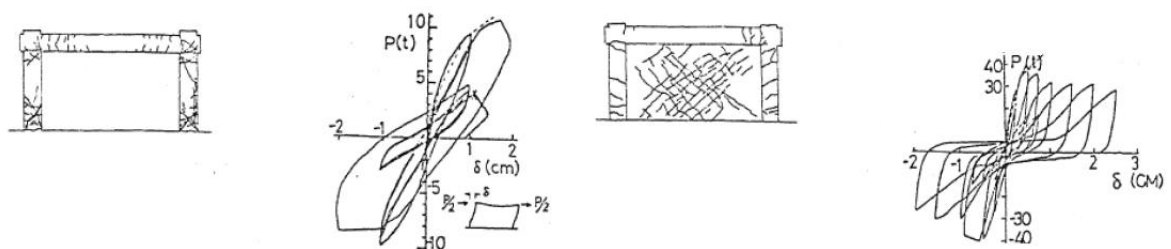
Figure 2.1: (a) Load-deflection curve of pure frame, (b) Load-deflection curve of RC infilled wall (Yoichi Higashi, Ohkubo111 and Shimizu, 1980)

In the same period, (Ohki and Bessho, 1980) tested two RC frames that were strengthened with infilled shear walls in 1:2 scale, five-storey, one-bay specimens. It was found that the initial stiffness of the infilled shear wall frame was about 19 times as high as that of the existing frame. As for the maximum strength of the infilled frame, it was 5.6 times as high as that of the bare frame. In Figure 2.2, the shear transfer mechanism of the frame with the infilled shear wall is illustrated.
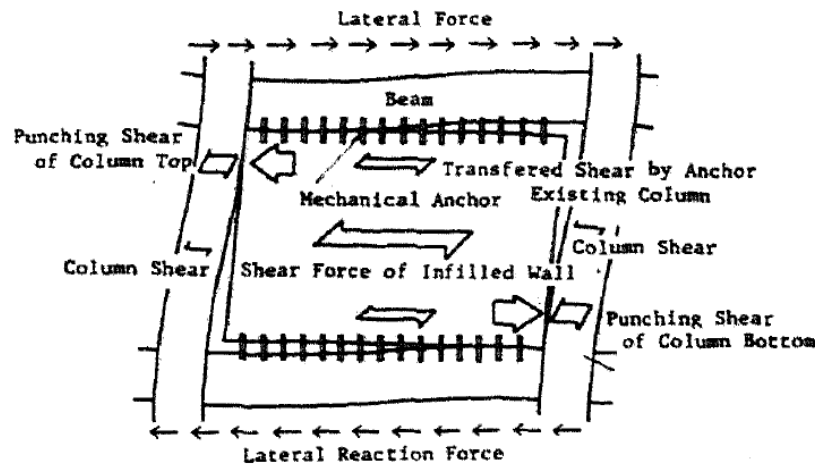
Figure 2.2: Shear Transfer Mechanism of the Frame with Infills' Shear Wall (Ohki and Bessho, 1980)

A few years later, Aoyama *et al.*, (1984), tested RC shear walls, into an existing frame for seismic strengthening and they observed that when the confining effect around a wall from the surrounding frame was increased, the shear strength of the infilled wall was increased. In the same period, Higashi, Ohkubo111 and Shimizu, (1980) tested the cyclic behavior of 1:7 scale, three-storey, single-bay specimens, with mechanical anchors on the top and bottom of the new web and expansive mortar at the lateral sides. They concluded that the specimens with RC infills' cast-in-place wall showed high strength.

After the 1980s, experiments were not only focused on the behavior of the RC infill walls but also their connection to the surrounding frames. Altin, Ersoy and Tamkut, (1992), Sinan Altin, Ozgur Anil, M. Emin Kara, (2012), and Sonuvar, Ozcebe and Ersoy, (2004), tested specimens with dowels all around, epoxy-grouted in the frame and extending well into the RC infill web and the similar three-bay ones in Canbay, Ersoy and Ozcebe, (2003); Ibrahim Erdem, Ugurhan Akyuz, Ugur Ersoy, (2006).

Aoyama *et al.*, (1984), studied the confining effect around a wall from the surrounding frame. They tested 12 specimens, about 1:3 in scale to investigate the confining effect of adjacent wall panels, the effect of flexural strength on shear strength, and the method of post-casting construction. All the specimens were single-storey, single-span walls, but the top girder was internationally made very stiff and strong to simulate the confining effect of multi-storey shear walls. They concluded that the shear strength of post-cast walls was increased with the confining effect. The confining effect was more effective in the form of increased flexural strength than that in the form of increased stiffness of the side columns. They also concluded that post-cast shear walls might fail in sliding along the interface of the old and new concrete, however, with large deformability. The improvement in construction methods reduced the amount of sliding and increased the strength accompanied by brittleness. The behavior of chemical anchors was generally satisfactory, and it was superior to the mechanical anchors, particularly in tension. Furthermore, an empirical design equation for shear strength was developed from the testing of post-cast shear walls, in the "Guideline for Repair and Strengthening Design of Existing Reinforced Concrete Buildings".

Added to these, Kato, Katsumata and Aoyama, (1984) also tested three multi-storey frames under lateral load reversals in 1:5 scale specimens. An arbitrary three-storey RC building with one-bay structural wall on footing foundation was chosen to be the prototype structure and a two-storey, three-bay portion of the frame with the structural wall in the central span was isolated from the prototype structure. The wall base rotation limited the input forces to the structural system and prevented damage to the wall. The beams though were forced to deform during the wall rotation. Regarding the behavior of the structural wall in low-rise buildings, three main modes of failure have been identified: the shear failure, the flexural failure, and the base rotation.

In order to investigate the strength and load-deflection characteristics of the interface connection between old and new concrete typical of that used in repair and strengthening of existing RC structures interface shear tests were carried out by Jirsa, (1988). Specimens were subjected to repeated cyclic loadings at various load levels up to failure. The tests indicated that the dowel embedment length, the number of dowels, the concrete surface roughness, and the concrete strength significantly influenced the interface performance. Specifically, the increased dowel embedment length and the number of dowels increased

the shear strength of the interface but not in a linear manner. Also, the concrete surface roughness influenced the interface performance, roughened surfaces reached higher strengths than plain surfaces, however, the degree of roughness, chipping, keying, sandblasting did not result in a significant difference in peak strength. Furthermore, the wall and base block reinforcement details had no discernible influence on strength. The concrete strengths of the base and the wall appeared to influence the shape of the failure surface but the influence on shear strength was not consistent. Also, it was shown that dowels generally provide more capacity than determined using code provisions for shear friction or development Jirsa, (1988).

A decade later, Canbay, Ersoy and Ozcebe, (2003) investigated the internal force distribution in RC frames with added RC walls. A 1:3 scale, two-storey, three-bay RC frame was initially subjected to damaging lateral-drift reversals and was then strengthened with the addition of RC wall to fill the middle bay, and then it was subjected again to drift reversals. The observed hysteresis loops from this test were stable even though a slip of the longitudinal bars was noted at the splices in the interior columns.

Furthermore, Sonuvar, Ozcebe and Ersoy, (2004), tested the behavior of RC infilled frames as rehabilitation for moderately damaged RC buildings. They tested five specimens and each specimen consisted of 1:3 scale, one-bay two-storey frames having the deficiencies commonly observed in residential buildings in Turkey under cyclic lateral loading until moderate damage occurred. Afterward, they introduced RC infills to the damaged specimens and these infilled frames were then tested under cyclic lateral loading until failure. The experiments illustrated that strength and stiffness were significantly improved by the introduction of the infill. The deficiency, which affected the behavior of infilled frames most adversely, was the presence of lap-splices in column longitudinal reinforcement. The length of the splices was much shorter than what is required by the codes.

Ibrahim Erdem, Ugurhan Akyuz, Ugur Ersoy, (2006), tested a 1:3 scale, two-storey three-bay RC frame specimen introducing an RC infill. The behavior of the specimen was dominated by the flexural action of the infill wall. Almost the total lateral load (about 90%) was carried by the RC wall. Since almost the total lateral load was carried by the infills, the most significant damage was concentrated on the infills at the end of the lapped splice region. The test was terminated when the decrease in strength was 24% due to

heavy damage in the RC infill. Pinching of hysteresis loops was observed towards the end of the test due to high deformations causing slip of the longitudinal bars of the boundary columns (shown in Figure 2.3).
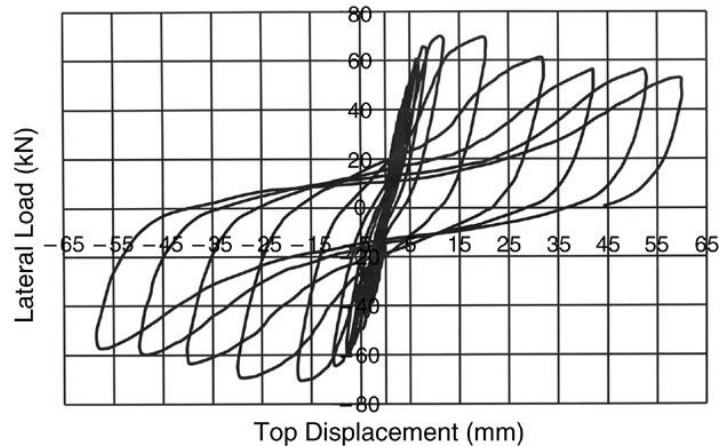
Figure 2.3: Hysteretic curve of specimen (Ibrahim Erdem, Ugurhan Akyuz, Ugur Ersoy, 2006)

Later, the placement configurations and the aspect ratio of the infilled wall were the parameters that were experimentally studied by Kara and Altin, (2006). They tested seven one-bay two-storey, 1:3 scale specimens under cyclic loading. The experimental results showed that partially infilled non-ductile RC frames exhibited significantly higher ultimate strength and higher initial stiffness than the bare frame without the infill. As the aspect ratio of the infilled wall increased, the lateral strength and rigidity were increased significantly. The strength and ductility inadequacies of the frame members influenced the lateral performance of the frame that was strengthened.

The behavior of RC frames with RC infills under lateral loads was also tested by Altin, (2007). They tested six 1:3 scale one-bay, two-storey specimens under cyclic lateral load. Test results illustrated that both the strength and stiffness were improved importantly by introducing infill. Like in other tests, the presence of lap-splices in column longitudinal reinforcement is observed mainly on the columns at just the floor level.

Simple structures, such as a four-storey shear wall with masses lumped at the floors or a single mass on a stick (Qin and Chouw, 2010) have also been tested on shake tables with the base fixed, or uplifting from the rigid table or a sand bed (Fardis, Schetakis and Strepelias, 2013).

The only experiment that was found in the literature in a full-scale multi-storey, multi-bay specimen that tested the interaction of the surrounding members of the existing

structure is the one of Chrysostomou *et al.*, (2013) and Poljansek *et al.*, (2014). The conversion of selected bays into new infilled RC walls for the retrofitting of multi-storey, multi-bay RC frame buildings was the subject of the project. The test took place at the European Laboratory of Structural Assessment (ELSA) of the Joint Research Centre (JRC) in Ispra, Italy. This experiment is discussed in detail in Chapter 3.

Several experiments were executed on one-bay RC frames converted into RC walls by adding a web, not thicker than the surrounding beams or columns, between the frame members by Dionysis Biskinis, Michael N, Fardis, (2016). A new wall incorporated the beams and both columns of the frame (as boundary elements). Then only the web of the wall was totally new, and it was fastened to the existing beams and columns all around the infilled panel so that the web shear and the tensile capacity of the web reinforcement were fully transferred to the frame members. As mentioned in Dionysis Biskinis, Michael N, Fardis, (2016), poor detailing and lack of a proper load-path between the old members and the new parts of the wall reduces the ductility or even causes brittle failure of the web panel. Moreover, if there is no integral connection between the existing and the new parts, the seismic behavior is uncertain, and the wall may not be confidently modeled and verified as a single integral element. The results of such tests have not been used as yet to develop rules for the calculation of those engineering properties of RC-infilled frame, which are essential for its analysis and design in the context of modern performance-based (and often displacement-based) seismic design, namely: the effective stiffness, the moment and shear resistance, the deformation at yielding and the cyclic deformation capacity (Dionysis Biskinis, Michael N, Fardis, 2016).

The most recent experimental study that was found about the response of RC frames strengthened by RC infill walls is Theocharis Papatheocharis, Philip C. Perdikaris, M.ASCE, (2019). In this study, the parameters to the experimental study included the infill-to-frame method of connection along the horizontal and/or vertical interfaces and the anchorage length of the shear connectors placed along the interfaces. The main results and conclusions of the experimental studies are discussed in sections 2.2.3.1 and 2.2.3.2.

2.2.3.1 *Experimental results*

From the experimental research studies, it was observed that the RC infills increased the lateral capacity of the frames as well as the strength and the in-plane stiffness of the

frames. Moreover, the energy dissipation of the frames was increased, but also led to a limited ductility and a rather abrupt failure after reaching the peak load. Nevertheless, they reduced the lateral displacement at failure. Furthermore, when the confining effect around a wall from the surrounding frames was increased, the shear strength of the infilled wall was also increased. Hence, the confining effect was more effective in the form of increased flexural strength than that in the form of increased stiffness of the side columns. In addition, it was noted that the improvement in construction methods reduced the amount of sliding and increased the strength accompanied by brittleness. It was also perceived that the aspect ratio of the infilled wall increased the lateral strength and rigidity.

The main modes of failure that have been identified were shear failure (including sliding at the interface), flexural failure, and base rotation. The wall base rotation limited the input forces to the structural system and prevented damage to the wall. It was also mentioned that the post-cast shear walls might fail in sliding along the interface of the old and the new concrete, however with large deformability. Nonetheless, the concentration of inelastic deformations and the most significant degradation was in the frame members that were bounding the panels. Slip of the longitudinal bars was observed several times at the splices in the columns. The length was much shorter than what is required in the codes. The strength and ductility inadequacies of the frame members influenced the lateral performance of the frame that was strengthened in some cases.

In Dionysis Biskinis, Michael N, Fardis, 2016, several specimens failed by sliding along the section which controls flexural yielding. Additionally, some specimens failed in diagonal tension after flexural yielding. Dionysis Biskinis, Michael N, Fardis, 2016 mentioned that for a wall produced in real life by infilling a frame bay, the most likely failure mode should be identified a priori, to calculate its cyclic force resistance and deformation capacity. Moreover, the contribution of shear keys to sliding shear resistance deserves further study according to Dionysis Biskinis, Michael N, Fardis, (2016).

Moreover, based on the results in the experimental work conducted by Haroun, M.A and Elbahar, M.R (2002) and the results reported in Mohamed Mohamed Salah El-Din Darwish, (2006) there is no evidence that the reinforcement of the infill wall had an effect on the seismic strength of the system or on its ductility. Also, it was concluded that the effect of the seismic strength of the system can be represented by following an equation

that is derived in Mohamed Mohamed Salah El-Din Darwish, (2006). It was also shown that the reinforcement of the columns had a direct effect on the seismic strength of the system as when the reinforcement of the columns was reduced the seismic strength of the system decreased while when the reinforcement of the columns was increased the seismic strength of the system increased. Based on the results conducted by Haroun, M.A and Elbahar, M.R (2002) and Mohamed Mohamed Salah El-Din Darwish, (2006), the reinforcement of the columns had a small effect on the cracking pattern in the infill wall which is expected as the major cracking occurs in the columns.

Furthermore, in Papatheocharis, Theocharis, Perdikakis, Philip C., Moretti, (2019) it was concluded that placing shear connectors along the infill-to-frame interface perimeter with an embedment length longer than that required for full activation of the dowel action led to the best overall response in terms of ultimate strength, in-plane stiffness, and energy dissipation capacity. In addition, it was concluded that the absence of any connection between the infill and the frame led to the complete separation of the infill from the bounding frame after the ultimate strength was reached with the measured beam-to-infill slippage being practically zero up to the peak load. On the other hand, in the case of the infilled frame specimens with dowels, the average horizontal relative slip along the infill/frame interfaces initiated at low drift levels of less than 0.05%, and relatively high slippage values were measured near the peak load. This had a detrimental effect on their post-peak response and integrity. Moreover, the presence of horizontal dowels along the frame-column/infill interfaces resulted in higher lateral-load carrying-capacity and considerably lower values of relative slip and opening displacements along these interfaces. However, when the frame columns were not strengthened by RC jacketing, the horizontal dowels led to localized concrete damage and lower ductility. Activation of the RC infill wall was observed only in the case of a relatively strong wall-to-frame connection but still without any significant damage in the infill. In Papatheocharis, Theocharis, Perdikakis, Philip C., Moretti, (2019) it is stated that the more effective the infill-to-frame connection scheme is, the more efficient the load transfer path is activated between the frame and the infill, thus increasing the load-carrying capacity of the infilled frame.

2.2.3.2 *Lack of data from experiments*

Despite the common field practice of new walls that encapsulate the frame members, the tests have been limited to small-scale specimens with new webs thinner than the surrounding beams or columns (possibly owing to the technical limitations of testing walls of very large shear force resistance) (Chrysostomou and Kyriakides, 2013a; Fardis, Schetakis and Strepelias, 2013). From the experimental studies that were studied, only the SERFIN experiment was full scale. Most of the experiments were on scale 1:3, 1:5, and 1:7, and only a few on 1:2 scale. In addition, it was noted that most of the experiments were testing one to three-storeys and just one was found to test five storeys, but even though they examined the effect of the number of storeys, they did not examine the number of bays. Most of the specimens were one-bay ones and very few specimens were three-bay. It is apparent that for practical reasons, the experimental research mainly targets on what was feasible and not on what is realistic and what is found in practice. Even in the extensive research on this subject, there is no experimental data for the taller full-scale specimens that reflect real building applications probably due to the practical difficulties associated with the high forces needed for the tests (Chrysostomou and Kyriakides, 2013a).

A common feature of all tests is the rather small thickness of the RC infill compared to the width of the frame members. This further penalizes the shear resistance of the composite wall and the new web-frame connection (Strepelias *et al.*, 2012).

Another drawback that was noted from the past investigations is that they did not propose or even follow a quantitative procedure for the design of the connection between the RC infilling and the surrounding frame members. That detail was empirically selected, almost non-engineered (Fardis, Schetakis and Strepelias, 2013). Furthermore, they have not led to, or supported, any procedure for the quantification of the engineering properties of the RC infilled frame which is essential for this analysis and design in the context of modern performance-based (and most often displacement-based) seismic design: the effective stiffness, the moment and shear resistances, the deformation at yielding and the cyclic deformation capacity (Strepelias *et al.*, 2012).

Nevertheless, it is evident from the research that the RC infill walls is an economic and practical way to strengthen the lateral stability of framed structures and to retrofit existing buildings to withstand earthquake loads.

2.3   Reinforced concrete hysteretic behavior

RC structures are made up of two materials with different characteristics. Steel can be considered a homogeneous material and its material properties are generally well defined. Concrete is, on the other hand, a heterogeneous material made up of cement, mortar, and aggregates, and its mechanical properties scatter more widely and cannot be defined easily. For the convenience of analysis and design, however, concrete is often considered a homogeneous material in the macroscopic sense (Kwak and Filippou 1990).

Considering the RC structure, it is designed on the principle that steel and concrete act together to withstand induced forces. The properties of thermal expansion for both steel and concrete are approximately the same. This, along with an excellent bendability property, makes steel the best reinforcement material in concrete structures. Another reason that steel works effectively as reinforcement is that it bonds well with concrete (Martín-Pérez and Pantazopoulou 2001).

The shear resistance in RC according to Martín-Pérez and Pantazopoulou 2001 comprises a component that collectively represents all other contributing mechanisms, namely:

(a) Bond of reinforcement to concrete and the tensile stress field mobilized in the concrete mass surrounding the reinforcement through this interaction,

(b) Residual diagonal tensile strength of cracked concrete,

(c) Dowel action of reinforcement intersecting the inclined cracks,

(d) Friction between crack faces and aggregate interlock

The nonlinear response of RC is caused by two major effects: cracking of concrete in cases of tension and yielding of the reinforcement or crushing of concrete in compression. Nonlinearities also arise from the interaction of the constituents of reinforced concrete, such as bond-slip between reinforcing steel and surrounding concrete, aggregate interlock at a crack, and dowel action of the reinforcing steel crossing a crack. The time-dependent effects of creep, shrinkage, and temperature variation also contribute to nonlinear behavior. (Kwak and Filippou 1990)

It is well established that the inelastic behavior of RC sections leads to a redistribution of moments and forces, resulting in an increased load-carrying capacity of the members and the indeterminate structure. As the applied load is increased, hinges start forming in

succession at locations where the hinge moment capacity is reached; with further increase in the applied load, these hinges continue to rotate until the last hinge forms converting the structure into a mechanism, fail. (Kheyroddin and Naderpour 2007)

A multitude of tests has been concluded to assess the performance of beams under seismic conditions. Under the reversed loading involving the inelastic extension of the reinforcement, failure has frequently been found to occur differently from that in a beam subjected to monotonic loading (Fenwick and Fong 1979). Tests have shown that the shear resisted by the concrete decreases under such conditions, and a diagonal tension-type of shear failure may occur unless adequate web reinforcement is provided (Fenwick and Fong 1979).

In all the tests, vertical cracks arose when the load was close to the specimen load-bearing capacity. Then the failure of the concrete cover followed, which was more pronounced in specimens with a high percentage of transverse reinforcement. The buckling of the longitudinal bars occurred during the softening branch of the stress-strain relationship. Furthermore, the rupture of some hoops was accompanied by the buckling of the longitudinal bars. (Barros *et al*., 2000)

In each series of tests, it was observed that the stress-strain (σ-ε) relationship obtained in specimen subjected to monotonic loading is the enveloping diagram of the σ-ε relationship registered in the specimens under cyclic loading. The results can also point out that the peak stress and the corresponding strain increase with the increment of the transverse reinforcement ratio, that by increasing the transverse reinforcement ratio the shape of the softening branch is smoothest, and that the energy absorption capacity increases with the increment of transverse reinforcement ratio. (Barros *et al*., 2000)

In RC members subjected to cyclic loading, the unloading/reloading stiffness and hysteretic energy dissipation decreased due to shear deformation caused by diagonal web cracking in the plastic hinge zone (see Figure 4) (Eom and Park 2013). The result showed that the longitudinal member elongation increased by cyclic loading has substantial effects on the shear deformation, and thereby, upon degradation of the stiffness and energy dissipation (Eom and Park 2013).

In the Figure 2.4, a force-displacement diagram is provided from the analytical study of Eom and Park (2013). It is obvious that there is hysteretic energy dissipation and that the

degradation of the stiffness and energy dissipation appears in the cyclic responses of members.
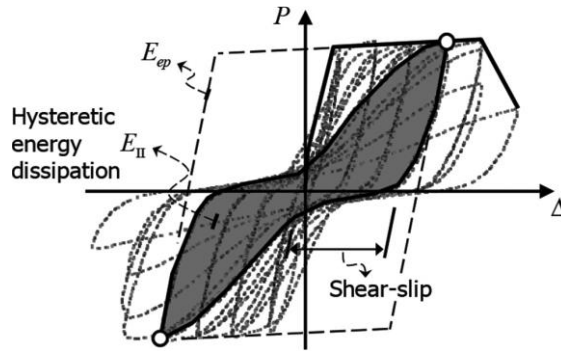
Figure 2.4: Cyclic behavior of RC members (Eom and Park 2013)

To accurately predict the cyclic response of RC members, including the degradation of stiffness and energy dissipation due to the shear deformation and longitudinal elongation, various nonlinear numerical analysis methods can be used (Palermo and Vecchio 2007; Petrangeli *et al.*, 1999; D'Ambrisi and Filippou 1999; Orakcal *et al.*, 2004; Massone *et al.*, 2009; Hsu 1988; Mansour and Hsu 2005; Mansour *et al.*, 2005). However, since the material nonlinearity of concrete and reinforcing bar and cyclic loading history are involved in the cyclic behavior of RC members, most of the existing methods require nonlinear numerical techniques and iterative step-by-step calculations (Eom and Park 2013).

The load cycle A-B-C-D-E-F-A in Figure 2.5 shows a general trend in the flexural and shear deformations of RC members showing ductile post-yield behavior as given in Eom and Park 2010. During the A-B, C-D, D-E, and F-A load cycles, shear deformation did not significantly increase, and the overall displacement of the member was attributed to the flexural deformation. On the other hand, during the B-C and E-F load cycles where the overall stiffness was significantly degraded, the overall displacement of the member was attributed to the shear deformation. This result indicates that the primary cause of the pinching in the cyclic response was shear deformation.
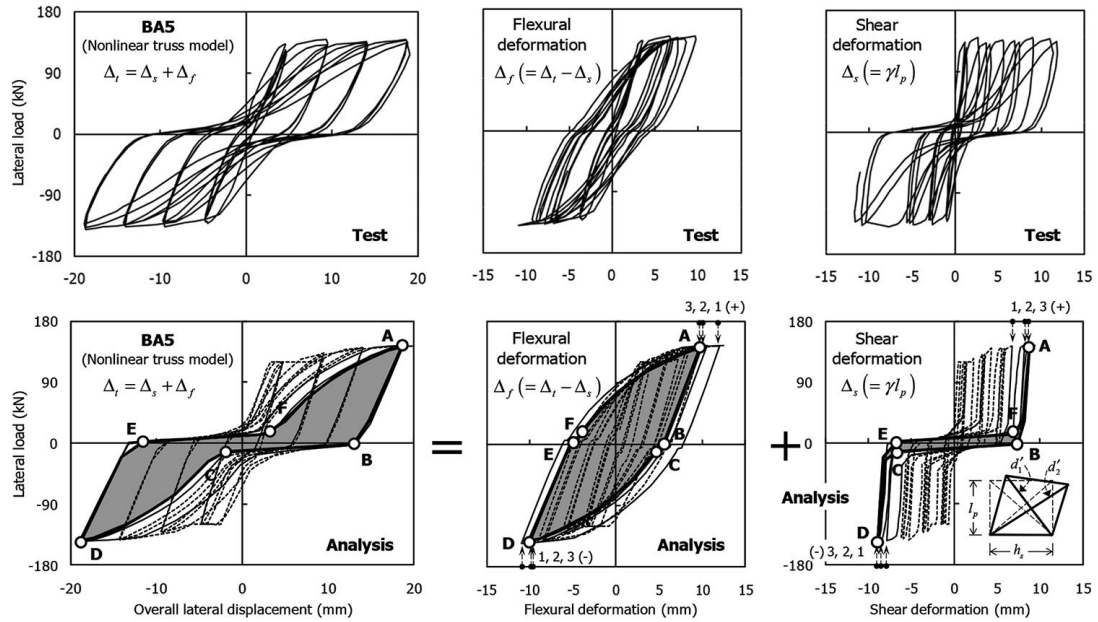
Figure 2.5: Cyclic behavior of beam specimen – Decomposition of total beam deformation into flexural and shear deformations (Eom and Park 2010)

As presented in Figure 2.5, the energy dissipation per load cycle is mainly attributed to flexural behavior, and the contribution of the shear deformation is limited. During cyclic loadings, the transverse reinforcing bars do not experience load reversals, remaining in tension. Therefore, the transverse reinforcing bars do not contribute to the energy dissipation (Eom and Park 2010; Park and Eom 2006). When RC members are subjected to a moderate axial compression load, the longitudinal elongation, and shear deformation decrease because the axial compression load restrains diagonal cracking in the web. Thus, hysteretic energy dissipation can increase due to the effect of moderate axial compression load. Nevertheless, significant axial compression load (that is, the load level greater than the balanced point) is not beneficial to hysteretic energy dissipation, increasing flexural pinching, and decreasing the deformation capacity of the member.

Eom and Park (2010) and Park and Eom (2006) investigated the energy dissipation mechanism of flexural members subjected to cyclic loading. According to their study, the overall energy dissipation is defined as the sum of the contributions of the energy dissipation due to the increase of the inelastic deformation and the energy of both the concrete in compression and the reinforcing bars in tension and compression.

26

In particular, modeling the behavior of RC under cyclic loading remains a challenge, and most of the research presented in the literature on the non-linear finite element analysis of RC is confined to the case of monotonic loading. Research performed on the cyclic behavior of RC is comparatively limited. Computational and numerical problems associated with the complex rules describing the stress-strain relationships of concrete and steel under cyclic loading are among the major constraints to the development of more-adequate design and analysis tools in this area. During the past 20 years, a limited number of refined models describing the behavior of RC under cyclic loading have been developed (Said *et al.*, 2005). These models though are generally based on empirical shear transfer functions.

Several studies investigated the shear transfer mechanisms for both reinforced and un-reinforced concrete subjected to cyclic loading. However, only a limited number of analytical models are available for such behavior. To account for the continually varying stiffness and energy absorption characteristics of concrete under cyclic loading, a suitable hysteretic model is considered necessary. (Said *et al.*, 2005)

2.3.1 The bond between concrete and reinforcing bars

The stress transfer capacity between concrete and a reinforcing bar is generally referred to as the bond of reinforcement. The bond mechanism is the interaction between concrete and reinforcement bars that engages the composite action of concrete and steel in RC construction (Murcia-Delso 2013). More specifically, bond stress is the shear stress that acts parallel to an embedded bar on the surface between the reinforcing bar and the concrete (see Figure 2.6) (Gan 2000). The bond mechanism has a strong influence on the fundamental behavior of a structure, for example in crack development and spacing, crack width and ductility.

Bond qualities affect anchorage, lap splices, cracking, and deformations of RC members, as well as the non-linear cyclic behavior of RC beam-column joints, which is complex and known to be sensitive to many factors interacting with each other. In seismic design, it affects stiffness and energy dissipation, and it is a significant property for ensuring adequate seismic performance. (Wei Yu 2006)
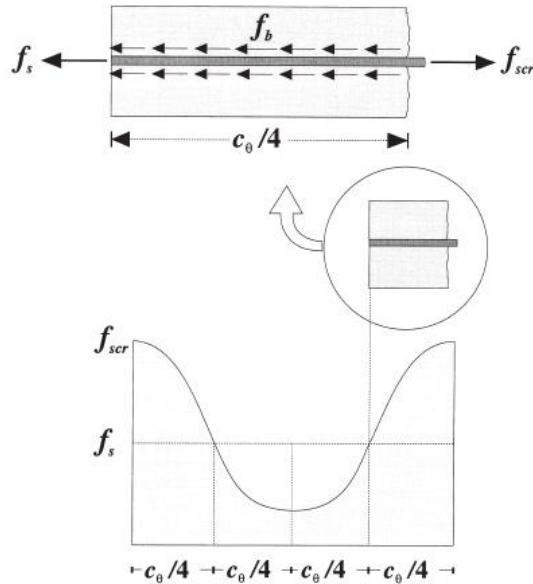
Figure 2.6: Variation of reinforcement stress and bond stress between successive cracks (Gan 2000)

As regards the bond between rebar and concrete, it depends upon many factors, such as the shape and geometry of ribs, the characteristics of the contact area, and the aspects related to the boundary conditions (Prabir *et al.*, 2004). It is also dependent on the slip between the steel bar and the concrete, as well as the stress in the reinforcing bar. American Concrete Institute (ACI) (2003) classifies the factors into three groups: concrete properties, bar properties, and structural properties. Concrete properties that have an important influence on the bond are the compressive and tensile strengths. Bar properties that have such influence include, but are not limited to, the bar size, the rib geometry, and the yield strength of the bar. Among the structural properties, the most relevant are the cover and spacing of bars, the transverse reinforcement, and the bar casting position. A more exhaustive list of factors and a detailed explanation of their effects are provided in the American Concrete Institute (ACI) (2003).

Two alternative basic hypotheses have been used in the past; in the first, the bond-stress is considered to be a linear function of slip (Ngo and Scordelis 1967), and in the second, it is considered that there is a nonlinear relationship between bond stress and slip (Gan 2000).

The strength of the bond between rebar and the surrounding concrete is generally made-up of three components: chemical adhesion between the steel and the concrete, friction

28

forces acting at the interface, and mechanical interlock between reinforcement and concrete (bearing forces of the bar ribs acting against the concrete) (see Figure 2.7) (Gan 2000; Lundgren 1999).
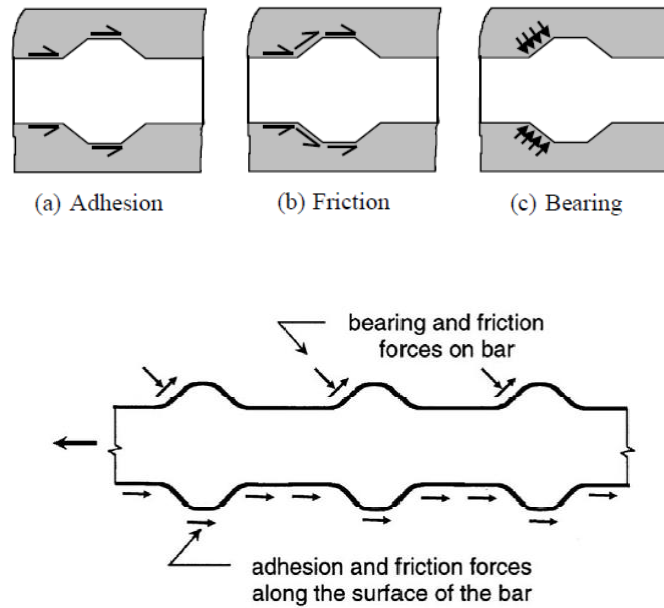
Figure 2.7: Idealized force transfer mechanisms (Lundgren, 1999)

The bond resistance resulting from the chemical adhesion is small; it is lost almost immediately when slipping between the reinforcement and the concrete starts, (American Concrete Institute (ACI) 1992). The inclined forces resulting from the bearing action of the ribs make it possible, however, to continue to transfer forces between the reinforcement and the concrete. This implies that bond action generates inclined forces that radiate outwards in the concrete. The inclined stress is often divided into a longitudinal component that is denoted the bond stress, and a radial component that is denoted normal stress or splitting stress, see Figures 2.8 and 2.9. (Lundgren 1999)
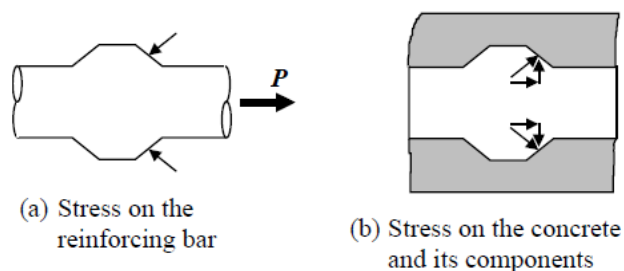
Figure 2.8: Bond and splitting stresses between a deformed bar and the surrounding concrete (Lundgren, 1999)
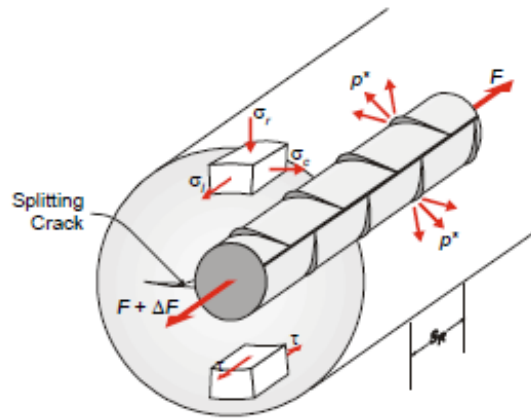
Figure 2.9: Splitting cracks due to circumferential tension (Lundgren, 1999)

Early experimental studies of the bond were concerned with determining bond failure strengths and the influence of surface deformations on them by the push-in test. Later, some researchers found that bond failure occurs at higher stress for a push-in test than for the normal pullout test. The explanation for this is simple. Primarily, the compressive axial stress developed in the bar during a push-in test causes an increase in bar diameter because of Poisson's effect, which, in turn, causes an increase in the radial pressure between bar and concrete. Since friction is an important element in a bond, this increase in pressure leads to increased bond strength; secondly, cracking is an important reason to cause degradation of bond strength. The lack of cracking in a push-in test leads to an increase in bond strength. (Gan 2000)

It should be noted that the presence of normal stresses is a condition for transferring bond stresses after the chemical adhesion is lost. When, for some reason, the normal stresses are lost, bond stresses cannot be transferred. This is what happens if the concrete around the reinforcement bar is penetrated by longitudinal splitting cracks, and there is no transverse reinforcement that can continue to carry the forces. This type of failure is called a splitting failure. The same thing happens if the reinforcement bar starts yielding. Due to the Poisson effect, the contraction of the steel bar increases drastically at yielding. Thus, the normal stress between the concrete and steel is reduced so that only low bond stress can be transferred. When the concrete surrounding the reinforcement bar is well-confined, meaning that it can withstand the normal splitting stresses, and the reinforcement does not start yielding, a pullout failure is obtained. When this happens,

the failure is characterized by shear cracking between two adjacent ribs. This is the upper limit of the bond capacity. (Lundgren 1999)

At low bond stress demands, there is some mechanical interlocking due to the roughness of the bar surface, and the bond between concrete and reinforcing bars is initially due to chemical adhesion (Gan 2000). As the chemical adhesion is overcome by increased demand (after bond stress from 0.5 to 1.0 MPa) even low bar-stress causes slip between the bars and the surrounding concrete (which mobilizes friction forces at the bar surface due to its roughness and bearing forces at the ribs caused by the wedging action against the concrete), sufficient to break the adhesion immediately adjacent to a crack in the concrete (Gan 2000). The pressure that the ribs exert onto the concrete creates micro-cracks, commonly referred to as Goto cracks (Goto 1971), starting at the tip of the ribs and propagating transversely away from the bar, as shown in Figure 2.10 (Murcia-Delso 2013). The opening of these micro-cracks allows further slippage of the bar with respect to the concrete (see Figure 2.11). As slip occurs, the wedging action of the ribs tends to introduce a radial expansion at the interface, which activates the passive confinement in the concrete (Murcia-Delso 2013).
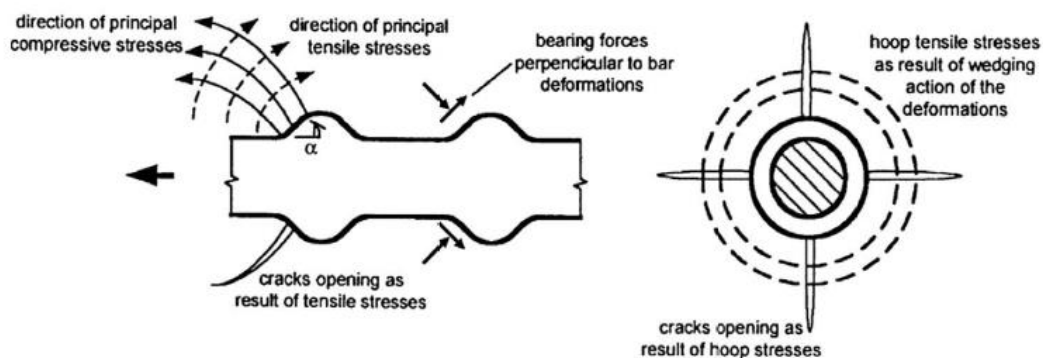
Figure 2.2: Cracking pattern due to bond-slip (ACI 2003)

Figure 2.10: Cracking pattern due to bond-slip (ACI, 2003)

<center>(a)   (b)</center>
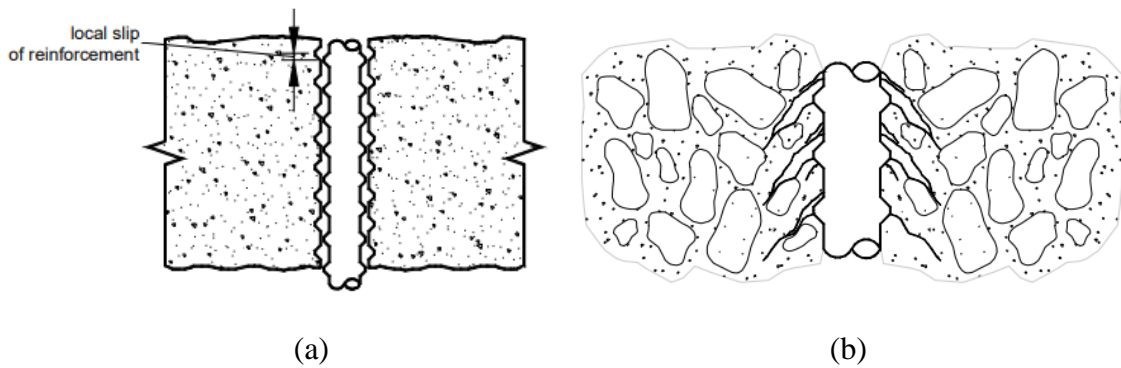
Figure 2.11: A typical scale of the bond response, (a) Local bond response, scale of the reinforcement, (b) Bond response, scale of the reinforcement lugs (Yu, 2006)

The inclined forces are balanced by ring tensile stresses in the surrounding concrete, as explained by Tepfers and Olsson (1992), see Figure 2.12. If the tensile stress becomes large enough, longitudinal splitting cracks will form in the concrete. Another type of crack that is directly related to the bond action is the transverse micro-cracks, which originate at the tips of the ribs, see Figure 2.13 (Goto 1971). These cracks are due to the local pressure in front of the ribs, which gives rise to tensile stresses at the tips of the ribs. These transverse micro-racks are also called bond cracks (Lundgren 1999).
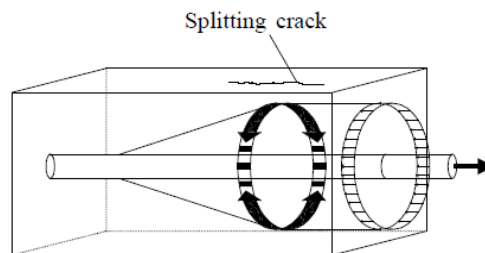
Figure 2.12: Ring tensile stresses in the anchorage zone (Tepfers and Olsson, 1992)
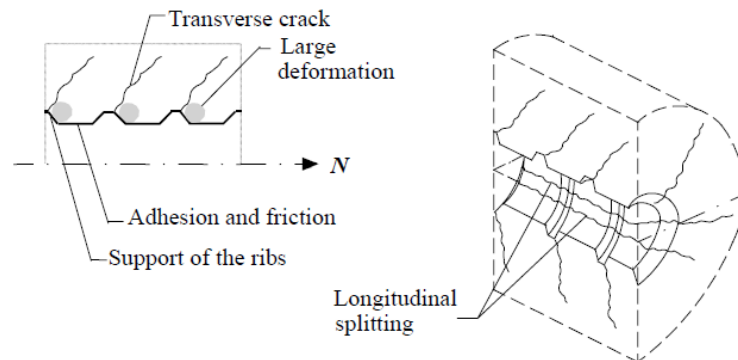
Figure 2.13: Deformation zones and cracking caused by bond, modified by (Magnusson J., 1997)

Further bond is also provided by the friction and wedging action between the cement paste and the pitting of reinforcing bars (Wei Yu 2006). Over the slipping length, only the friction drag remains, and the highest adhesive, bond stress can act only close to this slipping portion (Gan 2000). The interlock force eventually leads to internal bond cracks next to the deformations; at about the same time separation of concrete from the bars takes place in the region of flexural cracks. After separation, forces from the deformations to the surrounding concrete may lead to splitting cracks, typically parallel to the bars. If these cracks can propagate without restraint, bond-splitting failure occurs. Figure 2.14 shows a typical scale of bond response (Wei Yu 2006).

The mechanics of the bond are presented in Figure 2.14.
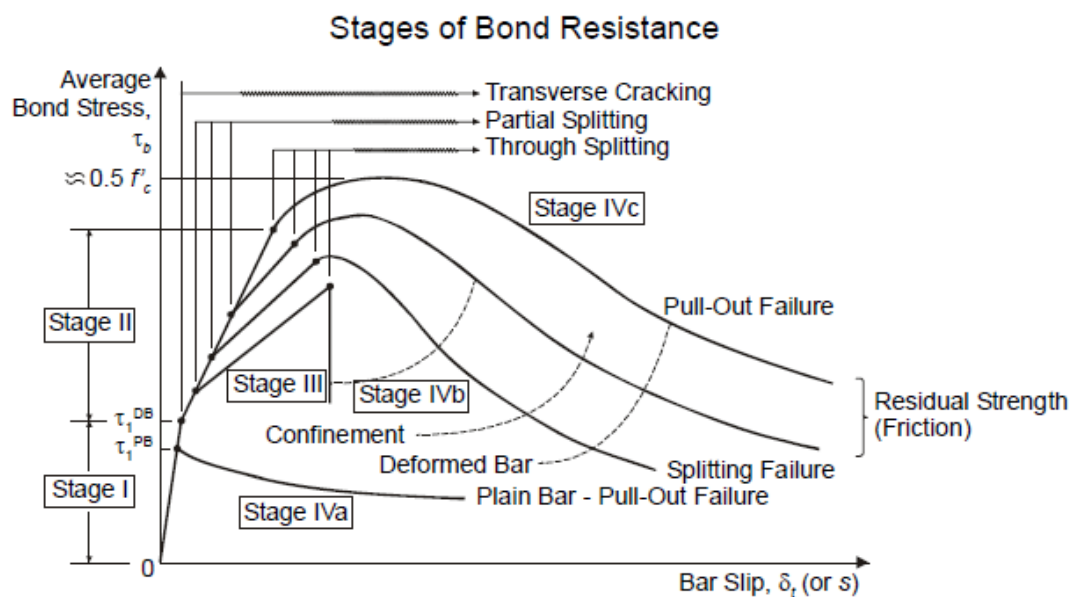
Figure 2.14: Mechanics of Bond (Yu, 2006)

Concerning radial expansion, it produces a hoop expansion in the concrete, which causes splitting cracks to develop at the surface in contact with the bar and propagates radially. This hoop expansion is restrained by the undamaged outer concrete ring as well as the confining reinforcement if any. The increase of the hoop stresses can still result in a splitting failure if the cover and the confining reinforcement are not sufficient. As soon as the concrete is well confined, splitting failure is precluded and higher bond strengths can be achieved. In this case, the bond fails due to the loss of the interlocking action caused by crushing and shearing of the concrete keys between the ribs. Finally, the bar is

pulled out from the concrete, and only a residual frictional resistance remains. This type of failure is referred to as a pullout failure. (Murcia-Delso 2013)

For low confinement conditions, splitting cracks propagate radially through the concrete cover and the bond fails abruptly, as shown in Figure 2.15. This type of failure is referred to as a splitting failure. Figure 2.16 shows a splitting failure obtained during a pullout test by Choi *et al.*, (2011).
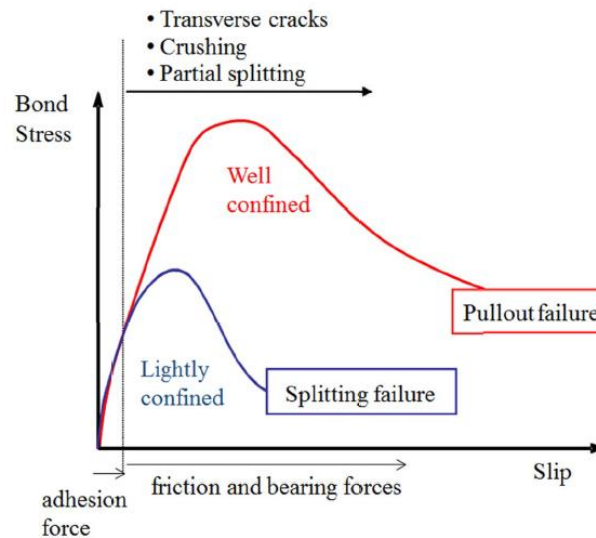
Figure 2.15: Bond stress versus slip for different confinement conditions (Choi *et al.*, 2011)
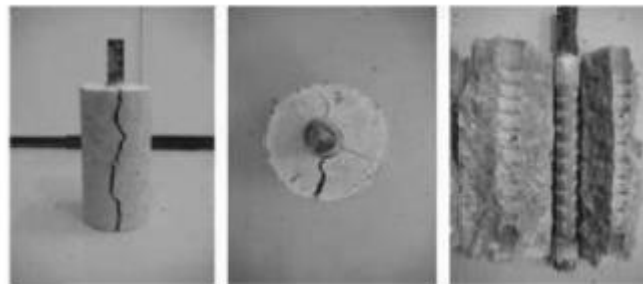
Figure 2.16: Bond failure by splitting of concrete (Choi *et al.*, 2011)

Clear cover over a reinforcing bar will be significant in bond resistance connection with splitting resistance. A thin cover can be easily split like Figure 2.17(a); a thick cover can greatly delay splitting if bars are not closely spaced laterally. If the number of bars is closely spaced with a thick cover in a beam, a splitting failure will occur as shown in Figure 2.17(b) (Gan 2000).
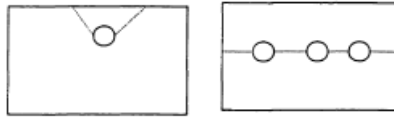
Figure 2.17: (a) Splitting mode of thin cover, (b) Splitting mode of thick cover (Gan, 2000)

Nonetheless, deformed bars change the behavior explained in the previous paragraphs and the most important parameters that are influenced are the confinement of the surrounding structure and yielding of the reinforcement (Gan 2000). Adhesion and friction still assist, but the primary resistance has been changed to mechanical interlocking for superior bond properties. With deformed bars, a pullout specimen nearly always fails by splitting; the concrete splits into two or three segments rather than failing by crushing against the lugs or by shearing on the cylindrical surface which the lugs tend to strip out (Gan 2000).

When reinforced concrete structures are modeled with finite element analysis, it is quite common to assume that the bond stress depends only on the slip. The confinement of the surrounding structure must then be evaluated before the analysis can be started, in order to choose an appropriate bond-slip correlation as input. Whether the reinforcement will yield or not must also be known in advance, for the same reason. (Lundgren 1999)

A typical response for the bond in cyclic loading is presented in a bond versus slip diagram in Figure 2.18 (Lundgren, 1999). The monotonic curve is followed for the first loading until point A in the figure. Thereafter steep unloading to point B occurs, and then an almost constant, low bond stress until the original monotonic curve is reached at point C. As for monotonic loading, the response depends on the structure, and the influencing parameters are the same. In addition, the response is also influenced by the type of cyclic loading. According to the American Concrete Institute (ACI) (1992), load cycles with reversed loading cause a greater degradation of bond strength and stiffness than the same number of load cycles with unidirectional loading. The peak value of the slip is a critical factor. Additional cycles between slip values smaller than earlier ones do not significantly influence the bond behavior, according to Eligehausen *et al*., 1982; Balazs (1992), and American Concrete Institute (ACI) (1992).
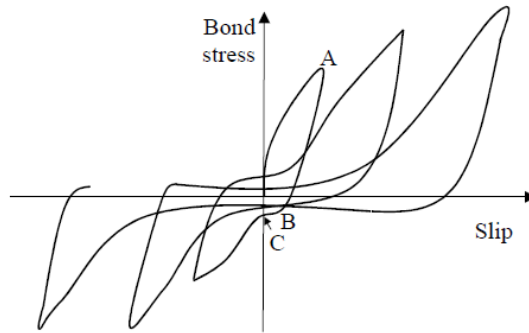
Figure 2.18: Typical bond versus slip for cyclic loading (Lundgren, 1999)

Anchoring deformed bars in concrete gives rise not only to bond stresses but also to splitting stresses. Although many experiments have been conducted to study bond stresses, splitting stresses have been less investigated. Tepfers and Olsson (1992) have done "ring tests" in which a reinforcement bar was pulled out of a concrete cylinder surrounded by a thin steel tube. By measuring the tangential strains in the steel tube, the splitting stresses could be evaluated. A few other researchers have also carried out tests to find solutions to the problems of measuring splitting stresses, for example, Malvar (1992). The effect on the bond of cyclic loading has been investigated by, among others, Eligehausen *et al.*, (1982) and Balazs and Koch (1995). However, no tests were found in the literature that show the effect of the splitting stresses measured during cyclic loading.

Therefore, steel-encased pullout tests subjected to reverse cyclic loading were carried out, such as Lundgren (1998). The results from the cyclic tests show a typical response for the bond in cyclic loading. When there was almost no bond capacity left, the measured strain in the steel tubes stabilized and remained relatively unaffected by the last load cycles (Lundgren 1999).

2.3.2 Bond-slip between concrete and reinforcing bars

Bond slip is the relative displacement between the bar and the concrete (Gan 2000). The stress transfer mechanism between reinforcing steel and surrounding concrete through bond and the resulting slip plays an important role in the hysteretic behavior of reinforced concrete structures (Ayoub and Filippou 1999).

The slips of the reinforcing bars and deterioration of the bond interfaces above the foundations and in the beam-column connections and plastic hinge regions play a crucial role in dictating the behavior of reinforced concrete frames under earthquake excitations.

These effects result in the reduction of stiffness and energy dissipation, leading to the characteristic pinched hysteretic loop (Limkatanyu and Spacone 2008).

Under the assumption of full composite action between the concrete and the steel rebars, the stiffness of RC structures is overestimated, as is the hysteretic energy dissipated during cyclic loads. Experimental tests on RC sub-assemblages have indicated large fixed-end rotations at the structural member ends. These fixed-end rotations resulted from the slippage of the rebars passing through the joints or being anchored into the footings. Under cyclic loads, the bond gradually deteriorates, and additional flexibility leads to the characteristic pinched hysteretic loops observed in several tests. The inclusion of the bond-slip effects into numerical models is a crucial step toward the development of accurate nonlinear techniques for the analysis of RC frame structures (Limkatanyu and Spacone 2008).

Most researchers believe that there are different relationships for local bond stresses versus local bond slips at different points of the interface of the steel bar and the concrete. Since the properties of the interface will not be different, this change can only come from stress effects. Some researchers believed that the relationship is a material property and, therefore, independent of location (Morita and Fujii 1982; Edwards and Yannopoulos 1978). They thought that there exists a unique bond-slip relationship that depends only on material properties and steel geometry (Giannopoulos 2006).

In Figure 2.19, the column deformations due to bar slip and the slip rotation and forces at the beam-column interface are illustrated (Eligehausen, Popov and Bertero, 1982).
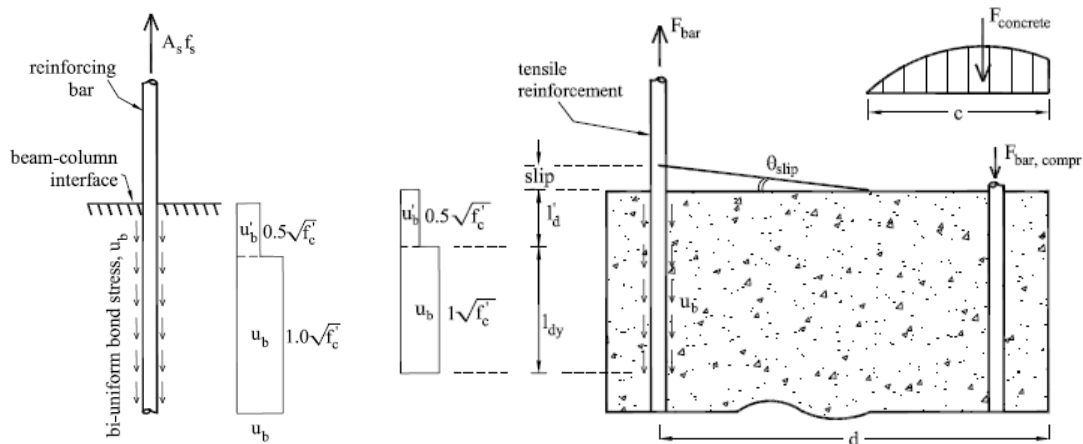
Figure 2.19: Column deformations due to bar slip (left), Illustration of slip rotation and forces at the beam-column interface (right) (Eligehausen, Popov and Bertero, 1982)

The bond-slip mechanism for bars with pullout failures under cyclic loading has been theorized by Eligehausen *et al*., (1982). Figure 2.19 shows the damage mechanisms and bond-slip behavior under cyclic loading as presented by Eligehausen *et al*., (1982). In Figure 2.20(a), it is assumed that the slip is reversed before horizontal shear cracks develop. After unloading (along path AF in the figure), the gap between the right side of the ribs and the adjacent concrete, caused by concrete crushing on the left side of the ribs, remains open with a width equal to the residual slip at point F. Only a small fraction of the slip is recovered by the elastic unloading of the concrete. Along path GH, when the slip is reversed, we see that some frictional resistance is built up. At H, the ribs are in contact again with the concrete, but a gap has opened on the left side of the ribs. Along path HI, a sharp increase in stiffness occurs because of a resumed contact with the concrete. With increasing load, the old, inclined cracks close, allowing the transfer of compressive stresses across them with no noticeable reduction in stiffness (with the monotonic loading curve recovered at this point). Inclined cracks perpendicular to the old ones appear as the stress increases in this direction. At the point I, a gap equal to the distance between points F and I has opened. When reversing the slip, the path IKL is similar to AFH, previously described. However, the bond resistance starts to increase again at L when the ribs start to press broken pieces of concrete against the previous bearing face. With further movement, the transverse cracks previously closed are opened and the cracks previously opened are closed. At M, the ribs and the concrete are in full contact and the monotonic loading curve is recovered.

If the slip reversal takes place after horizontal shear cracks have initiated, different behavior is revealed as shown in Figure 2.20(b). Along path HI, the ribs press against the concrete in between whose resistance has been lowered by the shear cracks when loading in the opposite direction. Therefore, the bond resistance is lowered compared to the monotonic curve. When reversing the slip again (along path IKLMN), the resistance is further lowered compared to that at the point I because of the additional shearing damage in the concrete.

When a large slip is imposed during the first cycle, almost all the concrete between the ribs can be sheared off and the behavior will be like the one shown in Figure 20(c). When moving the bar back (along path GH), the frictional resistance is higher than that for the previous cases, in which the slip in the first cycle is smaller, because the concrete surface

along the shear crack is rougher. When reloading in the opposite direction, the peak resistance (point I) is lowered. When reversing the slip again, the frictional resistance is lowered because the surface has been smoothened (path KL) (Murcia-Delso 2013).
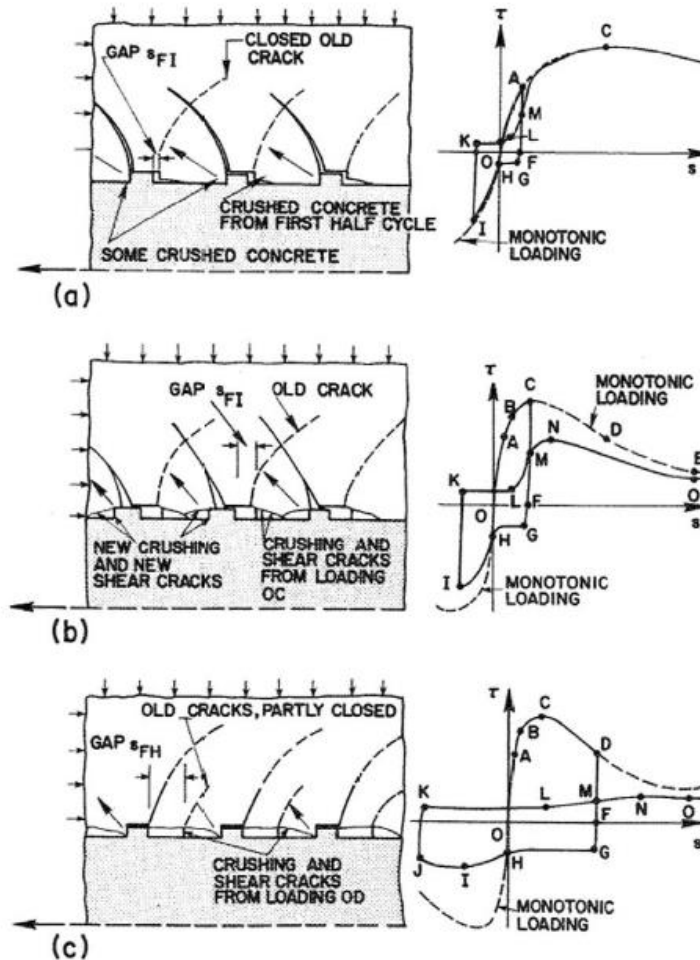
Figure 2.20: Cyclic bond-slip behavior in pullout failures (Eligehausen, Popov and Bertero, 1982)

2.4   Dowel action

The dowel action can have significant effects on the ductility of RC and as a shear transfer mechanism across cracks has long been recognized as an important component of the overall shear resistance capacity of RC beams, and it can be a significant factor if other contributions to shear transfer are relatively small (El-Ariss 2007). The analytical results generally agree more with experimental values when the dowel action is considered (He and Kwan 2001).

The dowel action of reinforcement bars is the bending of reinforcement bars at a crack plane, and usually, the dowel action is more important near peak load and at the post-peak stage (Martin 2007). The dowel force in a bar is the force resisting the transversal displacement or the slipping of two segments along a crack interface (Martin 2007). Dowel action can be comprised of bending, shear, or kinking of the bar (Martin 2007).

The bending of rebar happens at a crack plane due to the difference in direction of the principal tensile stress and direction of reinforcement (Martin 2007). The bending of the reinforcement results in the deterioration of the bond between the rebar and concrete in the vicinity of the crack leading to flaking of the concrete at the side where reinforcement is oblique to the crack plane; see Figure 2.21 (Martin 2007).
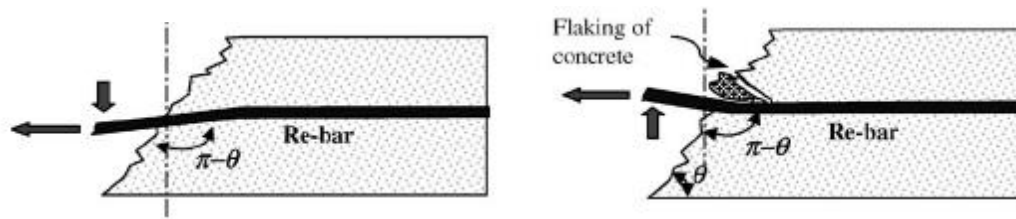
Figure 2.21: Flaking of concrete (Martin, 2007)

When plastic hinges develop in the reinforcement at both sides of the crack the kinking of the bar can occur (see Figure 2.22) (Martin 2007). This type of mechanism is possible when the members undergo very large shear displacements only; (Fédération internationale du béton 1999).

Studies revealed that the shear capacity of a dowel is affected by the compressive strength of concrete, the yielding strength of steel, the inclination angle of transverse reinforcement, and the size of the dowel bar (Ince *et al*., 2007). The shear capacity can be affected by specimen size and maximum aggregate size. It is noteworthy to mention that the shear capacity of the dowel specimen increases slightly with increasing maximum aggregate size (Ince *et al*., 2007).
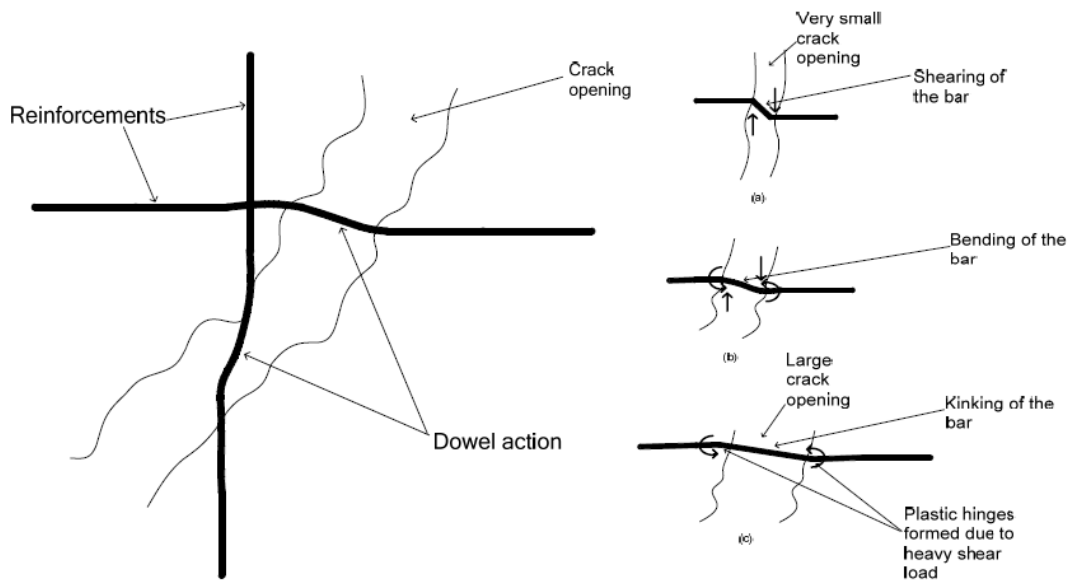
Figure 2.22: Dowel action in reinforcements at a crack opening (Martin, 2007)

In order to deal with the interaction between the reinforcement bar and the surrounding frame the "beam in elastic foundation" theory can be used (He and Kwan 2001). According to this theory, the foundation may be treated as a bed of springs so that the reaction force of the foundation at any point may be assumed to be proportional to the deflection of the beam at that point (He and Kwan 2001). This approach was first proposed in 1940 by Friberg (1940) and later referenced by several other researchers (see for instance Dei Poli *et al.*, (1992)).

If the reinforcing bar is cut at the face of the crack, the bar may be treated as a semi-infinite beam resting on an elastic foundation and subjected to concentrated dowel force (Vd) and moment (Mo) applied at its end as shown in Figure 2.23 (El-Ariss 2007).
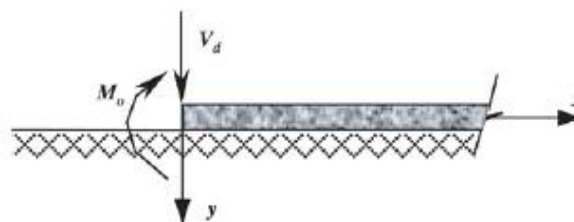
Figure 2.23: Semi-infinite beam on an elastic foundation (El-Ariss, 2007)

If we assume that an inflection point exists in the dowel at the center of the crack, the forces acting on the portion of the dowel within the crack width, z, are shown in Figure 2.24 (El-Ariss 2007).
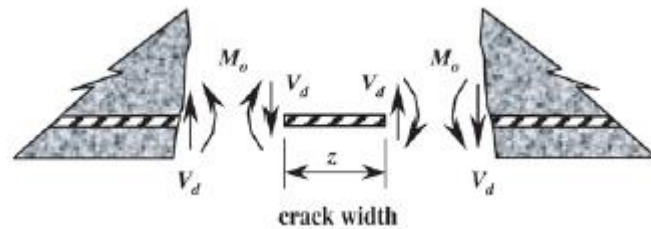
Figure 2.24: Forces acting in the dowel bar (El-Ariss, 2007)

It was found that the primary cause for the unsatisfactory performance of dowels was the excessive voids under the dowel bar, which prevented proper load transfer at the joint (Chen *et al.*, 2011). The main variables that cause the voids around dowels are the time of placement after grout mixing, the vibration time of grout, the slot width, and the maximum aggregate size (Chen *et al.*, 2011).

Dowel bars are often used to transfer shear forces at movement joints and also to create shear key connections, for example in precast concrete building (Norbert Randl, 2007). The way that a dowel cast-in on both sides under shear load functions was first, clearly and thoroughly, described by Paulay. T., Park, R. and Phillips, (1974). The effect of bending, shear resistance, and inclined tension (kinking effect) on dowels is shown in Figure 2.25. For design purposes, the bending resistance is of most importance, the inclined tension effect first builds up after considerable displacement (Norbert Randl, 2007). While the maximum bending moment occurs in each case slightly over or under the joint, the maximum shear under approximately symmetrical conditions results at the shear surface, the bending moment at this section is M=0. Failure under shear loading is, however, mostly not significant, because the concrete cannot withstand the high pressures on the walls of the hole without corresponding yielding. Failure finally occurs at a sufficiently large distance from the edge (min. 8-10 dowel diameters ds), and with a cast-in length of at least 5-6 ds through steel failure, although with increasing shear load the pressure on the hole walls rises strongly and it can happen. This spalling of the concrete further increases the inner lever arm of the load and the bar is increasingly loaded in bending. With a cast-in length of less than about 5ds, failure can occur by the concrete behind breaking out, and early concrete failure can also happen if the distance to the edge in the direction of the hole is small.

The bending moment and shear diagram of a central dowel bar obtained from the analysis as well as from the experiment in Swati Roy Maitra, K. S. Reddy, (2009), is shown in Figure 2.26.
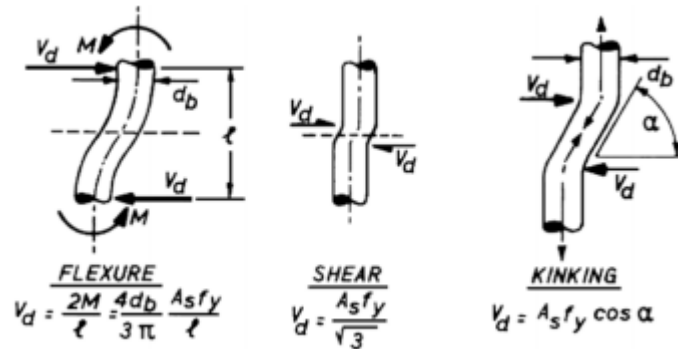
Figure 2.25: Dowel action according to (Paulay. T., Park, R. and Phillips, 1974)
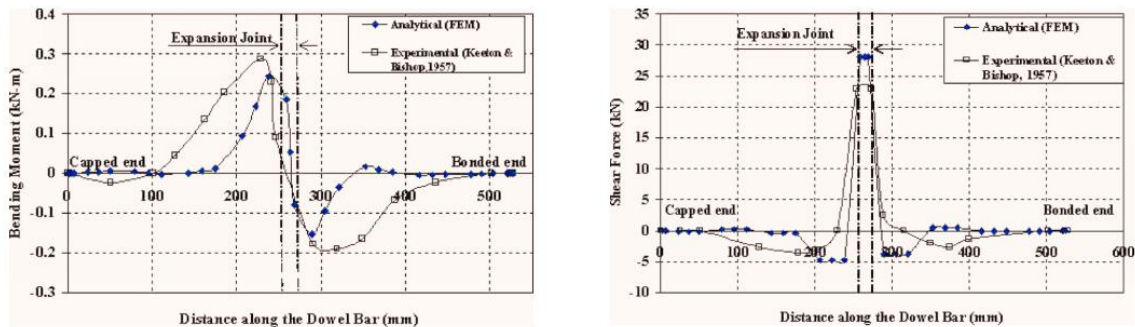
Figure 2.26: Bending moment diagram for a dowel bar (left) and shear force diagram for a dowel (right) (Swati Roy Maitra, K. S. Reddy, 2009)

The performance of epoxy dowels in tension is dependent on proper installation, sufficient embedment depth, and sufficient spacing between adjacent dowels. Installation should be in accordance with the preceding section. Spacing should be at least an embedment depth apart. It is often better as well as more economical to use bigger dowels at greater spacing than lots of small dowels at close spacing (Loring A. Wyllie, 1988). Once installation techniques are mastered, the other key element for epoxy dowels in tension is providing sufficient embedment length. Embedment depth should be sufficient to develop the strength of the dowel. A reading of current building codes for concrete construction ACI, (1983) would infer the dowel must be installed in a hole equal to a full development length. Although, tests by numerous researchers have shown that a shorter embedment length is sufficient for epoxy grouted dowels (Luke. Philip C.C; Chon, Carlos; Jirsa, 1985) . However, the embedment length should be sufficient to develop the

strength of the dowel. ACI 318-83 development lengths are normally based on 1.25 times yield of the steel, for Grade of steel 410MPa, 520 MPa (Loring A. Wyllie, 1988). For bars properly embedded to the recommended depths, ultimate bar strength in tension should be achievable. For important tension elements, such as chords of new shear walls into basement walls or other critical tension elements, it would be a prudent exercise of engineering judgment to increase these embedment depths 25 to 50% for that particular usage (Loring A. Wyllie, 1988).

Epoxy dowels resisting shear forces are possibly more prevalent than pure-tension situations. The attachment of infilled walls or new shear walls to existing concrete frames always requires a shear transfer between new and old concretes. The research has confirmed that shear transfer across an interface between new concrete and old concrete should be treated as shear friction per ACI, 1983. For seismic exposures, the existing concrete surface should be thoroughly roughened by heavy sandblasting or chipping. Dowels should be installed to provide an area of shear friction reinforcement according to ACI, (1983) and should be epoxied in holes in the existing concrete. Tests of Bass, Robert A., Corrasquillo, Ramon L., 1985 showed that roughened surfaces are most important to limit slip and dowels with full embedment are needed to maintain load after slip occurs. The experiments also illustrated several fine points of shear transfer that common sense would confirm. For example, in one specimen too much epoxy was placed in the holes and when the bars were inserted, puddles of epoxy about 100mm surrounded the dowels and this excess epoxy was not removed. This specimen, considering its variables, achieved a strength significantly below corresponding specimens with slightly different conditions. This test illustrated the need to ensure that all extra epoxy is cleaned off the interface, as the most effective region of the interface to transfer shear is close to the dowels (Loring A. Wyllie, 1988).

No tests have been conducted in that program nor reviewed in the literature for combined shear and tension loadings. Since the shear loading for concrete dowels is based on shear friction, which depends on the clamping force of the dowels across the interface, an addition of the demands for tension and shear (as shear friction reinforcement) would seem appropriate. A more favorable interaction expression should be possible for threaded rods attaching structural steel to concrete, although the author is not aware of experimental evidence to establish this relationship. (Loring A. Wyllie, 1988)

2.4.1 Dowel modeling

The action of a dowel is a very complicated mechanism. The modeling of the dowel action has not been mentioned in the literature for the finite element (FEM) analysis before 1991 (El-Ariss 2007). To analyze the details of the dowel action, the steel bars need to be individually modeled by finite elements and a very fine mesh must be used for concrete. Except for the large number of the finite elements, an individual modeling of the steel bars and concrete is not compatible with the common practice of modeling the concrete and steel together in the analysis of RC structures.

In experimental tests, the shear force transferred by the dowel action is quite difficult to measure because it is embedded with other shear transfer components (El-Ariss 2007). In fact, since the dowel action involves interaction between the reinforcement bars and the concrete near the cracks and the interaction stresses are extremely difficult to measure, many details of the dowel action have never been investigated (El-Ariss 2007). There are not adequate experimental data or theoretical analysis for the dowel action near the peak load and at the post-peak stage, where the dowels are more important.

During a seismic event, an anchor may be subjected to a combination of cyclic tension and shear forces. Furthermore, the anchor may be located in a crack that forms during the earthquake. Specifically, the direction of application of the actions (axial, shear, combined), the state of the surrounding concrete, quantity, and orientation of reinforcement in the vicinity of the anchorage, and the characteristics of the anchor, including load transfer mechanism, material properties, diameter, and embedment (R. Eligehausen, 2006).

A theoretical analysis of the resistance offered to a shearing force applied to the projecting end of a bar embedded in concrete was published by Timoshenko and Lessels in 1925. The bar was treated as a beam on an elastic foundation so that the support reaction on the embedded length was proportional to the transverse deflection. This approach was extended by others to the problem of dowel connections in concrete road slabs and the criterion of failure was assumed to be the direct compressive stress beneath the dowel bar at the face of concrete, the limit of which was considered to the cylinder strength of concrete. Marcus H., 1951, however, found that in tests of dowel bars embedded in concrete the average bearing stress at failure was often more than twice the crushing

strength, and suggested that the concrete criterion was the tensile strain causing splitting of the concrete below the dowel (E. W. Bennett, 1976).

The modeling of dowels for the purpose of this research is presented in Chapter 5.

3   SERFIN experimental test prototype model

The experimental test prototype model that was used for the calibration of the FE model was the specimen of the SERFIN (Seismic Retrofitting of RC Frames with RC Infilling) project. This was the only full-scale multi-bay, multi-storey specimen that was found in the literature since there is limitation regarding the experiments in real-scale specimens with the interaction of the surrounding members of existing structures. This prototype model reflects the real situation correctly and its results and data are very useful. In this chapter, the description of the SERFIN experimental study is presented. Also, the experimental results and data of this experiment that were used for the validation of the numerical model that was developed in DIANA FEA to study the behavior of RC infills within RC frames, are discussed. Specifically, the specimen geometry, design, and test are described. The full description, details, and results of this project can be found in Chrysostomou and Kyriakides, (2013b); Chrysostomou *et al.*, (2013), (2014a); Poljansek *et al.*, (2014).

The SERFIN project studied experimentally the effectiveness of seismic retrofitting of existing multi-storey RC frame buildings by the conversion of selected bays into new RC infilled walls. The experimental study was under the SERIES (Seismic Engineering Research Infrastructures of European Synergies) European 7th framework program, and within this program the project SERFIN was completed. The test took place at the European Laboratory of Structural Assessment (ELSA) of the Joint Research Centre (JRC) in Ispra (Italy). The subject of the project was the conversion of selected bays into new infilled RC walls for retrofitting of multi-storey, multi-bay RC frame buildings. This experiment aimed to study the efficiency of the retrofitting method and to examine the amount of web reinforcement in the walls and the connection details between the wall and the bounding frame. The main parameters that were examined in this experiment were the connection between the RC infill and the surrounding RC frame and the percentage of the reinforcement in the RC infill. The effect of these parameters was studied during the experiment, by using different connection details and reinforcement percentages for the two infilled frames.

3.1 Specimen geometry

The prototype building structure that was tested was a full-scale four-storey model consisted of two four-storey frames with RC infilling of the exterior frames only (Figures 3.1 and 3.2). The exterior frames were 12m tall and consisted of three-bays 8.5m long spaced at 6 meters as it is presented in Figure 3.1. The two exterior frames linked through 15cm slabs and 4 transverse beams (65x35cm). The infill walls were in the central bay of the specimen and they had the same thickness of 25cm with the columns and beams framing them. All the columns of the specimen had the same cross-section, 40cm in the longitudinal direction by 25cm in the transverse direction. The specimen geometry is illustrated in Figure 3.1.
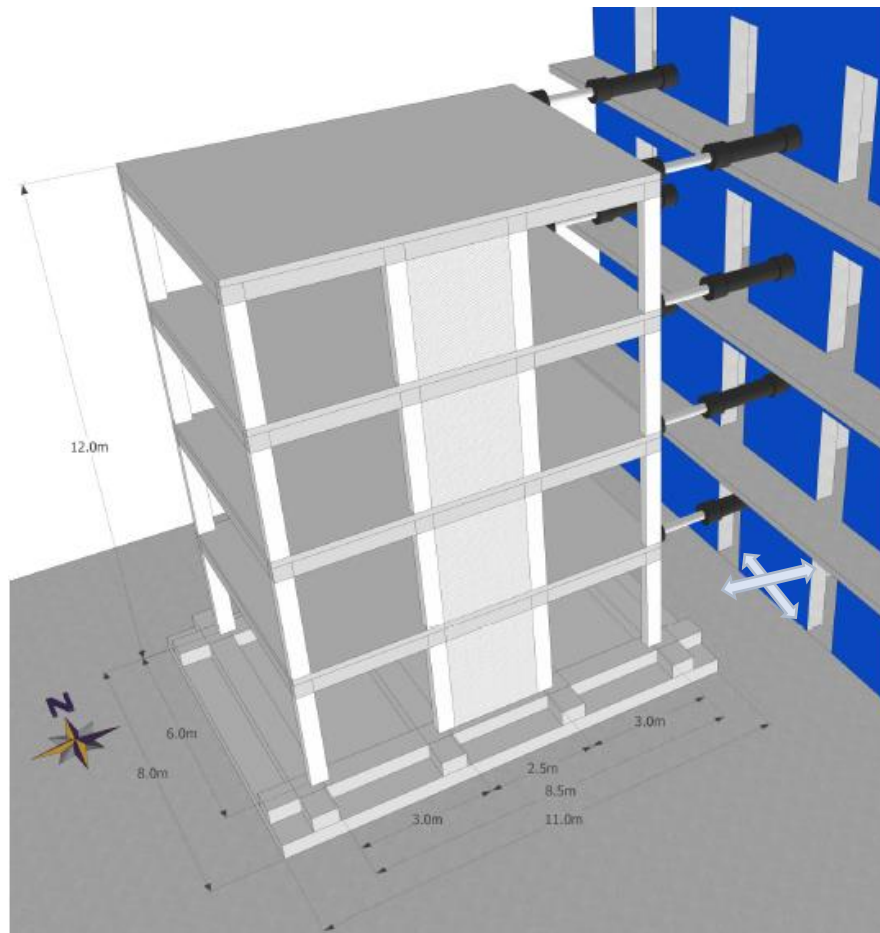
Figure 3.1: Geometry and dimensions of SERFIN specimen with an indication of the cardinal directions. The south frame with infill walls is visible in front. (Poljansek *et al.*, 2014)

3.2 Specimen design

The SERFIN structure was designed to represent a typical building in the late 70s and beginning of the 80s in Cyprus. Building structures at that time were designed for gravity loads only since there were no provisions for earthquake loading. There was no specific design standard in Cyprus and the authorities were accepting any standard that was acceptable in other countries. The mock-up was designed in such a way that all reinforcement details conformed to CP110:1972 and BS8110:1983.

The material properties that were used in the mock-up were constrained by the availability of materials in the Italian and European market. Concrete C20/25 was used for both the frame and the walls, with a unit weight of 25 kN/m³ and a modulus of elasticity E=30 GPa. The characteristic yield strength of the deformed steel reinforcement was equal to 400 MPa and it was used for all the members of the RC frame and the slab. For the RC infill and the dowels, steel reinforcement equal to 450 MPa was used. The 400 MPa characteristic yield strength steel represents the one used in Cyprus construction practice at that time, while the 450 MPa was the closest available in the Italian market to substitute for the 500 MPa steel that would be used today in the walls for retrofitting.

The self-weight of the structure was calculated using the unit weight of concrete. The imposed dead load was 3kN/m² and the live load was 1.5kN/m². Water was added to simulate the loads in the test as it is shown in Figure 3.2 and because of the slow nature of the PsD (pseudo-dynamic) method that was applied for the test, the water did not show any dynamic effects during the tests.

Figure 3.2: SERFIN specimen (Poljansek *et al.*, 2014)

The reinforcement details of the beams and the columns are displayed in Table 3.1. The columns had longitudinal reinforcement 4Y20 ribbed bars, one in each corner. The bars were spliced right above the footing and then above each slab with 55cm length (see Figure 3.3). This lap-splice was designed only for compression and not for tension since the specimen was designed for gravity loads only. Stirrups Y8/200 were evenly spaced throughout the height of each column starting at 50 mm from the top of the slab.

The longitudinal beams had 4Y12 longitudinal reinforcement at the top and the bottom and Y8/200 stirrups were evenly spaced throughout the length of each beam starting at 50 mm from the edge of the column (Table 3.1). The transversal beams had 2Y20 at the top and 5Y20 at the bottom (see Table 3.1). Stirrups Y10/150 were evenly spaced throughout the length of the beam starting at 50 mm from the edge of the column.

Table 3.1: Reinforcement details for the frame members (Poljansek *et al.*, 2014)
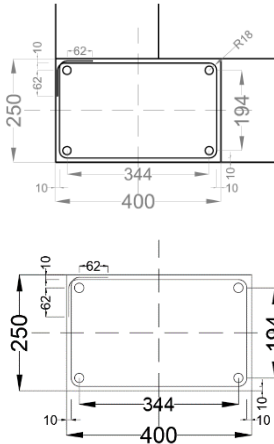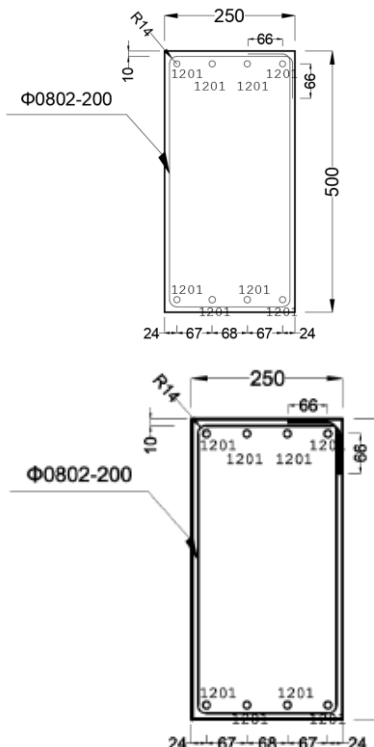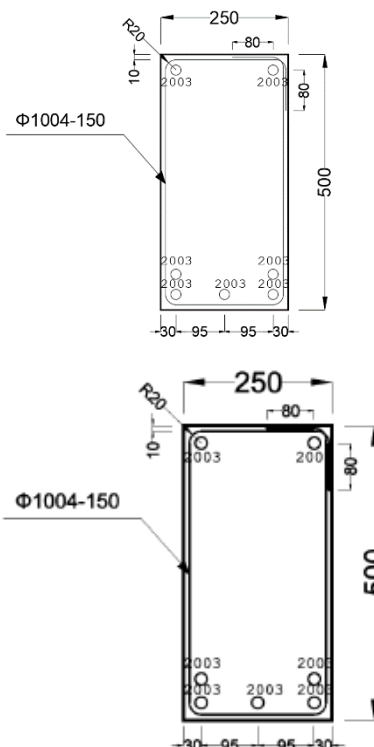
Columns reinforcement detail	Longitudinal beams reinforcement detail	Transversal beams reinforcement detail

Figure 3.3: Lap-splice of the columns (Poljansek *et al.*, 2014; Kyriakides *et al.*, 2015, Poljansek *et al.*, 2014)

For the FE model, only the columns and the longitudinal beams were simulated since only the South frame of SERFIN building was simulated. The transversal beams and the slabs

that linked the two exterior frames were considered in the FE model by adding their load to the designed frame.

3.2.1 RC infill walls and dowels design

In order to facilitate the study of the effect of as many parameters as possible, the north and south walls of the specimen were reinforced with different amounts and arrangements of reinforcements with the north wall being the stronger of the two. In this section, mainly the details and results of the south wall are presented, which was the one that was simulated in the FE model.

In Table 3.2, the amount of reinforcements for the south frame is illustrated. The details about the reinforcements of the north wall can be found in Poljansek *et al.*, (2014). It is important to mention that two distinct connection details were applied in the SERFIN experiment. An elaborate and varying system of dowels and starter bars was used to join the new walls with the existing frame. For the south wall, these details are shown in Figures 3.4 and 3.5.

In the first detail that was used to connect the new infill wall to the bounding frame, two reinforcement bars were used: the starter bars and the short dowels (Figure 3.4). The starter bars were used to connect the web bars of the wall to the surrounding frame through lap splicing with the same diameter starter bars. These starter bars were epoxy grouted into the frame members. The short dowels served to transfer shear at the interface between the wall and the frame member. In the second detail, only longer bars were used to act both as dowels and consequently to transfer shear to the interface, as well as for anchorage of the web panel to the surrounding frame (Figure 3.5). The dowels are considered as lap-spliced with the nearest web bars. In all cases, the dowels were positioned along the centerline of the elements at 125 mm from the face of the wall.

Table 3.2: Reinforcements for the south wall (Poljansek *et al.*, 2014)

South Wall									
		Embedment of web starter bars (mm)		Dowels					
					Embedment (mm)				
					Bottom & East		Top & West		
Storey	Web bars	In wall	In frame	Φ (mm)	In wall	In frame	In wall	In frame
1	Φ10/200	500	170	Φ20	160	160	500	160
2	Φ8/200	400	120	Φ18	145	145	400	145
3	Φ8/200			Φ16	400	130	400	130
4	Φ8/200			Φ16	400	130	400	130

Figure 3.4: First connection detail of the new infill wall to the bounding frame with starter bars and short dowels (Dowels, dowels and starter bars, dowels and starter bars, dowels starter bars and web reinforcement)

Figure 3.5: Second connection detail of the new infill wall to the bounding frame with only longer dowels (Dowels, dowels, dowels, and web reinforcement)

The first detail was used to connect the wall at the bottom beam, the second storey bottom beam, the left column at the ground floor, and the right column at the first storey (see Figure 3.6). In Figure 3.6, the short dowels that were used to transfer the shear at the interface and the starter bars that were used to connect the web bars of the wall to the surrounding frame through lap splicing are highlighted in yellow.

The second detail was used to connect the wall at the top beam of all the storeys, and the east and west columns of the ground and first storeys of the south frame, respectively (see Figure 3.6). In the third and fourth storey only the second detail was employed, while for the fourth storey only two dowels per wall interface were applied, to provide safety against failure of the wall out of plane. The second detail with the long dowels is highlighted in Figure 3.6 in grey.
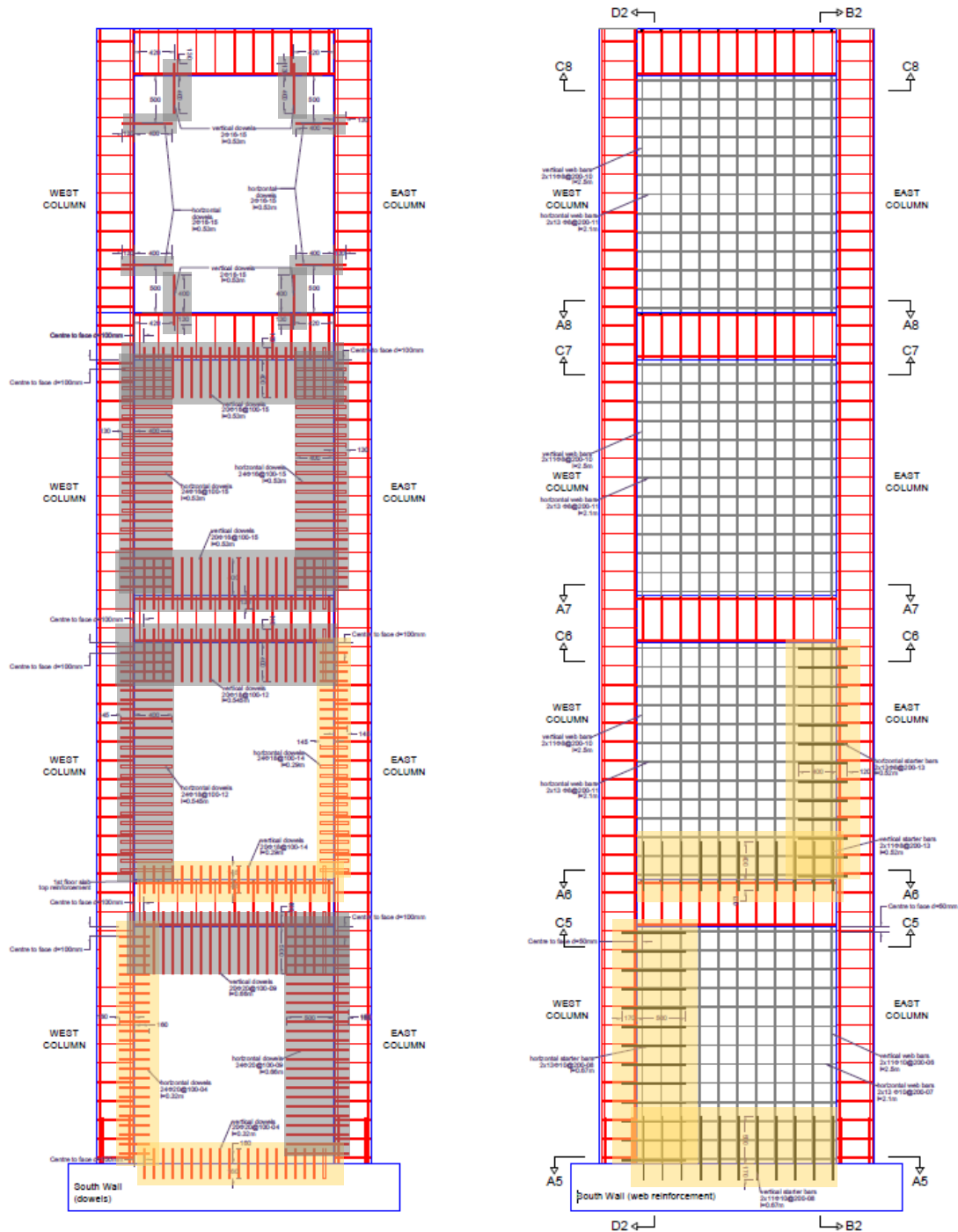
Figure 3.6: First and second connection details of the new infill south wall to the bounding frame

Additional retrofit was applied to reinforce the edges of the wall on the lap length at the ground floor based on the performance of the ground floor RC infill walls during the experiments. So, three-sided carbon fiber reinforced polymer (CFRP) jackets were applied to reinforce the edges of the wall at the ground floor with a height of 0.6m, since the lapping stop at 0.55m from the base of the column as it is shown in Figure 3.7. This

retrofit was crucial and constituted part of the proposed retrofit strategy. A lap splice failure would have taken place during the test, which could be detrimental to the whole experiment. Therefore, in order to safeguard against this type of failure and allow the experiment to be performed successfully, it was decided to reinforce the edges of the wall at the ground floor.

Figure 3.7: First and second connection details of the new infill south wall to the bounding frame

3.3   Specimen instrumentation

The SERFIN test structure was instrumented with 108 potentiometric displacement transducers, 22 inclinometers and 8 Heidenhain linear encoders. The description of the instrumentation is presented in this section, while the full description of the instrumentation can be found in Poljansek *et al.*, (2014).

In Figure 3.8, the displacement transducers are illustrated in yellow, red, brown, and orange for the south frame and they were installed to measure local displacements in critical areas. They were placed to monitor slip and crack opening between all walls and their bounding beams and columns, the displacements between the ground floor walls and the foundation beams, and the shear deformations of the two ground floor walls. Displacement transducers were also installed to measure the vertical elongation of the bounding columns on all storeys.

Inclinometers are shown in Figure 3.8, in blue on the frame. They were used to measure the rotation of beams and columns on the first storey. They were placed at the center joints and on beams and columns 30cm away from the joints. Inclinometers were also placed on selected columns 30cm above the foundation beam.

Heidenhain linear encoders were installed to measure the horizontal displacement of the two frames on each of the four storeys in the direction of testing. They served as reference displacement instruments for control in all tests.
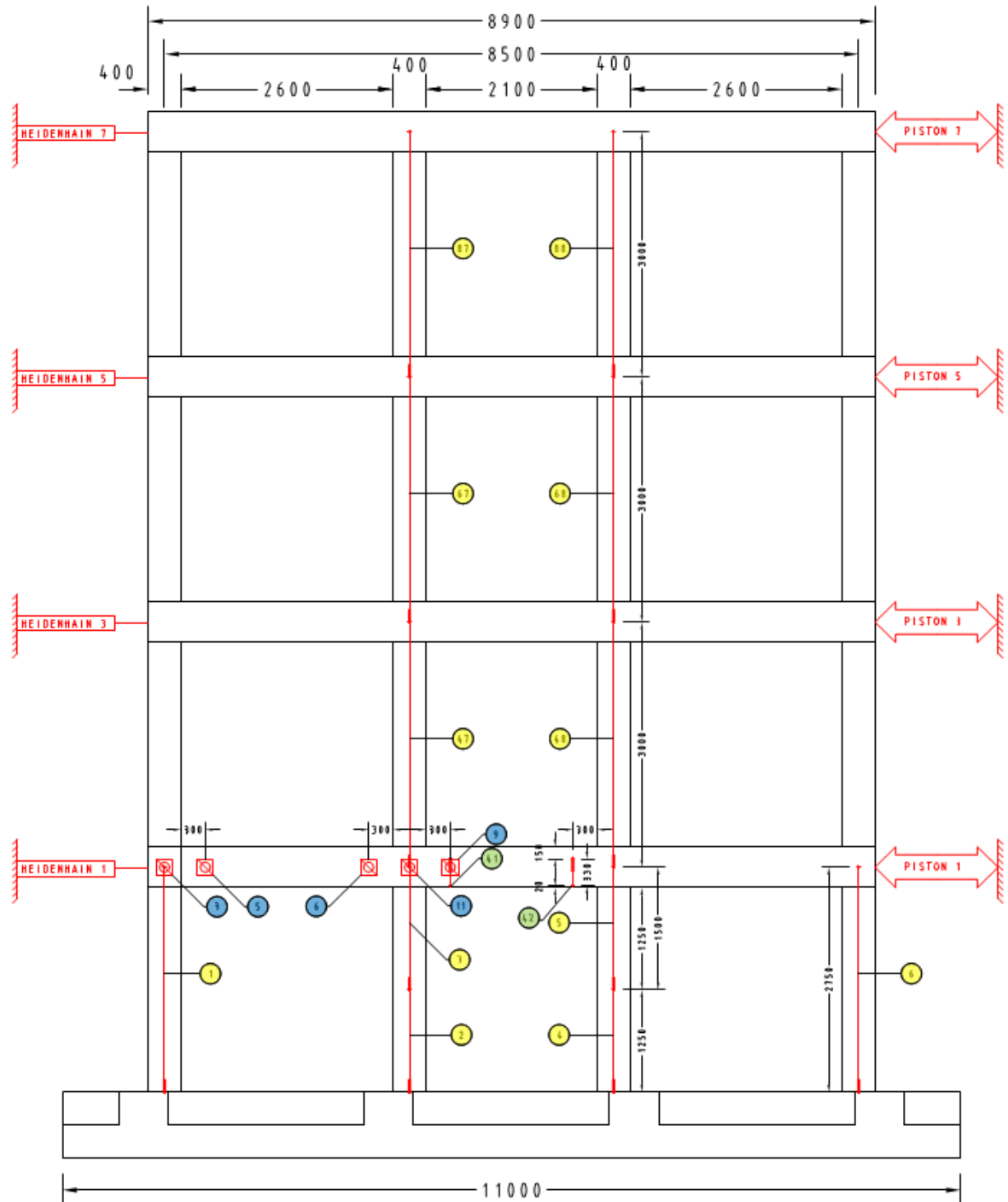
Figure 3.8: Instrumentation of the south wall outside (Poljansek *et al.*, 2014)
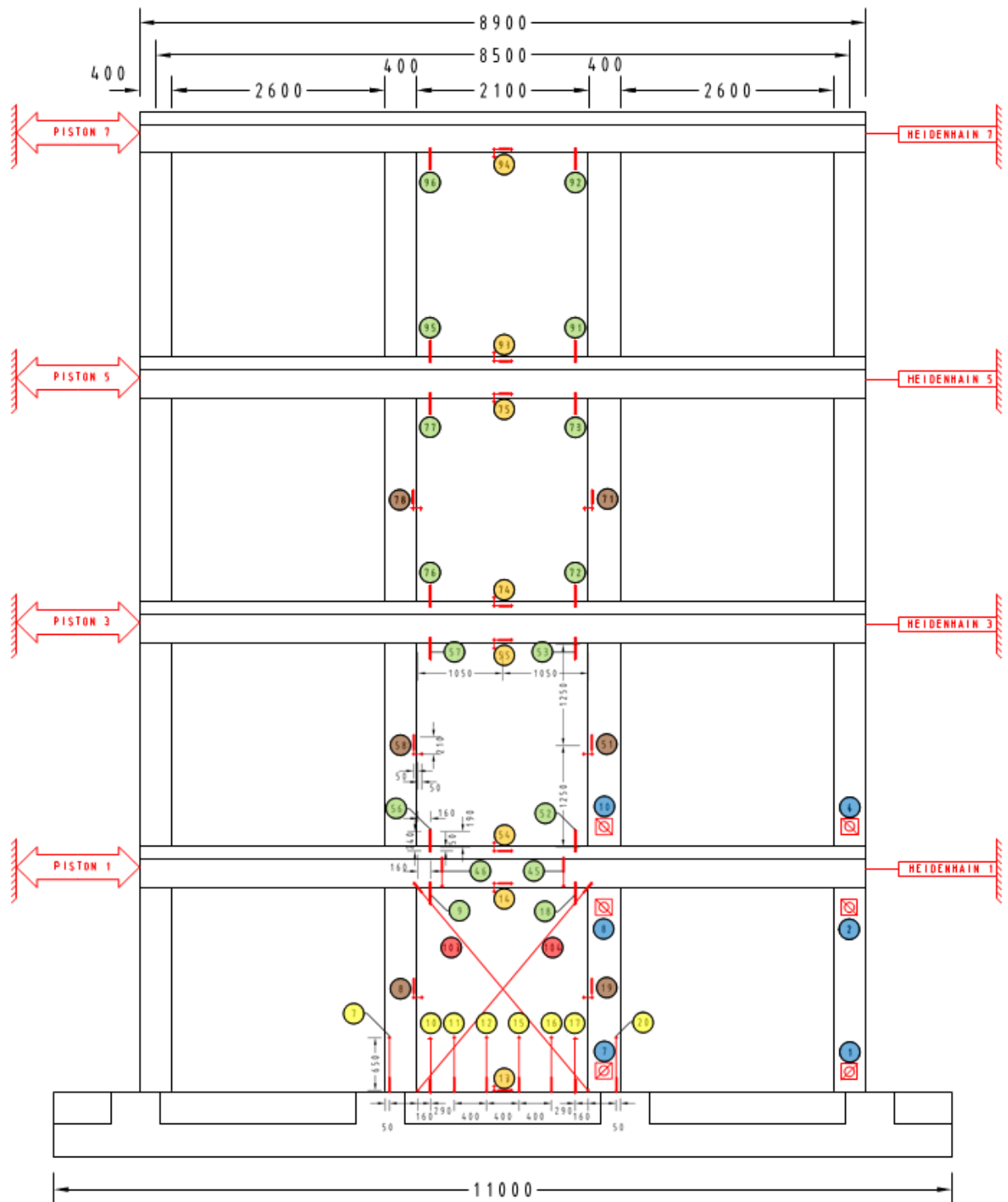
Figure 3.9: Instrumentation of the south wall inside (Poljansek *et al.*, 2014)

3.4 Specimen tests

The building specimen was tested with the pseudo-dynamic (PsD) method. Within the testing campaign, two PsD tests and one cyclic test were run. The accelerogram was

scaled to a maximum acceleration of 0.10g-first PhD test and 0.25g-second PsD test. For the final cyclic test, a history of displacements was imposed on the fourth storey, while maintaining a triangular distribution of loads along the height of the north frame and zero rotation on each of the four storeys.

In each storey, a pair of servo-hydraulic actuators applied horizontal loads as derived from the PsD test method. To connect an actuator to the structure, a system of steel beams was installed. One beam was passing above and the other under the slab (see Figure 3.2). The beams were then clamped together with prestressed bars. On the actuator side (east side) they were welded together to a sheen plate to which the actuators were bolted. Spacers were designed to allow the bottom beam to pass without leaning against the beams of the structure. All actuator generated load was thus transmitted to the structure by friction minimizing stress concentrations. This ensured the smooth transmission of forces also when the direction of loading was changed.

The Herzeg Novi (Montenegro 1979) accelerogram was scaled to 0.1g and 0.25g in order to execute the specimen tests (Figure 3.10). First, the 0.1g test was performed to induce minimum damage on the structure. Then, the 0.25g test performed to study the performance of the specimen at its ultimate capacity of the specimen up to a 20% drop of peak strength of the structure to establish the strength envelope of the specimen.

Herzeg Novi accelerogram scaled to 0.1g

Herzeg Novi accelerogtam scaled to 0.25g
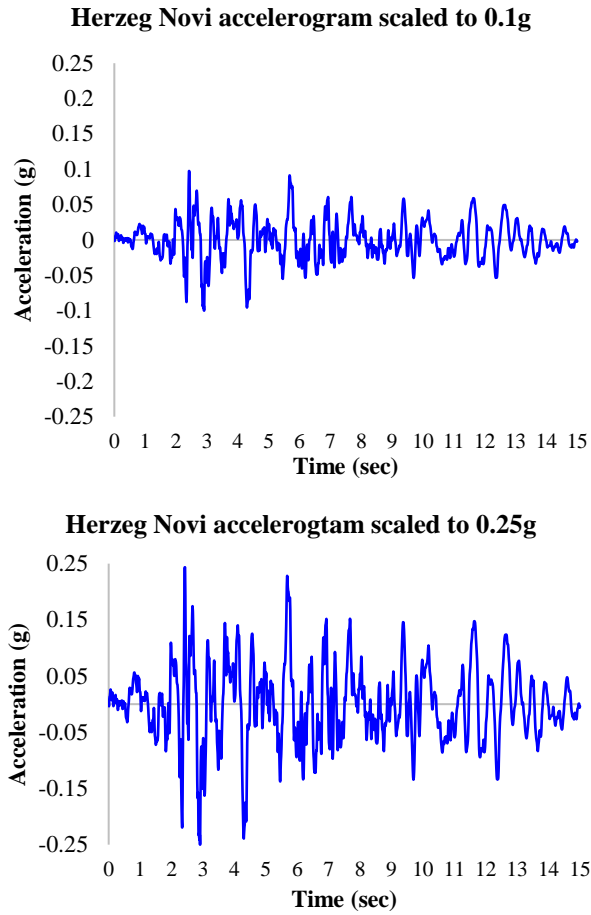
Figure 3.10: Herzeg Novi (Montenegro 1979) accelerograms scaled to 0.1g and 0.25g.

The results of 0.25g acceleration test were used for the validation of the numerical model and mainly these results are presented and discussed in sections 3.5 and 3.6

3.5 Specimen global results

A brief description of the first 0.1g acceleration test results and a more detailed description of the second 0.25g acceleration test results are discussed in this section. The full description of the results of all the tests of this project is given in Chrysostomou and Kyriakides, (2013b), Chrysostomou *et al.*, 2013, 2014a and, Poljansek *et al.*, (2014).

As it was previously mentioned, the 0.1g test was designed to induce minimum damage on the structure. After a visual inspection of the specimen, no visible cracks on the columns or walls could be noticed. Some hairline cracks that appeared on the surface of the wall at maximum displacement closed at the end of the experiment. Based on the

results of the test and the observed damage, it can be considered that both walls reached their cracking moment.

After the 0.25g acceleration test, the larger level of damage was for the south frame consisting of a crack that opened at the ground beam of the foundation at the base of the wall on both sides (Figure 3.11) and by a lap-splice failure due to tensile forces that appeared in the outer column on the east side of the south frame (Figure 3.12). The presence of the carbon fiber reinforced polymer (CFRP) on the bounding columns of the wall prevented a similar failure, thus allowing the completion of the experiment. Moreover, there was a failure of the cover on the first-storey column due to movement of the lap joint (Figure 3.12). In addition, some hairline cracks were developed in the wall (Figure 3.12). The places where these damages occurred are displayed in Figure 3.13. These were the main visual indications from the second test.
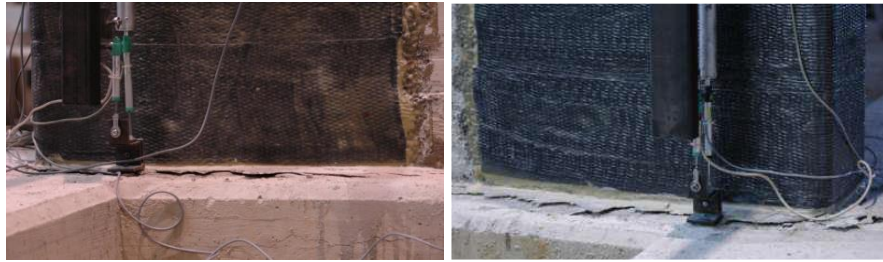
Figure 3.11: Crack that opened on the ground beam of the foundation on the base of the south wall in both sides (Poljansek *et al.*, 2014)

Figure 3.12: Lap-splice failure due to tensile forces appeared in the outer column on the east side of the south frame (left picture), lap-splice failure due to tensile forces appeared in the outer column on the west side of the south frame (middle picture) and hairline cracks that developed in the south wall (right picture) (Poljansek *et al.*, 2014)
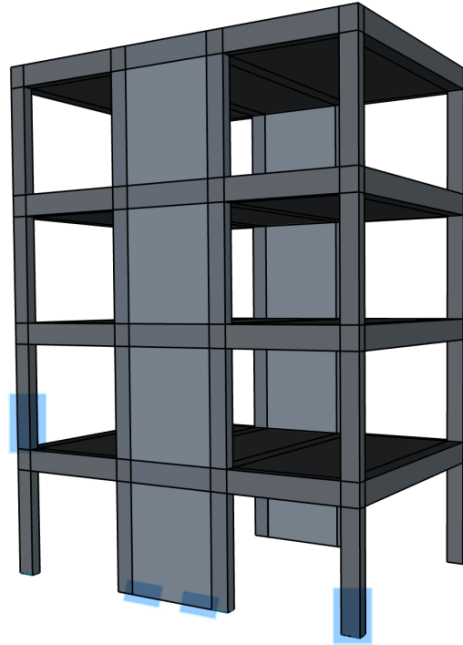
Figure 3.13: Places of failures shown in Figures 3.11 and 3.12

The response history of the base-shear force and the displacements of each storey of the specimen for the 0.25g acceleration test are illustrated in Figures 3.14 and 3.15, respectively. In Figure 3.16 the base shear force versus the top storey displacement for the south wall is presented. In Figure 3.16 it can be observed that the hysteresis loops are stable and provide energy dissipation. These results are compared with the DIANA FEA numerical model results in Chapter 5.
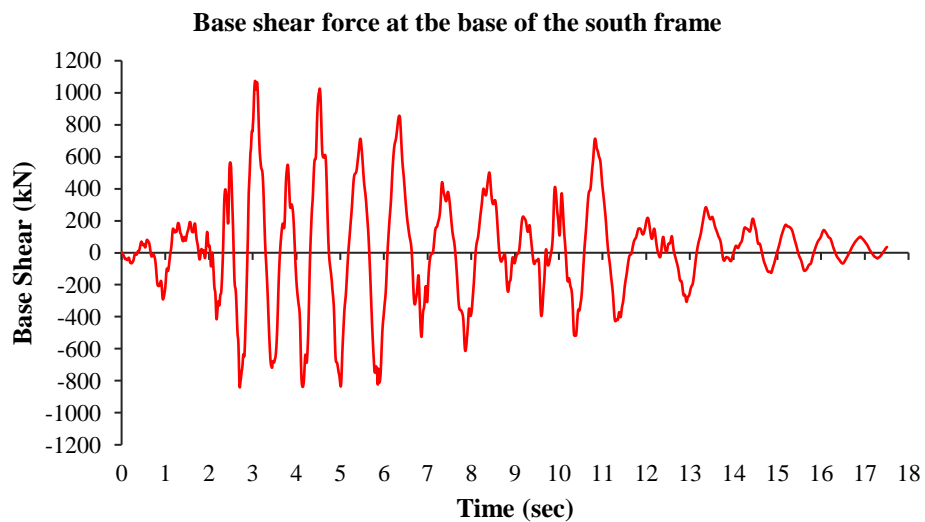
Figure 3.14: Base-shear force of the south wall of the specimen through the time (Poljansek *et al.*, 2014)
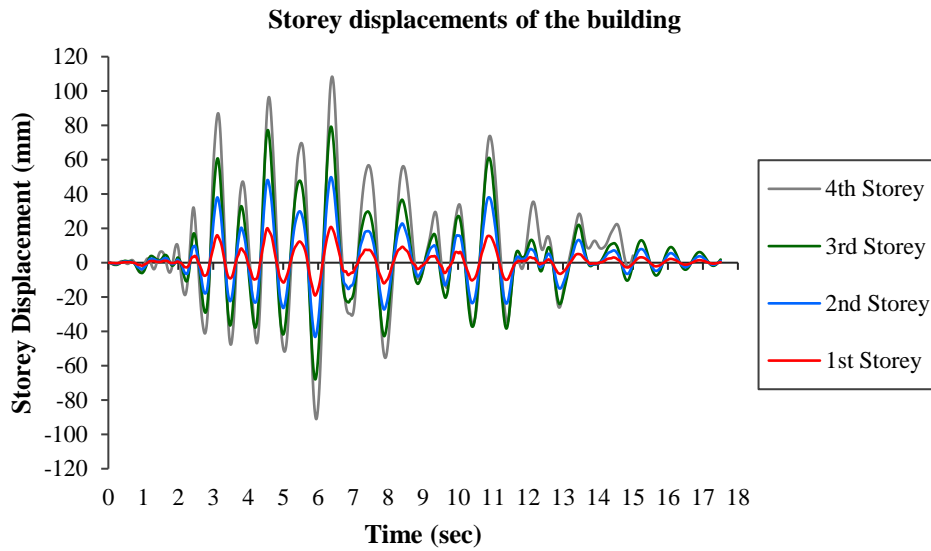
Figure 3.15: Storey displacements of the south wall of the specimen through the time (Poljansek *et al.*, 2014)
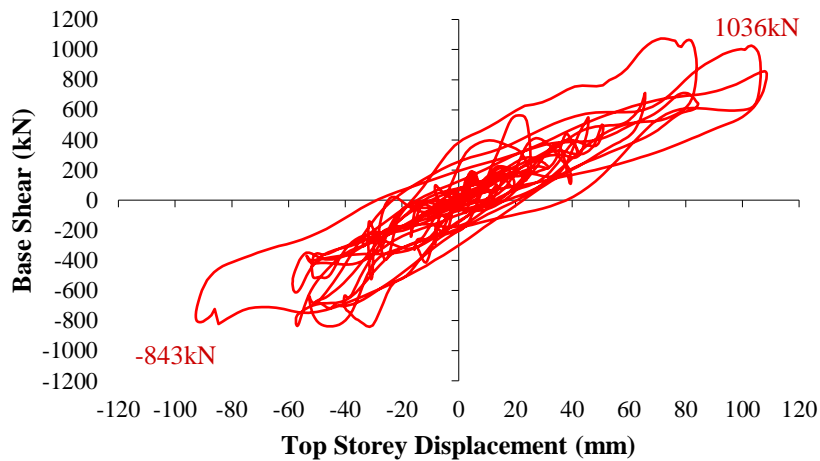
Figure 3.16: Base shear force versus top storey displacement of the south wall of the specimen (Poljansek *et al.*, 2014)

As shown in Figure 3.15, the maximum top storey displacement was 109 mm and the one in the opposite direction was -93 mm. In Figures 3.14 and 3.16 it is illustrated that the maximum base shear in the positive direction (when the specimen was moving in the east-direction, that is towards the reaction wall) was 1036 kN for the south frame, while a negative base shear of -843 kN was recorded for the south frame in the negative direction (specimen was moving towards the west, that is away from the reaction wall).

The general behavior of the specimen during the two PsD tests showed that its performance was in accordance with the damage expected from the retrofit design corresponding to a life-safety limit-state for the 0.25g earthquake (475 years return period). The structure managed to sustain an earthquake of 0.25g without significant damage. Although some column lap-splices failed with concrete spalling, the structure continued to carry load. Moreover, some vertical cracks appeared in the beams to both the exterior and the bounding columns close to the beam/column interface. Also, in nearly all the corner columns and storeys, a horizontal crack appeared at a height of 0.55 m, corresponding to the limit of the lap-splice; in some cases, spalling of the concrete cover was observed (see Figure 3.12). It is noteworthy to mention that the three-sided CFRPs protected the wall bounding columns on the first storey and prevented lap-splice failure. The horizontal crack that appeared on the ground-beam of the walls was the main cause for the loss of strength of the frame. However, no severe damage was observed, even though there were no ductile connections in the structure (Figure 2.11). There was no visible movement on the interface between the wall and the bounding frame (Chrysostomou and Kyriakides, 2013b; Poljansek *et al.*, 2014). Overall, the behavior of the wall was mainly flexural, although on the south-frame wall some hairline diagonal cracks appeared.

From the experimental outcomes that were discussed in this section, it can be concluded that this is a viable method for retrofitting, and it can be used to strengthen existing ductility and strength deficient structures (Chrysostomou *et al.*, 2014a, 2014b; Kyriakides Nicholas, Kotronis Panagiotis, Georgiou Elpida, 2014).

3.6 Specimen local results

Invaluable results have been obtained for the local behavior of the RC infilled frame by monitoring the local behavior of the walls and the bounding beams and columns. In this section, some local results from the second 0.25g acceleration test are presented and discussed. Full description and further discussion of the specimen local results can be found in Chrysostomou and Kyriakides, (2013b) and Poljansek *et al.*, (2014).

Figure 3.17 shows the strains of the ground floor columns of the south frame. On examining Figure 3.17, it can be observed that, as expected, the columns next to the wall (channel 2 & 3 and 4 & 5) had larger strains than the outer ones. This changed at about

5.95 seconds when the strain in the east column (channel 6) increased suddenly to 0.0035mm/mm, and it continued to be larger than the east bounding-column of the south wall (channel 4 & 5), in most of the cases and remained in tension for the rest of the experiment. This was associated with the sudden failure of the lap-splice of this column, and the formation of a crack which increased the recorded displacement, which resulted in a permanent strain of 0.00055mm/mm or 1.51mm, which is noticeable in Figure 3.17. Therefore, although the graph shows an increase in the strain of the outer column, this is not true since it is due to the formation of the crack. (Chrysostomou and Kyriakides, 2013b)
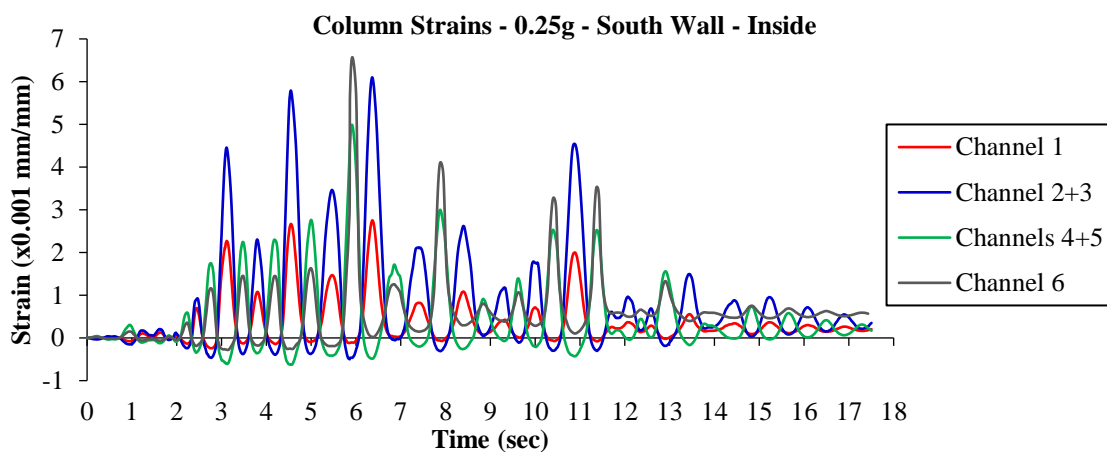
Figure 3.17: Strain distribution in ground-floor columns of the south frame (Poljansek *et al.*, 2014)

Figure 3.18 shows the distribution of strain along the base of the south wall including the bounding columns. The strains were monitored with 8 transducers covering the width of the wall horizontally (2.8m of a total for 2.9m since the first and the last were positioned at 50mm from the edge of the wall-column) and extending 650mm in the vertical direction as it is shown in Figures 3.8 and 3.9. This height was selected to be longer than the endpoint of the lap-splices of both the column reinforcement (550mm) and that of the wall web-reinforcement (600mm), in order to be able to catch any crack that would possibly be formed at that level. The lines plotted correspond to the points shown in Table 3.3. It should be noted that the lines plotted for the maximum compressive strain on the west edge and for the maximum tensile strain on the east edge coincide; therefore, only three lines appear in Figure 3.18.
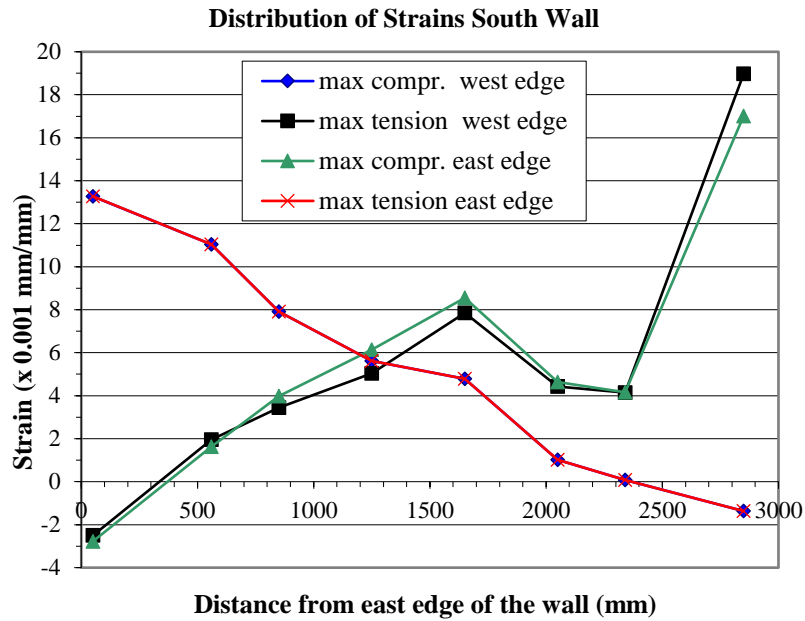
Figure 3.18: Strain distribution on the base of the south wall (Chrysostomou *et al.*, 2014b)

Table 3.3: Maximum tensile and compressive strains in the south Wall (Chrysostomou *et al.*, 2014b)

	Time(s)	South wall (x10^{-3})
Max compression west edge	5.9	-1.4
Max tension west edge	6.4	19.0
Max compression east edge	4.6	-2.8
Max tension east edge	5.9	13.3

Examination of Figure 3.18 indicates that distribution of strains is more or less linear, except for the tension on the west side of the wall. This can be attributed to the crack that formed in the ground beam on that location, on which the transducers were anchored (Figure 3.11). While this did not have any effect on the measurements in the compression phase, the recorded measurements in the tension phase were affected (smaller measurements) due to the opening of the crack.

The overall maximum compressive strain for the south wall was 0.0028 on the East edge, which is at about 80% of the ultimate concrete compressive strain of 0.0035. The overall maximum tensile strain was about 0.019 on the west side and 0.013 on the east side for the south wall, which is well beyond the yield strain of 0.0023. The location of the neutral axis was about 400mm from the two edges of both walls (total length of wall including the two bounding columns is 2900mm). This positions the neutral axis at the interface between the bounding column and the wall (width of columns is 400mm). This is the limit specified by EC8-1 beyond which additional confinement reinforcement is required. For this experiment, it seems that the provision of the CFRP at the edges of the wall provided the necessary confinement that prevented the lap-splice failure and at the same time allowed the walls to sustain loads close to its ultimate capacity.

Figures 3.19 and 3.20 show the strain distribution along the bounding columns of the south wall. Both in the east and west side, the strains in the columns of the ground floor (Channel 2+3 for the west side and Channel 4+5 for the east side) are considerably larger compared to those of the 1st storey, while the ones for the 2nd and 3rd storeys are negligible. It should be noted, since these strains are averaged for the total length of the column, much smaller values are obtained compared to the ones shown in Figures 3.19 and 3.20.

Strain distribution South Wall Columns (west side)
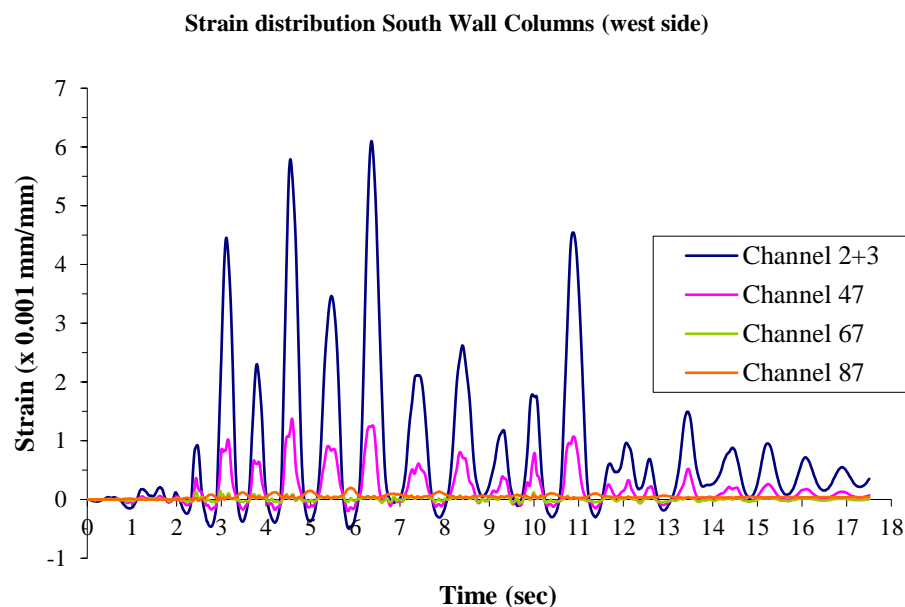
Figure 3.19: Strain distribution along the west side bounding-columns of the south wall (Chrysostomou *et al.*, 2014b)

Strain distribution South Wall Columns (east side)
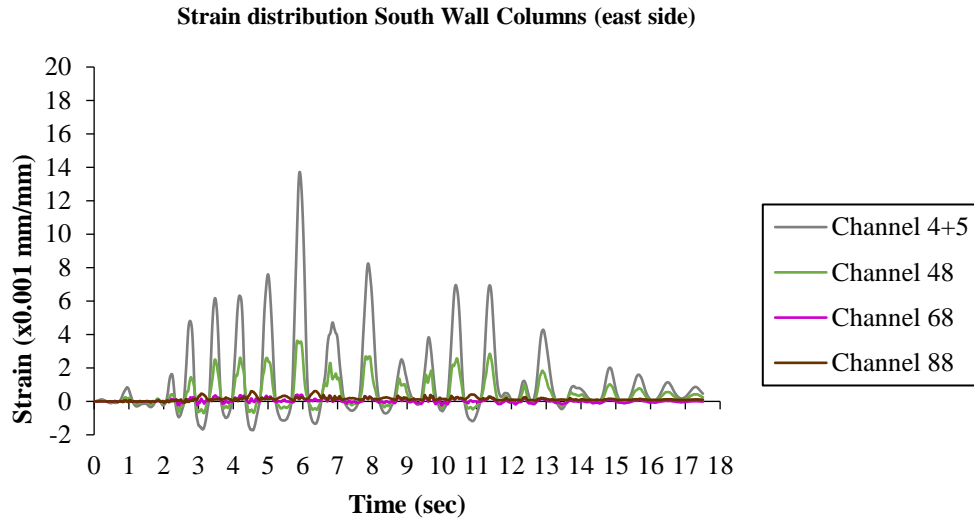
Figure 3.20: Strain distribution along the west side bounding-columns of the south wall (Chrysostomou *et al.*, 2014b)

Figure 3.21 shows the slip displacement between the wall and the bounding beam of the ground floor, for the south wall. The maximum displacements are of the order of 0.8mm for the south wall. The displacements are larger on the interface between the wall and the ground beam in comparison with the interfaces of the upper levels for the whole duration of the test.

Slip displacement of ground beam and GF top beam - S Wall
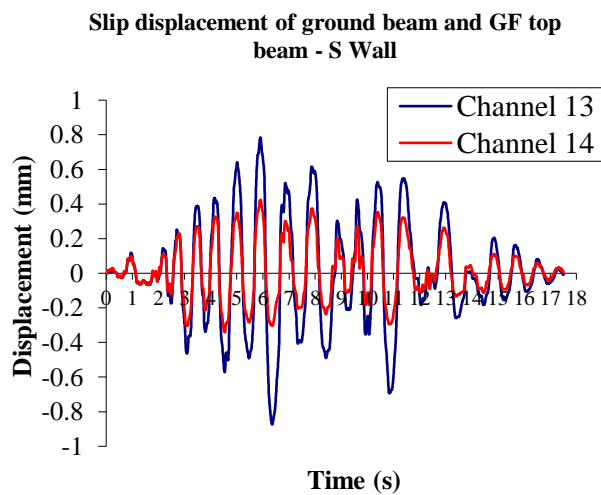
Figure 3.21: Slip displacement on the ground beam and ground floor top beam for the south wall (Chrysostomou *et al.*, 2014b)

The global and local results of the SERFIN experiment that were presented in this Chapter are compared with the numerical results in Chapter 5.

4 Numerical simulation

In order to draw general conclusions about the seismic retrofitting of RC frames with RC infill walls, numerical experiments and parametric studies were performed through the simulation of SERFIN full-scale PsD tested specimen, which correctly reflects the actual behavior. The DIANA FEA tool was used to generate the numerical model and to simulate the SERFIN experimental results. Specifically, the SERFIN experiment was simulated by a FE model and the experimental results were validated considering the hysteretic action of materials to capture and evaluate the performance of RC infills. In this way, with the validated FE model, the numerical experiments and the parametric studies were generated and a reliable investigation of the proposed system that would complement the experimental results could be performed. More specifically, the contribution of dowels, which was the main aim of this research, was parametrically studied.

In this Chapter, the FE model of the south frame of the SERFIN experiment that was simulated with the same geometry of SERFIN specimen and the calibration of the model are described and presented. Specifically, the FE model's initial conditions and assumptions, the elements, the mesh and material constitutive laws, the loads that were applied to the model and the analysis procedure are presented. Finally, the comparison of the numerical global and local results to the experimental ones, (FE model calibration) are described and displayed in Chapter 5. The capabilities of the FE model that simulated the experimental nonlinear cyclic behavior of the tested RC building are presented.

4.1 Finite element model simulation in DIANA FEA

In this section, the simulation of the south frame of the SERFIN prototype specimen model in DIANA FEA is presented. The numerical model that was developed is a 2D continuum FE model. The assumptions and the initial conditions that were made for the development of the FE model, the elements, and the constitutive material laws that were selected from the DIANA FEA library and the mesh that was generated are presented. In addition, the loads that were applied to the model and the analysis procedures are described.

Much of the focus was on the behavior of the individual models that were used for the modeling and how they were validated, so they would correctly reflect the overall model behavior. Suitable elements for the simulation of the RC infills, reinforcement, and frame members were selected along with material models for concrete and reinforcement, which included hysteretic behavior with strength and stiffness degradation. In this way, the FE model considers the nonlinear hysteretic behavior of materials during a seismic excitation to capture and evaluate the behavior of RC infills. Furthermore, a detailed analysis was obtained considering the nonlinear behavior of the materials at the local level (nonlinear transient analyses were performed) to simulate the experimental results.

Two distinct numerical models were developed in DIANA FEA and they consisted of the existing RC frame and the new RC infill wall, like the prototype model. Initially, the first numerical model was developed without the consideration of the interaction between the existing bounding frame and the new RC wall (model I displayed in Figure 4.10) to verify the experimental results and several parameters of the model and analysis being tested. The most influential parameter was Young's modulus of concrete. Eventually, the experimental results (displacements, base shear force) were verified. In the first model, the infills were monolithic with the bounding frame and all reinforcing bars being modeled to carry axial loads only. In the second numerical model (model II shown in Figure 4.11) that was developed in DIANA FEA, the interaction between the existing bounding frame and the new RC wall was modeled through interface elements, to allow for the separation of the bounding framing members and the RC wall at the interface when they are in tension (caption of tension cut-off behavior). In this case, the dowels were modeled in such a way so they can take shear and axial forces, and moments, as in the case of the real structure. Both numerical models are described and presented along with their results in this chapter.

4.1.1 Model characteristics and assumptions

The initial conditions and assumptions that were made for the simulation and the analysis of the FE model are described in this section. Specifically, a rigid foundation was simulated, and pin supports (X and Y translational constraints) were applied at the base of the building model (see Figure 4.1). Moreover, the CFRPs that were applied at the SERFIN specimen (see Chapter 3) were not considered in the DIANA FE model. The

units that were used for the model were N, m, and kg. In Figure 4.2 the geometries of concrete and reinforcement members in DIANA FEA are illustrated.
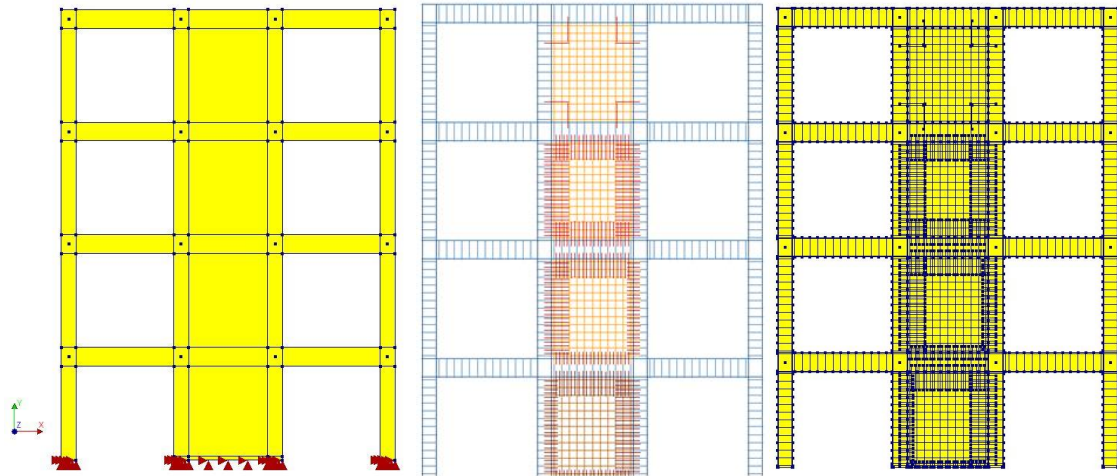
Figure 4.1: (a) Concrete geometry shapes of the FE model, **(b)** Embedded reinforcement bars for the existing frame and web reinforcements of the infill wall and dowels, **(c)** Complete geometry of the FE model

The additional weight of half of the experimental slab and transverse beams was added to the 16 joints of the model through mass point elements. The dead and live loads were applied on the beams as edge pressure load with the same values as the prototype model and the earthquake signal with 0.25g peak acceleration was added as body force for base excitation with the earthquake time-history function.

Then, the nonlinear transient analysis was executed in DIANA FEA. In order to perform a nonlinear transient analysis, the Rayleigh damping coefficients were defined in DIANA FEA using 0.25% damping ratio. The secant Newton method (quasi-newton), which is an iterative method, was applied, together with the line search method. The convergence tolerance was applied for force and displacement.

4.1.2 Element and mesh

The elements and the mesh that were selected and applied for all the members of the frame in DIANA FEA are presented in this section. Different elements were used to simulate the concrete elements of the frame, the frame reinforcement, the web reinforcement of the infill, the dowels that connect the new infill wall to the existing frame and the interface between the existing frame and the new infill walls. In addition, as it

was mentioned before, point mass elements were used to add half the mass of the specimen (slabs and transversal beams see Chapter 3) to the 2D FE frame.

It is important to mention that for the second FE model (model II) the frame and the RC infills web-reinforcement were modeled differently than the dowel reinforcement. The reinforcing bars of the RC frame and the web reinforcement of RC infills were modeled to carry only axial loads, whereas the dowels were modeled to capture not only axial loads but shear and moment as well.

4.1.2.1   *Concrete mesh*

The concrete frame members (columns, beams, and joints) and the infill wall were simulated using the 2D regular plane stress quadrilateral elements with 8 nodes (CQ16M) shown in Figure 4.2 from the DIANA FEA element library. Plane stress elements are characterized by the fact that the stress components perpendicular to the face are zero: σ_{zz} = 0. These elements may only be applied if there is no bending outside the plane of the structure, like in walls, deep beams and the like (DIANA FEA BV, 2019). In addition, the plane stress elements can be combined with the bond-slip reinforcement elements in DIANA FEA in case we do not want perfect bonding between concrete and reinforcement steel (DIANA FEA BV, 2019).
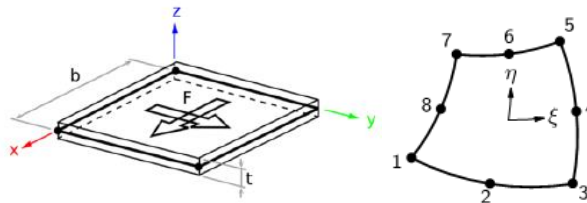
Figure 4.2: Plane stress elements characteristics (DIANA FEA BV, 2019)

4.1.2.2   *Reinforcement mesh*

For the first FE model I the frame reinforcing bars, the web reinforcement of the RC infills, and the dowels were modeled as reinforcement steel bars and for their mesh, 1D embedded bar reinforcement inside plane stress elements were used (Figures 4.3 and 4.4), which can carry only axial loads. More specifically, the embedded reinforcement has strains and stresses in the longitudinal direction only. For model II, only the frame reinforcing bars and the web reinforcement of the RC infills were modeled with these elements, since the dowels were modeled in such a way so they can take not only axial

load but also shear load and bending moment (see section 4.1.2.3). The reinforcement steel bar elements that were applied for the reinforcement in the two developed models are described in this section.

These reinforcement elements are fully embedded in the structural elements in which they are located, the so-called "mother elements" and they are fully coupled (they do not allow relative slip). They do not contribute to the weight of the element and they do not have degrees of freedom of their own while they add stiffness to the FE model. The contribution of the reinforcement stiffness to the stiffness of the respective mother element is automatically calculated by the software. If for the respective element the option NOBOND is defined, this reinforcement does not contribute to the stiffness matrix. By default, in embedded reinforcement, the strains in the reinforcement are computed from the displacement field of the mother elements. This implies a perfect bond between the reinforcement and the surrounding material unless the user chooses the no bond option in order to specify the non-bonded behavior. The technique of embedding allows the lines of the reinforcement to deviate from the lines of the mesh. This permits the user to generate the FE mesh without having to anticipate the location of reinforcement.

Moreover, such reinforcement can be embedded in all structural interface elements and they are applied when it continues from one structural part into another and have a considerable effect on the cracking or sliding of the connection between these two parts. Such reinforcement was applied in the FE model that was generated.

In DIANA FEA, reinforcement is defined by its location in the model, the material properties, the physical properties, i.e., cross-section area, the integration schemes, and the loading, if applicable. The location points are determined automatically, as DIANA identifies the elements that are intersected by the embedded reinforcement (the embedding elements), which is called "element-by-element" discretization method. For reinforcement that is passing through interfaces, an alternative discretization method is available that is based on section (section wise). This method of discretization was applied for the dowels in model II for the dowels. As mentioned before, the contribution of the reinforcement stiffness to the stiffness of the respective mother elements is automatically calculated. If for the respective element the not bonded option is defined, this reinforcement does not contribute to the stiffness matrix. The total length of the bar is divided in several "particles". By definition, a particle must be completely inside a

structural element. The so-called "location points" define the position of the particles in the FE model.
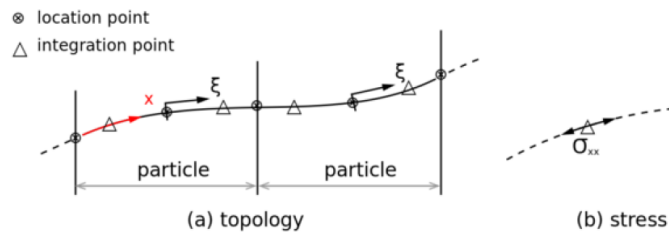
Figure 4.3: Reinforcement bar location points and integration points (DIANA FEA BV, 2019)

For the generated FE models, the bar reinforcement is embedded in the regular plane stress elements that was used for the concrete members of the FE model. To embed the bar reinforcement in plane stress elements, DIANA needs for each plane stress element the location points of the particle that is embedded in that element (see Figure 4.4). These location points are generated by the discretization of the reinforcement. For the FE model of the south wall that is examined, four cross-section areas of bars (Y8, Y10, Y12, Y20) were used like in the prototype model (see Chapter 3). The reinforcing bars that were applied in the FE models are given in Tables 4.1 to 4.4.
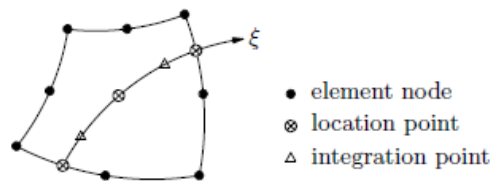
Figure 4.4: Reinforcement bar particle in plane stress element (DIANA FEA BV, 2019)

Table 4.1: Reinforcing bars for frame members

Frame members	Longitudinal reinforcing bars	Shear links
Longitudinal beams	4Y12 Up + Down	Y8/200
Columns	4Y20	Y8/200

Table 4.2: Infill wall reinforcing web bars

Infill Wall	Vertical web bars	Horizontal web bars
Ground Floor web bars	Y10/200# (2x11 bars)	Y10/200# (2x13 bars)
1st Storey web bars	Y8/200# (2x11 bars)	Y8/200# (2x13 bars)
2nd Storey web bars	Y8/200# (2x11 bars)	Y8/200# (2x13 bars)
3rd Storey web bars	Y8/200# (2x11 bars)	Y8/200# (2x13 bars)

Table 4.3: FE model dowel bars

Dowels	West column	East column	Foundation beam	Storey beam
Ground floor infill wall (W1)	24Y20/100 (l=320mm)	24Y20/100 (l=660mm)	20Y20/100 (l=320mm)	20Y20/100 (l=660mm)
1st Storey infill wall (W2)	24Y18/100 (l=545mm)	24Y28/100 (l=290mm)	20Y18/100 (l=290mm)	20Y18/100 (l=545mm)
2nd Storey infill wall (W3)	24Y16/100 (l=530mm)	24Y18/100 (l=530mm)	20Y16/100 (l=530mm)	20Y16/100 (l=530mm)
3rd Storey infill wall (W4)	2Y16 (l=530mm)	2Y16 (l=530mm)	2Y16 (l=530mm)	2Y16 (l=530mm)

Table 4.4: FE model starter bars

Starter bars	West column	East column	Foundation beam	Storey beam
Ground floor infill wall (W1)	2x13Y10/200 (l=670mm)	-	2x11Y10/200 (l=670mm)	-
1st Storey infill wall (W2)	-	2x13Y18/200 (l=520mm)	2x11Y18/200 (l=520mm)	-

The variables for a bar reinforcement are the strains ε_{xx} and the stresses σ_{xx} oriented along the longitudinal direction of the vector. DIANA FEA performs numerical integration of each particle of a reinforcement bar. In each integration point, DIANA FEA determines

a vector tangential to the bar axis and the integration scheme for the bar reinforcement is derived from the one for the embedding structural element (mother elements).

4.1.2.3 Dowels mesh

As it is shown from the literature, even though the dowel reinforcing bars (shear connectors) between the existing bounding frame members and the new infill wall affect the behavior of RC infills and the overall shear resistance capacity of a building, it is not clear how to design them. This is because their behavior is based on a complicated mechanism (see Chapter 2). In order to study the contribution of dowels and to investigate further their design and construction, they were modeled in the FE model II and their modeling in DIANA FEA is presented in this section.

As discussed in section 4.1.2.1, the frame was modeled with plane stress elements that do not have rotational degrees of freedom and the reinforcement elements that were used for the existing frame reinforcements and the web reinforcement of the infill wall can only take axial loads. As already stated, the local behavior of dowels in the FE model is important in order to study their contribution. Therefore, the shear that the dowels carry in actual cases was important to be included in the FE model. In this way, for the FE model II, bond-slip beam-element reinforcement (BAR LINE, INTERF BEAM) that are available in DIANA FEA element library as embedded lines in regular plane stress elements were used to capture the real behavior of dowels in the FE model.

In this case, the reinforcement bars are internally modeled as beam elements, which are connected to the mother elements in which they are located by line-plane elements. In bond-slip reinforcement, elastic or nonlinear bond-slip material behavior may be defined. For this case, the material behavior that was defined is described in section 4.1.3. Moreover, bond-slip reinforcement may be applied for modeling slip of steel reinforcement in concrete. For example, the bond-slip reinforcement can be used to describe the pull-out of an anchor of a bar reinforcement. However, this was not studied in the specific FE model that is presented.

No integration schemes can be defined for bond-slip reinforcement because in general beam elements have different integration schemes. The applied elements for bond-slip reinforcement use the default integration schemes of these elements.

The material parameters of the bond-slip reinforcement define both the material for the beam elements as well as the interface elements. The applied material models and parameters for the dowels are described in section 4.1.3. The geometry properties of beam elements must be defined as geometric properties of the reinforcement. The perimeter of the interface can be either specified or calculated using the dimensions already specified for the beam elements. For circular beam cross-sections that were applied in the FE model that was developed, DIANA calculates the diameter and perimeter internally. DIANA uses the diameter or perimeter to convert the shaft into interface tractions.

The deformation of bond-slip reinforcements may be different from for the elements in which they are located since relative slip is allowed. The reinforcement is connected with interface elements to the continuum elements in which it is located. Material and geometry properties are defined both for the reinforcement bar and for the bond-slip interface. The characteristics of the reinforcement is defined by the location, material, and dimensional properties.

A bond-slip reinforcement bar in a plane stress element is defined as it was described for the embedded bar reinforcement. The calculation of the intersections of the bar reinforcement and the plane stress elements can be done by reinforcement sections with location points being defined by nodes or b global XYZ coordinates. The type of the beam reinforcement element in plane-stress elements (mother element, CQ16M) that is internally used is automatically determined as CL9BE.

For the FE model II, three diameters (Y20, Y18, Y16) of circular beam elements with different lengths were used for the dowels, as shown in Table 4.5, and correspond to the ones of the prototype model described in Chapter 3. The geometry of the dowels as added in the FE model II is shown in Figure 4.5.

Table 4.5: FE model dowel bars

Infill Wall	Vertical dowels-connecting beams		Horizontal dowels-connecting columns	
	West side	**East side**	**Down**	**Down**
Ground Floor	24Y20/100 (length=320mm)	24Y20/100 (length=660mm)	20Y20/100 (length=320mm)	20Y20/100 (length=660mm)
1st Storey	24Y18/100 (length=545mm)	24Y18/100 (length=290mm)	20Y18/100 (length=545mm)	20Y18/100 (length=290mm)
2nd Storey	24Y16/100 (length=530mm)	24Y16/100 (length=530mm)	20Y16/100 (length=530mm)	20Y16/100 (length=530mm)
3rd Storey	2Y16 (length=530mm)	2Y16 (length=530mm)	2Y16 (length=530mm)	2Y16 (length=530mm)
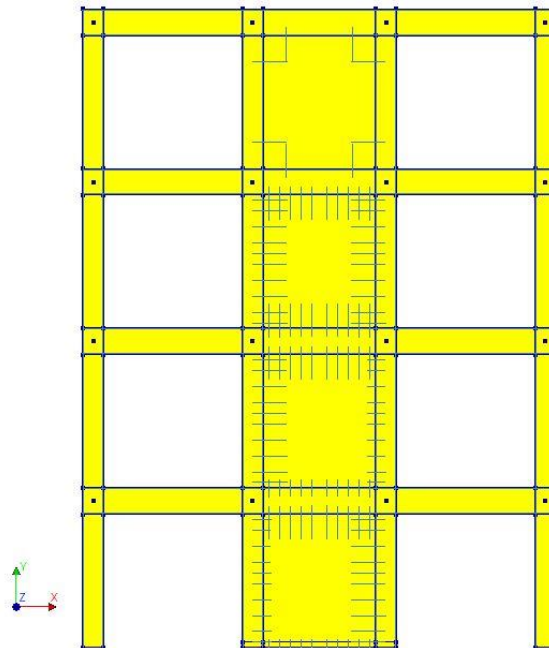
Figure 4.5: Dowels geometry in the FE model

4.1.2.4 Interface mesh

The interface area between the wall and the frame was modeled in the FE model II to capture the tension cut-off behavior between the existing frame and the new infill wall. This allows for a more realistic contribution of the dowel's reinforcement bars to the resistance of the model. For the interface between the frame and the walls, the two-dimensional (2D) line interface (CL12I) from the DIANA element library was applied.

The structural interface elements describe the interface behavior in terms of a relation between the normal and shear tractions and relative displacements across the interface. The 2D line interface elements of the DIANA library that were applied were placed between the edges of the two-dimensional elements of concrete frame members and the concrete wall. For 2D line interface elements, the thickness (out-of-plane) is required to be specified by the user for plane stress. For the applied interface elements, the same thickness of plane stress elements of 250mm was applied. For this type of 2D line interfaces elements, DIANA determines the direction in which the thickness is measured from the element shape.

The basic variables for structural interfaces are the nodal displacements $\Delta\mathbf{u_e}$. The derived values are the relative displacements $\Delta\mathbf{u}$ and the tractions $\mathbf{t}$. The structural interface elements describe a relation between $\mathbf{t}$ and $\Delta\mathbf{u}$ across the interface and DIANA can output the derived values in the integration points. The variables of two-dimensional structural line interfaces are oriented in the local xy axes (Figure 4.6). The normal traction t_{ny} is perpendicular to the interface; the shear traction t_{sx} is tangential to the interface (Figure 4.6).

$$\mathbf{u}_e = \left\{ \begin{array}{c} u_x \\ u_y \end{array} \right\} \qquad \Delta\mathbf{u} = \left\{ \begin{array}{c} \Delta u_{sx} \\ \Delta u_{ny} \end{array} \right\} \qquad \mathbf{t} = \left\{ \begin{array}{c} t_{sx} \\ t_{ny} \end{array} \right\}$$

(a) displacements   (b) relative displacements   (c) tractions
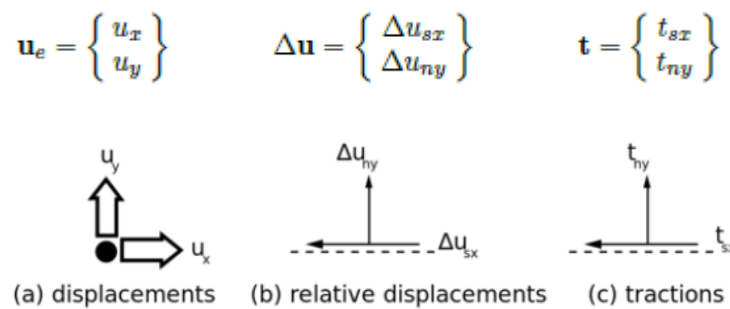
Figure 4.6: Variable of two-dimensional line interfaces (DIANA FEA BV, 2019)

The CL12I element that was applied is an interface element between two lines in a two-dimensional configuration. The local axis xy axes for the displacements are evaluated in the first node with x from node 1 to node 2 (see Figure 4.7). Variables are oriented in the xy axes.
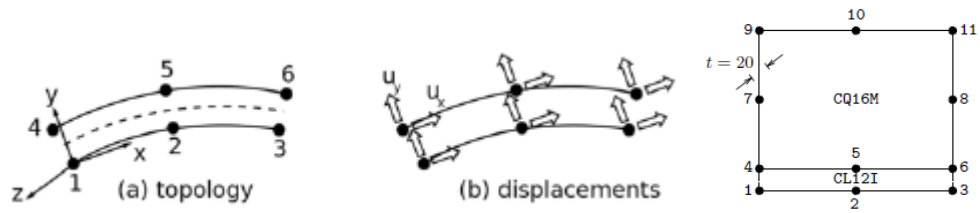
Figure 4.7: Line interface CL12I, topology and displacements (DIANA FEA BV, 2019)

4.1.2.5 Mass mesh

As it is described in chapter 3, the SERFIN specimen was a full-scale prototype model and since the FE models of the south frame of the specimen that were generated are 2D models, the mass of half the weight (312Tons) of the prototype building was added in the models by using the point mass elements (PT3T) on the 16 joints of the frame (see Figure 4.1).

The point mass elements (shown in Figure 4.8) that were applied in the models, may be applied to add mass, or damping to the FE model without influencing the stiffness. The point elements do not have any post-analysis results like strains or stresses. As point mass, these elements are typically used to correct the deadweight or to affect the inertial mass in a dynamic analysis. If a damping coefficient is specified by the user, then these elements act as dashpots in the global *XYZ* directions to simulate continuous damping in dynamic analysis. For the generated FE models, the point mass elements were applied to add mass without influencing the stiffness. Specifically, they were used to correct the deadweight of the simulated frame and to affect the inertial mass, since a dynamic analysis was then executed. In the specific case, the point mass was used in 2D elements, thus the direction without stiffness was supported. The material properties for mass elements are illustrated in section 4.1.3.
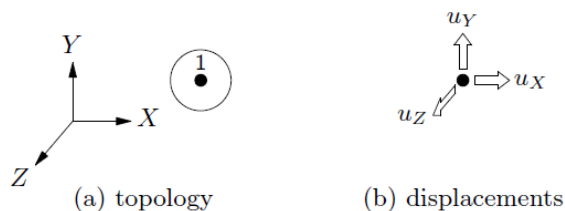
Figure 4.8: 1 node point mass element PT3T topology and displacements (DIANA FEA BV, 2019)

The PT3T element is a one-node translation mass/damping element; it acts as a concentrated mass in the finite element model. The basic and the only variables of the PT3T element are the translations in the global *XYZ* directions (see Figure 4.9).

$$\mathbf{u}_e = \left\{ \begin{array}{c} u_X \\ u_Y \\ u_Z \end{array} \right\}$$

Figure 4.9: Point mass element variables (DIANA FEA BV, 2019)

4.1.2.6 Generated mesh

The generated mesh of concrete members, reinforcement, interface areas, dowels, and mass points in the FE models that were developed in the environment of DIANA FEA are shown in Figure 4.10 and Figure 4.11 for the first and second models, respectively.

In Figure 4.10, the first 'monolithic' model that was generated is presented. As shown, all the concrete members were meshed with the plane stress elements, and the mass point elements are shown at the 16 joints of the frame. It is also shown that the frame, the web reinforcing bars, and the dowels are meshed as 1D embedded reinforcement in the plane stress elements.
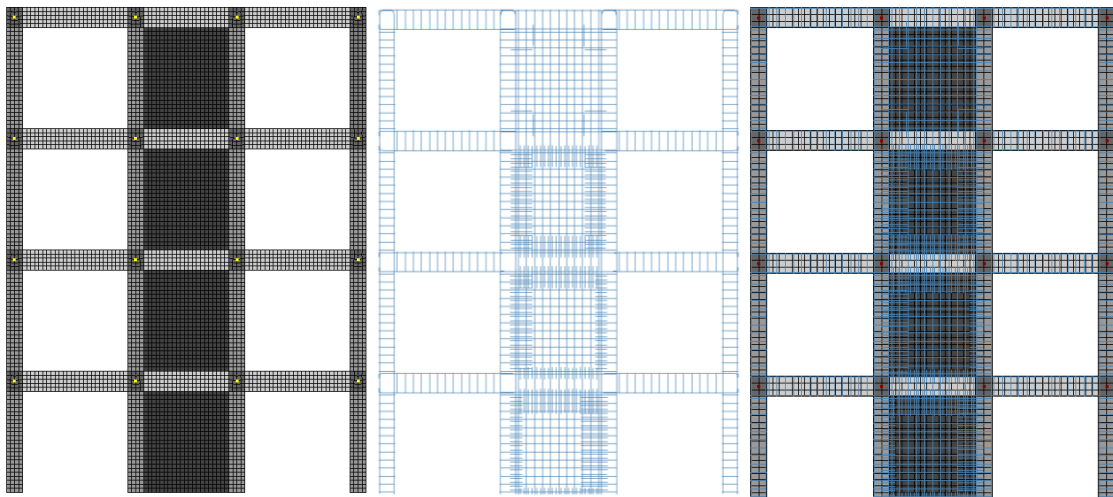
Figure 4.10: (a) Monolithic RC frame with RC infills with plane stress elements, (b) Embedded reinforcement bars for the existing frame and web reinforcements and dowels, (c) Complete FE model I (DIANA FEA BV, 2019)

In Figure 4.11, the second 'non-monolithic' FE model is presented. In Figure 4.11(a), the plane stress elements that form the frame with the infill walls is illustrated along with the

mass point elements at the joints of the frame. Added to that, in this model the 2D line interface elements between the new infill wall and the bounding frame (blue lines) are shown. In Figure 4.11(b), the frame reinforcing bars (in blue), the web reinforcement of the infill wall (in orange) and the dowels connecting the new infill wall to the bounding frame (in red) are displayed. In Figure 4.11(c) all the elements of the model that was developed are shown.
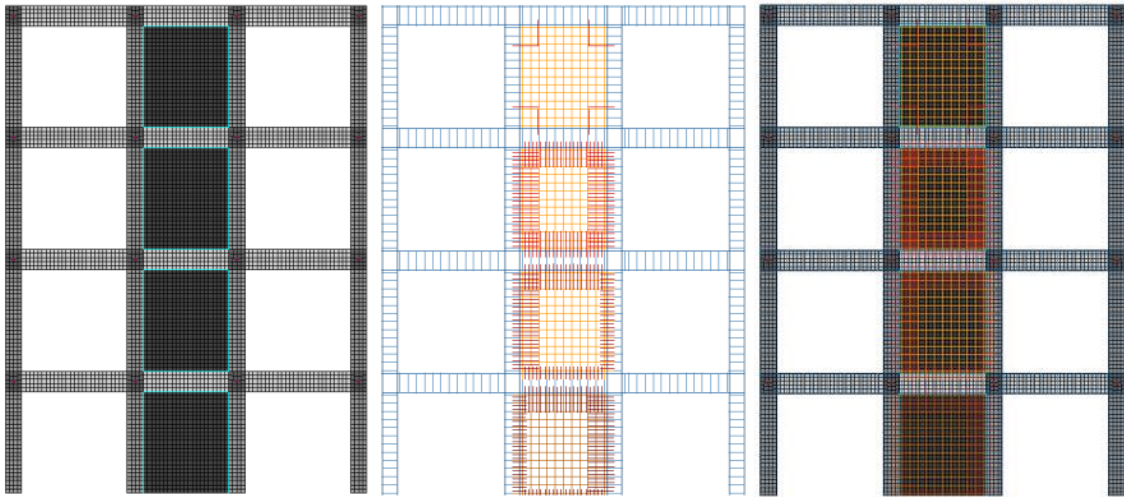
Figure 4.11: (a) RC frame with 2D line interface elements at the interfaces and plane stress elements, (b) Embedded reinforcement bars for the existing frame and web reinforcements and dowel special elements which can take shear forces, (c) Complete FE model I (DIANA FEA BV, 2019)

In Table 4.6, the elements that were selected from the DIANA FEA element library, and the parameters that were defined for the generation of their mesh are presented.

Table 4.6: Elements that were selected from DIANA FEA element library and defined parameters

Members:	Concrete	Reinforcement steel bars (frame and web reinforcement of infill walls)	Dowels	Interface	Mass
Applied elements:	2D regular plane stress quadrilateral elements with 8 nodes '*CQ16M*'	Embedded bar reinforcement in plane stress elements	Bond-slip reinforcement with beam elements '*BAR LINE, INTERF BEAM*'	2D line interface elements '*CL12I*'	Point mass elements '*PT3T*' translation, point mass/damping, 1 node
Defined parameters:	Thickness:*250mm* Size:*100x100mm*	Cross section-area of bars: *Y8, Y10, Y12, Y20*	Diameter of circle: *Y16, Y18, Y20*	Thickness (width): *250mm*	Half weight of the prototype building: *275,260kg/16 points*

4.1.3 Material constitutive laws

The material models that were selected from the DIANA FEA material library for both concrete and reinforcement steel materials describe the hysteretic behavior of materials under cyclic loading. More specifically, the constitutive laws of the materials model the stiffness and strength degradation and the material softening behavior which causes localization and redistribution of strains in the structure (plasticity). The materials' constitutive laws that were applied for all the materials of the developed FE models are described in this chapter.

4.1.3.1 Concrete constitutive law

For concrete members, the pure elastic damage models or pure elastic-plastic constitutive laws are not satisfactory to describe the behavior of concrete. These models indeed, fail to reproduce the unloading slopes during cyclic loading which experimentally define the value of the damage in the material (Omidi and Lotfi 2010). Numerous concrete models

have been proposed in previous years. Although it has been proved that the models derived from the theory of plasticity and the continuum damage theory can accurately simulate the observed behavior of concrete, its application in the engineering practice is limited. This is motivated by the great number of parameters that are usually required and the difficulty to obtain them through conventional laboratory tests (Sima *et al.*, 2008). In this research though such a material model was used for concrete, which describes the hysteretic behavior of concrete under cyclic loading (strength and stiffness degradation) and it is described in this section.

Initially, the material model that was chosen for concrete from the DIANA FEA material library was the 'Modified Maekawa model' since it was the only one in the library of the software that could describe the hysteretic behavior of the concrete under cyclic loading. This model uses different constitutive equations to describe the behavior of concrete before and after its cracking and it combines a multi-axial damage plasticity -model based on the total strain of the tensile regime. However, code bugs and instabilities were noticed while dealing with unstable and unreasonable outcomes. It should be noted that these problems with the material models were confirmed by the developers of the software and they replaced the Modified Maekawa model with the 'Maekawa-Fukura' model. For the FE models that were developed in order to avoid the unstable and unexpected spikes in the force results that were noticed from the application of the Maekawa concrete model since the options for the shear transfer models had bugs in the implementation in DIANA, the 'Total-strain based crack model' with rotating crack orientation was used and the Maekawa cracked concrete model was applied only for the compressive behavior of concrete. For the tensile behavior of concrete, the fib Model Code for Concrete Structures 2010 tensile curve was chosen.

The Total-strain based crack model is based on total strain and is developed along the lines of the Modified Compression Field Theory, originally proposed by Vecchio & Collins (Vecchio, Frank J, 1986). This model follows a smeared approach for the fracture energy. For more information about the concept of smeared cracking see (DIANA FEA BV, 2019). A constitutive model based on total strain describes stress as a function of the strain. This concept is known as hypo-elasticity when the loading and unloading behavior is along the same stress-strain path. In the current implementation in DIANA, the behavior in loading and unloading is modeled with a secant unloading (Figure 4.12).

85
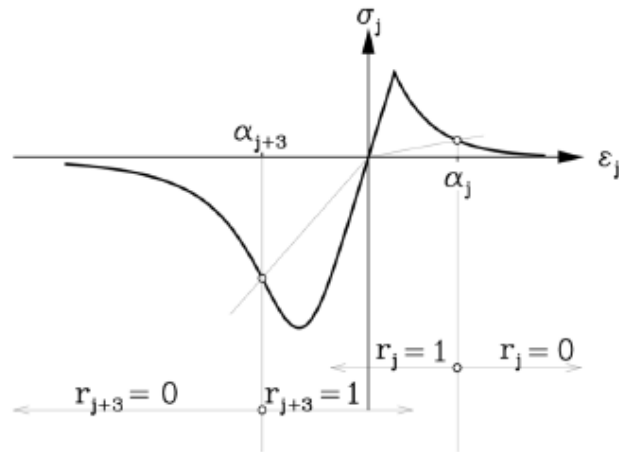
Figure 4.12: Loading-unloading (DIANA FEA BV, 2019)

Within the total stress-strain relations, various approaches are possible. One commonly used approach is the coaxial stress-strain concept, in which the stress-strain relations are evaluated in the principal directions of the strain vector. This approach, also known as the rotating crack model, is applied to the constitutive modeling of reinforced concrete during a long period and has shown that the modeling approach is well suited for reinforced concrete structures. So, this approach was selected for the developed FE model. The basic concept of the Total Strain Crack models is that stress is evaluated in the directions that are given by the crack directions.

In the meantime, during loading concrete is subjected to both tensile and compressive stress, which can result in cracking and crushing of the material. In a fixed stress-strain concept, the shear behavior is modeled explicitly with a relation between the shear stress and the shear strain. A more detailed explanation of the calculation of these constraints is given in DIANA FEA BV, 2019.

In an incremental-iterative solution scheme, the equilibrium between the internal force vector and the external load vector is achieved with Secant (Quasi-Newton) iterative procedure for the developed FE model. For this purpose, the constitutive model should also define the stiffness matrix, which is utilized to achieve equilibrium. In DIANA two approaches to the stiffness matrix are used, the *secant stiffness matrix* and a *tangent stiffness* matrix (secant stiffness matrix was chosen for the studied FE model). The first approach has proved to be robust and stable in RC structures with extensive cracking. The

latter has shown superiority in an analysis where localized cracking and crack propagation are the most important phenomena.

For the Total Strain Crack model, several functions based on fracture energy are implemented, which are all related to a crack bandwidth as is usual in smeared crack models. For the developed FE model as mentioned above, the tensile behavior of concrete that was applied is the nonlinear tension softening according to Paragraph 5.1.8.2 of the "fib Model Code for Concrete Structures 2010" (Figure 4.13) (DIANA FEA BV, 2019) where the tensile curve was used with 2.6 MPa tensile strength (f_t).
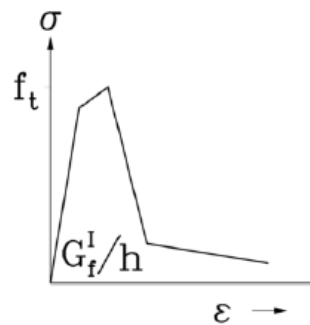
Figure 4.13: fib Model Code for Concrete Structures 2010 tensile behavior of concrete (FIB, 2013)

For the compressive behavior of concrete, the Total Strain Crack Model assumes that the compressive behavior of concrete is influenced by lateral cracking. To model the lateral confinement effect, the parameters of the compressive stress-strain function, f_{cf} and ε_p, are determined with a failure function, which gives the compressive stress that causes failure as a function of the confining stress in the lateral directions. If the material is cracked in the lateral direction, the parameters are reduced for the peak strain and peak stress with the factors $\beta\varepsilon_{cr}$ and $\beta\sigma_{cr}$ respectively (for the equations see DIANA FEA BV, 2019). It is tacitly assumed that the base curve in compression is determined by the peak stress value $fp=\beta\sigma_{cr} f_{ct}$, and the corresponding peak strain value $\alpha_p=\beta\varepsilon_{cr} \varepsilon_p$. The base function in compression, with the parameters f_p and α_p, is modeled with several different predefined and user-defined curves. The predefined curves are the constant curve and the brittle curve. Also, available are linear hardening curve and the saturation-hardening curve. The curve that was selected from the available hardening-softening curves in compression from the DIANA material library is the Maekawa Cracked Concrete curves (see Figure 4.14).

When the Maekawa Cracked Concrete curve is selected, automatically the unloading and reloading curves in both tension and compressive regime are applied in the Total Strain Crack model. For this model, the compressive strength f_c under uniaxial stress situations is defined. Young's modulus E is specified in the material properties and strain ε_c at the compressive strength in case of uniaxial loading conditions is calculated from equation 1. The reduction factor for the tensile strength Rf was set to linear, which specifies that the reduction factor of the tensile strength is equal to the damage factor K: $Rf=K$. It is noted that the Maekawa Cracked Concrete curves in their essence are calibrated in the experimental data. The compressive strength of the model only matches with the maximum compressive stress under uniaxial loading conditions when the specified Young's modulus and Poisson's ratio are close to realistic values for concrete.

$$\varepsilon_c = 2.0 \frac{f_c'}{E} \tag{1}$$

The Maekawa Cracked Concrete curves are uniaxial stress-strain relations for loading, unloading, and reloading conditions in, respectively, the tensile and compressive strain domains. In the main directions of the coordinate system related to the active crack, the stresses are calculated with these equations using the equivalent strain. Figure 4.14 shows the typical uniaxial stress-strain development as defined by the Cracked Concrete curves. In this figure the following stages can be distinguished: 0-1 compressive loading, 1-2 compressive unloading, 2-3 compressive reloading, 3-4 compressive unloading, 4-5 tensile loading, 5-6 tensile loading, 6-7 tensile unloading, 7-8 tensile reloading, 8-9 tensile unloading, 9-10 compressive reloading, 10-11 compressive loading. The equations that define the Maekawa Cracked Concrete curves can be found in Maekawa, Koichi, Okamura, H., Pinanmas, 2003.
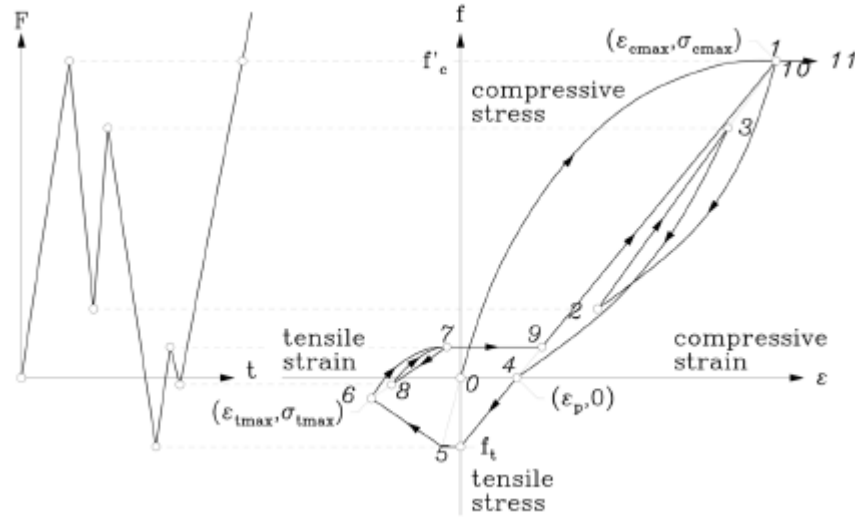
Figure 4.14: Hysteresis for Maekawa model for compressive behavior of concrete (Maekawa, Koichi, Okamura, H., Pinanmas, 2003)

The specific crack-reclosing behavior concerns both the compressive reloading and the tensile unloading mode. During the unloading mode, the strain decreases from the maximum tensile strain that has ever been felt, ε_t, to the compressive plastic strain, ε_p. During the compressive reloading mode, the strain decreases from the compressive plastic strain, ε_p, to the maximum compressive strain that has ever been felt, ε_c. Without the crack-reclosing option, the stress developed in the tensile unloading model according to a cubic function with the strain until the crack-bond stress, σ_{cb} (from Equation 2), when the strain equals the plastic strain, ε_p.

$$\sigma_{cb} = f_t \left(0.05 + 0.15 \frac{\varepsilon_t - \varepsilon_p}{5 f_t} E \right) \tag{2}$$

In an incremental-iterative solution scheme, the equilibrium between the internal force vector and the external load vector is achieved with for instance a Newton-Raphson iterative procedure. For this purpose, the constitutive model should also define the stiffness matrix, which is utilized to achieve equilibrium. In DIANA, the *secant stiffness matrix* is used for the total strain crack model that was applied for the FE model. This approach has proved to be robust and stable in RC structures with extensive cracking.

The direct input that is needed to apply in the Modified Maekawa model as implemented in the standard DIANA code, is Young's modulus and Poisson's ratio, the selection of the total strain crack model (fixed, rotate, non-orthogonal), the compressive strength *fc*

under uniaxial stress situations and the stress confinement function. In Table 4.7, the material properties of concrete that were defined in the model are shown.

For the compressive behavior of concrete, the Maekawa Cracked Concrete curve is used with compressive strength of 33 MPa. It is important to mention that the Young's modulus of concrete was calibrated in the model in order to get the real behavior of the building that was already cracked. Therefore, Young's modulus was reduced from 30GPa to 15GPa. The attractive points of the selected concrete model are that it is defined by engineering parameters such as the tensile and compressive and tensile strength and that it covers all loading conditions. The validated parameters that were applied for the FE model are shown in Table 4.7. Moreover, a detailed description of the material constitutive model that was applied for concrete can be found in Maekawa, Koichi, Okamura, H., Pinanmas, 2003.

The hysteretic behavior of the applied material model for concrete was assessed under cyclic loading (by applying compressive and tensile force loads in one plane stress element) after the definition of the necessary parameters in the software. The stress-strain diagrams that were obtained from the DIANA results and are illustrated in Figure 4.15 reveal that the concrete model can provide the hysteretic loops with the defined tensile and compressive strengths and according to the defined properties in the FE model. It is shown that the model expresses the energy dissipation during cyclic loading paths according to the properties that were given.

Table 4.7: Concrete material model parameters defined in DIANA FEA

Linear material properties		Total strain based cracked model	Tensile behavior "Fib Model Code for Concrete Structures 2010"		Compressive behavior "Maekawa cracked concrete curves"	
Young's modulus (E)	15GPa (reduced)	Rotating crack orientation	Tensile strength	2.6MPa	Compressive strength	33MPa
Poisson's ratio	0.2		Mode-I tensile fracture energy	136.98N/m	Stress confinement	No increase
Mass density	2500kg/m³		Crack bandwidth specification	Rots		
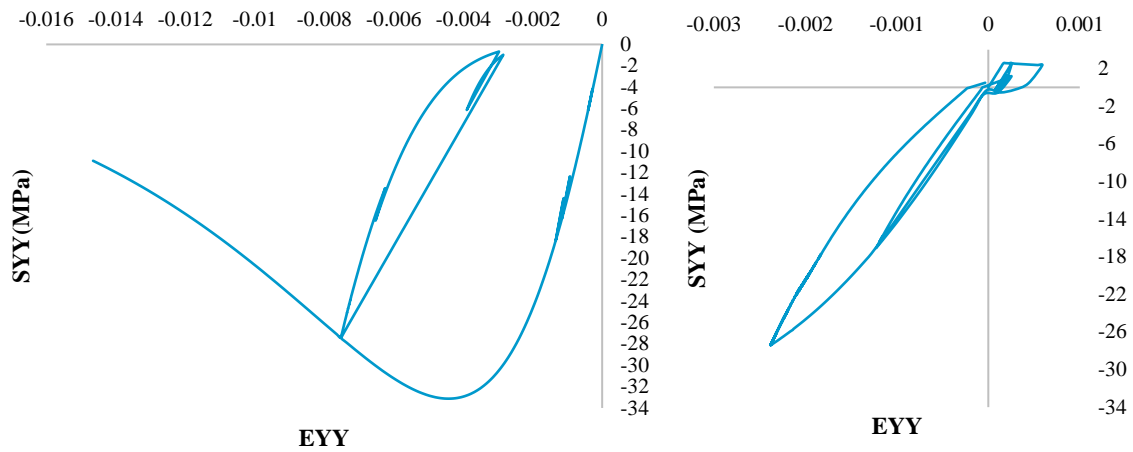
Figure 4.15: Stress-strain diagrams derived from DIANA FEA for the applied concrete material

4.1.3.2   *Reinforcement constitutive law*

The classic explicit models for reinforcement steel modeling are the Giuffre and Pinto (1970), Menegotto and Pinto (1973), Monti and Nuti (1991), Monti and Nuti (1992). In the DIANA FEA material library, the Monti-Nuti, the Menegotto-Pinto, and the Dodd-Restrepo constitutive laws were available for cyclic loading. In this section, the applied constitutive law for reinforcement steel is presented and discussed.

The Menegotto-Pinto model is one of the classic explicit models for reinforcement steel modeling and it was employed to represent the hysteretic stress-strain behavior of reinforcing steel elements of the existing frame and for the web reinforcements of the FE model II and the dowels of the FE model I. The Menegotto-Pinto model has the same expression as the Monti-Nuti model with the difference between the models being the hardening rules in relation to the load cycles. Between the two models, the Menegotto-Pinto model is more computationally stable and as shall be explained later in this section, it is one of the most common uniaxial steel models that can simulate the strain-hardening of reinforcing bars.

The Monti-Nuti material model was found to be very sensitive to severity problems depending on the formulation of the material model used (Fragiadakis *et al*., 2008;). More specifically, even a tiny notch in the stress-strain path may lead to a very large overestimation of the corresponding stress and it has been noticed that in the case of partial unloading and then reloading, a common situation when a structure is subjected to

seismic actions, the model might greatly overestimate the corresponding stress (Fragiadakis *et al*., 2008). This is because the bilinear envelope, defined by the Menegotto-Pinto model adopted by Monti and Nuti, becomes too narrow and the curves are not capable of "fitting" within it. Therefore, this inauthentic behavior is generated because the same algebraic expression used for the skeleton curve is also used when small unloading and loading back takes place. Consequently, the spurious branches of Figure 4.16(b) are developed, with a shape that depends on the ratio between the tie spacing and the bar diameter L/D (Fragiadakis *et al*., 2008). In addition, the Monti and Nuti's model predicts steeper softening in a small strain region and restricts the minimum compressive stress to 0.4fy (Dhakal and Maekawa, 2002).
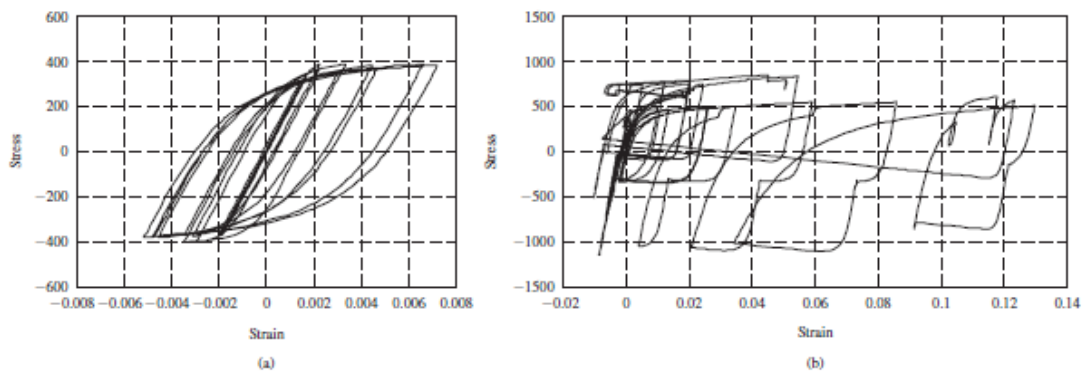
Figure 4.16: Stress-strain diagrams for reinforcing bars (Fragiadakis, Pinho and Antoniou, 2008)

Apart from the Monti-Nuti material model, the Dodd-Restrepo model was also an option from the DIANA FEA material library for the steel reinforcement definition. Dodd-Restrepo was tested for nonlinear behavior under cyclic loading but from the assessment procedure, it did not exhibit reliable results. In particular, the stress-strain diagram of the steel reinforcement with the Dodd-Restrepo model was not reducing the stress capacity even after the yield stress that was defined in the model (as shown in Figure 4.17), therefore not representing accurately the Bauschinger effect.
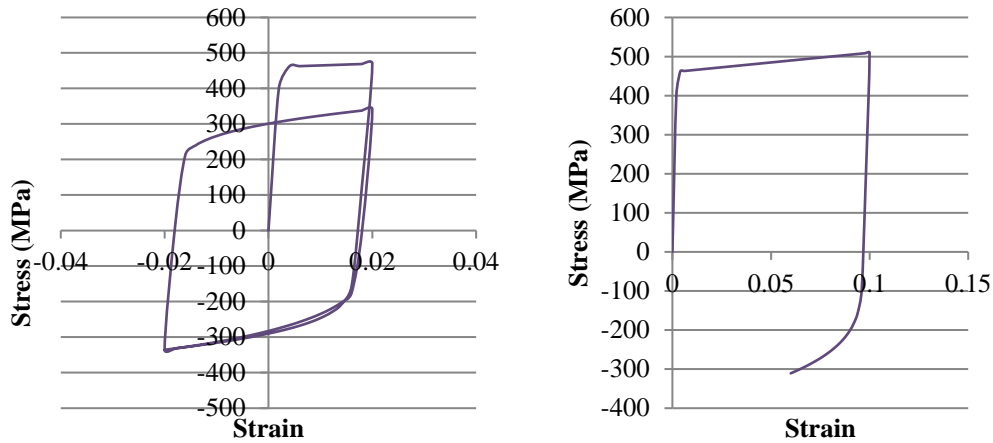
Figure 4.17: Dodd-Restrepo model hysteresis loops

Consequently, the Menegotto-Pinto (shown in Figure 4.18) model was chosen for the simulation of the reinforcement bar elements in the FE model. This model is based on the isotropic plasticity and it is a special plasticity model for the cyclic behavior of steel available for embedded reinforcements. The basic expression of the Menegotto-Pinto model (Filippou, Popov and Bertero, 1983, Menegotto and Pinto, 1973) is shown in DIANA FEA BV, 2019. The model consists of one-dimensional stress-strain relations for branches between two subsequent load reversal points. In order to find the loading/unloading curve between two subsequent inversion points, the model uses the normalized equation of Menegotto and Pinto 1973. The material state parameters re-updated after each load reversal. The model is expressed in terms of a dimensionless stress σ_s* and a scaled strain ε_s*, which are expressed in the strain-stress coordinates of the last point and in the stress-strain coordinated of the updated yield point. The shape of the transition curve allows a good representation of the Bauschinger effect.

Generally, what can be observed from the Menegotto-Pinto model is that the softening behavior that modifies both the monotonic and the elastic curves of the reinforcement bars is considered. It is also a model of both symmetrical and non-symmetrical cyclic strain histories and it is even reliable in the presence of buckling after yielding. Furthermore, the model is computationally very efficient, and it can employ either stress or strain relations for the loading branches.

The parameters that are necessary for the calculation of the model relations are the yield stress, the elastic modulus, the hardening ratio, and the weighting coefficient and in the

93

case of buckling. The yield stress of the existing frame reinforcement was 400MPa and the yield stress of the infill-wall web-reinforcement and dowels was 450MPa. The material properties that were defined for reinforcement bars in DIANA FEA are shown in Table 4.8.
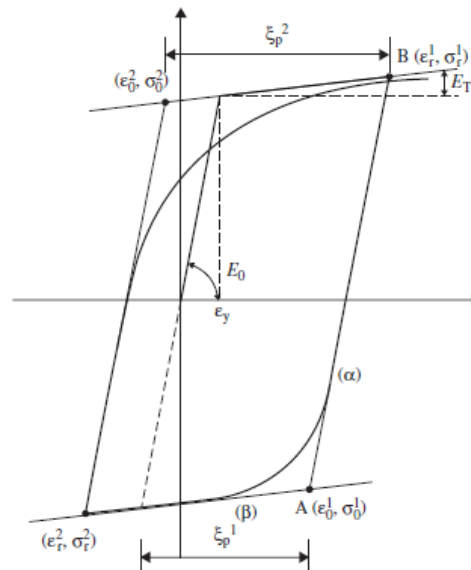
Figure 4.18: Stress-strain relationship of the Menegotto-Pinto model (Faur and Mircea, 2012)

Table 4.8: Reinforcement steel material model parameters defined in DIANA FEA

Linear elasticity		Menegotto-Pinto	
Young's modulus (E)	*200GPa*	Yield stress	*400MPa for frame members*
			450MPa for walls
Mass density	*7800kg/m³*		
		Initial tangent slope ratio	*0.05*
		Initial curvature parameter	*20*
		Constant a1	*20*
		Constant a2	*18.5*
		Constant a3	*0.02*
		Constant a4	*3*
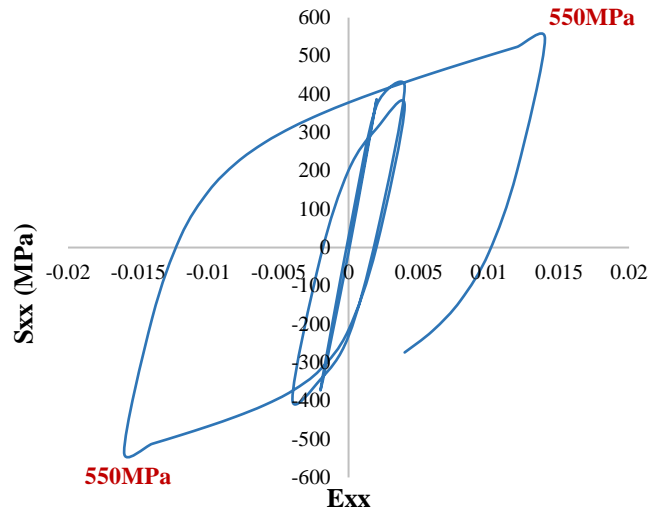
Figure 4.19: Stress-strain diagram derived from DIANA FEA for Menegotto-Pinto model

The hysteretic behavior of the steel model was examined in a 1D element (uniaxial) that was in a plane stress element by applying compressive and tensile loads. In this way, it was ensured that the applied material model presents the actual behavior of reinforcement steel under cyclic loading (see Figure 4.19).

4.1.3.3 Dowels constitutive law

The actual behavior of dowels under shear is shown in Figures 2.25 and 2.26 according to (Paulay. T., Park, R. and Phillips, 1974; Swati Roy Maitra, K. S. Reddy, 2009). As explained earlier in this chapter, the application of dowels in DIANA was achieved through a different modeling since the frame was modeled with plane stress elements that do not take shear forces or moments. So, for the dowels that were modeled to capture the shear stress in the FE model II, the Menegotto-Pinto model was replaced with the Von-Mises plasticity model since the latter can also be applied to control both axial and shear stresses for cyclic loading of the reinforcement, whereas the Menegotto-Pinto model is appropriate for the reinforcement elements that can solely take axial loads. As a result, it can only control the tensile and compressive stresses. The Von-Mises plasticity model parameters are presented in Table 4.9 as defined in DIANA FE model. Also, the Von-Mises stress-strain diagram as specified in the DIANA FE model is shown in Figure 4.20.

Table 4.9: Von-Mises plasticity models parameters defined in DIANA FEA

Linear elasticity	Von Mises plasticity nonlinear model	Bond-slip interface
Young's modulus (E) – 200GPa	Yield stress – 450MPa	Normal stiffness modulus – 2e11N/m³
Mass density – 7800kg/m³	No hardening function	Shear stiffness modulus – 2e14N/m³
		Bond-slip interface failure model – *Shima bond-slip function* • Compression strength: 33MPa • Diameter per bar: 20, 18, 16 • Factor to shear-stress: 1

(a)   (b)
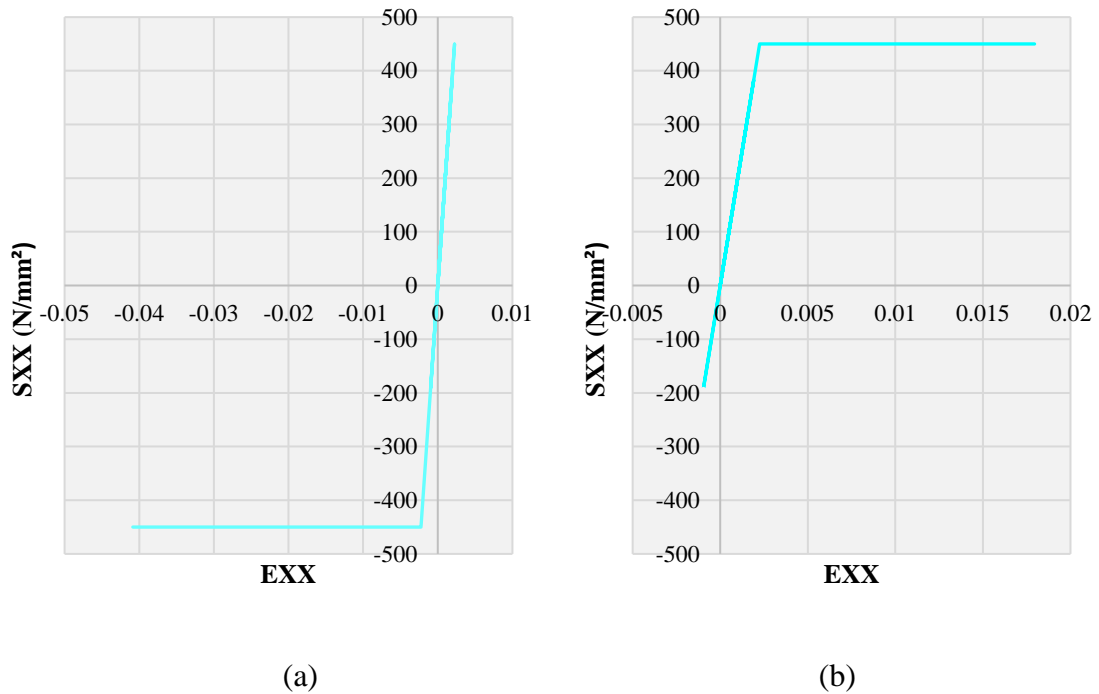
Figure 4.20: Stress-strain diagram derived from DIANA FEA for Von-Mises plasticity model (a) reaching ultimate compressive stress (b) reaching ultimate tensile stress

For the verification of the dowel's proper modeling in DIANA, a push-over test with a beam and a wall with an interface between them and a dowel was executed. In this test, the parameters of the Coulomb friction model that was applied at the interface (cohesion

and friction) were set to zero and only the gap-criterion was applied. Therefore, the dowels would take all the shear force that was applied. As it is shown in Figures 4.21 and 4.22, the expected moment and shear diagrams of dowels that were taken from the literature were obtained in the finite element model and the dowels took the shear force that was applied to the model. It is obvious that this model is close to reality and the expected moment and shear-force diagrams of dowels according to the literature were captured. More specifically, in Figures 4.21 and 4.22 it is shown that the maximum shear force and zero moments at the interface are like the diagrams that are given in the literature.
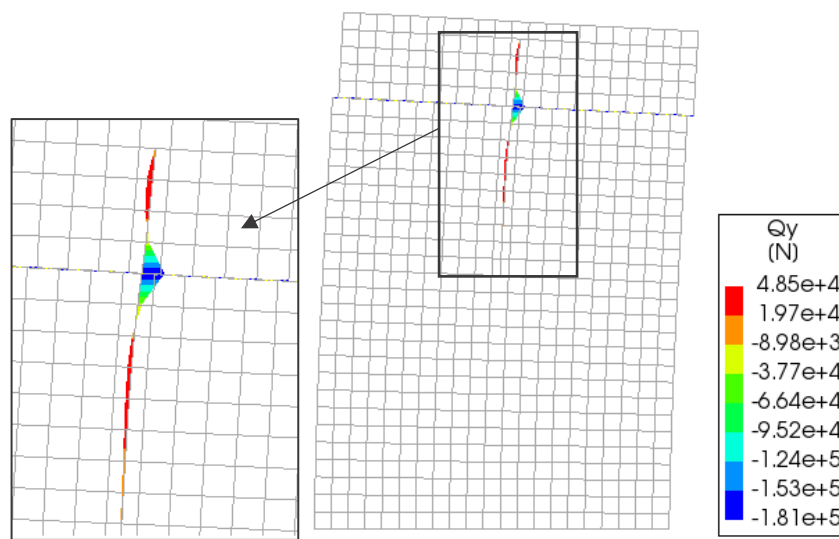
Figure 4.21: Moment diagram of dowel at the interface in DIANA FEA
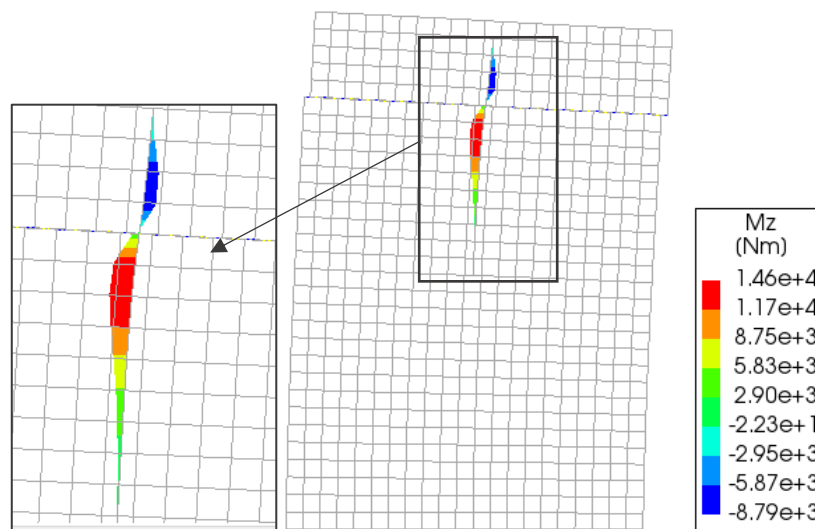
Figure 4.22: Shear force diagram of dowel at the interface in DIANA FEA

4.1.3.4 *Interface constitutive law*

As mentioned before, the new infill wall and the bounding existing frame were constructed at different times and the actual actions of these areas should be properly modeled in the FE model. Specifically, the interface area between the new infill wall and the surrounding frame members should represent the cohesion and the friction between the interfaces. In addition, the dowel action should be active at the interface between the two members. The general concept of interface material modeling and the specific interface material model that was used from the DIANA FEA material library for the FE model II are presented and discussed in this section.

In general, the behavior of an interface between two parts of a structure is governed by friction. This behavior can be modeled with the Coulomb friction model, which has close resemblance with the Mohr-Coulomb plasticity model for continuum elements. This model was used to represent the cohesion and the friction between the interfaces in FE model II, which at the same time provides the option of the gap criterion in the case of tensile stress between the two interfaces. To achieve this aim, the brittle gapping model was applied with very small tensile strength, in order to let the dowels, carry the shear stresses at the interface. The linear material properties of the Coulomb friction model were set through trials to achieve the outcomes that were the closest to the results of the test specimen.

The Coulomb friction model is given by the yield surface and the plastic potential surface given in DIANA FEA BV, 2019. Where *tan (φ)* the friction coefficient (also commonly known by the symbol μ), and *c* the cohesion. It is important to mention that it is possible to extend the friction criterion with a gap criterion, where DIANA assumes that a gap arises if the tensile traction t_n normal to the interface exceeds a certain value. After a gap formation, t_n is immediately reduced to zero (brittle cracking). The full description and details of the Coulomb friction material model can be found in DIANA FEA BV, 2019. The Coulomb friction criterion is shown in Figure 4.23 and the material properties that were defined for the FE model II are given in Table 4.10.
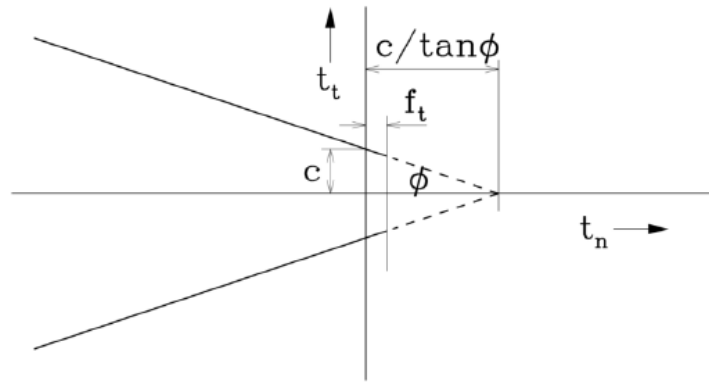
Figure 4.23: Coulomb friction criterion (DIANA FEA BV, 2019)

Table 4.10: Coulomb friction model parameters defined in DIANA FEA

Linear material properties for "2D line interface"	Coulomb friction	Interface opening model "Gapping model"
Normal stiffness modulus-y *2000N/m³*	Cohesion-*1e7Pa*	Tensile strength-*1e-6Pa*
Shear stiffness modulus-x *2000N/m³*	Friction angle-*0.5 rad*	Mode-II shear (model for gap appearance) - *Brittle*
	Dilatancy angle-*0 rad*	

4.1.4 Loads

The loads that were applied in the FE model are presented in this section. The same values of dead and live loads with the SERFIN prototype model were applied on the beams as edge pressure load in the DIANA FEA model as is illustrated in Figure 4.24. The earthquake signal Herzeg Novi accelerogram of the Montenegro earthquake in 1979 was scaled to 0.25g acceleration and was applied as body force in the FE models for the base excitation with the earthquake time history function (shown in Figure 4.25).
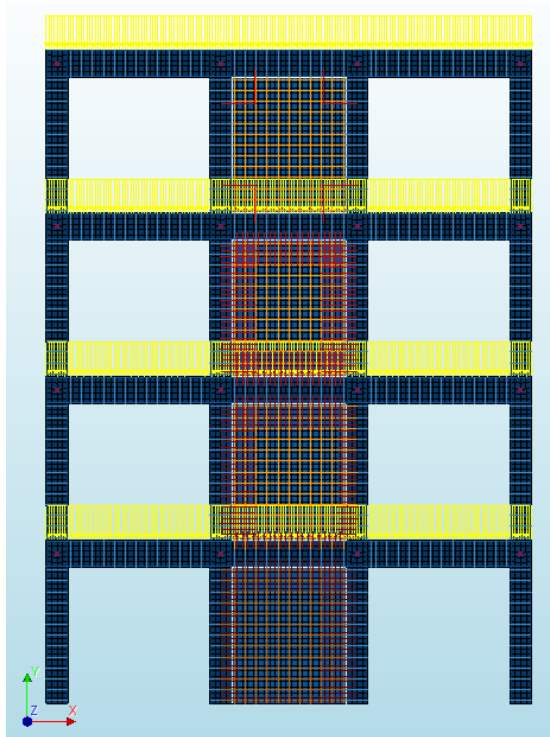
Figure 4.24: Gravity vertical load applied in the FE model
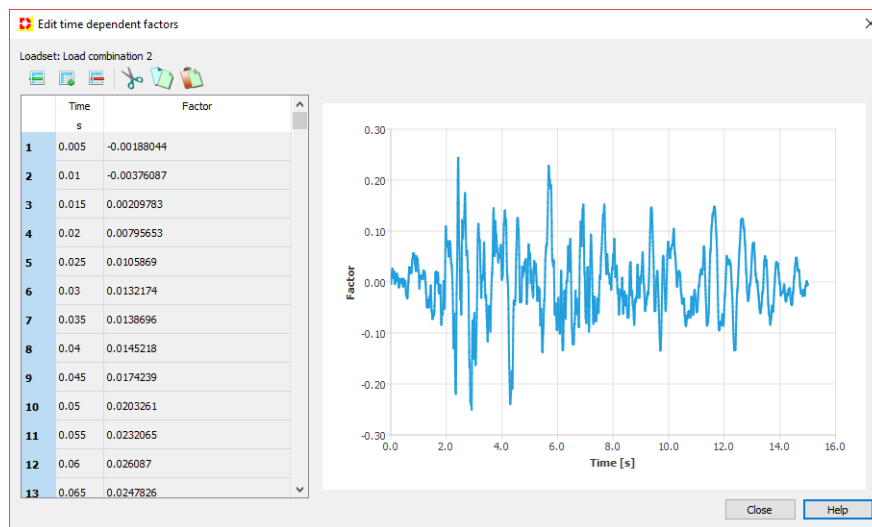
Figure 4.25: Base excitation with time history function (0.25g) applied in the FE model

4.1.5 Analysis

The analysis procedure that was executed in DIANA FEA, iterative methods, and the convergence tolerance that were applied are discussed in this section. The analysis procedure that was executed in DIANA FEA was a structural physically nonlinear

analysis with dynamic effects in order to execute the earthquake excitation load that was imposed.

Nonlinear analysis poses far more challenges than solving a system of equations in a linear elastic regime because there is not a unique solution procedure that is suitable for solving all nonlinear problems. For nonlinear analysis, an appropriate solution procedure must be selected. When the model definition is not suitable or the solution procedures are not properly chosen, convergence issues may arise in nonlinear analyses. Apart from that, convergence issues can arise because the iterative solution method is unable to find a solution for the nonlinear problem. So, the procedure of the completion of the nonlinear analysis was a time-consuming procedure and a lot of trial-and-error trials were executed in order to complete an entire nonlinear transient analysis of the model. When convergence difficulties are found in nonlinear structural analyses, usually the solution procedures must be updated to find a solution. In addition, the model set-up should be checked, since wrong or not appropriate modeling definitions (e.g., elements with connectivity issues, lack of support, etc.) may exacerbate the nonlinear analysis. There are many issues during the modeling (errors in boundary conditions, element coupling, irregular element shapes, etc.) which can be identified simply by performing a linear elastic analysis and others are exclusively related to the nonlinear analysis behavior itself (Kesio Palacio 2013).

Since the analysis that was executed in DIANA FEA was with transient effects, the consistent mass and damping matrix were calculated during the analysis with the Newmark time integration method (with Beta=0.25 and Gamma=0.5) in DIANA FEA. The Rayleigh damping a factor for the mass matrix and β factor for the stiffness matrix were calculated from the equations of Rayleigh damping equation in 4. The Rayleigh factors were calculated for ζ=0.25% and the initial and the final frequencies of the SERFIN frame were used for the calculation of the factors as F_i=2.56Hz and F_j=99Hz.

$$C= \alpha M+\beta K \tag{4}$$

$$\alpha=\zeta*(2\omega_i\omega_j / (\omega_i+\omega_j))$$

$$\beta=\zeta*(2 / (\omega_i+\omega_j))$$

The iterative method that was applied for the equilibrium iteration for both FE models was the secant (quasi-newton), which is an implicit algorithm iterative method applied in addition to the line search method.

The convergence tolerance and time step that were applied for the two FE models were not the same. For the first FE model, the convergence tolerance that was applied was 1% for force and displacement. The time-step for the transient analysis was set to 0.005 seconds and in total there were 3000 steps executed since the imposed earthquake load had a duration of 15 seconds. For the second FE model, which was more demanding in analysis, the convergence tolerance was 0.2% for both forces and displacements. The time-step for the transient analysis was set to 0.002 seconds, so 7500 steps were executed for the completion of the analysis. A very demanding analysis was necessary especially for the second FE model because of the fine generated mesh, the nonlinear transient analysis procedures, the interfaces, and the modeling of the dowels. The duration of the transient analysis for the first FE model took three hours to be completed and for the second FE model took seven to thirteen hours to be completed on a laptop computer with Intel® Core™i7-6700HQ CPU @ 2.60GHz 2.59GHz processor.

5 Numerical calibration

In order to validate the FE model that was developed as explained in Chapter 4, and use it for numerical experiments, the global results of the south wall of the SERFIN experiment were compared with the DIANA FE model results. Initially, the first FE model (model I) was calibrated to capture the global experimental results, and then the second FE model (model II) was calibrated to capture the local behavior of dowels. Furthermore, the main local results that were obtained during the experimental testing of the specimen are compared with the second FE model results. The comparison of the experimental results and the numerical results for the two FE models that are described in Chapters 3 and 4 are shown in Figures 5.1 to 5.7. The calibrated model II was used to perform the numerical experiments discussed in Chapter 6. This model is referred to as the 'Validated Model' in the following chapters. In this chapter, the numerical results are compared to the SERFIN experimental results of the south frame.

5.1 Global results comparison

The response history of the top-storey displacements of the frame is compared in Figure 5.1 and the response history of the base shear force of the frame is compared in Figure 5.2. Moreover, the top-storey displacement versus the base shear force is compared in Figure 5.3 in order to examine energy absorption and stiffness degradation of the model.
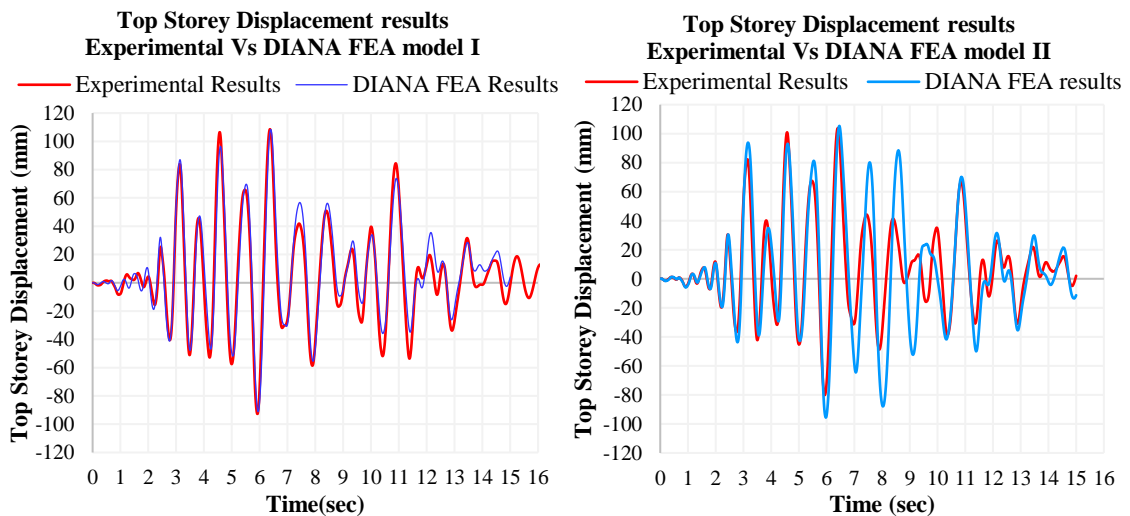
Figure 5.1: Fourth storey displacements versus time (FE model I and II in left and right graphs, respectively)
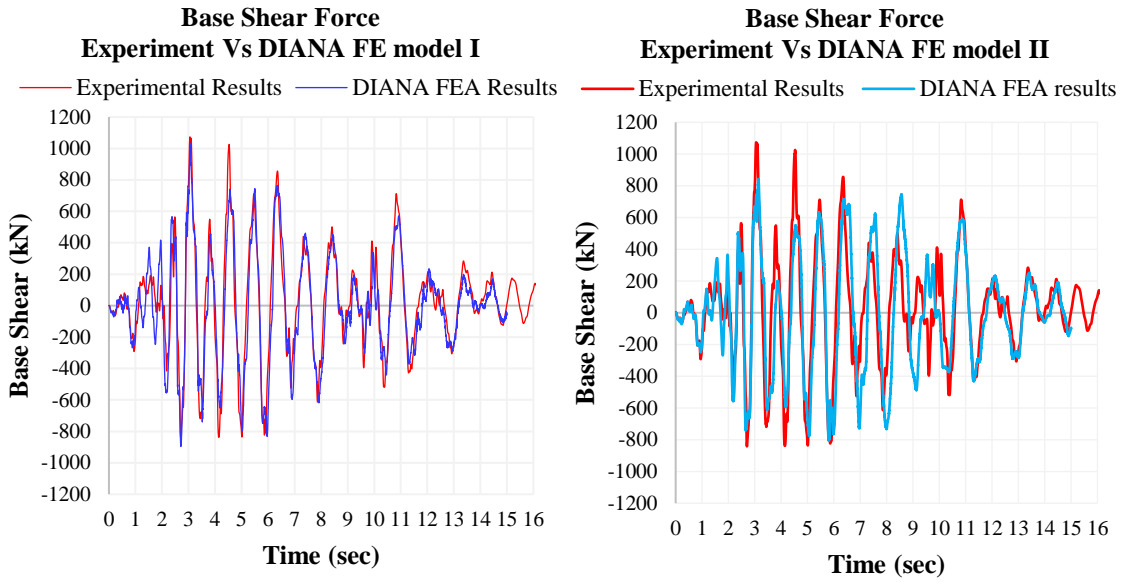
Figure 5.2: Base shear force versus time (FE model I and II in left and right graphs, respectively)
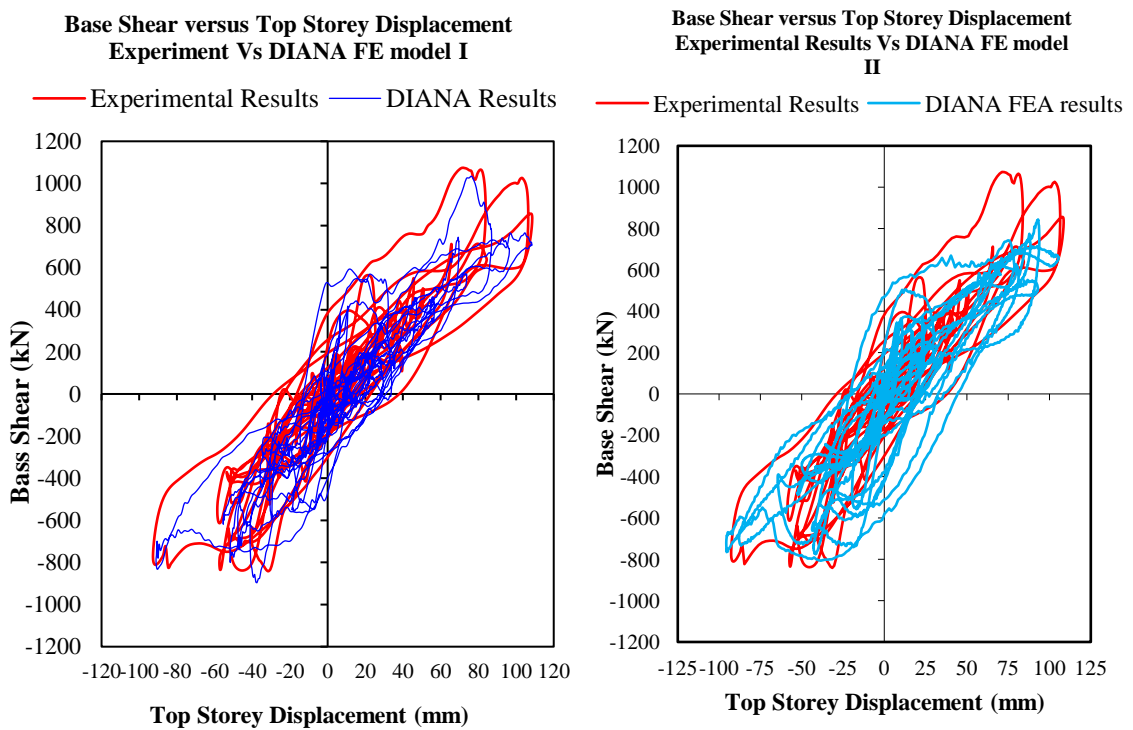
Figure 5.3: Base shear force versus top-storey displacement (FE model I and II in left and right graphs, respectively)

From the FE models global results, it is apparent that both FE models match the experimental results very well. As shown in Figures 5.1 and 5.2 the peak values are captured for both the forces and the displacements, and it is clear that the FE models

104

capture the frequency of the actual structure. In addition, the stiffness degradation is captured very well (Figure 5.3).

5.2   Local results comparison

In this section, the local results that were taken from the SERFIN specimen and discussed in section 3.6 are compared with the numerical results obtained from model II. The strain distribution on the ground floor columns of the wall (Figure 5.4) and the slip displacement on the ground beam (Figure 5.5) are compared with the numerical results. Moreover, from the experimental results, the main failures that occurred was the crack opening at the bottom of the column-wall in both sides of the wall and the failure of the east column at the bottom (see Chapter 3). These results are also compared with the DIANA FEA results in Figures 5.6 to 5.8.

As shown in Figures 5.4 and 5.5, the strain distribution on the bounding columns of the wall at the ground floor were captured in the FE model, as well as the slip in the middle of the ground beam of the wall.
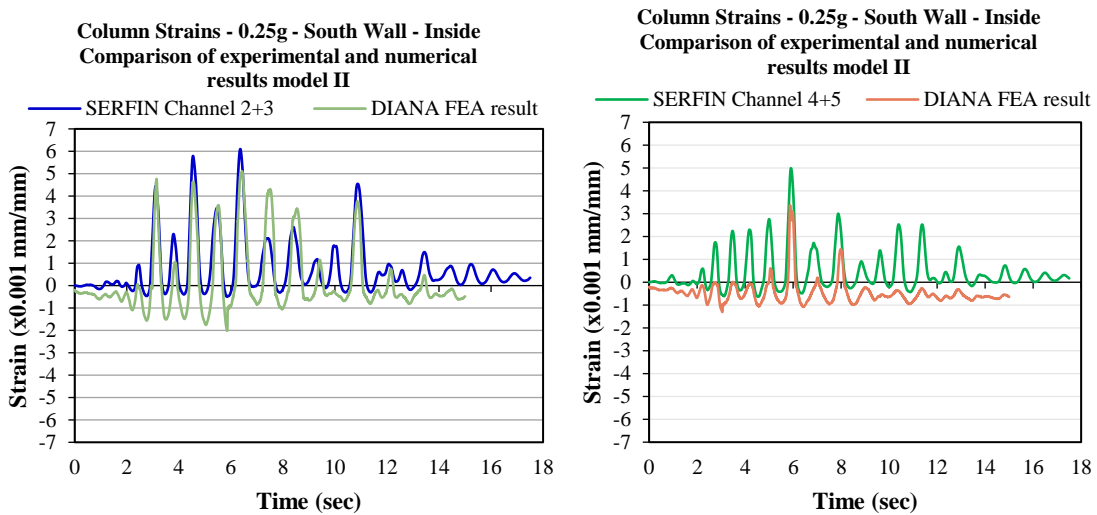
Figure 5.4: Strain distribution on the ground floor bounding columns of the wall comparison between the experimental and numerical results using model II

Beam (miidle) Slip - South Wall - Inside - 0.25g
Comparison of experimental and numerical results model II
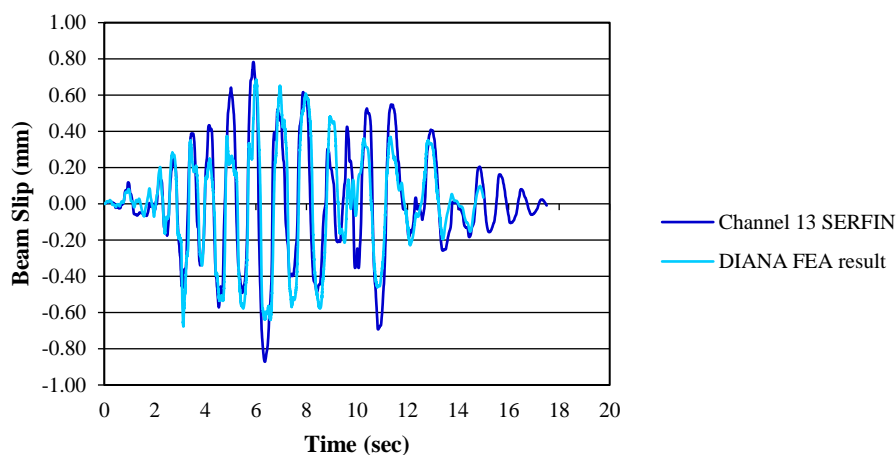
Figure 5.5: Slip in the middle of the ground beam comparison between the experimental and numerical results using model II

The hairline cracks that developed in the wall are also shown in Figure 5.6 in the FE model from the shear stress distribution results of the validated model. From the pictures of the shear stress distribution in Figure 5.6, the formation of the diagonal strut was also captured in both sides of the wall. Moreover, the crack that opened on the ground beam of the foundation at the base of the wall is captured in DIANA FE model in both sides of the wall as presented in Figure 5.7. Also, the tensile forces in the outer column at the east side of the frame were captured in the FE model as shown in Figure 5.8, where the tensile stress of concrete was reached in the east side of the column.
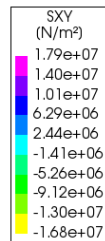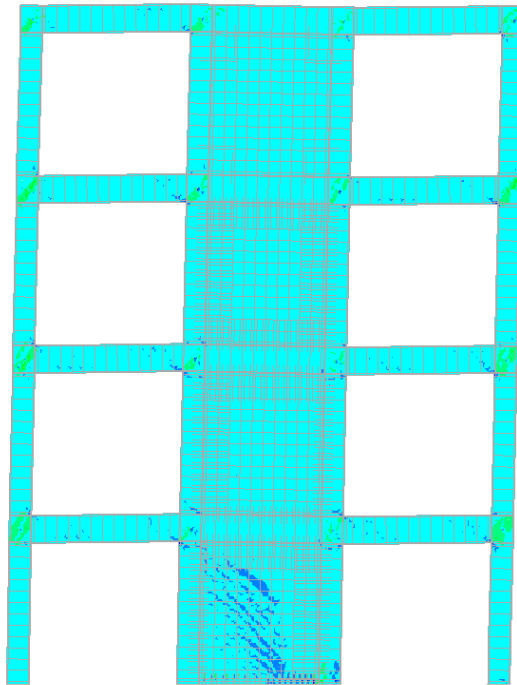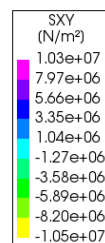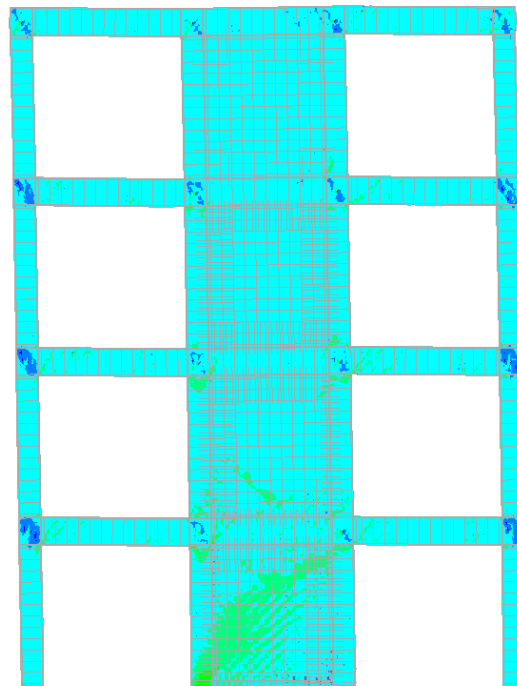
Figure 5.6: Shear stress distribution in the FE model at the maximum base shear in both directions
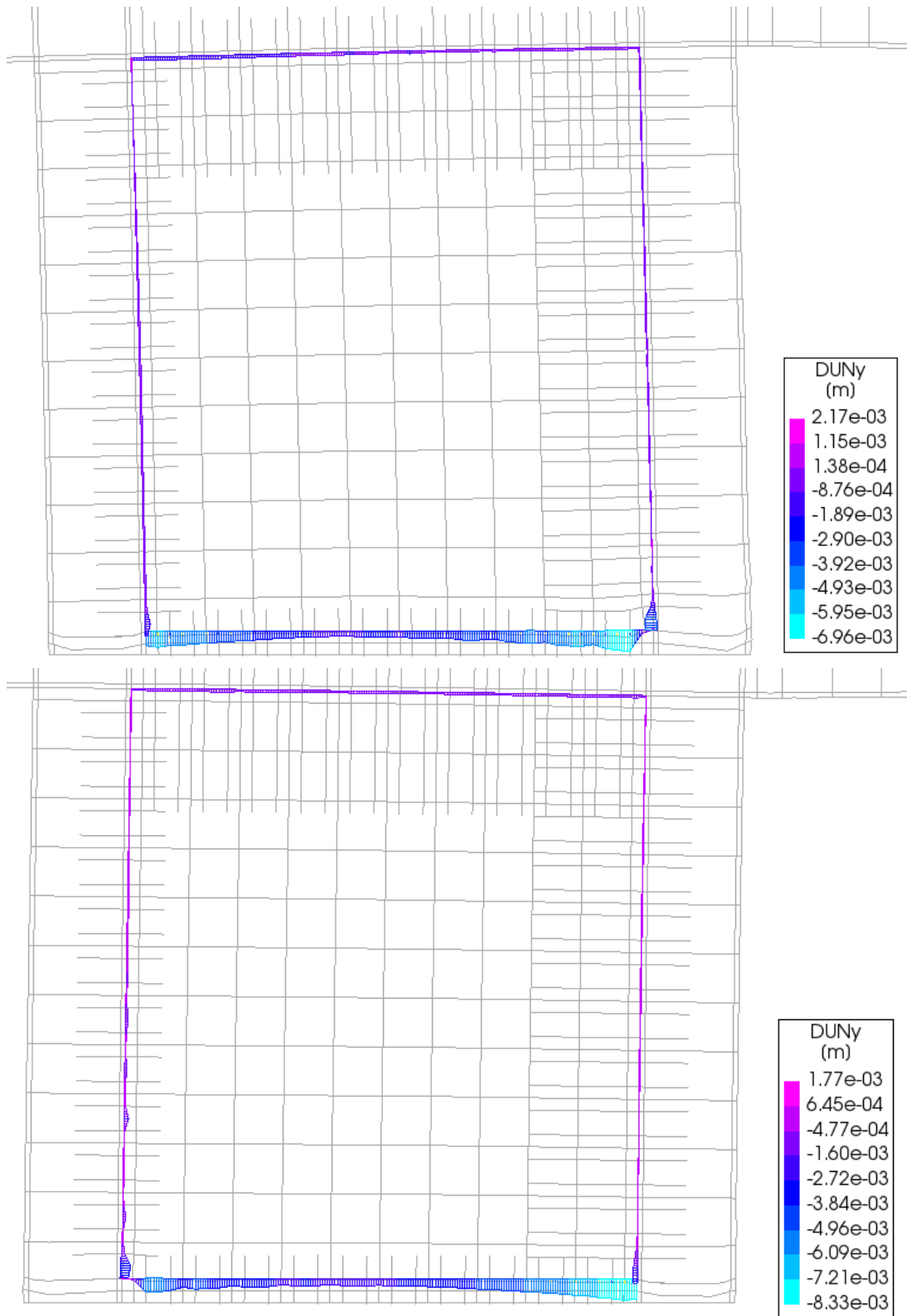
Figure 5.7: Opening at the base interface of the wall at maximum displacements of the frame in both directions

Figure 5.8: Tensile stress of 2.6MPa at 5.968seconds (maximum displacement of the frame in the west direction) at the east column of the frame

5.3 Summary

It is obvious that there is a good agreement between the real case study and the results of the 2D FE models, both model I and model II, despite the number of the influencing factors regarding the simulation and analysis. More specifically, the factors that influenced the simulation and analysis of the results of the model were the type of elements, the mesh, the material models capacity, the nonlinear time history analysis, the iteration methods, and the convergence criteria. It is important to mention that a very good calibration of the model was necessary regarding the nonlinear analysis parameters and methods and regarding the normal and shear stiffness modulus of the interface and bond-slip material models in order to get these results. This is because there are no clear values for these mechanisms since they are complicate, and their characteristics are difficult to measure in actual tests.

It can be concluded that the aim of developing a reliable model of RC infills and its interaction with the surrounding frame through the dowel action and starter bars contribution at the interface was achieved by the FE models presented in this section, but in particular by model II, which was proved to be able to capture not only the global

response as did model I, but also the local response of the infilled frame. Consequently, this validated model of RC infills (model II) could be used to study the configurations with reduced number of dowels to complement the experimental results and to study the interaction between RC infills and bounding frame both in the local and global level.

6   Numerical simulations through a parametric study

After the model calibration, numerical simulations were performed by varying the number and the arrangement of dowels connecting the wall to the bounding frame. A parametric study was performed that covers a range between monolithic behavior and that of a non-integral infilled frame and is presented in this Chapter. In this way, the experimental results of the SERFIN project were complemented through the numerical experiments. In this way, the interaction between the RC infills and the bounding frame both in the local and global level could be studied further.

The validated model that was calibrated in DIANA FEA (in Chapter 5), had the same number of dowels as the SERFIN experiment (24 dowels connecting the wall to the columns and 20 dowels connecting the wall to the beams). It was then decided to perform another eight different cases of the number of dowels in the model. These parametric-study scenarios are shown in Table 6.1. In Table 6.1, the name of each case scenario is shown in the first row of the table, which is the number of dowels connecting the wall to the beams of the frame. Also, in Table 6.1, the number, the diameter, the spacing and the area of all the dowels that are connecting the wall to the bounding columns and beams are presented for all the floor levels of the frames. For the last case scenario (Case 8), where there are no dowels in the model, the only connection between the new infill wall and the existing frame members is the cohesion between the two interfaces.

Table 6.1: Case scenarios for parametric study

Case scenarios		Case 1 Validated model		Case 2 13 Dowels connecting the beams		Case 3 10 Dowels connecting the beams		Case 4 6 Dowels connecting the beams	
Number, diameter, spacing and area of dowels connecting the wall to the bounding frame									
1st storey	Columns	24Y20/**100**	7539.8cm²	16Y20/**150**	5026.5cm²	12Y20/**200**	3769.9cm²	8Y20/300	2513.3cm²
	Beams	20Y20/**100**	6283.2cm²	13Y20/**150**	4084.1cm²	10Y20/**200**	3141.6cm²	6Y20/300	1884.96cm²
2nd storey	Columns	24Y18/100	5089.4cm²	16Y18/150	4071.5cm²	12Y18/200	3053.6cm²	8Y18/300	2035.8cm²
	Beams	20Y18/100	5089.4cm²	13Y18/150	3308.1cm²	10Y18/200	2544.7cm²	6Y18/300	1526.8cm²
3rd storey	Columns	24Y16/100	4021.2cm²	16Y16/150	3217cm²	12Y16/200	2412.7cm²	8Y16/300	1608.5cm²
	Beams	20Y16/100	4021.2cm²	13Y16/150	2613.8cm²	10Y16/200	2010.6cm²	6Y16/380	1206.4cm²

4th storey	Columns	2Y16	402.1cm²	2Y16	402.1cm²	2Y16	402.1cm²	2Y16	402.1cm²
	Beams	2Y16	402.1cm²	2Y16	402.1cm²	2Y16	402.1cm²	2Y16	402.1cm²

Table 6.1 (cont.): Case scenarios for parametric study

Case scenarios		Case 5 4 Dowels connecting the beams		Case 6 2 Dowels		Case 7 2 Dowels only on beams		Case 8 No Dowels	
Number, diameter, spacing and area of dowels connecting the wall to the bounding frame									
1st storey	Columns	5Y20/**500**	1570.8cm²	2Y20	628.3cm²	-	-	-	-
	Beams	4Y20/**500**	1256.6cm²	2Y20	628.3cm²	2Y20	628.3cm²	-	-
2nd storey	Columns	5Y18/500	1272.3cm²	2Y18/	508.9cm²	-	-	-	-
	Beams	4Y18/500	1017.9cm²	2Y18	508.9cm²	2Y18	508.9cm²	-	-
3rd storey	Columns	5Y16/500	1005.3cm²	2Y16	402.1cm²	-	-	-	-
	Beams	4Y16/500	804.2cm²	2Y16	402.1cm²	2Y16	402.1cm²	-	-
4th storey	Columns	2Y16	402.1cm²	2Y16	402.1cm²	-	-	-	-
	Beams	2Y16	402.1cm²	2Y16	402.1cm²	2Y16	402.1cm²	-	-

The nonlinear dynamic analysis procedure that was followed was the same for all the case scenarios and it has been explained in Chapter 4. The time-history of an earthquake record with peak acceleration of 0.25g was used for all the parametric-study scenarios and the results of the parametric study are illustrated and analyzed in the following sections.

6.1 Global numerical results of the parametric study

In this section, the global results from the parametric study of the effect of the number of dowels are illustrated and discussed. More specifically, the number and therefore the distance between dowels at the interface between the existing frame and the new wall is examined in order to capture the effect of dowel action. The results with positive values in the graphs in the following sections are the ones that represent the behavior of the frame while it is moving towards the reaction wall (east direction) and the ones with negative

values are the results when the frame is moving away from the reaction wall (west direction).

The eigenvalue analysis results, the displacements, the inter-storey drift (ISD) and the shear forces of the building, the moments at the base of the frame members and the axial and shear forces of the dowels are presented and discussed in the following sections for all the case scenarios that were performed. Furthermore, the correlation of these results to the total area of the provided dowel reinforcement and to the spacing of the dowels is examined and some conclusions are drawn. Eventually, some preliminary design recommendations are considered regarding the effect of the dowels for the strengthening of existing structures with RC infills within existing frames.

6.1.1 Eigenvalue analysis

The eigen value analysis was executed for the validated model in order to verify the FE model total mass, which consist of the self-weight of half the SERFIN specimen and the dead loads that were applied on it (total mass of half of the SERFIN specimen is 312 tons). Then, the fundamental frequency f_n of the FE frame was compared with the fundamental frequency that was obtained from the analysis of the same frame in Cast3M in Kyriakides *et al.*, 2015. The eigen value analysis was executed for the first four eigenmodes and the corresponding eigenfrequencies are presented in this section for all the case scenarios.

The fundamental period T_n and fundamental frequency of the building for the first four eigenmodes are presented in Table 6.2 for all the case scenarios examined. As it is shown, the fundamental frequency and the stiffness of the building is reduced with the reduction of the number of dowels, and consequently its fundamental period is increased. It is interesting to note that for the eighth case scenario, in which there are no dowels, the fundamental period increases considerably compared to cases 6 and 7 in which two dowels on columns and beams, and two dowels on beams are used, respectively. This indicates that it is beneficial to use even two dowels to connect the wall to the beams instead of having no dowels at all.

Table 6.2: Eigen value analysis results for parametric cases

First eigenmode   Second eigenmode   Third eigenmode   Fourth eigenmode
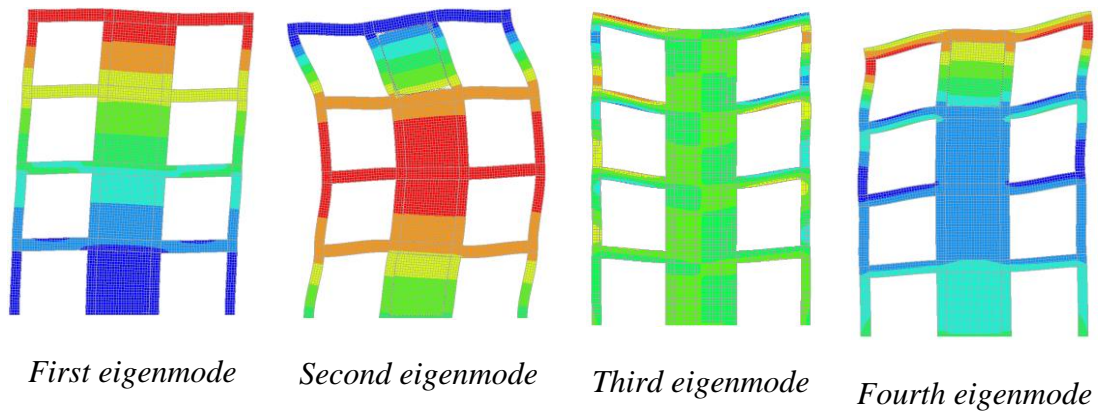
Case
scenario

	f_1 (Hz)	T_1 (sec)	f_2 (Hz)	T_2 (sec)	f_3 (Hz)	T_3 (sec)	f_4 (Hz)	T_4 (sec)
1	2.3507	0.4254	7.9601	0.1256	10.185	0.0982	10.392	0.0962
2	2.3135	0.4322	7.8094	0.1281	10.176	0.0983	10.383	0.0963
3	2.2868	0.4373	7.6862	0.1301	10.168	0.0983	10.377	0.0964
4	2.1593	0.4631	7.1871	0.1391	10.129	0.0987	10.351	0.0966
5	2.0906	0.4783	6.8699	0.1456	10.096	0.0990	10.331	0.0968
6	1.9315	0.5177	6.2080	0.1611	10.002	0.0999	10.234	0.0977
7	1.5393	0.6496	4.6214	0.2164	7.6804	0.1302	9.6421	0.1037
8	0.18835	5.3093	0.18844	5.3067	0.18844	5.3067	0.18844	5.3067

6.1.2   Top storey displacements

The top storey displacements of the frames are illustrated for all the case scenarios in Figure 6.1. In each graph, two cases are presented for a better comparison between the cases.

From these results, it is shown that the top-storey displacement for the first five case scenarios is about the same. When the dowels are reduced to two, in the sixth case scenario, it is illustrated that there is a permanent deformation in the east direction since

the oscillation of the frame remains in the positive side of the graph after the peak value of the top-storey displacement at about 6 seconds. For the seventh case scenario, two dowels connecting only the beams of the surrounding frame to the RC infill wall, the top-storey displacement is increased during the analysis. This is an indication that the building is less stiff in this case, which is evident from Figure 6.1 and as a result, the deformations of the building are higher. Moreover, for the eighth case scenario, it is displayed that the top-storey displacement is increased relative to the previous case scenarios.

Moreover, from Figure 6.1, it is observed that the elastic characteristics of the frame have changed with the reduction of the number of dowels after the sixth case scenario. This is an indication that the stiffness and the fundamental frequency of the frame are reduced, with the reduction of the dowels. It is also noteworthy to mention that even with just two dowels connecting the wall to the bounding frame (seventh case scenario) the displacements of the building are significantly decreased in comparison to the eighth case scenario, in which case we have just an infilled frame. This is consistent with the observation made regarding the fundamental period of the frames in the previous section.

From these results, it can be concluded that the top-storey displacement of the frame is about the same in both directions for the first five case scenarios. The deformations then increase, with the eighth case scenario having considerably larger deformations. The permanent deformation of the frame in one direction is obvious for the fifth and sixth case scenarios while this vanishes for the seventh and eighth one. From the waveform the change of the fundamental characteristics of the frame are observed after the sixth case scenario.
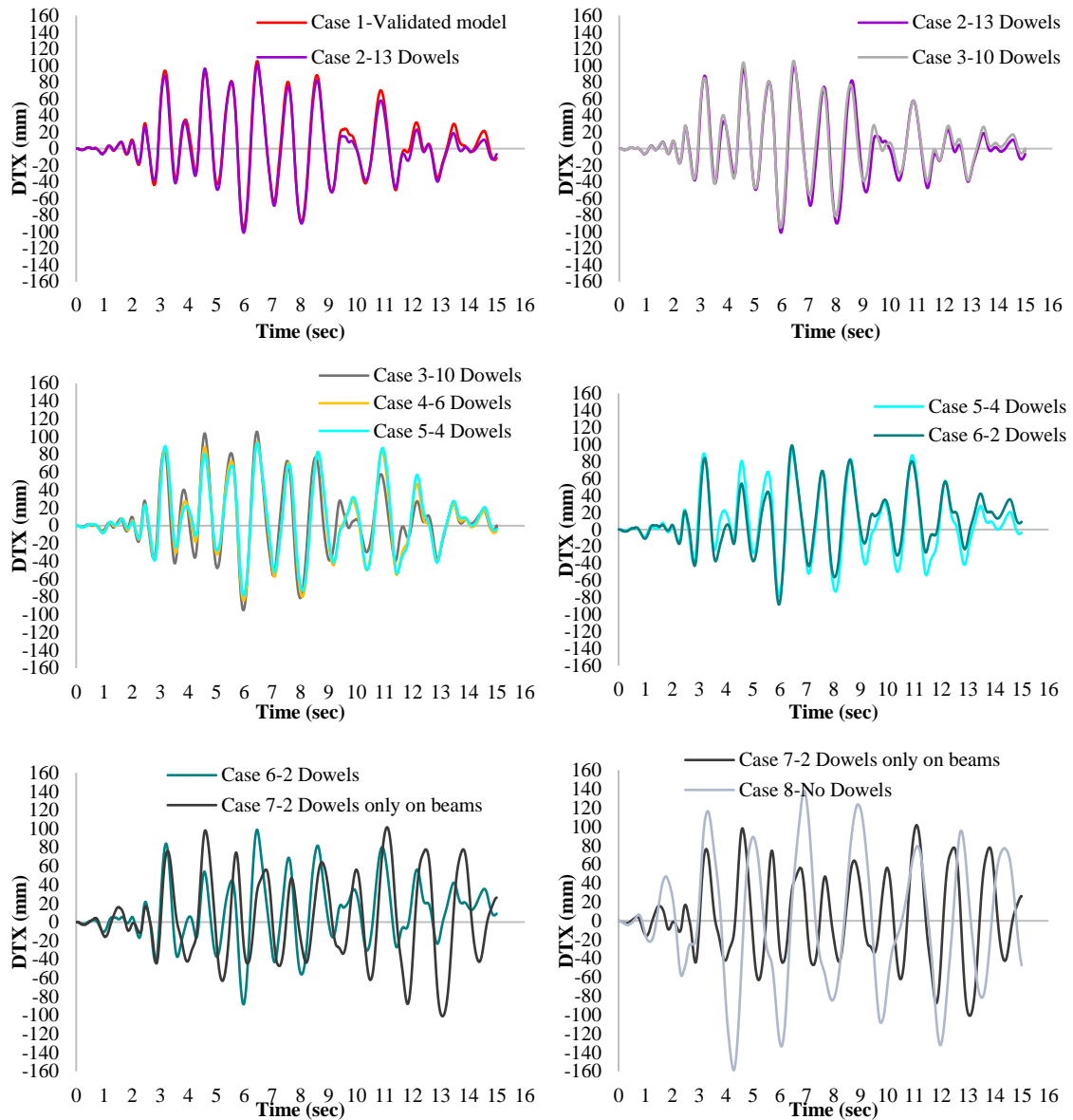
Figure 6.1: Top-storey displacement for all case scenarios

6.1.3   Inter-storey drift results

The inter-storey drifts (ISDs) for each case scenario are presented in Figure 2 for all the storeys of the frame. The comparisons of ISD results between the case scenarios are shown in Figures 6.3 to 6.6. In each graph, two cases are presented for a better comparison between the cases.

In general, the ISDs of the first storey of the frame (level 1 in Figure 6.2) are the largest and for the fourth storey of the frame are the smallest for the first five cases. For the sixth and seventh cases, the ISD of the first storey is lower than that of the upper storeys of the

frame, while for the eighth case there is no consistency in the comparison of the ISD of the various storeys.

In the first four case scenarios, the ISDs are fluctuating between 30mm in both directions. On the other hand, for the fifth and sixth case scenarios the nonlinearities started to be apparent as it is shown in Figure 6.2 where permanent displacements appear to occur in the end of the response history. For the seventh and eighth cases, these nonlinearities disappear. These results present that the frame has permanent deformations in the east direction, for the cases mentioned above, after the peak displacements at around 6.4 seconds. In addition, from the waveforms of the last two case scenarios, it is obvious that the dynamic characteristics of the frame have changed and there is a different behavior of the frame from the beginning of the analysis.

The ISD of the fourth storey is displayed for all the case scenarios in Figure 6.3. From the comparison of the five first cases, it is shown that the ISD remains at the same levels. In the sixth case scenario, the ISD of the fourth storey of the frame is reduced at some points in relation to the previous cases and after the peak values at around 6 seconds the oscillation of the fourth storey of the frame is only in the east direction (positive values of the graph). This is an additional indication that the deformations of the frame are permanent in the east direction of the frame in the sixth case scenario. For the seventh case scenario, there is an obvious change of the ISD of the fourth storey of the frame relative to the previous cases. In that case, it is illustrated that the ISD of the fourth storey of the frame is higher than the previous cases after about 3seconds of the response history. Furthermore, once again it is illustrated that the dynamic characteristics of the frame have changed in this case, with the frame being less stiff. For the last case scenario, the ISD of the fourth storey of the frame is increased in relation to all the previous cases and the dynamic characteristics of the frame are changed.
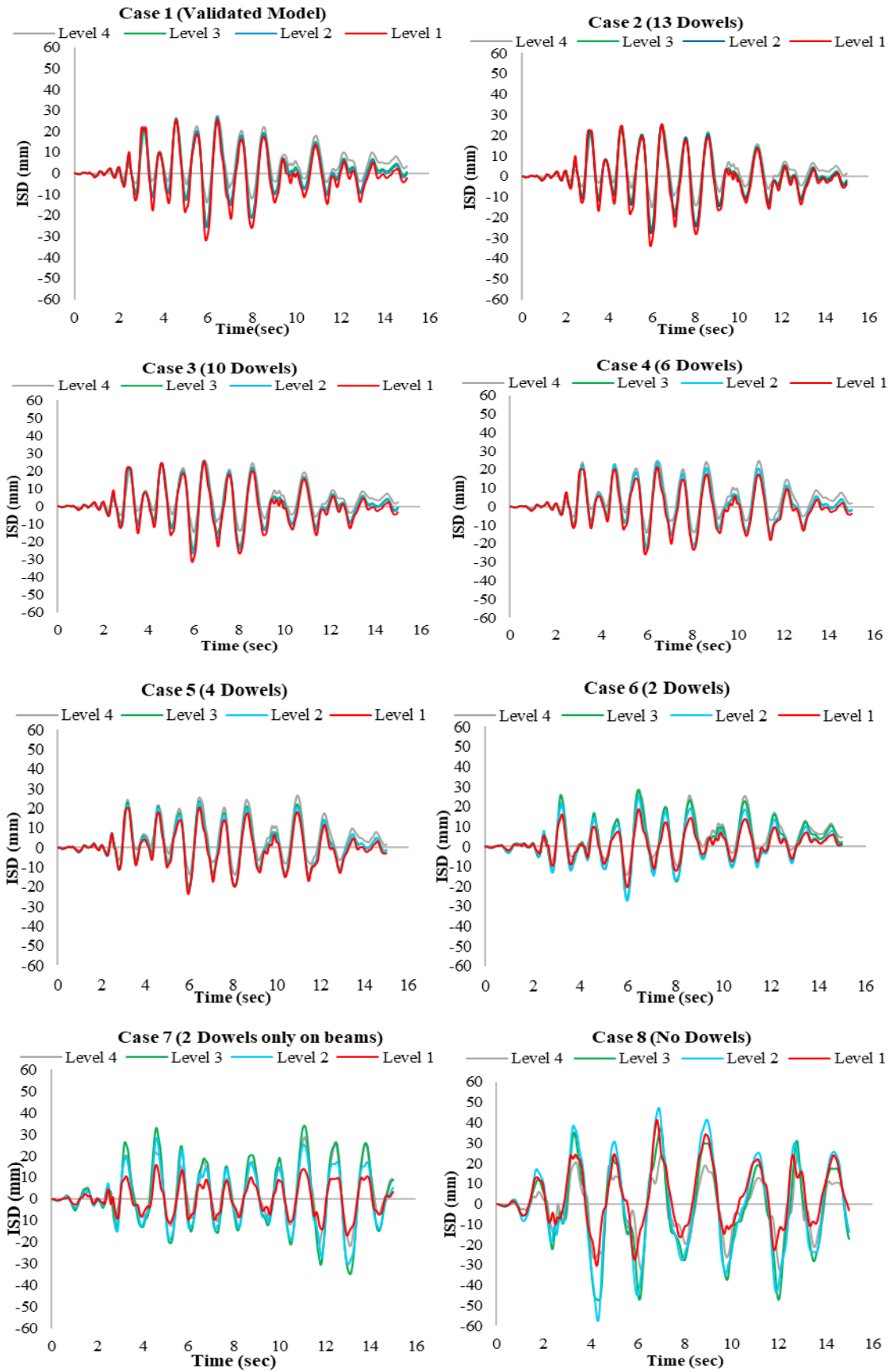
Figure 6.2: Inter storey drifts for all case scenarios

118
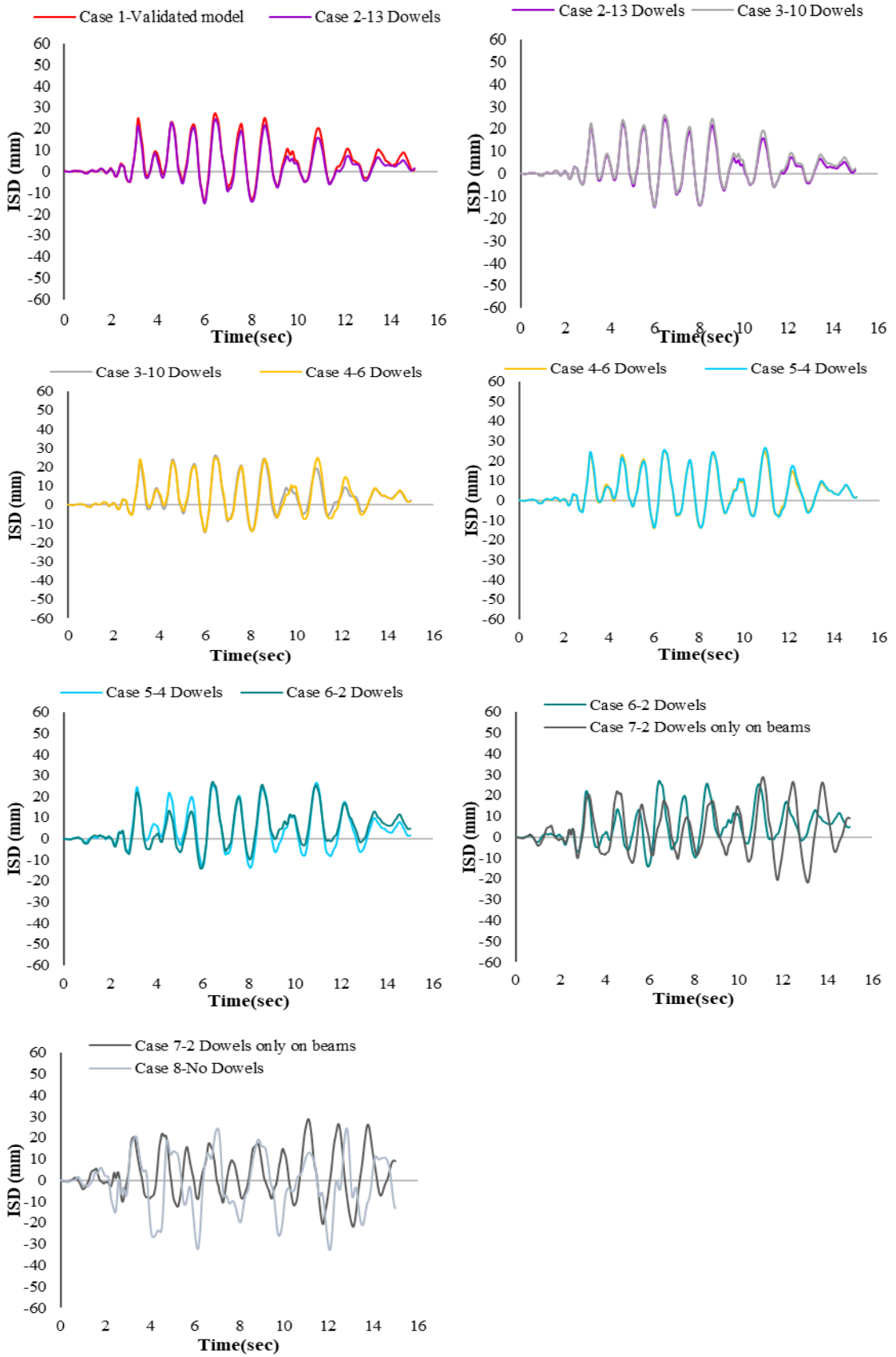
Figure 6.3: Inter storey drift of the fourth storey for all case scenarios

The comparison of the ISD of the third storey of the frame is displayed for all the case scenarios in Figure 6.4. The observations that were made from these graphs are the same as for the ISDs of the fourth storey of the frame. However, the increase of the ISD of the third storey of the frame is higher for the last two case scenarios in comparison to the increase of the ISD of the fourth storey of the frame for the last two case scenarios in Figure 6.2.
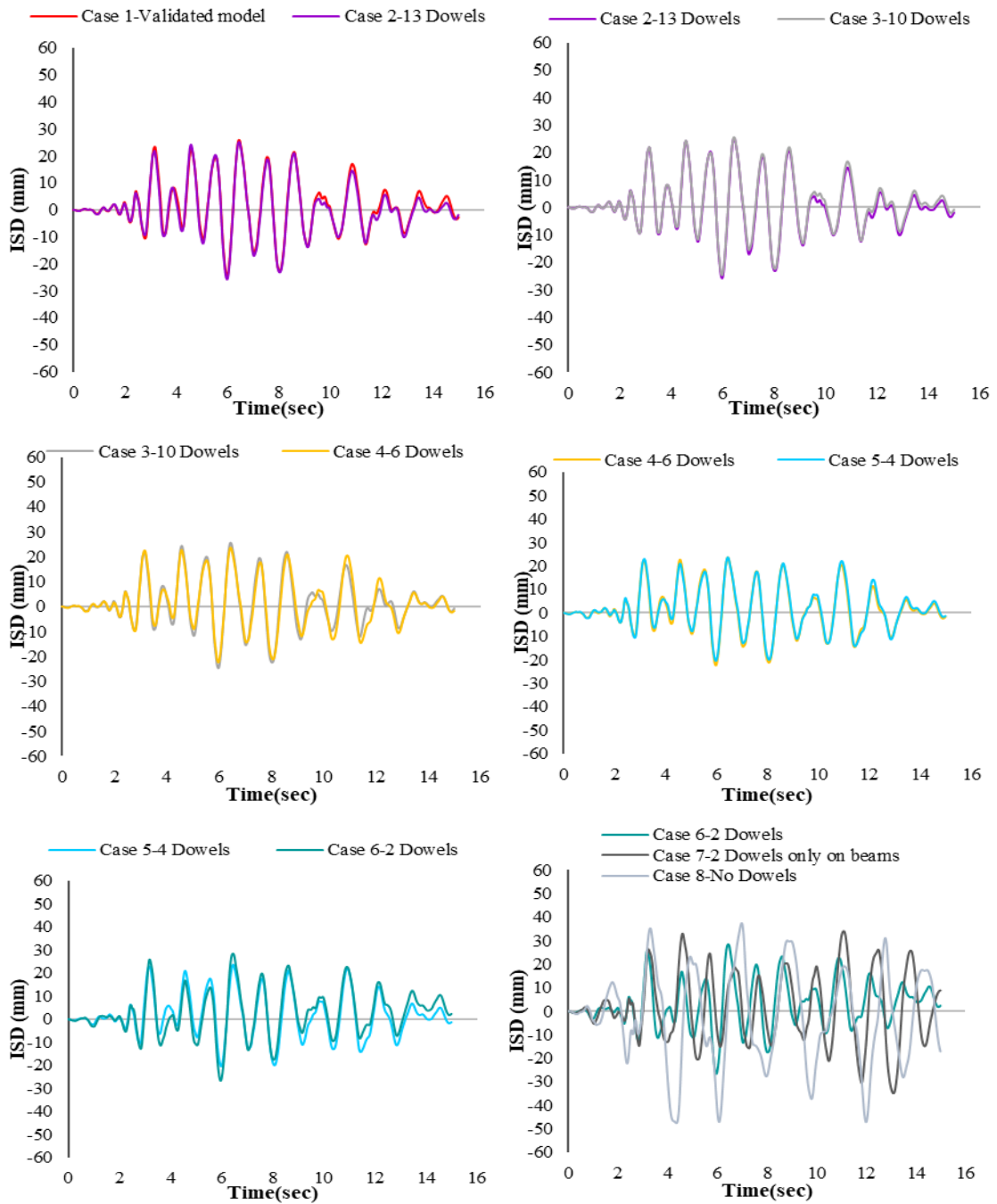
Figure 6.4: Inter storey drift of the third storey for all case scenarios

The ISDs of the second and first storeys of the frame are presented in Figures 6.5 and 6.6, respectively. The same observations with the ISDs of the third storey of the frame (Figure 6.4) are shown. It is observed that, for the second storey of the frame, the increase of the ISD is larger than the upper floor levels of the frame in the sixth case scenario. Moreover, the ISD of the second storey of the frame in the fourth case scenario is larger compared to the fifth case scenario. This was not observed in the upper storeys of the frames between the fourth and fifth case scenarios (Figures 6.2 to 6.4).
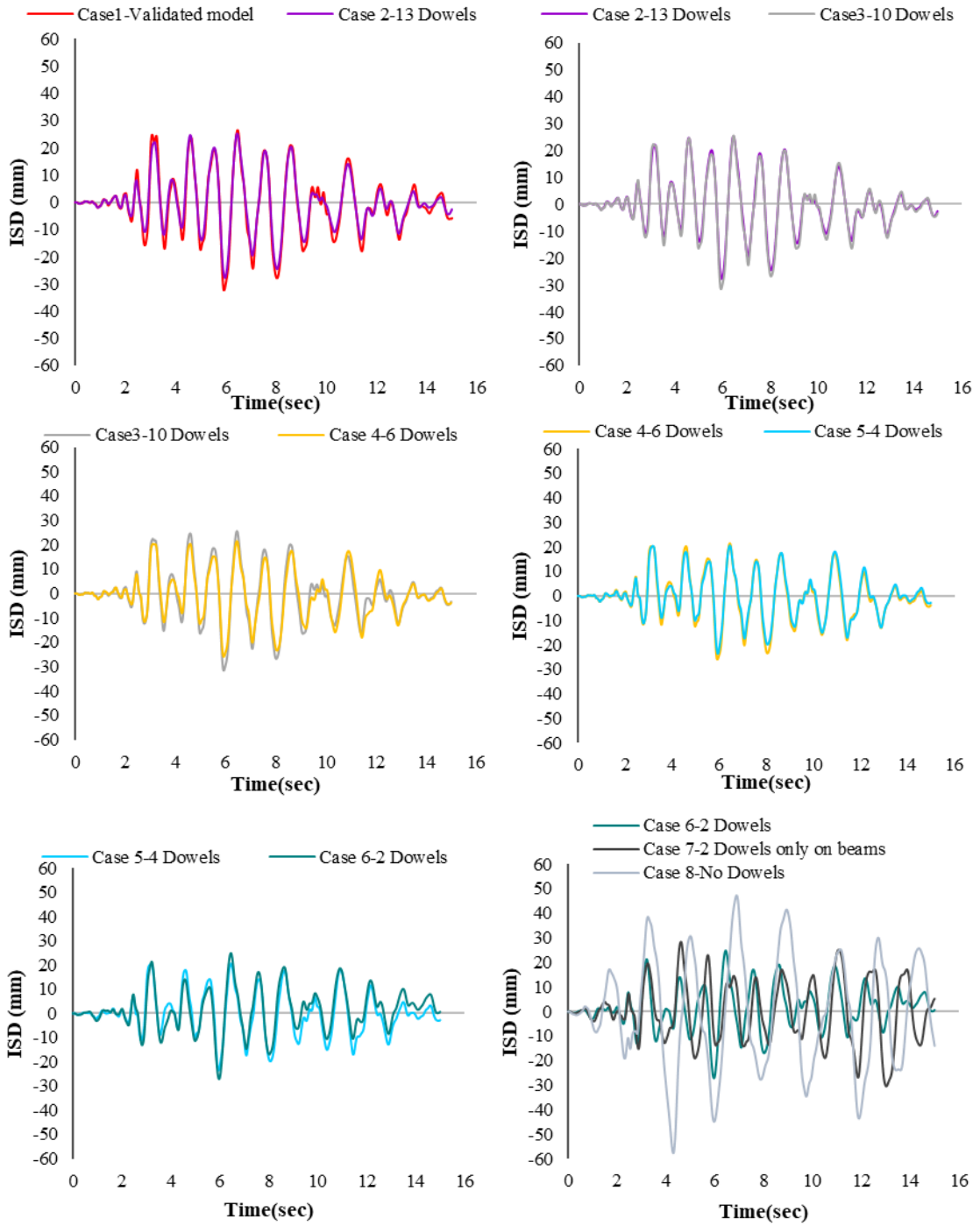
Figure 6.5: Inter storey drift of the second level for all case scenarios
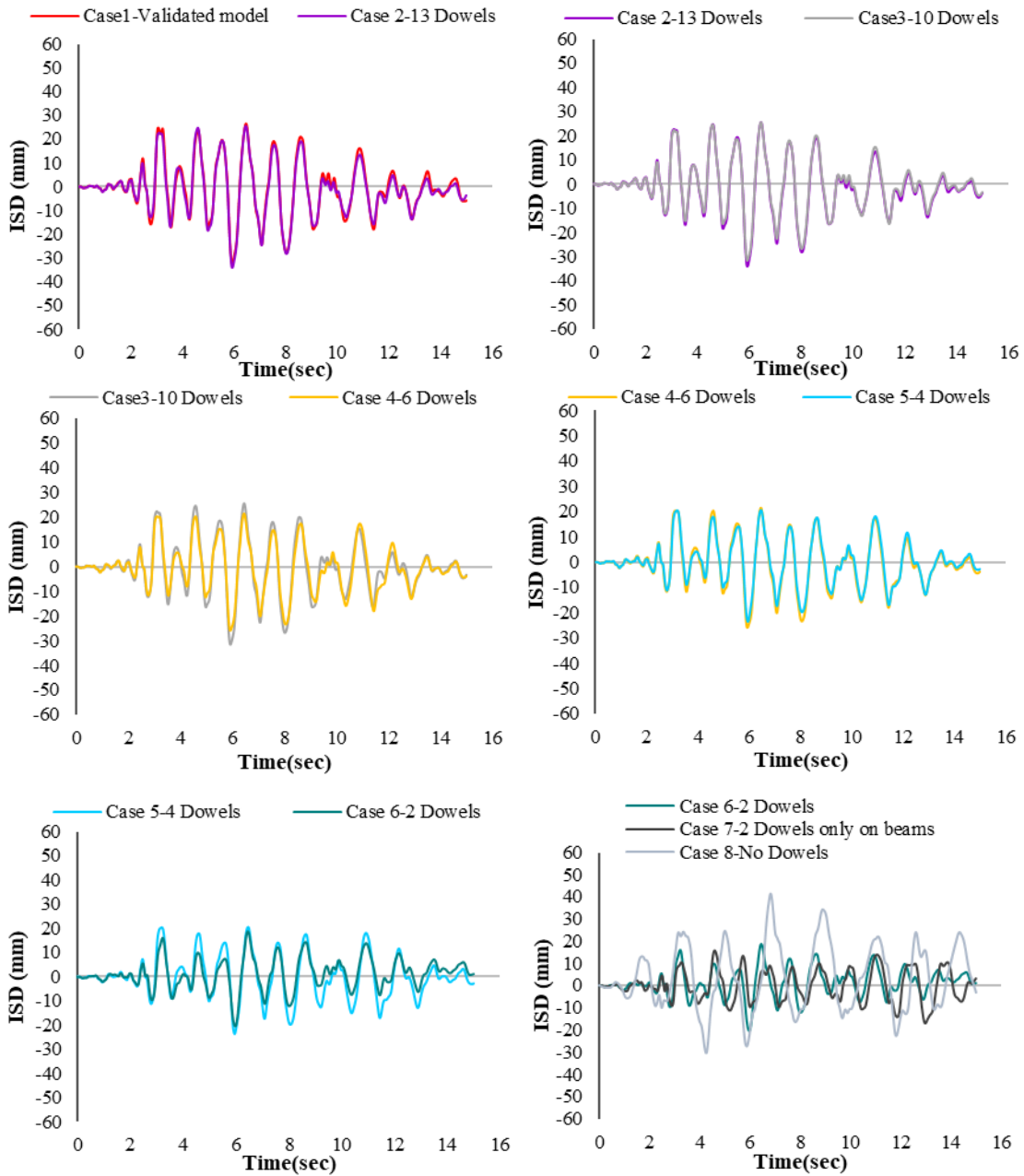
Figure 6.6: Inter storey drift of the first storey for all case scenarios

Overall, from the ISD results of the frames, it is shown that the frame suffered some permanent deformations in the east direction after the peak displacements of the frame at about 6.4 seconds at all floor storeys after the fifth case scenario. In addition, it is observed that for the fourth storey of the frame (that is connected by two dowels per side of the wall for all cases), the permanent deformations are apparent for all the case scenarios. Consequently, the reduction of the number of dowels to two dowels per side of the wall leads to permanent deformations at all floor levels after a peak of such an earthquake

signal as the one used in this analysis. It is also shown that the lower the floor level the larger the displacement are. This observation verifies that at the lower storeys the shear is larger and causes larger deformations, which gradually migrate to the upper floors. Moreover, the change of the dynamic characteristics of the frame, as indicated from the waveform in Figures 6.2 to 6.6, is obvious after the sixth case scenario.

6.1.4 Base shear force results

The shear forces at the base of the frame were calculated from the numerical analyses and they are illustrated and discussed in this section. The base-shear force of the frame models and the distribution of this shear force to the members of the frame that resulted from the response-history analysis is presented and discussed. Additionally, the base-shear force of the frame versus the top-storey displacement as well as the shear force of each member at the base of the frame versus the first-storey displacement are presented and discussed.

The base-shear force for each case scenario model was calculated by adding the shear forces of all the frame members at the base of the frame. More specifically, the presented results of the shear at the base of the frame in the following paragraphs concern the four columns of the frame and the wall with the dowels. These members are shown in Figure 6.7 for the first storey. The two outer columns of the frame are displayed as C11 (west side outer column of the frame) and as C14 (east side outer column of the frame). The two columns bounding the wall are illustrated as C12 (west bounding column) and as C13 (east bounding column).
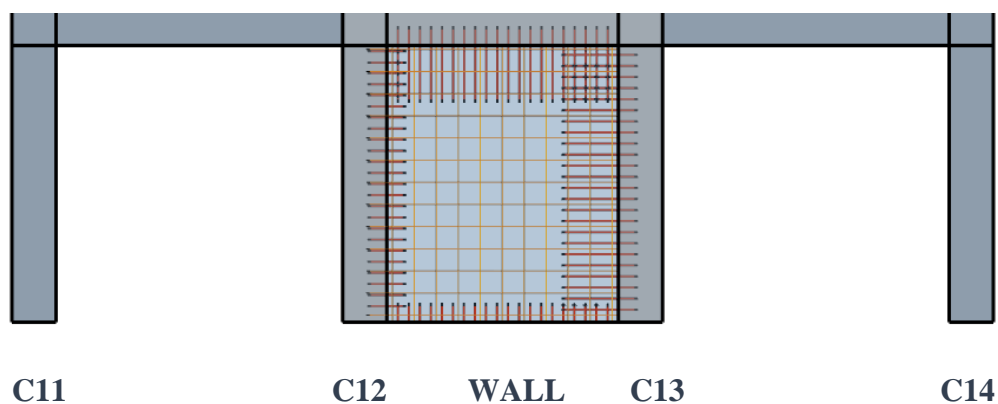
Figure 6.7: Inter storey drift of the first storey for all case scenarios

6.1.4.1 Total base-shear force response-history

The response-history of the shear forces at the base of the frame for the eight case scenarios are displayed and discussed in this section. In Figure 6.8, the total base shear force is illustrated for all the case scenarios.
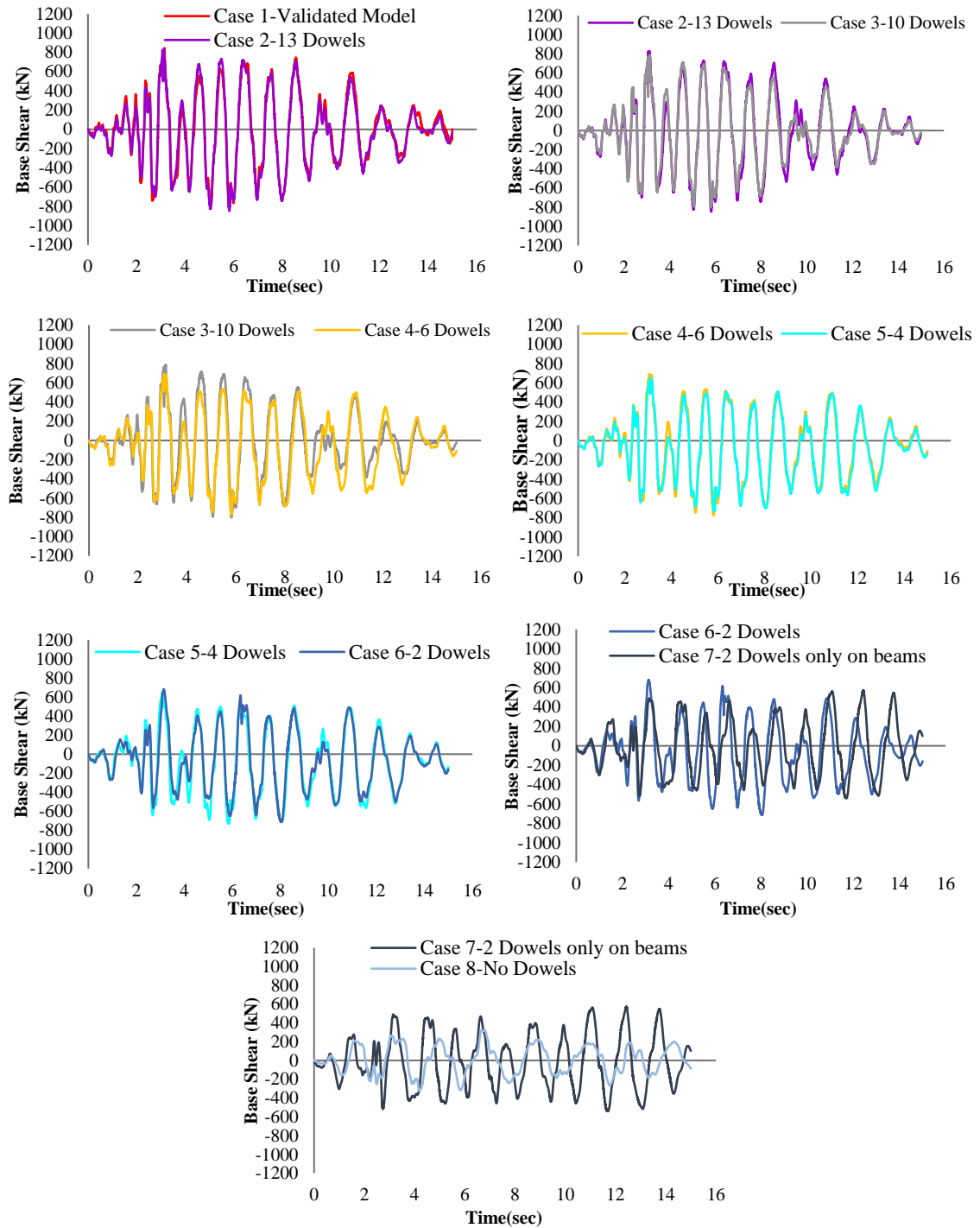
Figure 6.8: Base-shear force for all case scenarios

For the first two case scenarios, the total base shear force of the frame is about the same. There is a reduction of the base shear force when the dowels are reduced to half of that of the first case, in the third case. For the fourth case, the base shear is reduced up to the ninth second and after that there is an increase compared to the second case. The base shear for the fourth, fifth and sixth case scenarios is about the same. For the seventh case scenario, where the dowels connecting the bounding columns to the wall were removed, there is a reduction of the base shear up to the ninth second and after that there is a considerable increase. For the last case, with no dowels, the base shear is reduced considerably.

A general trend that was observed is that the lower the number of dowels, the lower the base shear.

6.1.4.2 *Base shear forces of members response-history*

The response history of the shear force at the base of the outer columns (C11, C14) of the frame is illustrated separately in this section for all the case scenarios in Figures 6.9 and 6.10. In addition, the response history of the shear at the base of the wall (which includes the contributions of column C12, the wall with dowels, and column C13 and it applies for all the instances that "wall" is referred to in the next sections), is presented in Figure 6.11 for all the cases. Moreover, the shear capacity of the frame members was calculated according to EC8-3 (equations A.12 and A.15) and it is compared with the analysis results that are examined in this section.

The response history of the shear force at the base of the west outer column of the frame (C11) is illustrated in Figure 6.9 for all the case scenarios. From these graphs, it can be observed that the base shear at the base of C11 is higher when the structure is moving towards the west side (negative values). The behaviour of this column is about the same for the first five cases. The maximum base shear force for this column is about 95kN and the minimum about 50kN for all the case scenarios as presented in Figure 6.9. This shear force is near the shear capacity of this column that was calculated according to the equation A.12 of EC8-3 for all the cases (about 113 kN at the maximum base shear of the frame, for 275mm compression zone depth and 1141kN axial force). For the sixth case scenario, there is a reduction of the shear force of this column in the west direction after about 7 seconds and for the seventh and eighth case scenarios, the base shear force response history at the base of these columns is different compared to the previous cases.

The response history of the shear force at the base of the east outer column of the frame (C14) is presented in Figure 6.10 for all the cases. These graphs demonstrate that unlike column C11 column C14 receives higher shear when the structue is moving towards the east direction (positive values). The behavior of this column is about the same for the first five cases, as in the case of C11. The maximum base shear force for this column is about 98kN and the minimum about 50kN in all cases as displayed in Figure 6.10 and these values are lower than the shear strength of this column that was calculated to be about 153kN (at the maximum base shear of the frame, for 175mm compression zone and 1246kN axial force) according to EC8-3.For the sixth case scenario there is a slight reduction of the shear force of this column when the structure moves in the east direction and for the seventh and eighth case scenarios, the shear forces vary between positive 80kN and negative 60 kN and are more symmetric about the zero axis.

Generally, it can be concluded that both outer columns of the frame are near their shear capacity even from the first case scenario and they take a maximum laod of about 95kN. Their behavior is about the same for the cases 1 to 6 with C11 taking the higher shear when the structure is moving towards the west and C14 when the structures is moving towards the east. The behavior of the columns is modified for cases 7 and 8 when their response become more symmetrical about the zero axis and the loads very between 80 and 60 kN.

The shear force at the base of the wall is presented in Figure 6.11 for all the case scenarios. As shown in these graphs, in the third case scenario, the wall reaches reduced shear forces after the first positive peak value at about 3 seconds relative to the first two case scenarios. Then, for the next cases, the wall gradually reaches lower shear values, and this reduction is more obvious in the sixth case scenario. For the last case scenario, it is shown that the contribution of the wall to shear is very small since it is not connected to the bounding frame and it behaves as an infilled frame. Moreover, it is shown that for all cases the base shear for the wall is lower than 750kN. The calculated maximum shear strength of this wall is 1978kN according to equation A.15 of EC8-3. Therefore, the wall in the model does not reach its shear capacity in any of the case.
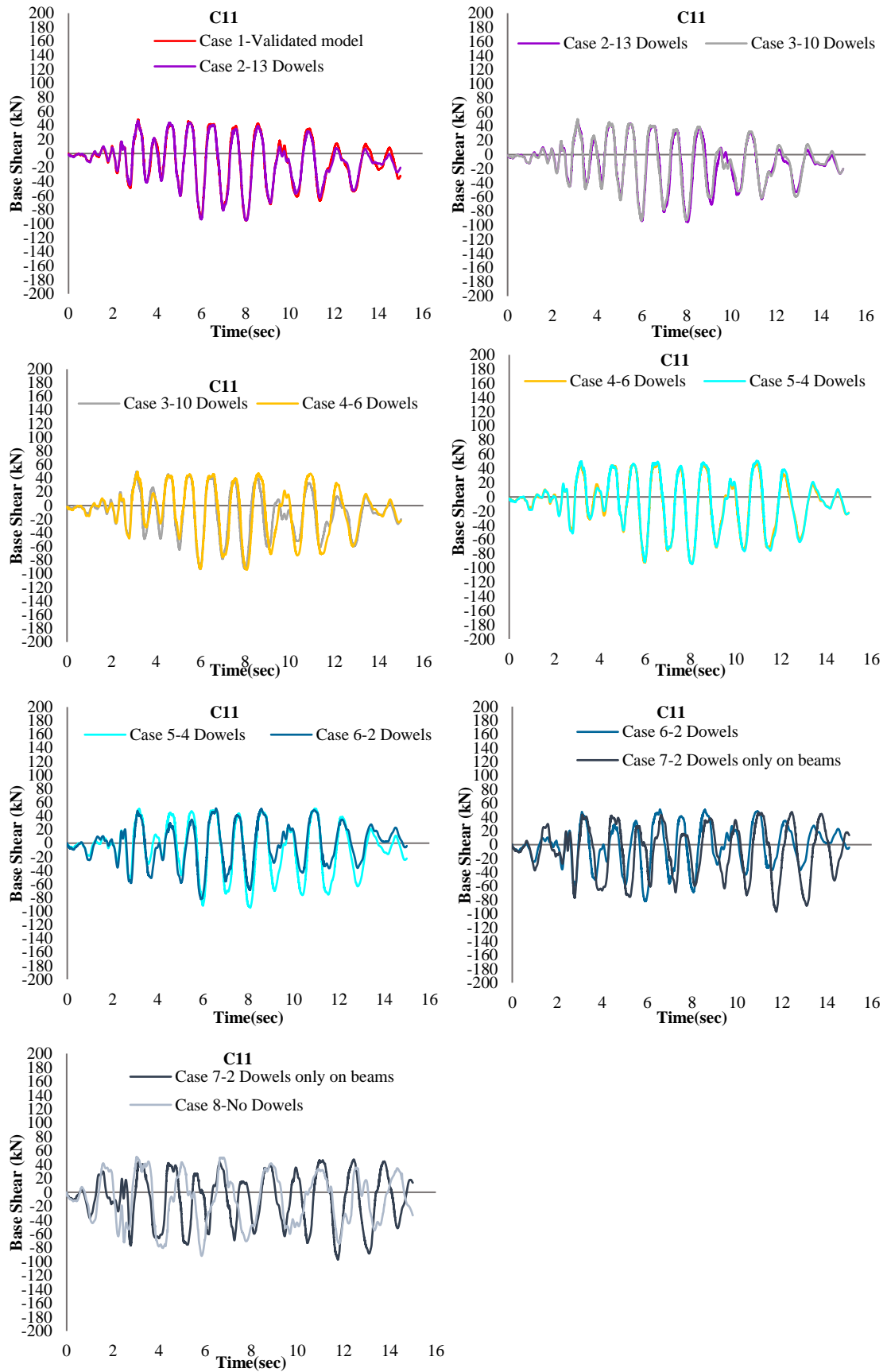
Figure 6.9: Shear force at the base of the west outer column (C11) for all case scenarios

128
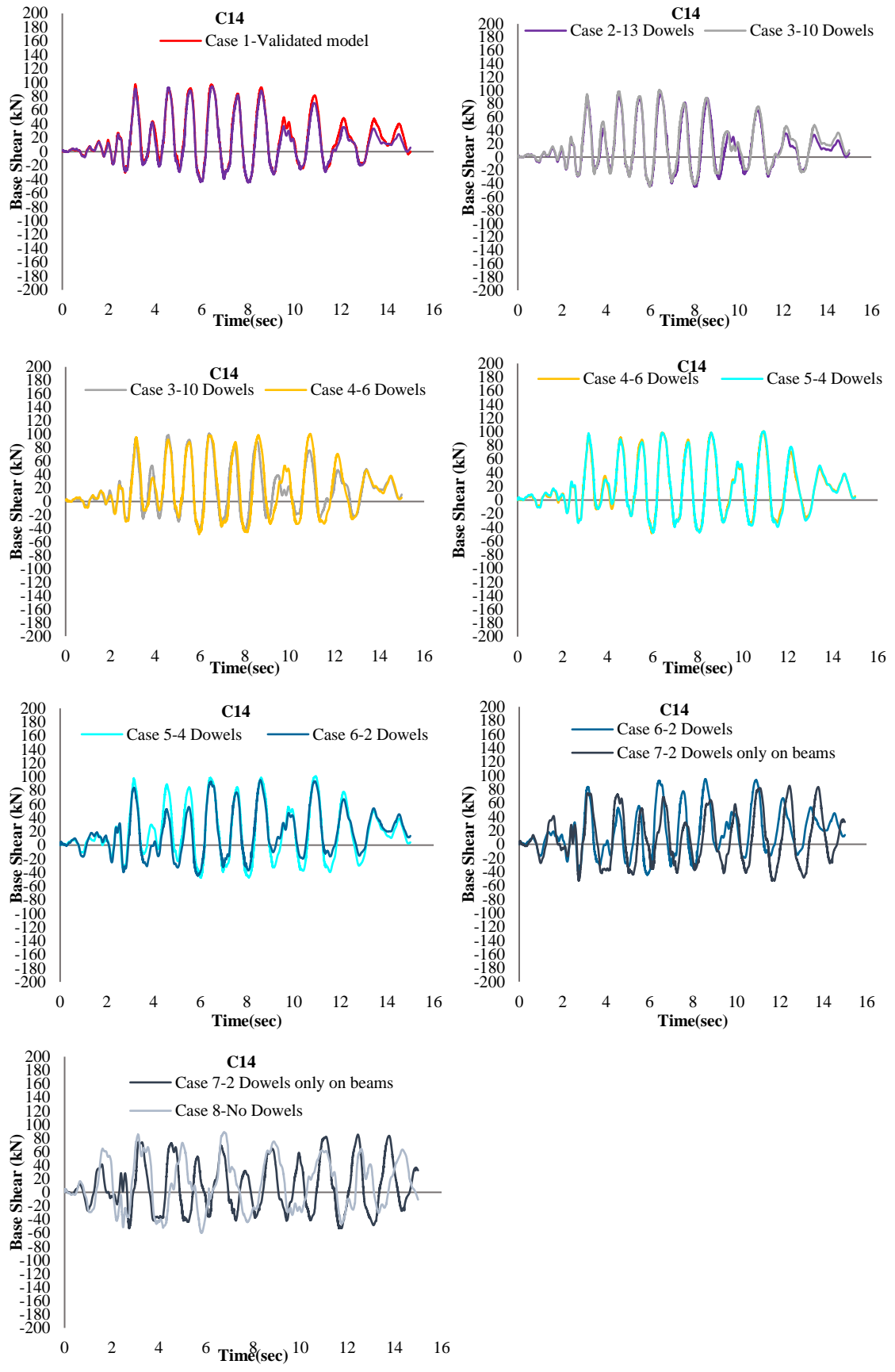
Figure 6.10: Shear force at the base of the east outer column (C14) for all case scenarios
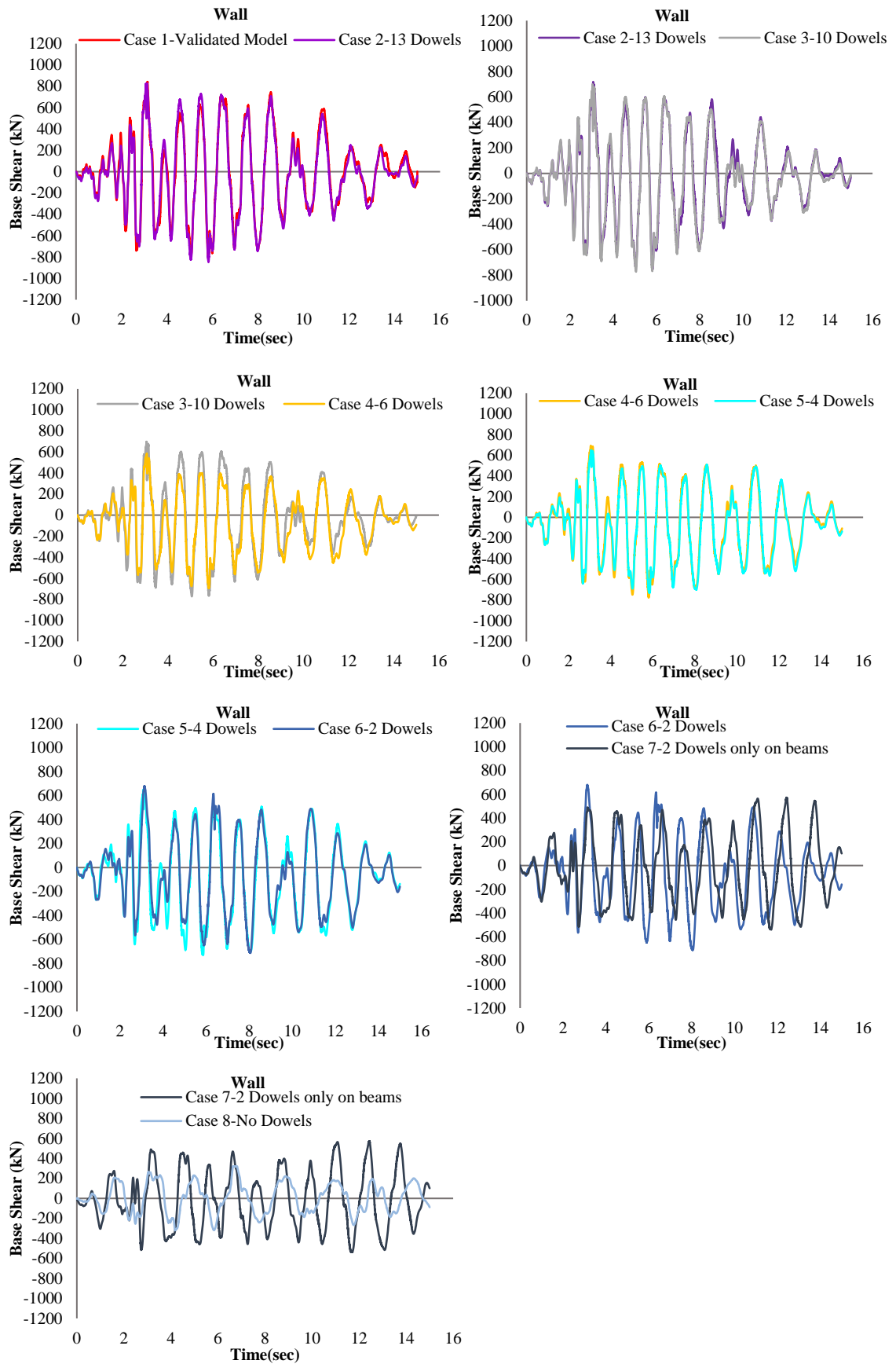
Figure 6.11: Shear force at the base of the wall for all case scenarios

From the results in this section, it is illustrated that the shear force in the wall is gradually reduced with the reduction of the number of dowels. The outer columns of the frame reduced their contribution to the base shear mainly after the sixth case scenario. Furthermore, it is shown that the frame members have not reached their shear strength in any of the cases, even though the outer columns of the frame reach shear values close to their shear capacity.

6.1.4.3   Base shear force distribution versus top-storey displacement

The base shear forces of the frame versus the top-storey displacements are illustrated and discussed in this section for each case scenario. Conclusions are drawn on the effect of the reduction of dowels on the overall stiffness and energy dissipation of the structural system as a whole, as well as of the first-storey members.

Regarding the base shear force, as shown in the previous sections and once again in the graphs in Figure 6.12, it is reduced with the reduction of the number of dowels. However, the top-storey displacement of the frame is about the same for the first five cases. After the fifth case scenario, the top-storey displacement is higher in relation to the previous cases. This can also be seen in the results in sections 6.1.2 and 6.1.3. From the results of all the case scenarios in Figure 6.12, it is demonstrated that the highest values of shear forces were reached for the first two case scenarios. In these two cases, also the stiffness of the frame is about the same.

As shown in Figure 6.12, for the third case scenario, the stiffness of the frame dropped as well as the base shear and the top-storey displacement of the frame. For the third, fourth fifth, and sixth case scenarios the peak shear and displacement values and the stiffness and the energy dissipation of the frames are about the same. For the seventh case scenario, as already mentioned from the results in previous sections, the frame takes lower base shear force and higher top-storey displacement than the previous case scenarios. For the eighth case scenario with no dowels, the reduction of the stiffness and the base shear force is significant and the top-storey displacement is very high.

In general, from these graphs, it is illustrated that the stiffness of the frame is reduced with the reduction of the number of dowels. However, it is shown that the stiffness and the energy dissipation of the frame are not varying considerably for the first two case scenarios. A more considerable reduction of the energy dissipation is observed for the

third case scenario in comparison with the first two cases. Then, the stiffness and the energy dissipation for the third, fourth, and fifth cases are almost the same. However, when the dowels are reduced to two only on beams in the seventh case, the decrease of the base shear force of the frame is apparent and the stiffness and energy dissipation reduction is obvious. Added to that, one can observe that when there are no dowels (eighth case scenario), the stiffness of the frame is obviously reduced in comparison to the previous case scenario. This indicates that even with just two dowels connecting the bounding columns with the wall (seventh case), not only their contribution to the total shear force is important, but also their contribution to the stiffness of the frame is significant.
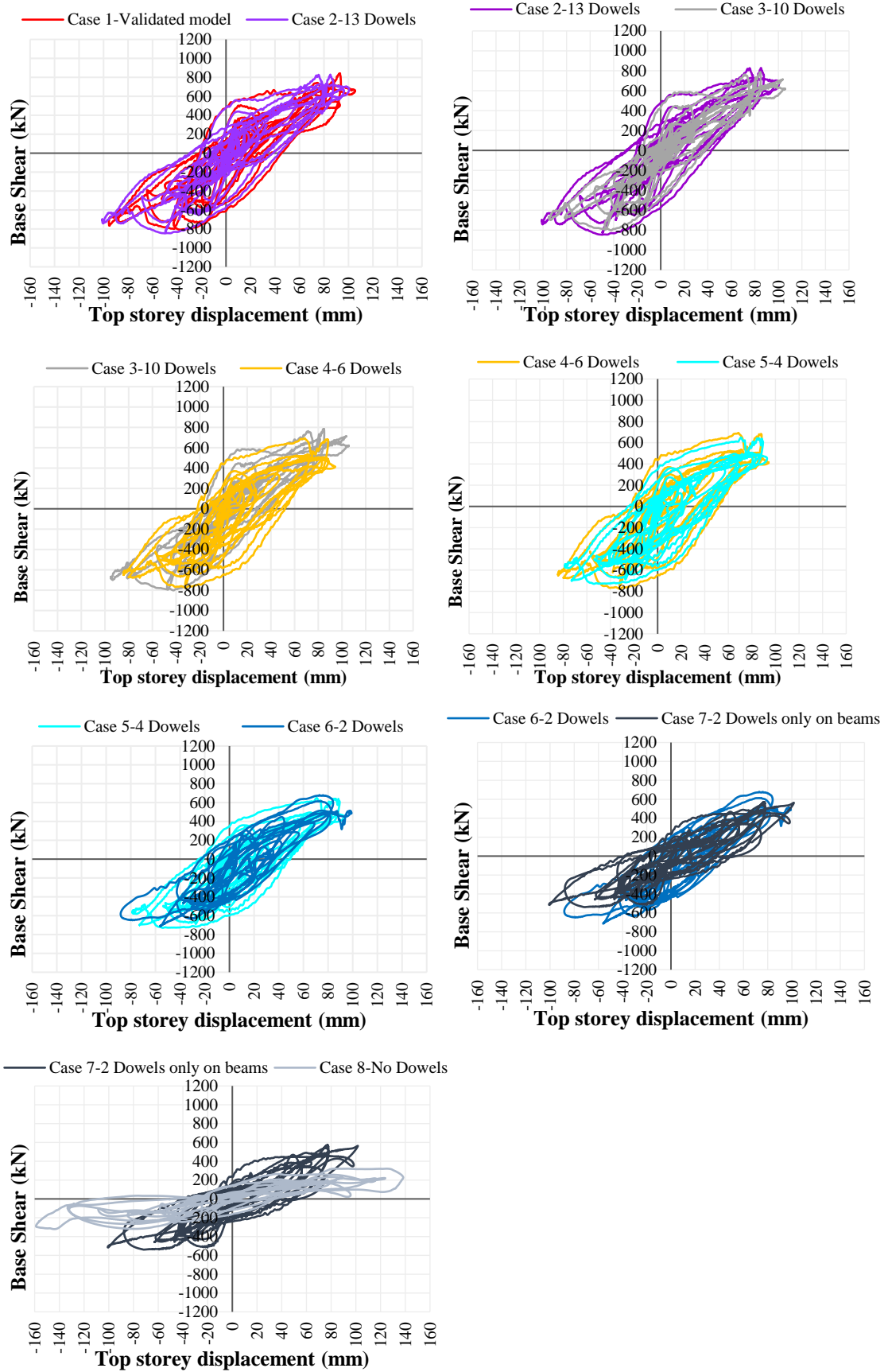
Figure 6.12: Base shear force versus top-storey displacement for all case scenarios

6.1.4.4   Base shear forces of members versus first-storey displacements

In Figures 6.13 to 6.20, the base shear force of each structural member versus the first-storey displacement of the frame during the response history analysis are displayed separately for each case scenario. In all cases, except for the last two cases, it is shown from the graphs that the highest energy dissipation occurs in the wall. Moreover, these graphs demonstrate that even though the wall has the highest energy dissipation during the earthquake for all the cases, with the reduction of the number of the dowels the other members of the frame increase their contribution regarding the energy that they dissipate. Therefore, with the reduction of the number of dowels the columns' contribution to the base shear is increased.

Figure 6.13: Base shear force versus first-storey displacement of the frame members for the first case scenario

For the first case scenario, it is apparent that the wall dissipates the most energy during the earthquake. In the right graph in Figures 6.13 and 6.14 where the wall is not shown, it is illustrated that the outer columns of the frame (C11 and C14) have an almost linear behavior, while in Figures 14 to 19, as the contribution of the columns increase, they enter into nonlinear behavior. Furthermore, in the left graph in Figure 6.13 it is shown that the outer columns of the frame do not have a high contribution to the base shear and energy dissipation during the earthquake; while the wall takes 91.1% and 83.6% of the maximum base shear of the frame in the west and east directions, respectively, the outer columns take only 8.9% and 16.4% in each direction, respectively.

134
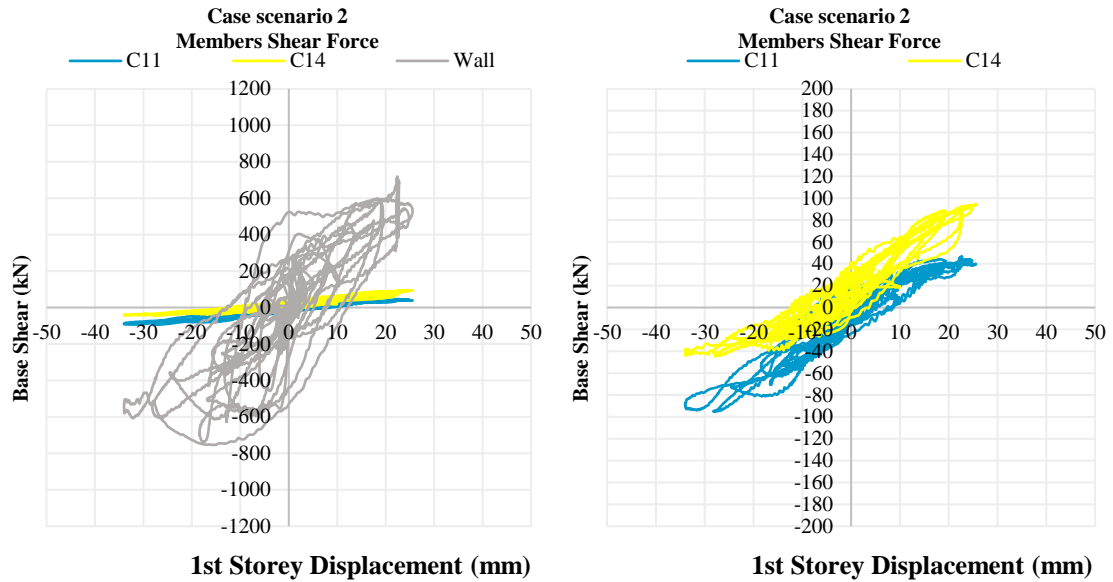
Figure 6.14: Base shear force versus first-storey displacement of the frame members for the second case scenario

For the second case scenario, the wall dissipates most of the energy during the earthquake (Figure 6.14) like in the first case scenario. In this case, the contribution of the outer columns to the maximum base shear is 14.1% and 16.4% in the west and east directions, respectively, whereas in the previous case it was 8.9% in the west direction and 16.4% in the east direction. This shows that the outer column on the west side of the frame (C11) increases its contribution to the base shear in the west direction, while the wall decreases its contribution to the base shear in the west direction (85.9%) in relation to the first case scenario.
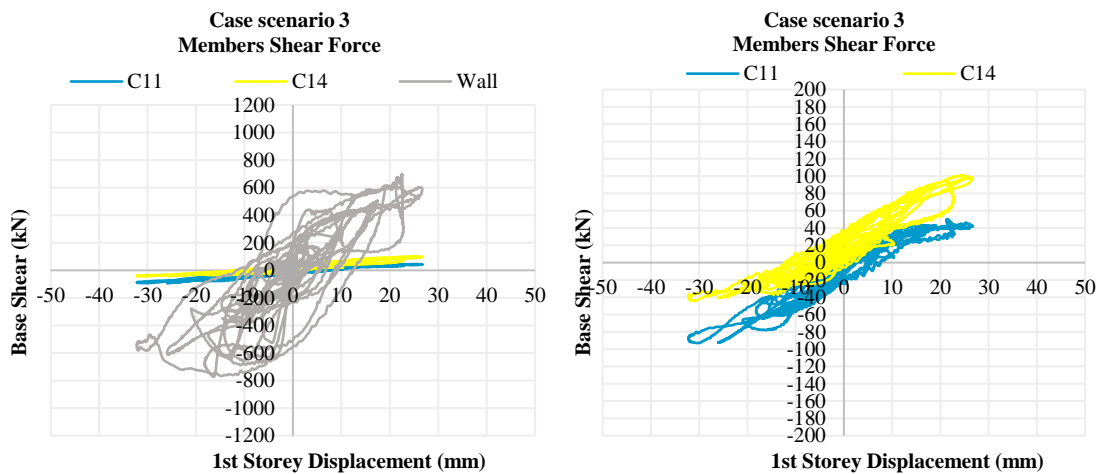
Figure 6.15: Base shear force versus first-storey displacement of the frame members for the third case scenario

135

In the third case scenario in Figure 6.15, it is illustrated that the wall reaches about the same shear forces and displacements in relation to the previous case scenarios. Moreover, in this case, the outer columns of the frame have about the same contribution to the base shear of the frame compared to the first and second cases. In the west direction, the wall contributes 89.2% and the outer columns contribute 10.8% to the maximum base shear of the frame, respectively, whereas in the east direction the wall contributes 83%, and the outer columns 17% to the maximum base shear.

In the fourth and fifth case scenarios, the same behavior of the frame members as the third case scenario is observed (Figures 6.16 and 6.17).

Figure 6.16: Base shear force versus first-storey displacement of the frame members for the fourth case scenario
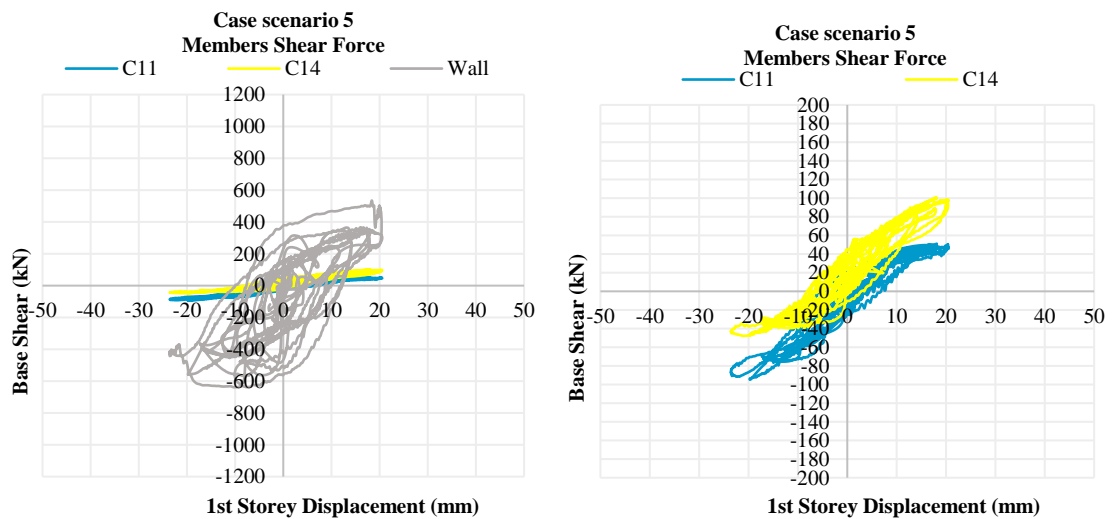
Figure 6.17: Base shear force versus first-storey displacement of the frame members for the fifth case scenario

136

In the sixth case scenario (Figure 6.18), there is a considerable change in the contribution of the frame members to the base shear is observed and it is illustrated that the wall has lower energy dissipation from all the previous case scenarios in relation to the outer columns of the frame. In this case, the wall reaches a base shear lower than 400kN in the east direction and lower than 300kN in the west direction.

In Figure 6.19, where the dowels that connect the bounding columns to the wall are removed and only two dowels are connecting the bounding beams to the wall (seventh case scenario), it is shown that all the members of the frame have dominant energy dissipation. Besides, it is seen that in this case the wall takes the lowest shear values at the base of the frame and it appears to have the lowest contribution to the base shear force concerning all the previous cases. In this case, the outer columns of the frame have 27.1% in the west direction and 23.1% in the east direction contributing to the maximum base shear.
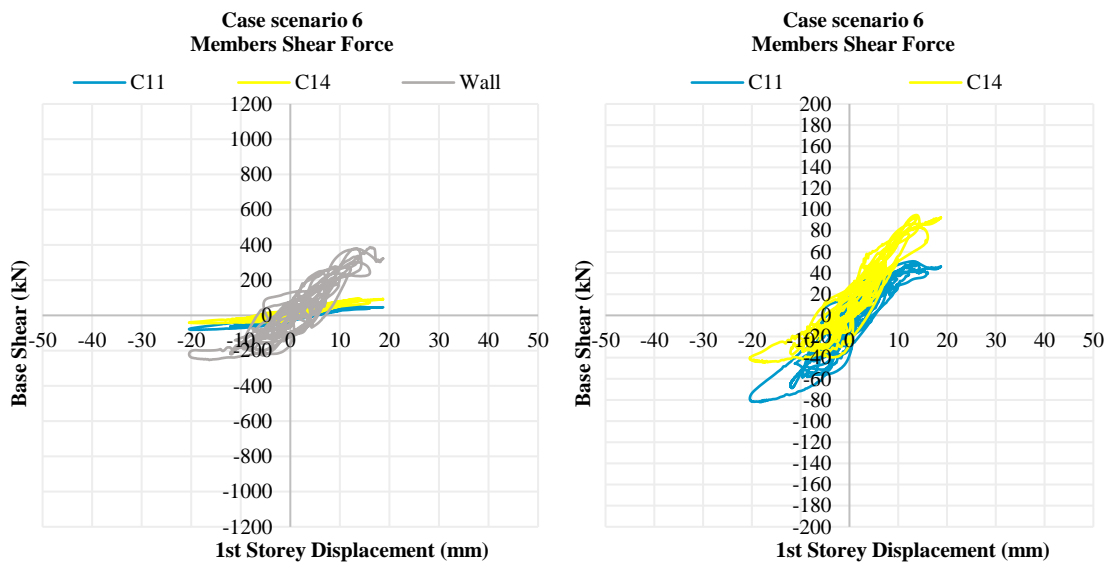
Figure 6.18: Base shear force versus first-storey displacement of the frame members for the sixth case scenario
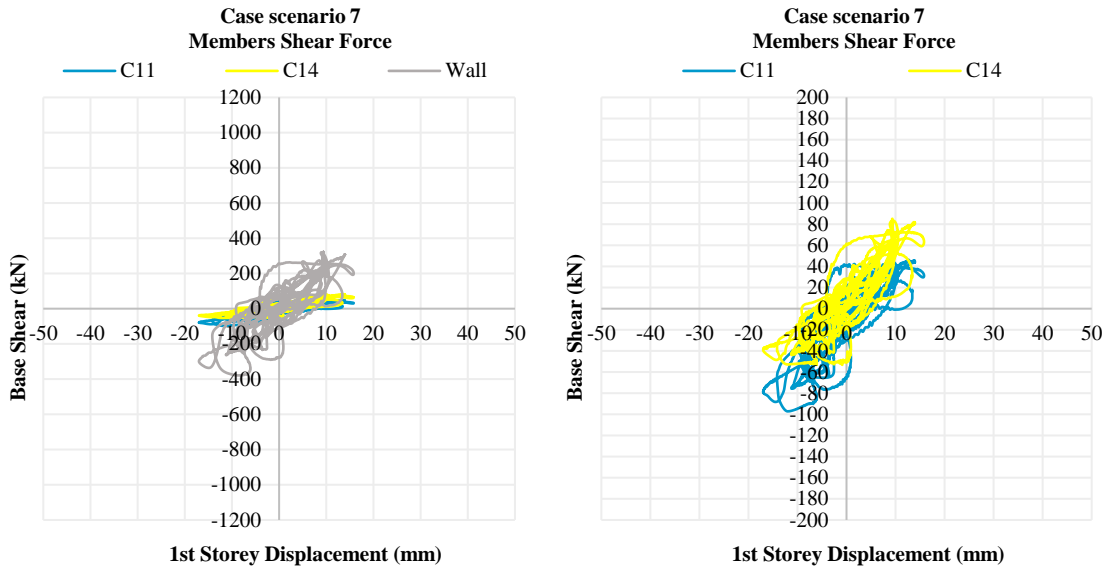
Figure 6.19: Base shear force versus first-storey displacement of the frame members for the seventh case scenario
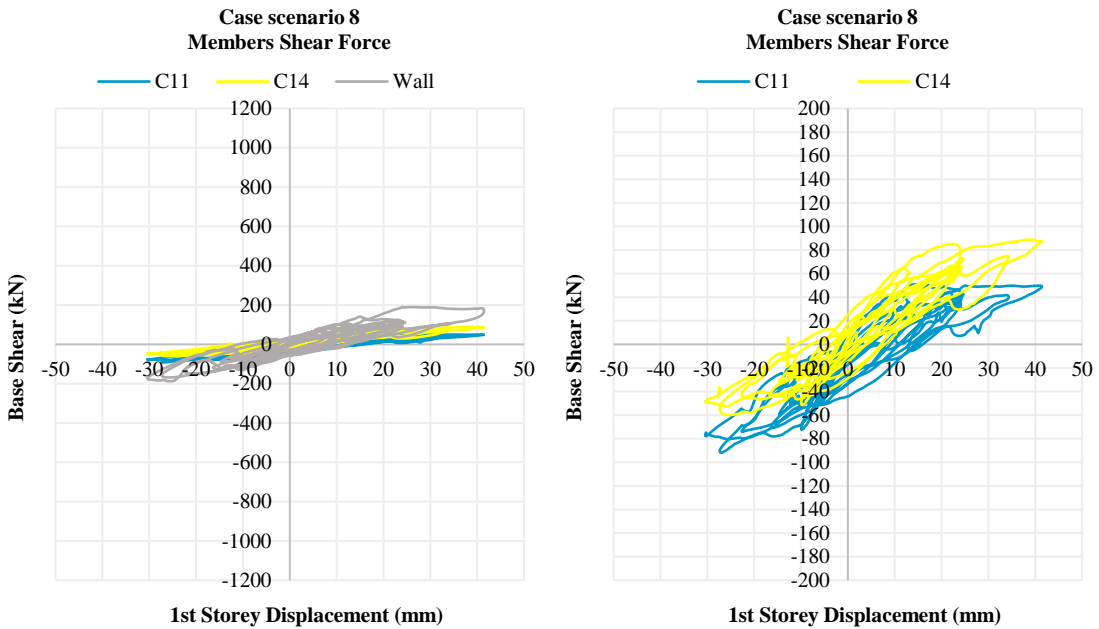
Figure 6.20: Base shear force versus first-storey displacement of the frame members for the eighth case scenario

The last case scenario (with no dowels) in Figure 6.20, represents the wall with the lowest base shear and stiffness in relation to all the previous cases since it behaves as an infilled frame. In this case, the outer columns have the largest contribution to the base shear for all the cases, with 41.4% and 40.9% contribution in the west and east directions, respectively.

In Figures 6.21 to 6.27, the results shown in the previous section are plotted again but here comparison is made between the various members for two case scenarios at a time, on the same graph.
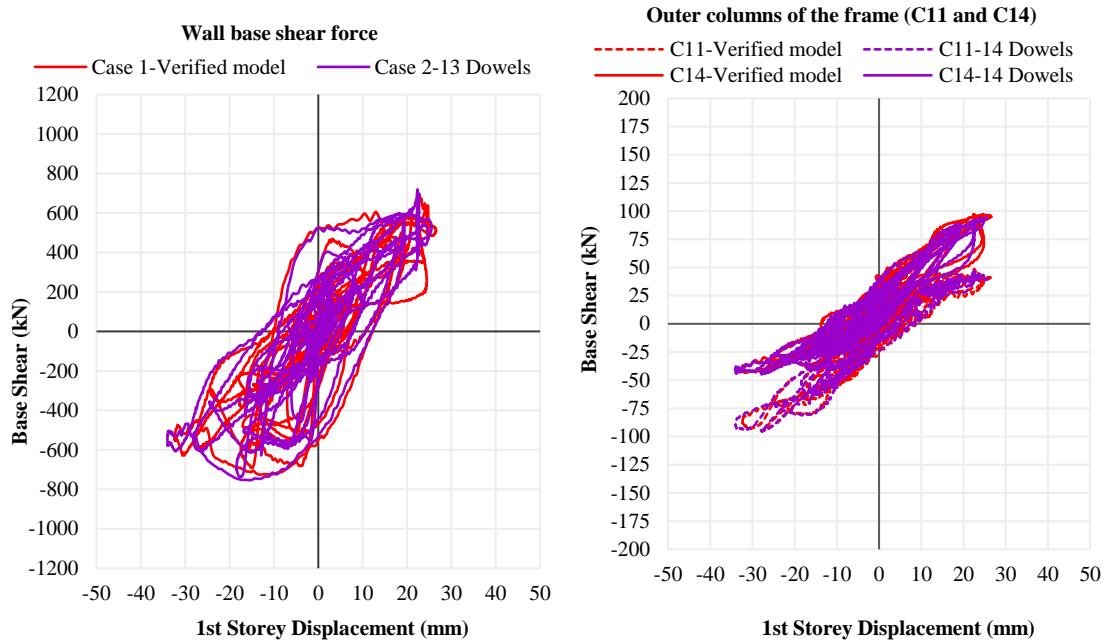
Figure 6.21: Base shear force versus first-storey displacement of the frame members for the first and second case scenarios

The comparison of the members' behavior for the first three case scenarios is shown in Figures 6.21 and 6.22. It verifies that the stiffness of the wall and the outer columns of the frame (C11 and C14) are about the same for the first three case scenarios.
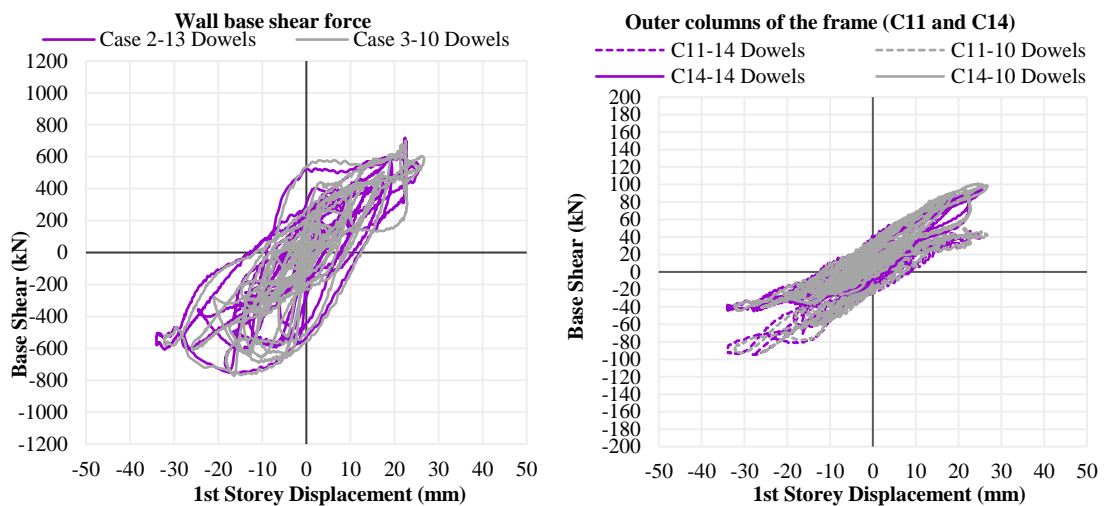
Figure 6.22: Base shear force versus first-storey displacement of the frame members for the second and third case scenarios

Figure 6.23 shows the comparison between the third and fourth case scenarios. It is shown that the wall of the frame of the fourth case scenario reaches lower values of base shear and of displacement in relation to the third case scenario. In addition, the outer columns of the frame of the fourth case scenario reach lower displacements and about the same base shear values in relation to the third case scenario. Moreover, the members of the frame dissipate less energy in the fourth case scenario as shown in Figure 6.23. It is observed that the stiffness of the frame members in the third and fourth case scenarios is the same.
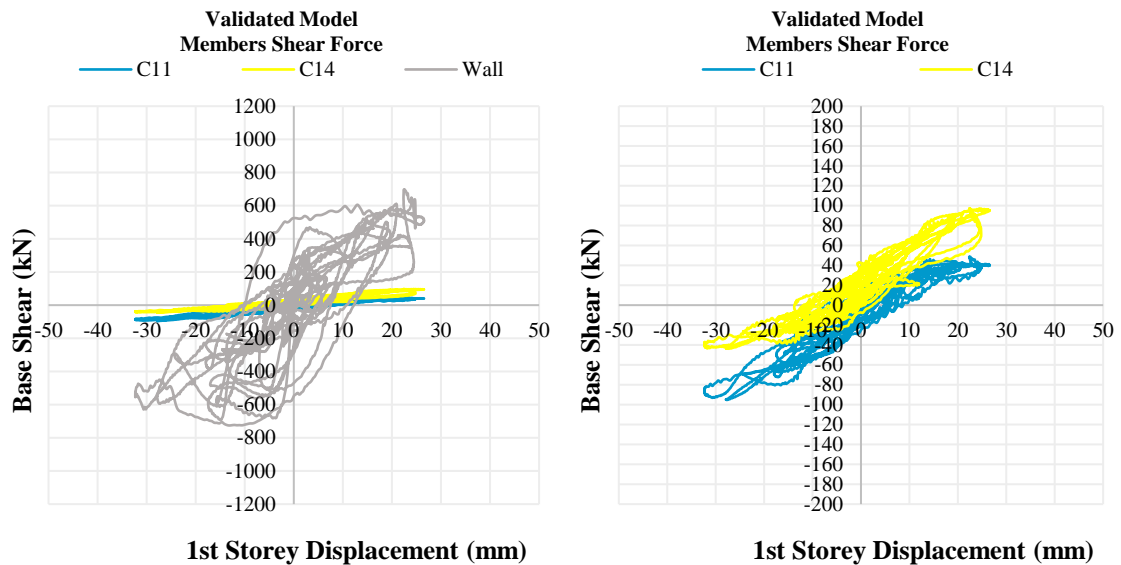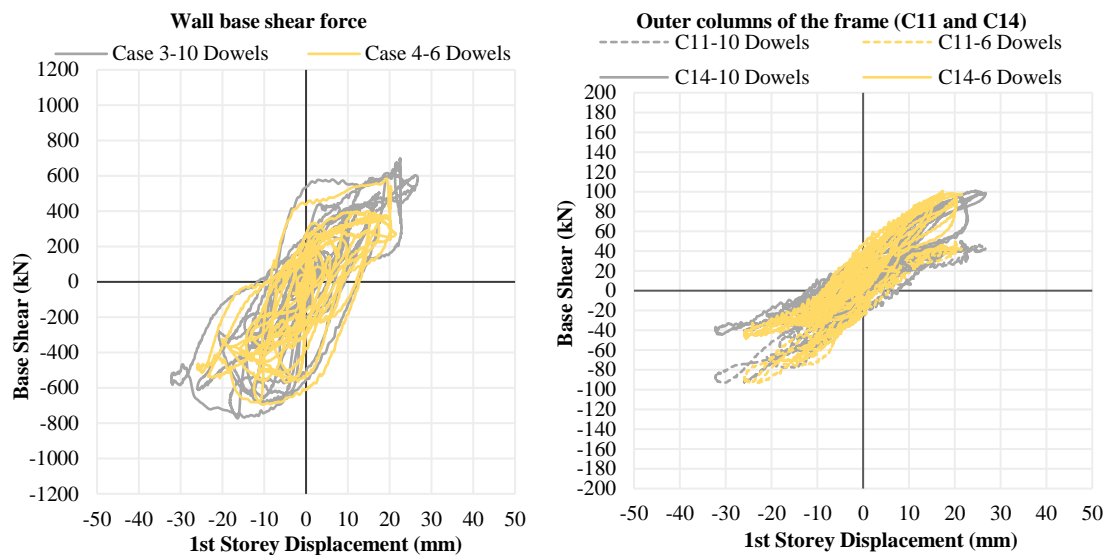

Figure 6.23: Base shear force versus first-storey displacement of the frame members for the third and fourth case scenarios

When the dowels are reduced to four (fifth case scenario), the members' behavior is approximately the same as the fourth case scenario with the six dowels and third with the half dowels from Figure 6.24. In Figure 6.24 it is shown that the wall of the fifth case scenario reaches lower values of the base shear in relation to the previous case scenario. It is also shown that the frame of the fifth case scenario reaches lower storey displacements in the west direction and about the same in the east direction. Moreover, as shown in the graph in Figure 6.24, it seems that the stiffness and the energy dissipation of the wall are about the same. The behavior of the outer columns of the frame in the fifth case is similar to the fourth case scenario.
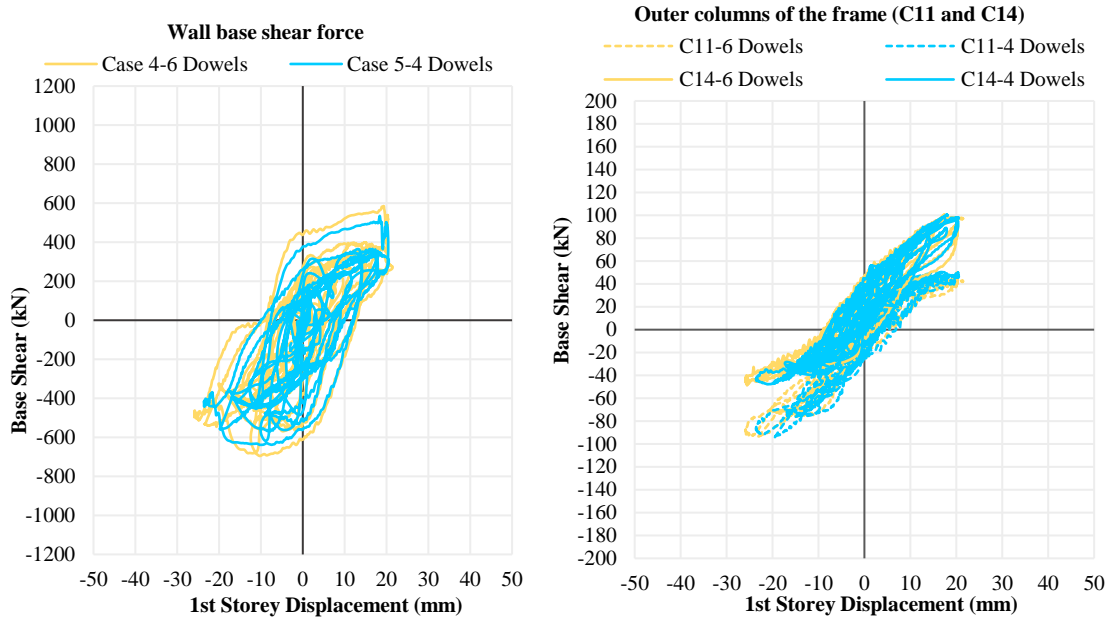
Figure 6.24: Base shear force versus first-storey displacement of the frame members for the fourth and fifth case scenarios

The comparison of the shear force at the base of the frame members for the fifth case scenario with the four dowels and the sixth case scenario with the two dowels are illustrated in Figure 6.25. The different behavior of the frame members is more apparent in these graphs when the dowels are reduced to two in the sixth case. The wall reaches lower base shear values than the previous case scenario. In these graphs, it is obvious that the wall and the outer columns of the frame with the two dowels dissipate lower energy compared to the previous case.
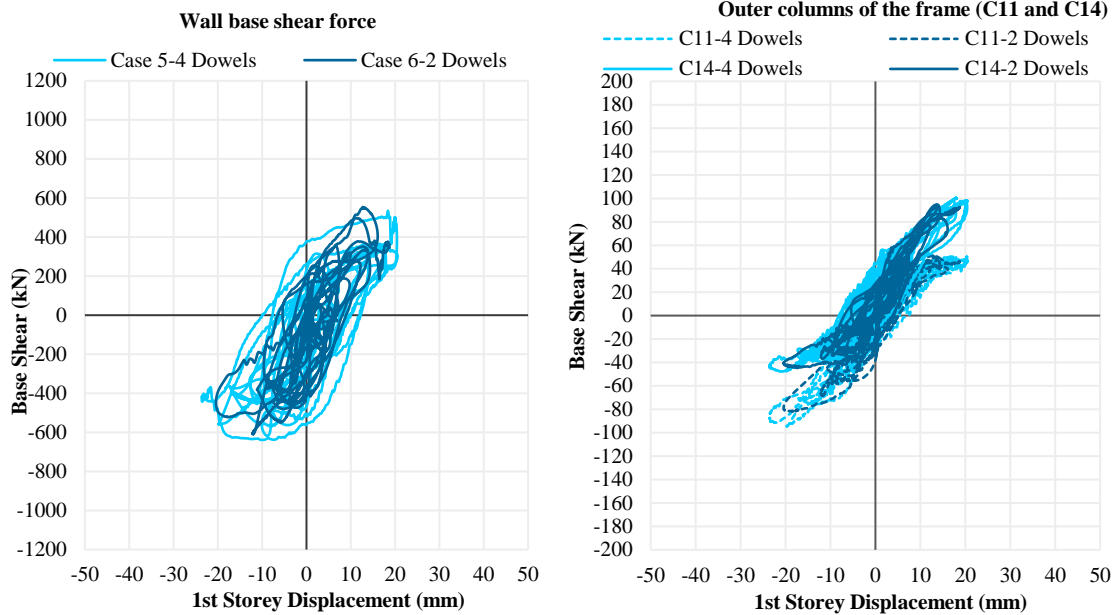
Figure 6.25: Base shear force versus first-storey displacement of the frame members for the fifth and sixth case scenarios

The comparison of the base shear force between the frame members for the sixth and seventh case scenarios is illustrated in Figure 6.26. Again, from these results, it is apparent that the behavior of the frame members is different after removing the dowels that connect the bounding columns with the RC infill wall. It is shown that the wall reaches lower base shear forces for the seventh case scenario, especially in the west direction. It is also apparent that the wall dissipates lower energy in the seventh case scenario. On the other hand, there is an increase of the base shear force carried by the outer columns of the frame in the west direction.
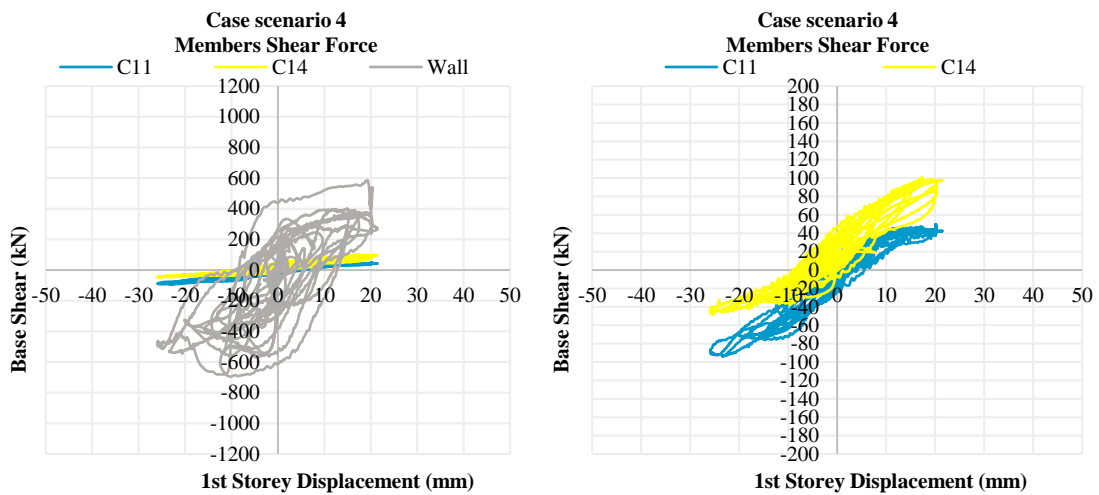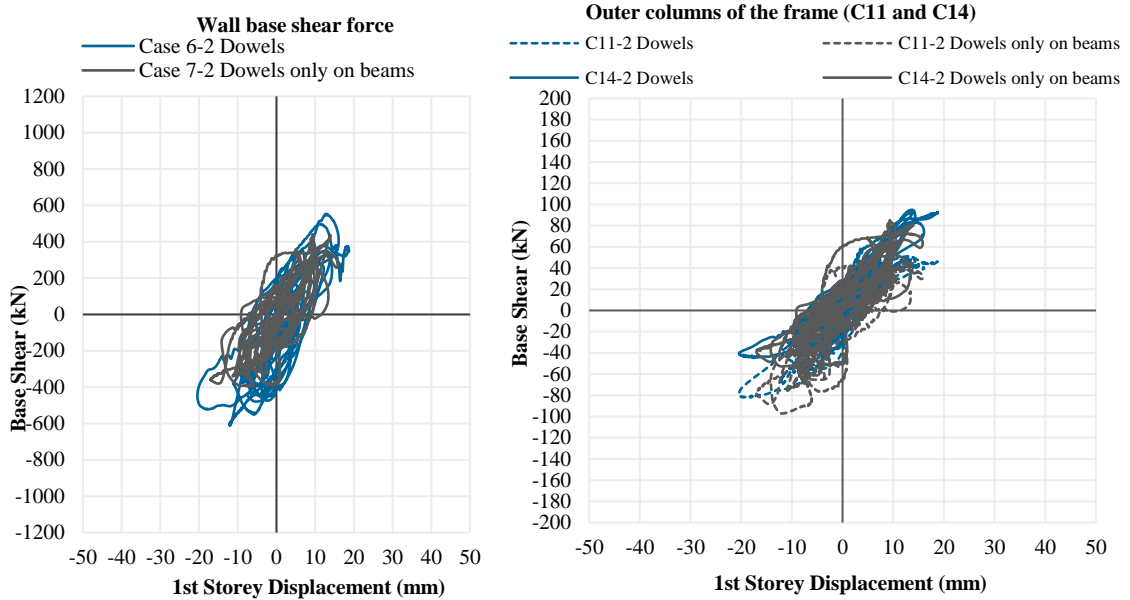
Figure 6.26: Base shear force versus first-storey displacement of the frame members for the sixth and seventh case scenarios
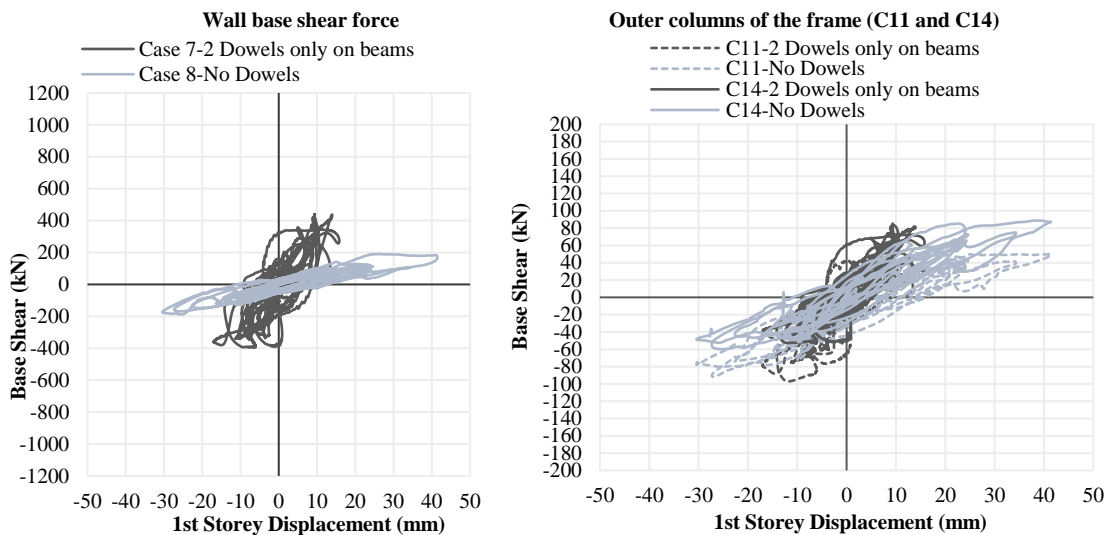
Figure 6.27: Base shear force versus first-storey displacement of the frame members for the seventh and eight case scenarios

From the comparison of the behavior of the members regarding the base shear force between the last two case scenarios in Figure 6.27, it is shown that when no dowels are connecting the wall to the columns, the wall has a smaller contribution to the base shear. On the other hand, the outer columns of the frame have a higher contribution to the base shear and higher energy dissipation compared to the previous case scenario. In addition, the reduction of the stiffness of the wall is apparent in Figure 6.27. Once again, it can be concluded that with the addition of even just two dowels, the contribution of the outer

143

columns of the frame to the base shear and the energy dissipation of these columns is decreased.

The conclusions that were deducted from the graphs in Figures 6.1 to 6.27are gathered in this paragraph. Figures 6.1 to 6.11 and Table 6.2 illustrate that the period of oscillation is higher with the reduction of the number of dowels, so it can be implied that the stiffness of the frame is changing (it is decreased) with the reduction of the number of dowels. The fewer the dowels, the lower the stiffness of the frame. Moreover, the same trend for the energy dissipation of the frame is observed (less energy being dissipated) (see Figure 6.12) with the reduction of the number of dowels in the frame. These reductions are more obvious after the sixth case scenario with the two dowels connecting the infill wall to the bounding frame. It is also shown that for the seventh case scenario (two dowels connecting only the beams to the wall) the overall behavior of the frame changes (base shear force, top-storey displacement of the frame, stiffness, energy dissipation). Added to that, it is shown that the distribution of the base shear force is relocated from the wall to the outer columns of the frame.

6.1.4.5 Stiffness of the frames

The initial stiffness of the frames was calculated and is presented in Figure 6.28 for all the case scenarios. These results were derived from the initial slope of the graphs in Figure 6.12 when the top-storey displacement is 10mm (when the frames are still in a linear condition).

Initial stiffness of the frame for all the case scenarios

Values shown: 10124.0, 10567.0, 10406.0, 9980.6, 9906.2, 9062.0, 6786.6, 2597.8

$$y = -61.0x^3 + 517.2x^2 - 1286.6x + 11160.3$$

Y-axis: Slope/Stiffness [N/mm]
X-axis: Case Scenarios
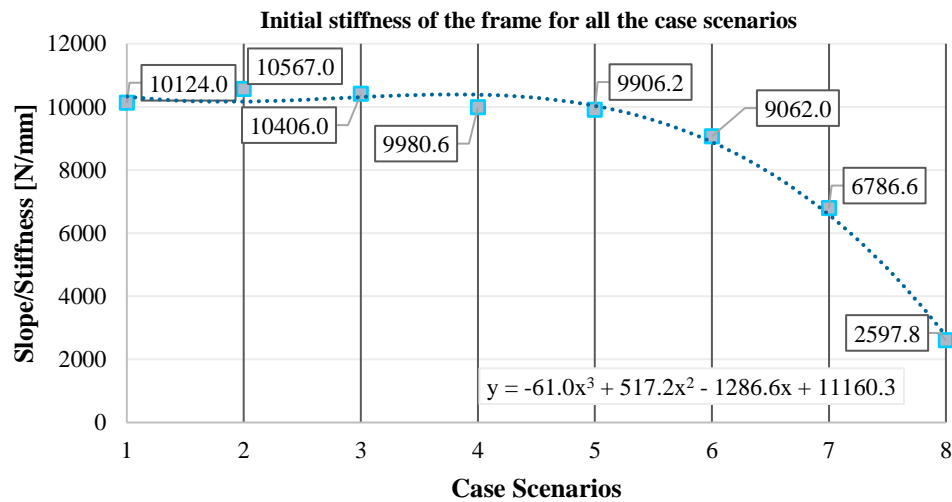
Figure 6.28: Initial stiffness of the frames for all cases

144

As shown in Figure 6.28, the initial stiffness of the frames is about the same for the first three case scenarios. For the fourth and fifth case scenarios, there is a decrease in the initial stiffness of the frame compared to the previous cases. Nevertheless, the initial stiffness for these cases is not varying considerably. For the sixth case scenario, there is about 10% reduction of the initial stiffness of the frame compared to the fifth case, whereas for the seventh and especially for the eighth case scenarios, as already mentioned, the initial stiffness is significantly reduced. Added to that, one can observe that when the dowels are reduced to two only on beams (seventh case scenario), the stiffness of the frame is significantly reduced (by 25%) in comparison to the sixth case, with two dowels on beams and two dowels on columns. For the eighth case scenario with no dowels, the reduction of the stiffness is noteworthy (62%) compared to the previous case, since the wall behaves as a non-integral infill.

In general, Figure 6.28 illustrates that, as expected, the initial stiffness of the frames is progressively reduced with the reduction of the number of dowels. The important point in Figure 6.28 is that it is shown that for the first three cases the stiffness is about the same and that the drop of the initial stiffness of the frames for the seventh and eighth cases is more apparent concerning the reduction observed in the previous cases. The former observation indicates that using 10 dowels (case 3) instead of 20 dowels (validated case) the initial stiffness remains the same. The latter observation demonstrates how important is the addition of dowels not just on beams but on columns as well and even more, it is shown how dominant is the addition of just two dowels even only on beams compared to a non-integral infill.

Moreover, the initial stiffness and the ultimate capacity stiffness of the validated frame (first case scenario), as well as the stiffness corresponding to the 20% decrease in the capacity compared to the ultimate capacity (near collapse capacity), as derived from the results, is presented in Figure 6.29. It is shown that the ultimate capacity stiffness of the frame, about 7790 N/mm, is reduced by 23% compared to the initial stiffness of the frame, which is about 10124 N/mm, and the near collapse stiffness, which about 5428 N/mm, is reduced by 30.3% compared to the ultimate capacity stiffness, or 46.4% compared to the initial stiffness of the frame.
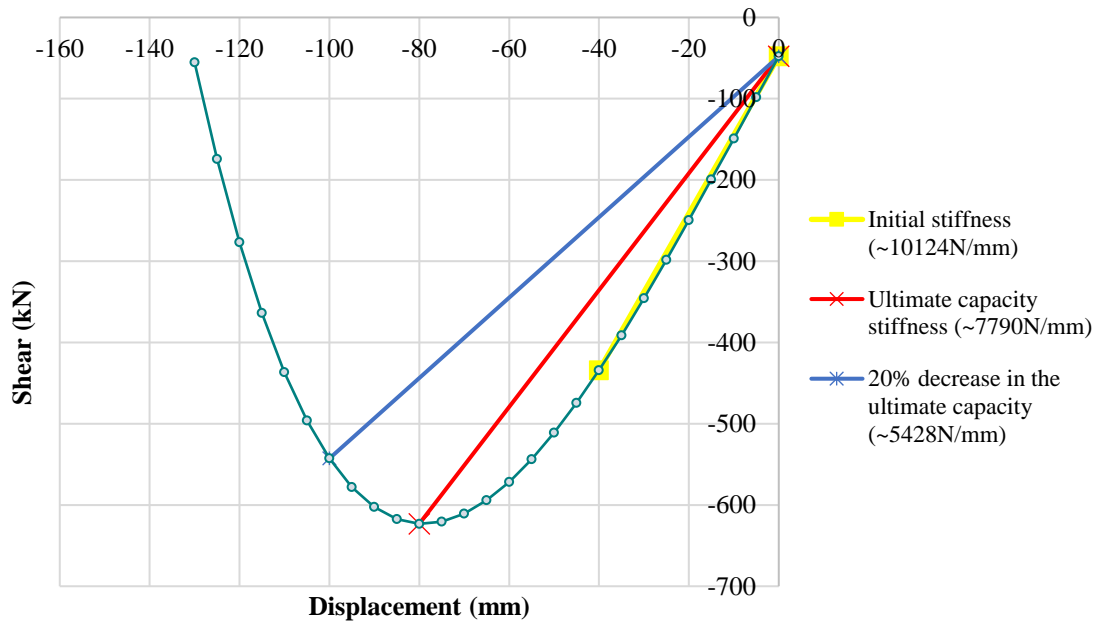
Figure 6.29: Initial and ultimate capacity stiffness of the frames for the validated FE model

6.1.4.6   Base shear force distribution on members

In Figure 6.30, the contribution of each member of the frame to the base shear force in terms of percentage is illustrated for all the case scenarios when the total base shear force (see section 6.1.5.1) is maximum (frame is moving towards the east) and when it is minimum (frame is moving towards the west).

Figure 6.30 shows that the wall (including the bounding columns) contributes the most to the base shear force for the first seven case scenarios in both directions. The contribution of the wall is stable (81% to 91% contribution) through the first six case scenarios in both directions, while for the last two case scenarios the contribution of the wall to the base shear force of the frame is decreased. Specifically, the contribution of the wall for the seventh case scenario is less than 80% (12.4% decrease in the west direction and 4.5% decrease in the east direction in relation to the sixth case scenario), while the contribution of the outer columns is increased in the seventh case scenario concerning the previous cases. For the last case scenario, the wall contribution to the base shear force is very small, whereas the outer columns of the frame take the 97.7% and 78.9% of the base shear force in the west and east directions, respectively. Henceforth, before the sixth case scenario (2 dowels per wall side) the contribution of the wall to the base shear is dominant and the outer columns of the frame contribute less than 20% to the base shear of the frame.

146

Therefore, it is illustrated that the contribution of the outer columns to the base shear force of the frame is not high in comparison to the contribution of the wall. Nevertheless, for the seventh case scenario (two dowels connecting only the beams to the wall), the contribution of the wall to the base shear is reduced compared to the previous cases and the contribution of the outer columns to the base shear is increased by more than 20%. The difference between the last two case scenarios is shown once again in Figure 6.30 and this presents that the connection of the new wall to the bounding frame even with the addition of two dowels only on the beams adds a lot to the behavior of the frame.

Furthermore, in Figure 6.30, it is presented that the outer columns of the frame have a higher contribution when the frame is moving towards their direction. The west outer column of the frame (C11) has higher contribution when the frame is moving towards the west, and the east outer column of the frame (C14) has higher contribution when the frame is moving towards the east. This indicates that the members of the frame contribute more to the shear when they are in compression.

CONTRIBUTION OF FRAME MEMBERS TO THE MAXIMUM TOTAL BASE SHEAR IN THE WEST DIRECTION

CONTRIBUTION OF FRAME MEMBERS TO THE MAXIMUM TOTAL BASE SHEAR IN THE EAST DIRECTION
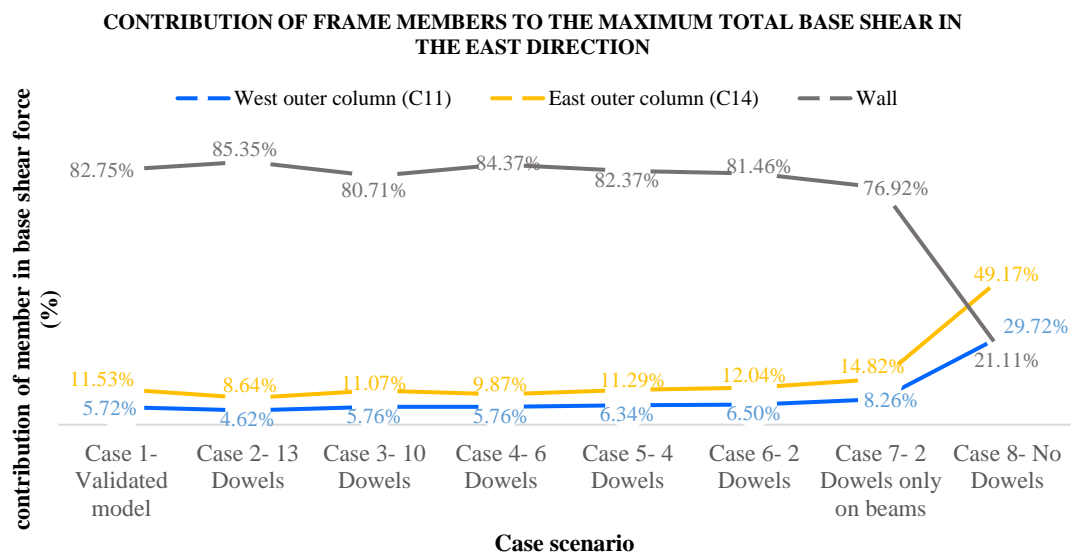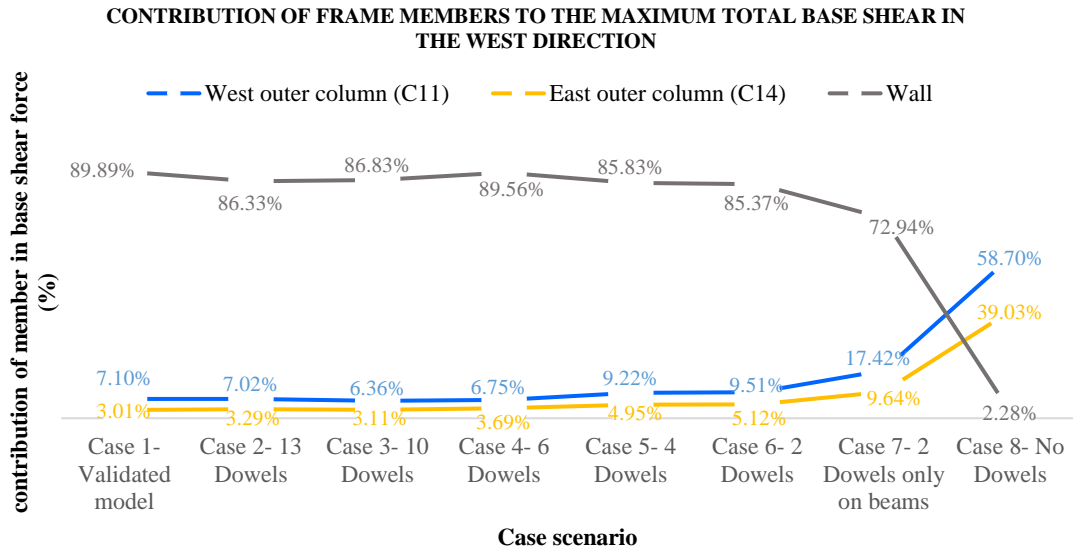
Figure 6.30: Contribution of the frame members to the base shear force for all case scenarios when the base shear force is maximum in both directions

In general, from the graphs in Figure 6.30, it can be concluded that the wall with the bounding columns contributes the most to the base shear of the frame for all the case scenarios, except the last case scenario with no dowels. Nonetheless, even though the contribution of the outer columns of the frame is relatively low (less than 13% in both directions), it is increased with the reduction of the number of dowels, especially in the last two cases. This is an indication that with the reduction of the number of dowels the shear force at the base of the wall is transferred to the outer columns of the frame and this

confirms that the less the dowels connecting the wall to the surrounding frame members, the more the outer columns of the frame suffer in shear.

6.2 Local numerical results of the parametric study

In this section, the local results from the parametric study of the effect of the number of dowels are presented and discussed. More specifically, the number and therefore the distance between dowels at the interface between the existing frame and the new wall is examined in order to draw conclusion about the effect of dowel action.

6.2.1 Dowel results

The behavior of dowels at the base interface of the wall during the analysis is displayed and discussed in this section for the time-steps when the frames experience their maximum top-storey displacements (DTX) and their maximum base shear forces (FBX) during the response-history analysis in both directions for the first five case scenarios. As shown in section 6.1.4, the frames reach their maximum base shear forces at about 3.1 seconds in the east direction and around 5.8 seconds in the west direction. The maximum top-storey displacements of the frames occur at around 6 seconds and 6.5 seconds in the west and east directions, respectively. The exact time-steps for each case scenario are displayed in the graphs.

In sections 6.1.5.1 and 6.1.5.2 the results show the behavior of each dowel at a local level; the axial (N_x) and shear forces (Q_y) of each dowel at the base interface along the length of the wall. Specifically, each marker on the graphs displays the results of the dowel that is located at the actual position of the dowel in the model. The length of the wall without the bounding columns (C12 and C13) is 2.1m as already mentioned in Chapter 3. The x-axis of the graphs displays the length of the wall, with 0m the west edge of the wall and 2.1m the east edge of the wall. For instance, in the first case scenario where the dowels were spaced at 100mm at the base of the wall in the x-axis of the graphs, there is a value for each dowel at every 0.1m. Consequently, for all the case scenarios, the corresponding position of each dowel is shown in the graphs. The y-axis of the graphs displays the corresponding axial or shear force of each dowel.

6.2.1.1 *Local axial forces of dowels at the base interface of the wall*

The axial load of each dowel at the base interface is presented along the length of the wall in Figure 6.31. The graphs in Figure 6.31, show the axial forces of dowels when the total base shear force (graphs on the left) and the top-storey displacement (graphs on the right) of the frames are at maximum in both directions. The positive values on the graphs display the compressive forces and the negative values the tensile forces of each dowel. Also, the design yield strength of dowels is shown in the graphs. As shown in these graphs, the maximum values occur at different instances during the analysis for each case.

In Figure 6.31, it is illustrated that the dowels of the validated model in the first case scenario take the lowest tensile forces in comparison with the other case scenarios since the infill wall behaves monolithically with the bounding frame, resulting in an even distribution of the axial force among the dowels when the frame experiences its maximum base shear and top-storey displacement in both directions. In this case, the position of the neutral axis is in the middle of the wall. In the second and third case scenarios, the dowels reach higher axial forces in comparison with the first case scenario and some dowels reach their yield strength capacity. In addition, in the first three case scenarios, the position of the neutral axis is in the middle of the wall, thus, there is an even distribution of the axial force among the dowels for these cases. During the fourth and fifth case scenarios, more dowels are in tension and more dowels yield, while the position of the neutral axis shifts closer to the edges of the wall, approaching the bounding columns. So, it can be seen that the position of the neutral axis shifts closer to the edges of the wall with the reduction of the number of dowels. Therefore, the smaller the number of dowels the larger the number of dowels that are in tension and the larger the number of dowels that yield.
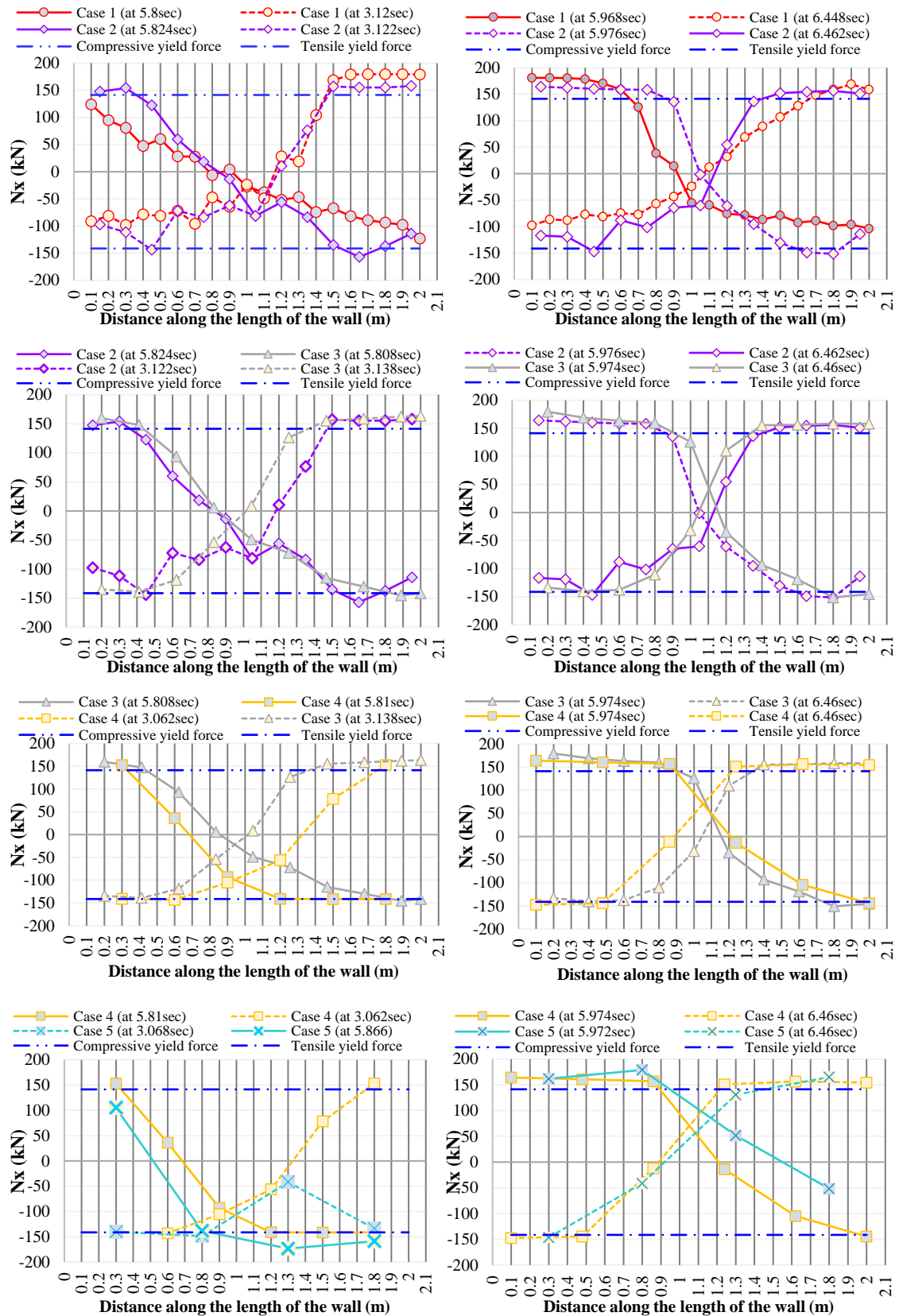
Figure 6.31: Axial force of each dowel along the length of the wall at the base interface when the base shear is at maximum in both directions (graphs on the left) and when the top-storey

displacement is at maximum in both directions (graphs on the right). Compression is positive and tension is negative on the graphs

6.2.1.2   Local shear forces of dowels at the base interface of the wall

The shear force of each dowel at the base interface of the wall is shown in Figure 6.32 when the base shear force is maximum in the west and east direction and in Figure 6.33 when the top-storey displacement is maximum in the west and east direction. Also, the design shear capacity of the dowels at the joint interface is shown in the graphs.

Figure 6.32 shows the dowels of the first two case scenarios taking shear forces lower than 20kN along the length of the wall when the base shear is at maximum in both directions. In the third case scenario, more dowels reach shear forces close to 20kN compared to the previous cases and in the fourth case scenario, more dowels reach shear values close to 20kN in relation to the previous cases. In the fifth case scenario, one dowel reaches 33.3kN shear force, very close to the design shear capacity of the dowel when the base shear is maximum in the west direction. Generally, Figure 6.32 shows that the fewer the dowels, the more dowels are active in shear. Also, it can be seen that the dowels that are in compression they are not active regarding the shear load. On the other hand, the dowels that are in tension take higher shear forces compared to the dowels that are in compression.
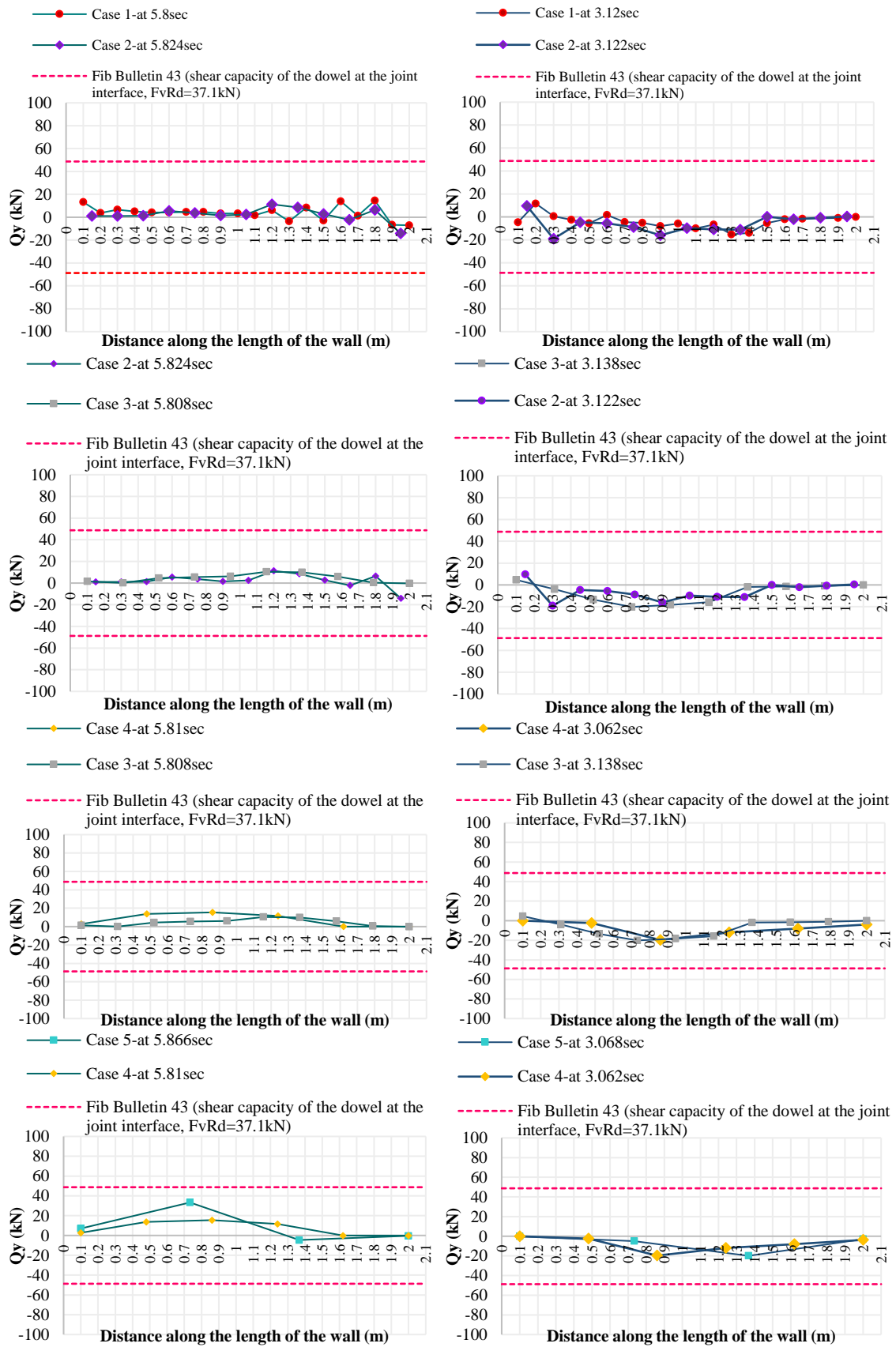
Figure 6.32: Shear force of each dowel at the base interface when the base shear is at maximum in the west and east directions (left and right graphs, respectively)

153
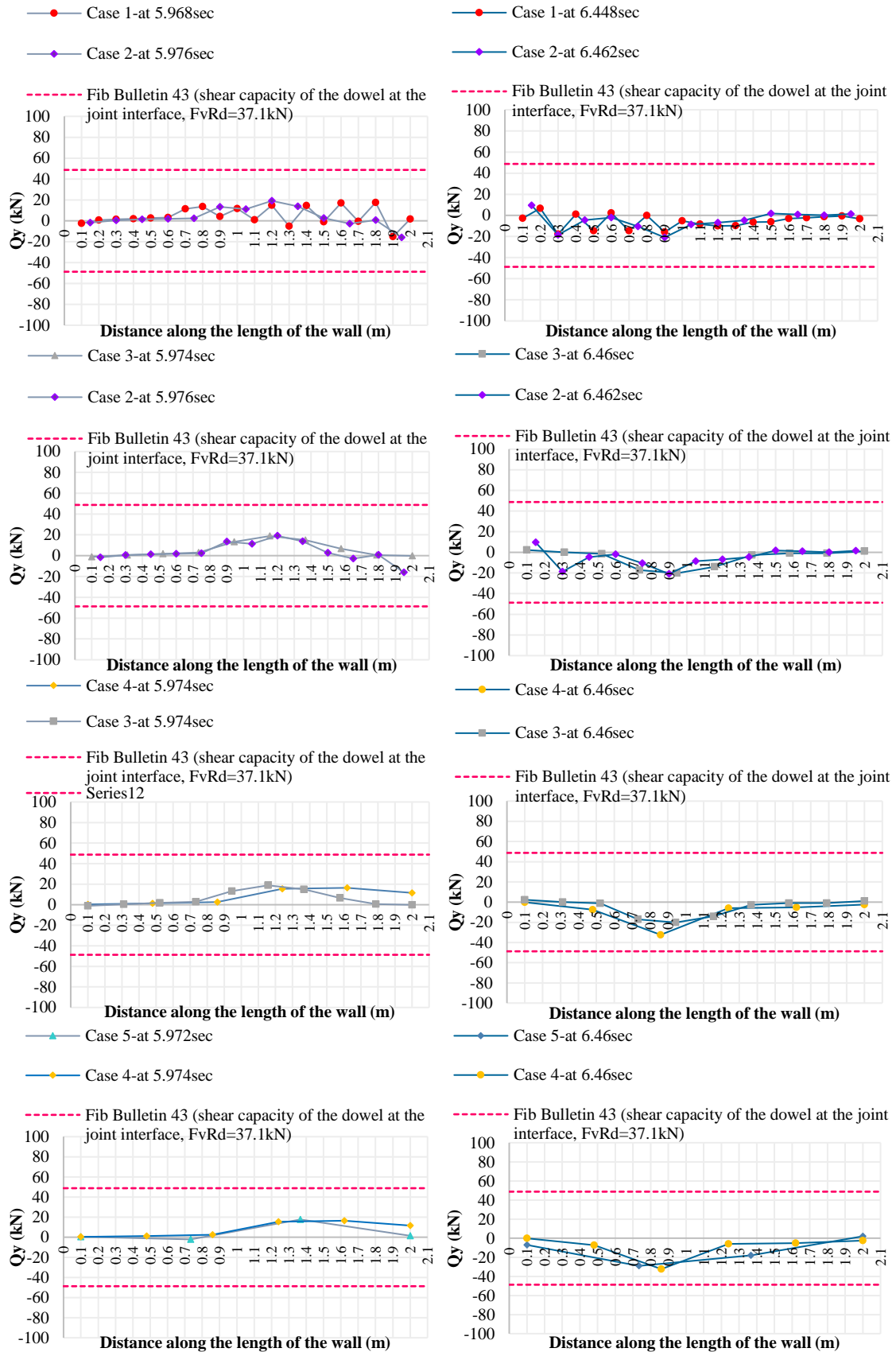
Figure 6.33: Shear force of each dowel at the base interface when the top-storey displacement is at maximum on the west and east directions (left and right graphs, respectively)

Figure 6.33 shows, that more dowels take higher shear forces along the length of the wall during high displacements than during high base shear. This is indicated from the two first case scenarios, where more than half the number of dowels (dowels along the 2/3 length of the wall) are active regarding the shear load, whereas during high base shear, dowels along half the length of the wall are active regarding shear load. For the third case scenario, the behavior of dowels is about the same with the second case, while the dowels reach slightly higher shear forces along the length of the wall for the third case scenario. The fourth and fifth case scenarios demonstrate that even though the behavior of dowels is similar with the third case scenario, one dowel almost reaches its shear capacity when the top-storey displacement is maximum in the east direction.

In all cases, it is indicated that the shear load mainly is distributed on dowels that are located on the opposite side from the moving direction of the frame, in other words, the dowels that are located in the side of the wall that is in tension. Consequently, when the frame experiences its maximum top-storey displacement in the east direction, the shear force in the dowels on the west side of the wall increases and in some of them, it almost reaches their shear strength. Moreover, it is shown that the higher the spacing is among the dowels and thus the less their number, the larger the length of the wall that is in tension and the more the dowels that are active in shear.

6.2.2 Moment demand at the base of the frame members

The moment demand at the base of the frame members is shown and discussed in this section. The moment demand at the base of the wall as obtained from the axial forces at the base of the wall (excluding the bounding columns) is presented in Figures 6.34 and 6.35 when the frames experience their maximum base shear force and top-storey displacement in each direction. Also, the moment at the base of the outer columns of the frame is shown in Figures 6.36 and 6.37. Figure 6.37 shows the moment results for each column at the maximum base shear force and top-storey displacement of the frames in both directions. The positive values of the moment results in the graphs (Figures 6.34 to 6.37) are clockwise and the negative values are anticlockwise.

**Moment at the base of the wall
at maximum base shear force**

	at FBX maximum in the west	at FBX maximum in the east
■ Case 1	-1553.26	1844.51
■ Case 2	-1199.50	1219.58
■ Case 3	-929.33	1049.68
□ Case 4	-734.40	497.98
□ Case 5	-588.88	352.12
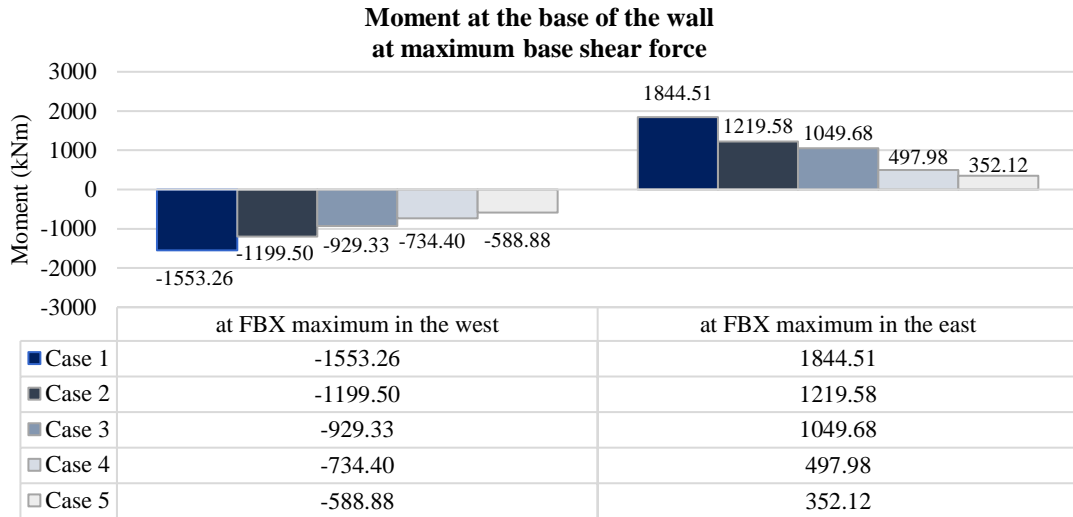
Figure 6.34: Moment demand at the base of the wall, at maximum base shear force in both directions

**Moment at the base of the wall
at maximum top-storey displacement**

	at DTX maximum in the west	at DTX maximum in the east
■ Case 1	-2654.31	2427.89
■ Case 2	-1487.96	1741.53
■ Case 3	-1447.60	1219.75
□ Case 4	-764.41	698.17
□ Case 5	-757.20	490.92
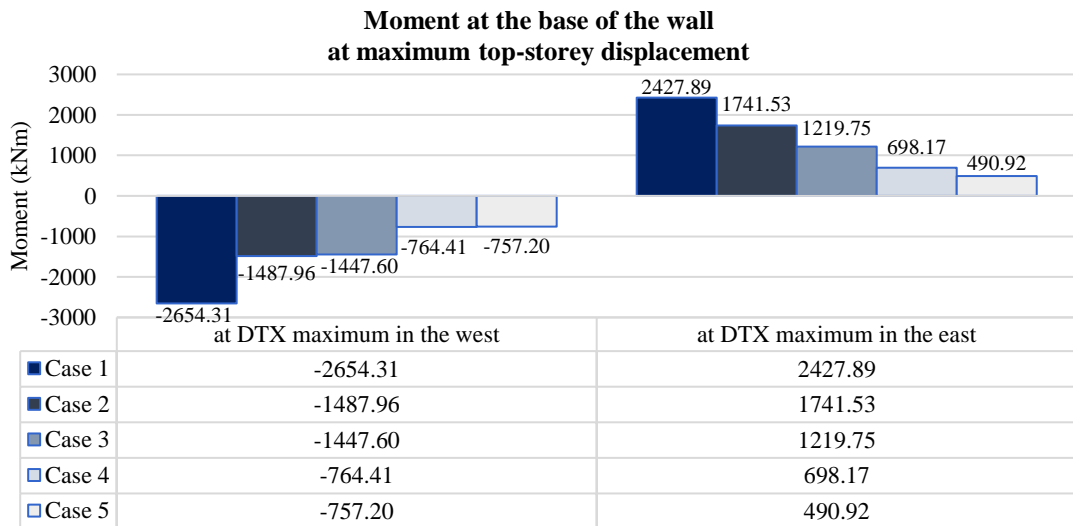
Figure 6.35: Moment demand at the base of the wall, at maximum top-storey displacement in both directions

Figures 6.34 and 6.35 illustrate that the moment at the base of the wall is decreased with the reduction of the number of dowels. Generally, it is presented that the moment demand at the base of the wall is 1.2 to 1.9 times higher with the increase of the number of dowels from one case scenario to the other. These results indicate that the more the dowels that connect the wall to the bounding frame, the more is the moment demand at the base of the wall. This is reasonable since these dowels add high axial forces at the base of the wall. Also, it is illustrated that the moment demand at the base of the wall is higher at the

maximum top-storey displacement of the frame (Figure 6.35) rather than at the maximum base shear force of the frame (Figure 6.34). This observation shows that the high displacements of the frame lead to higher moments at the base of the wall rather than the high base shear forces of the frame.

The moment demand at the base of the outer columns of the frame as presented in Figures 6.36 and 6.37 shows that each column demands higher moments at their base when the frame is moving towards their direction compared to the moment demand when the frame is moving away from their direction. This is due to the higher compressive forces that these columns take at their base during the response-history analysis when the frame is moving towards their direction. Moreover, it is presented that the moment demand at the base of the outer columns of the frame is increased with the reduction of the number of dowels in most of the cases. However, this is not observed in all cases, while in some cases the moment demand at the base of the outer columns of the frame is more or less stable.

Furthermore, the correlation of the moment demand at the base of the frame members concerning the reduction of the number of dowels is discussed in section 6.2.4.

WEST OUTER COLUMN OF THE FRAME(C11)

	at FBX maximum in the west	at FBX maximum in the east
Case 1	-274.80	84.58
Case 2	-248.11	80.10
Case 3	-281.60	82.79
Case 4	-271.06	120.71
Case 5	-314.58	126.71

EAST OUTER COLUMN OF THE FRAME (C14)

	at FBX maximum in the west	at FBX maximum in the east
Case 1	-143.62	127.93
Case 2	-136.13	247.24
Case 3	-167.29	256.76
Case 4	-168.61	205.46
Case 5	-171.88	211.68
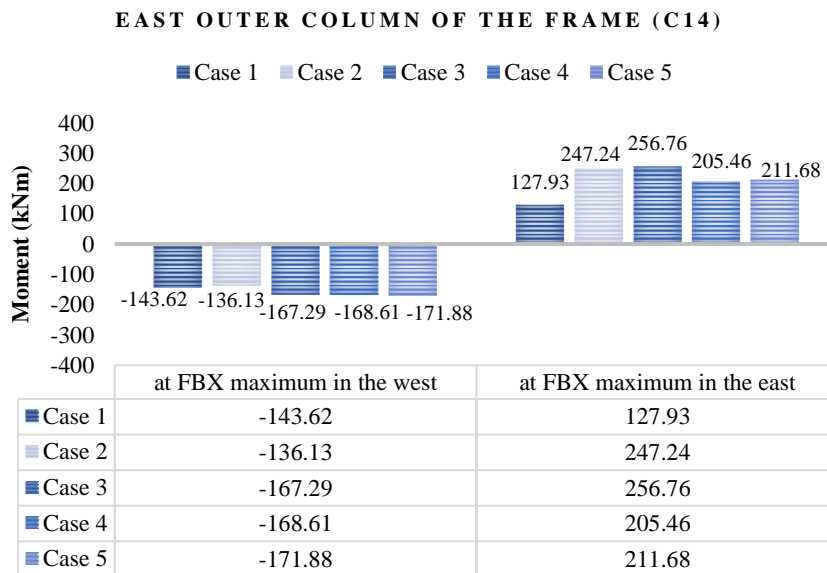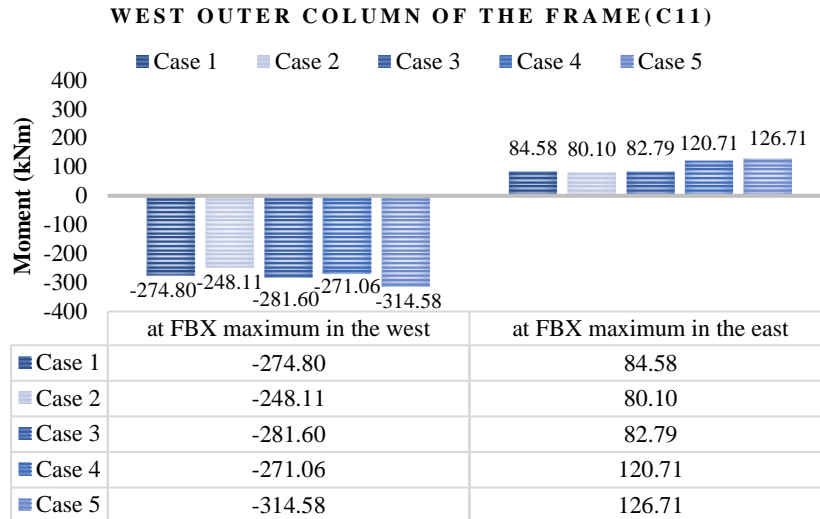
Figure 6.36: Moment demand at the base of the outer columns of the frame at the maximum base shear force of the frame in both directions

WEST OUTER COLUMN OF THE FRAME (C11)

	at DTX maximum in the west	at DTX maximum in the east
Case 1	-319.75	81.85
Case 2	-324.41	78.16
Case 3	-321.29	81.17
Case 4	-315.57	79.42
Case 5	-309.57	87.86

EAST OUTER COLUMN OF THE FRAME (C14)

	at DTX maximum in the west	at DTX maximum in the east
Case 1	-99.31	125.78
Case 2	-138.37	146.36
Case 3	-137.90	148.28
Case 4	-140.21	146.13
Case 5	-142.84	148.83
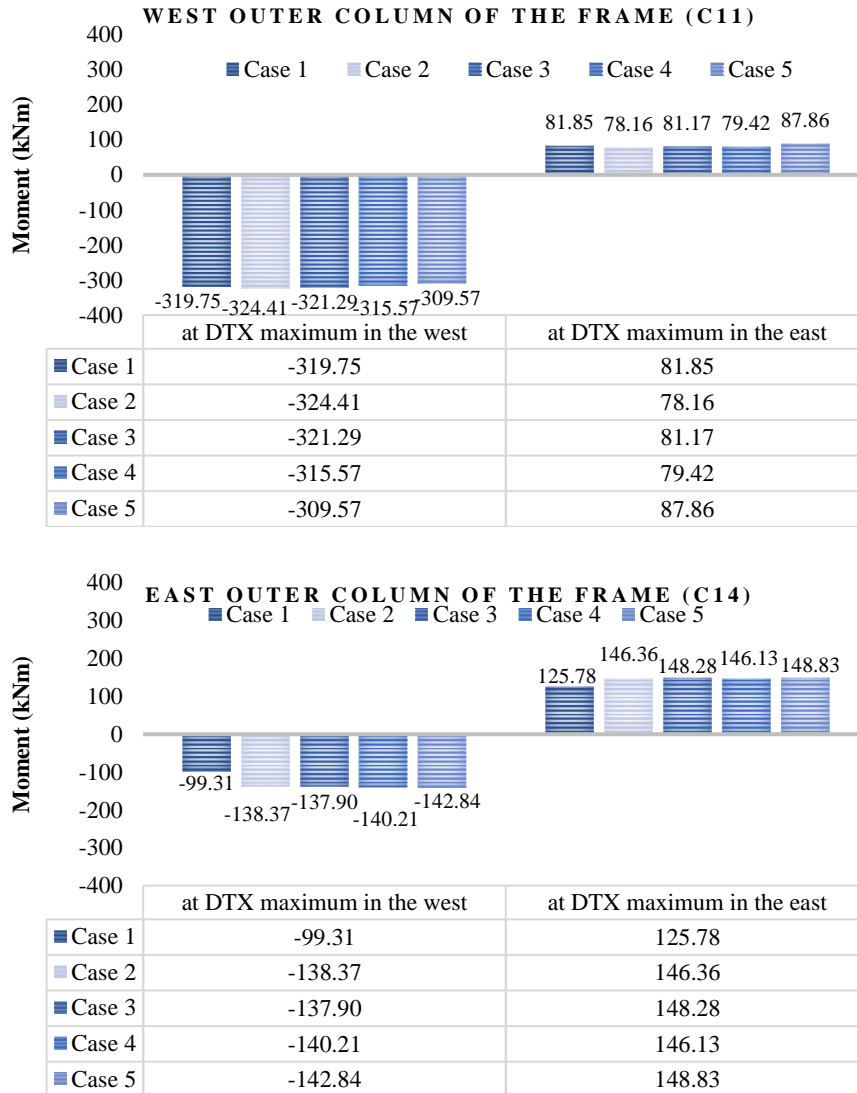
Figure 6.37: Moment demand at the base of the outer columns of the frame at the maximum top-storey displacement of the frame in both directions

6.2.3   Correlation of results

The correlation of the results in the above sections was made to draw some conclusions, which are discussed in this section. Specifically, the correlation of the tensile forces (Nx) on dowels in Figure 6.31 with the shear forces (Qy) on dowels in Figures 6.32 and 6.33 is made, and some conclusions are drawn and are discussed below. Additionally, the number of dowels that were provided in terms of the total area of reinforcement (As, mm²) for each case is correlated with the stiffness, the shear strength, the displacement of the frames, and the moment at the base of the frame members, for each case. Furthermore, the arrangement of dowels along the length of the wall (spacing, in terms of the dowel

159

diameter, ds) is related to the forces on dowels and the moment demand at the base of the frame members and some conclusions are drawn and discussed in this section. The As and ds are shown in Table 6.3 for each case scenario.

Table 6.3: Total area and spacing of dowels for all the case scenarios

Case scenario	Number of dowels connecting the wall to the beams	Total area of dowels (As, mm²)	Spacing of dowels in terms of dowels diameter (ds, mm)
1	20Y20/100	6283.2	5ds
2	13Y20/150	4084.1	7.5ds
3	10Y20/200	3141.6	10ds
4	6Y20/300	1885	15ds
5	4Y20/500	1256.6	25ds
6	2Y20	628.3	-
7	2Y20	628.3	-
8	-	-	-

6.2.3.1   Tensile and shear forces on dowels

The tensile forces and the corresponding shear forces of dowels when base shear and top-storey displacement of the frames are maximum were correlated in Figures 6.38 and 6.39 and their interaction observations are discussed in this section. Only dowels in tension are considered.
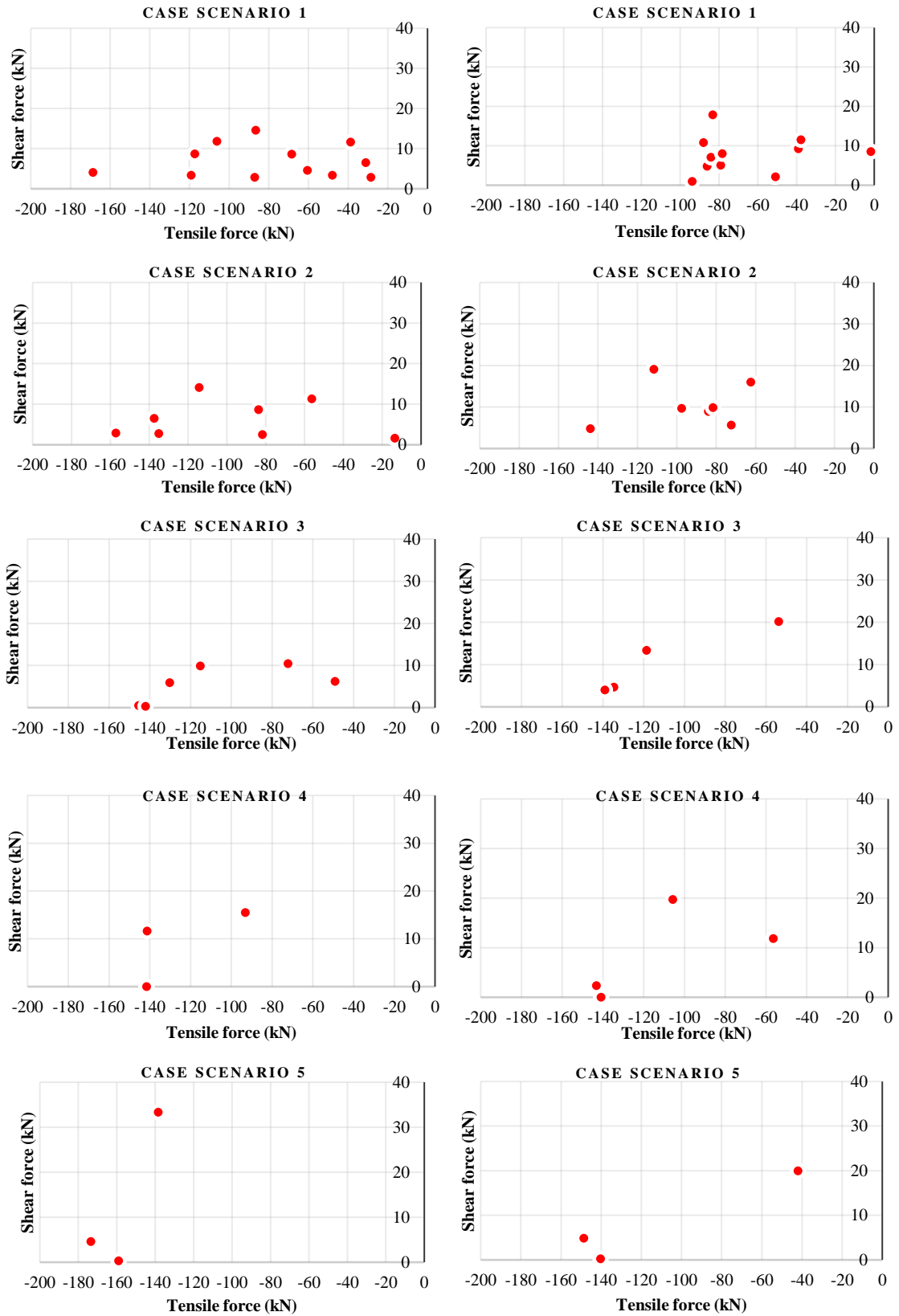
Figure 6.38: Correlation of the tensile forces (Nx) on dowels with the shear forces (Qy) on dowels when the base shear of the frames is maximum in both directions (graphs in the left in the west direction and graphs in the right in the east direction) for all the case scenarios

161
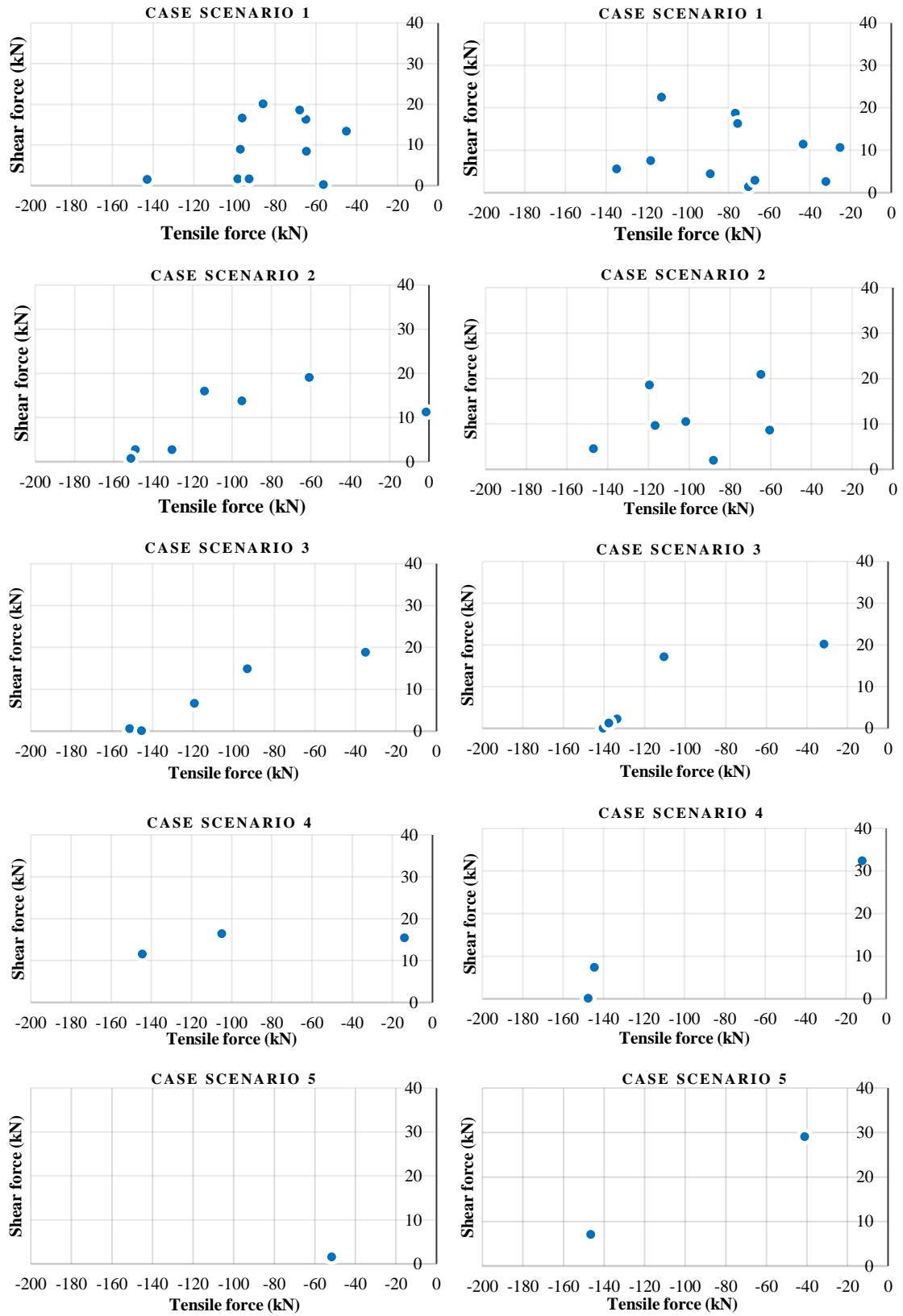
Figure 6.39: Correlation of the tensile forces (Nx) on dowels with the shear forces (Qy) on dowels when the top-storey displacement of the frames is maximum in both directions (graphs in the left in the west direction and graphs in the right in the east direction) for all the case scenarios

From the correlation of the tensile and shear forces on dowels, it is observed that for tensile forces on dowels lower than 40kN, the shear force on these dowels is less than 2kN for the first two cases (dowels spacing lower than 10ds), while for the third case scenario (dowels spacing=10d$_s$) some dowels get 20kN shear force, and for the fourth case scenario (dowels spacing larger than 10ds), one dowel gets 33kN shear force, which is near the shear strength of the dowel. Another observation is that for the fifth case scenario no dowel takes tensile force lower than 40kN.

Furthermore, it is observed that for tensile forces higher than 40kN but lower than 100kN, the dowels in all case scenarios take shear forces lower or equal to 20kN. Moreover, it is noted that the dowels that take tensile forces higher than 100kN but lower than 140kN (their yield strength is 141kN) take shear forces lower than 25kN for the first four case scenarios, whereas, for the fifth case scenario, one dowel takes shear force of 33kN which is near the shear capacity of the dowel. Also, it is observed that the dowels that take tensile force higher than 140kN, take shear force lower than 5kN for the first three case scenarios, while for the fourth and fifth cases they take higher shear forces than 5kN but lower than 12kN.

Consequently, these observations show that the arrangement of dowels along the length of the wall (spacing) affects the interaction of the axial and shear force on a dowel since for the first two cases (spacing less than 10d$_s$) the dowels with low tensile forces take low shear forces as well. On the other hand, for the cases with dowels spacing more than 10d$_s$, the dowels with low tensile force reach high shear values. Moreover, it is shown that when the dowels exceed their tensile yield strength, they do not contribute to the shear load, which is in agreement with the results in Takase, (2019).

6.2.3.2 *Stiffness, shear strength, displacement of frames, and moment demand at the base of the frame members concerning the dowels provided*

The correlation of the number of dowels that were provided in the frame models in terms of dowels area (Ad$_s$, in mm²) with the stiffness, shear strength, displacement of the frames, and moment demand at the base of the frame members for each case scenario is presented in Figures 6.40 to 6.44. The outcomes from these correlations are discussed in this section.
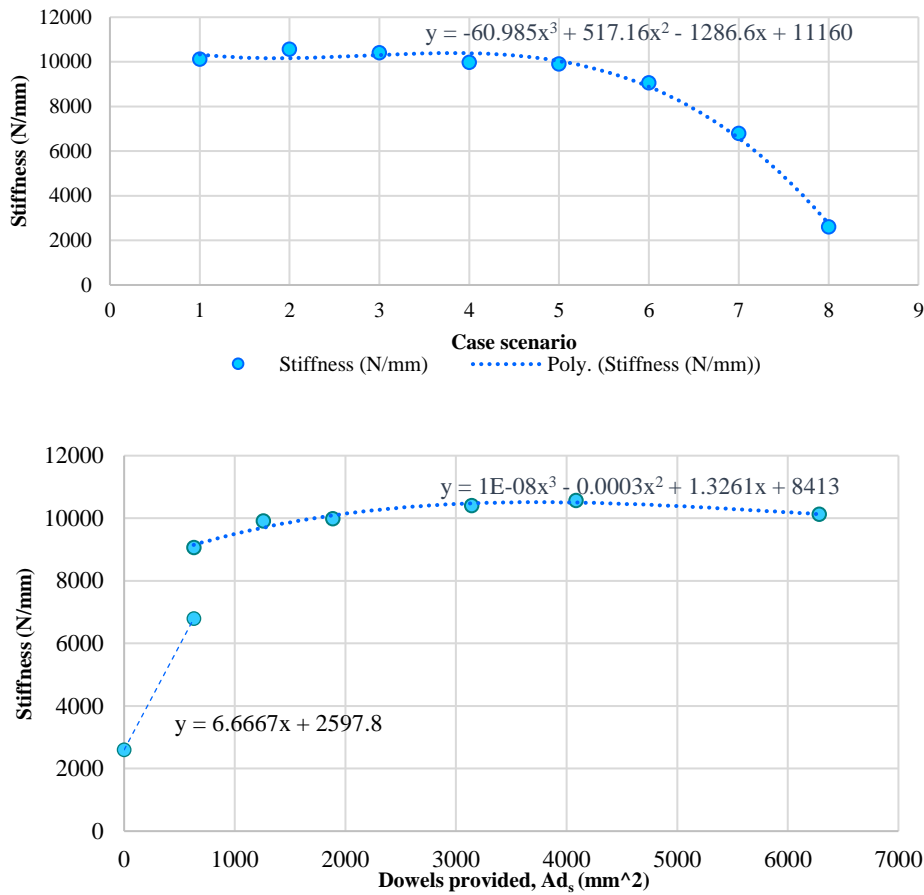
Figure 6.40: Stiffness of the frames concerning the area of dowels provided (Ad$_s$, mm²)

As displayed in Figure 6.40, the stiffness of the frame is reduced with the reduction of the number of dowels as already mentioned in section 6.1.4.5. The relation of the number of dowels with the reduction of stiffness is shown in Figure 6.40 and it illustrates that the less the dowels that are provided, the less is the stiffness of the frame. When the dowels that are provided are more than 2000mm², the stiffness of the frame is not changing considerably. One can say that there is no need to add dowels more than 3000mm² to add to the stiffness of a frame. However, it is shown that when the provided dowels are less than 2000mm², the stiffness of the frame is significantly reduced. On the other hand, in the case of an existing bare frame, by adding just 2Y20 (628.32mm²) only on beams or around the perimeter of the frame, or by adding just 4Y20 (1256.64mm²) around the perimeter of the frame, the addition to the stiffness of the frame is remarkable.
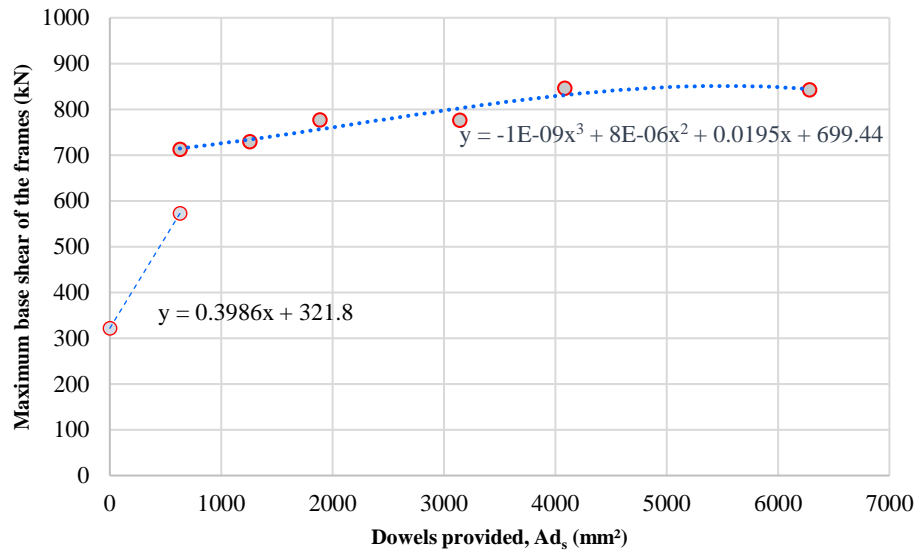
Figure 6.41: Maximum base shear of the frames concerning the area of dowels provided (Ad_s, mm²)
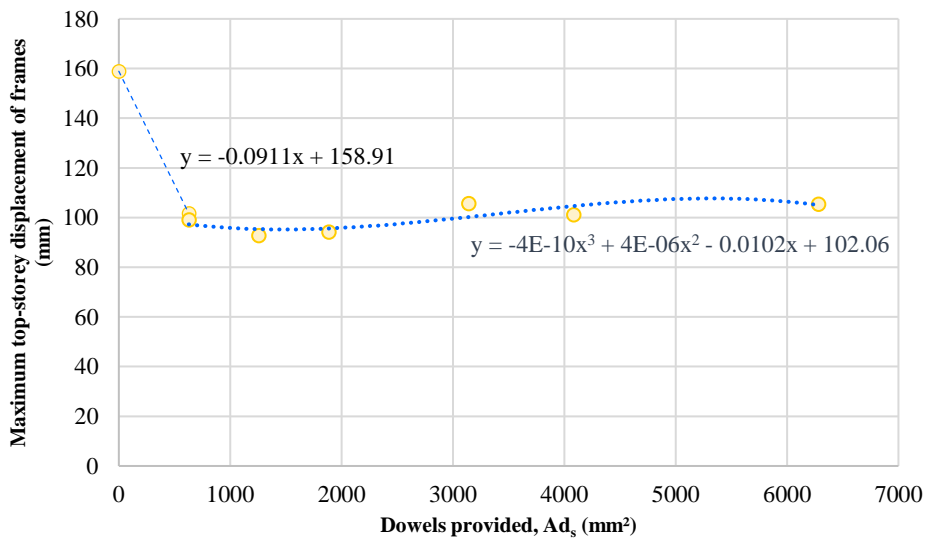
Figure 6.42: Maximum displacement of the frames concerning the area of dowels provided (Ad_s, mm²)

The relation of the provided dowels to the shear strength and the displacement of the frame is presented in Figures 6.41 and 6.42. It shows that the relation of the number of dowels to the shear strength of the frame is similar to the relation to the stiffness of the frame. Nevertheless, the addition to the shear strength of the frame when the provided dowels are more than 3000mm² is increased, in contrast to the stiffness addition when the

provided dowels are more than 3000mm². This indicates that in the case where the aim is to increase the shear strength of the frame, the more the number of dowels, the more the shear strength of the frame.

Moreover, it is illustrated that the relation of the dowels that are provided, to the displacement of the frame, as expected, is the opposite of the stiffness. The less the dowels provided, the higher the displacement of the frame, especially for provided dowels of less than 1000mm². Nevertheless, the displacement of the frame is more or less the same when the dowels that are provided are more than 3000mm². Consequently, as shown in Figure 6.42, there is no need to add more than 3000mm² when the aim is to minimize the displacements of an existing frame.

Relation of the number of dowels (As) and moment at the base of the wall when base shear force of the frame is maximum

$y = 0.2467x + 175.36$

○ Moment at the base of the wall when base shear is maximum (kNm)

.... Linear (Moment at the base of the wall when base shear is maximum (kNm))

Relation of the number of dowels (As) and moment at the base of the wall when top-storey displacement of the frame is maximum

$y = 0.3895x + 72.021$

○ Moment at the base of the wall when top-storey displacement is maximum (kNm)

.... Linear (Moment at the base of the wall when top-storey displacement is maximum (kNm))

Figure 6.43: Moment demand at the base of the wall concerning the area of dowels provided (Ad$_s$, mm²) when the base shear force and the top-storey displacement of the frames is at maximum

Figure 6.43 shows the moment demand at the base of the wall when the frame experiences maximum base shear force and top-storey displacement concerning the number of the provided dowels. The moments shown in Figure 6.43, are the average values of the moments taken from Figures 6.34 and 6.35 at the maximum base shear forces and top-storey displacements of the frame in each case scenario. It is illustrated that there is a linear relationship between the moment demand at the base of the wall and the provided dowels. So, the more the provided dowels, the more is the moment demand at the base of the wall. As already mentioned, this is due to the additional axial forces that the dowels take along the length at the base of the wall.

Figure 6.44 displays the moment demand at the base of the outer columns concerning the provided dowels. The values of moments in Figure 6.44 are the average values of the moments in Figures 6.36 and 6.37, when the frame is moving to the west (graphs on the left side of Figures 6.36 and 6.37) and east direction (graphs on the right side of Figures 6.36 and 6.37). As shown in Figure 6.44, the moment demand at the base of the outer columns of the frame is not varying considerably among the different provided total area of dowels.

**Relation of the number of dowels (As) and
moment at the base of C11
when the frame is moving in the west direction**

$$y = -2\text{E-}06x^2 + 0.016x - 325.35$$

Moment (kNm) vs Dowels provided, Ad_s (mm²)

○ Moment at the base of west outer column of the frame (C11) when the frame is moving in the west direction (kNm)

**Relation of the number of dowels (As) and
moment at the base of C11
when the frame is moving to the east direction**

$$y = 3\text{E-}06x^2 - 0.0242x + 134.68$$

Moment (kNm) vs Dowels provided, Ad_s (mm²)

○ Moment at the base of west outer column of the frame (C11) when the frame is moving to the east direction (kNm)

**Relation of the number of dowels (As) and
moment at the base of C14
when the frame is moving to the west direction**

$$y = 7\text{E-}07x^2 + 0.0022x - 161.66$$

Moment (kNm) vs Dowels provided, Ad_s (mm²)

○ Moment at the base of east outer column of the frame (C14) when the frame is moving to the west direction (kNm)

**Relation of the number of dowels (As) and
moment at the base of C14
when the frame is moving to the east direction**

$$y = -7\text{E-}06x^2 + 0.0473x + 125$$

Moment (kNm) vs Dowels provided, Ad_s (mm²)
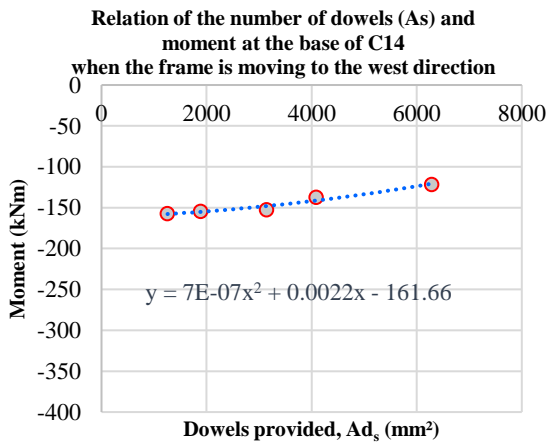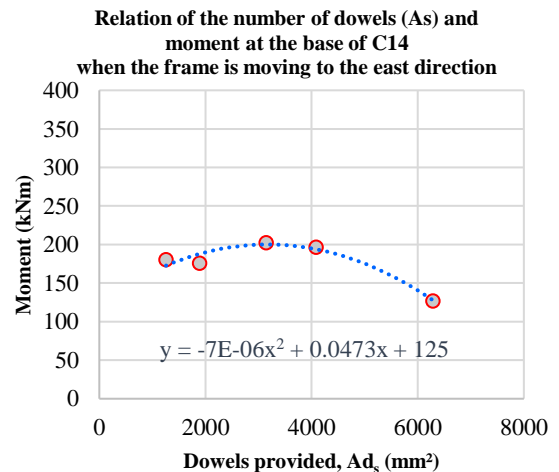
○ Moment at the base of east outer column of the frame (C14) when the frame is moving to the east direction (kNm)

Figure 6.44: Moment demand at the base of the outer columns of the frame (C11 and C14) concerning the area of dowels provided (Ad_s, mm²) when the base shear force and the top-storey displacement of the frames is at maximum in both directions (west and east direction, graphs on the left and right graphs respectively)

Therefore, it can be concluded that the provided dowels that are added to connect the new RC infill wall to the surrounding existing frame members, depends on the aim of the strengthening of the existing building. More specifically, if the aim is to add to the shear strength of the building, the more dowels provided, the more is the shear strength of the building. Otherwise, if the goal is to increase the stiffness of the frame as much as possible or to minimize the displacement of the frame, it seems that there is not much difference

if one adds more than 3000mm² dowels. However, the additional moment demand at the base of the new wall should be considered, since the more the provided dowels the more the moment demand is at the base of the new wall. On the other hand, if the target is to provide the minimum possible dowels to the frame and at the same time to strengthen the building for such an earthquake event as the examined one, even the minimum provided dowels (2Y20, which is less compared to the KANEPE suggested minimum of 3Y16 around the frame members) increase the stiffness as well as the shear strength of the frame and decrease the displacement of the frame significantly.

6.2.3.3 *Arrangement of dowels and local results at the base interface and on dowels*

The arrangement of dowels along the length of the wall in terms of spacing (related to the provided diameter of dowel bar, d_s) between the dowels is correlated to the forces on dowels (the maximum values as taken from Figures 6.31 to 6.33) in Figures 6.45 and 6.46. Moreover, the moment demand at the base of the frame members is related to the spacing of the dowels in Figures 6.47 and 6.48. These results are discussed in this section and some conclusions are drawn.
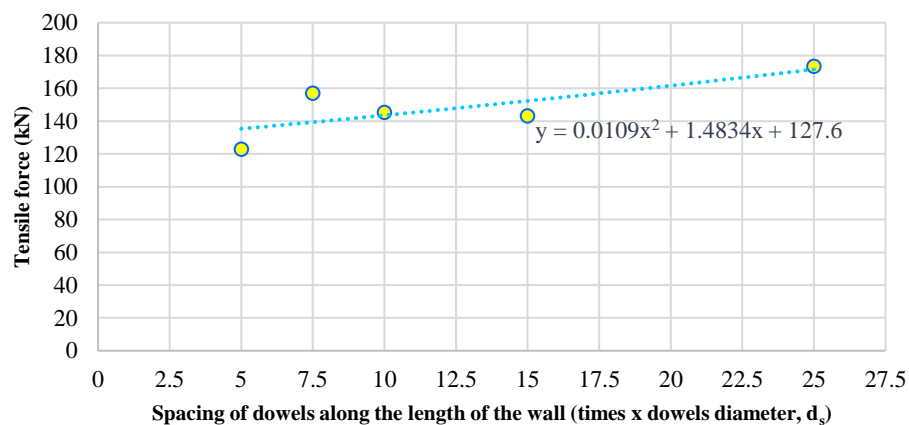
Figure 6.45: Maximum tensile forces of dowels concerning the arrangement of dowels (d_s, mm)
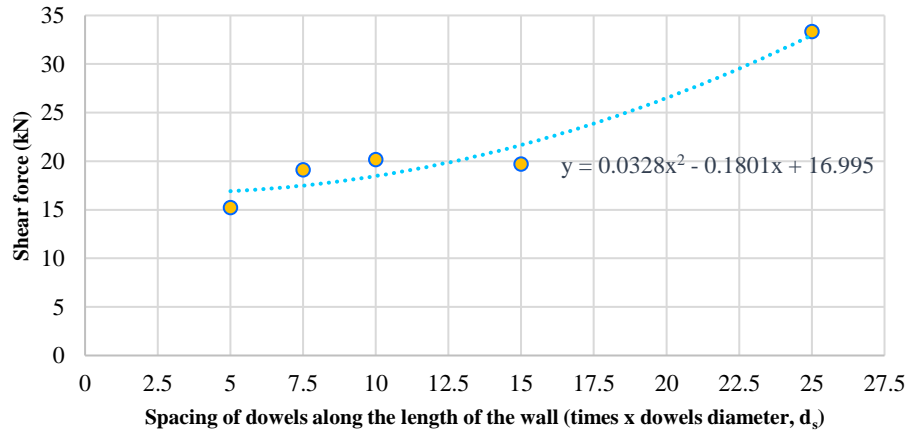
Figure 6.46: Maximum shear of dowels concerning the arrangement of dowels (d_s, mm)
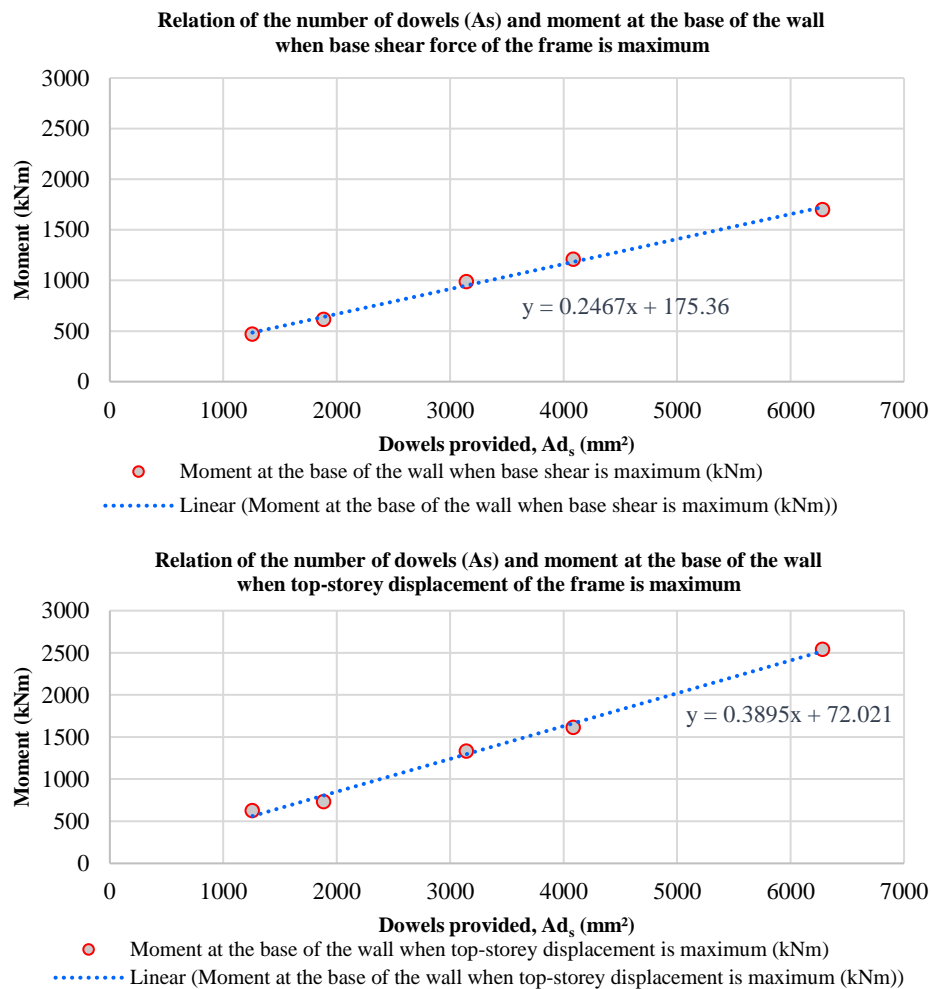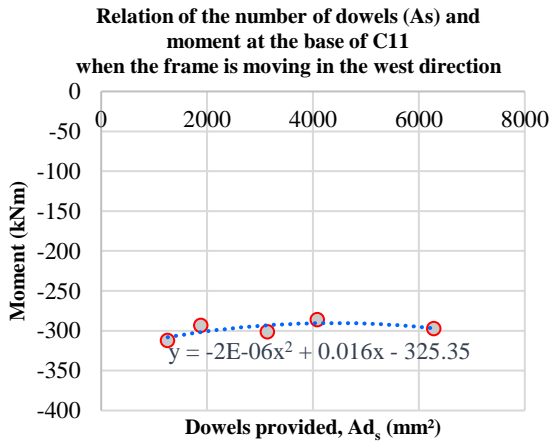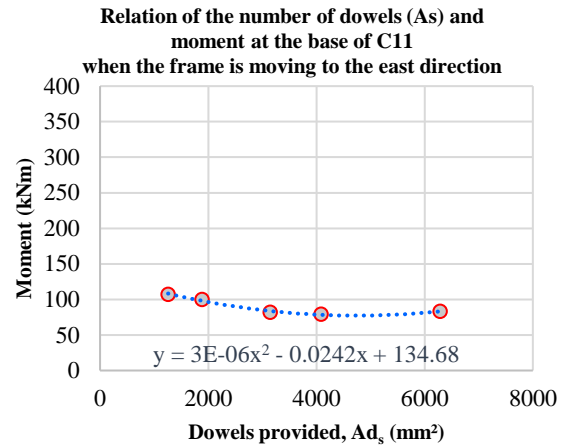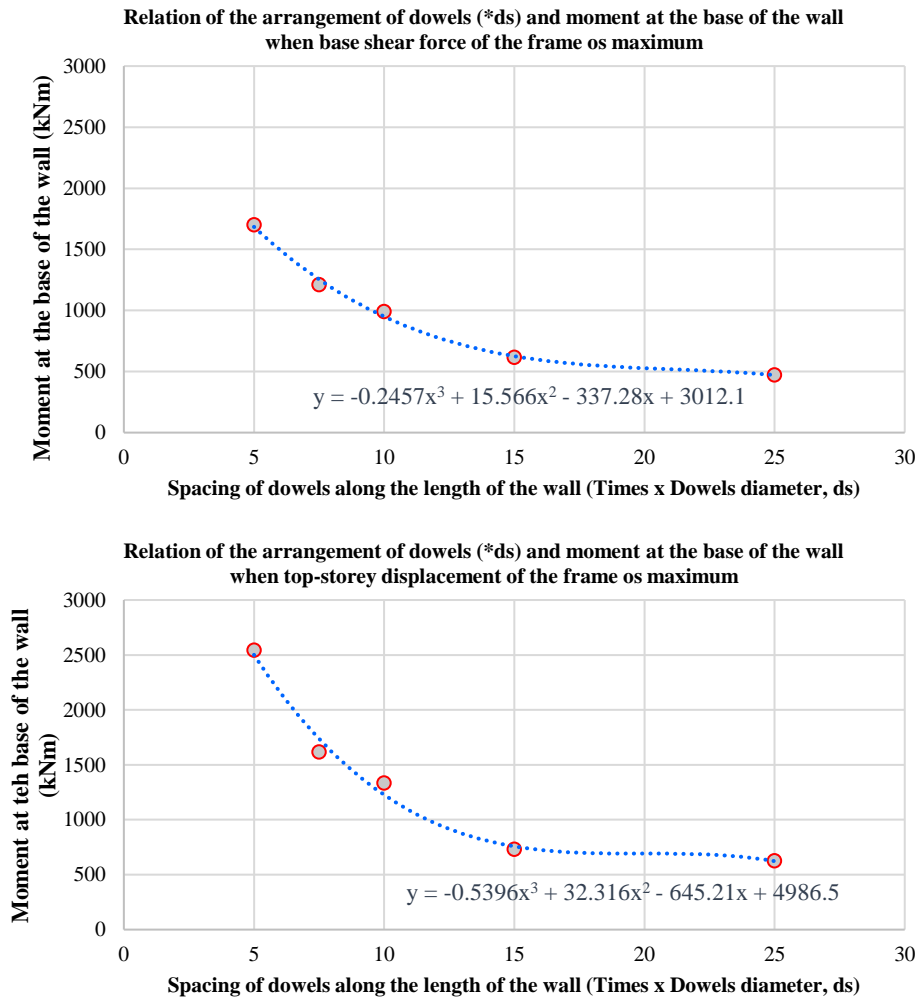

Figure 6.47: Moment demand at the base of the wall concerning the arrangement of dowels (d_s, mm) when the base shear force and the top-storey displacement of the frames is at maximum (above and below graphs respectively)

Also, the spacing of the dowels is related to the moment demand at the base of the wall as shown in Figure 6.47, and at the base of the outer columns of the frame as shown in Figure 6.48. It is presented that the moment demand at the base of the wall is a polynomial function of the spacing of the dowels at the base of the wall and as the spacing of dowels is increased, the moment demand at the base of the wall is decreased. This is due to the less axial forces that are generated at the base of the wall because of the reduced number of dowels. The moment at the base of the outer columns of the frame is not varying considerably through the several arrangements of dowels as shown in Figure 6.48.
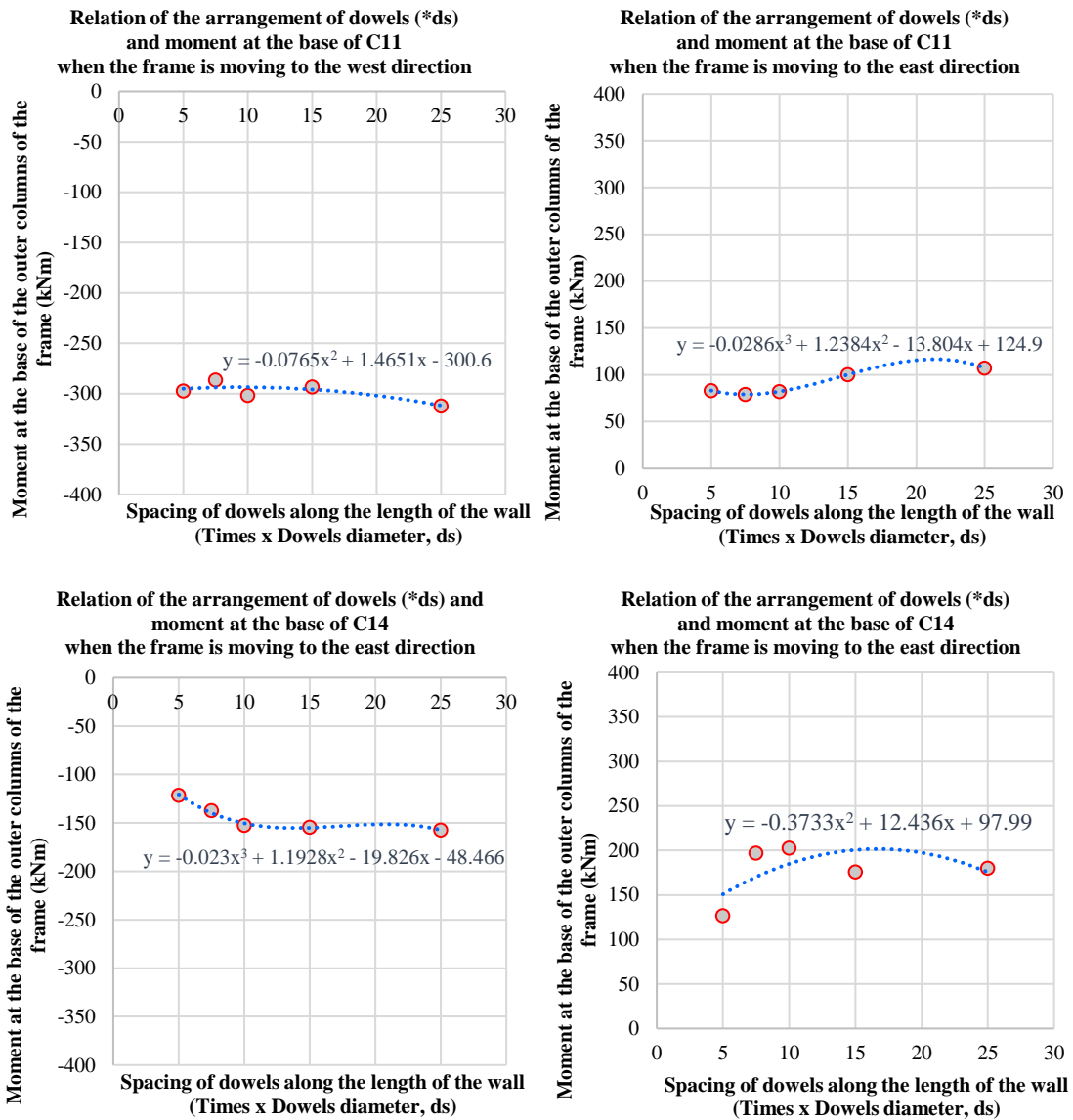
Figure 6.48: Moment demand at the base of the outer columns of the frame (C11 and C14) concerning the arrangement of dowels provided (d_s, mm) when the base shear force and the top-

storey displacement of the frames is at maximum in both directions (towards the west and east direction, graphs on the left and right respectively)

The correlation of the spacing of the dowels to the maximum axial and shear forces that the dowels take, as shown in Figures 6.45 and 6.46, indicates that the lowest tensile and shear forces on dowels happen when the spacing of dowels is $5d_s$ (as suggested in KANEPE). Then, the maximum tensile and shear forces are increased for spacing higher than $7.5d_s$ and reach their highest values for the highest spacing as shown in Figures 6.45 and 6.46. Also, the moment demand at the base of the wall is increased when the spacing of the dowels is less than $15d_s$. The graphs in Figures 6.45 and 6.46 indicate that if the aim is to keep the tensile and shear forces on dowels low, then the spacing of the dowels must be minimum of $5d_s$ (as proposed in KANEPE). Otherwise, for spacing of dowels higher than $5d_s$ but lower than $15d_s$, some dowels may reach their tensile strength while the maximum shear forces on dowels are about the same. These results indicate that the spacing of the dowels should not be more than $15d_s$. So, it could be recommended as a minimum arrangement of dowels in cases when an existing bare frame is infilled for strengthening reasons.

6.3 Design recommendations for RC infills connections

The provided area of dowels and their arrangement were examined in the previous sections and some of the conclusions that are drawn are discussed further in this section. Moreover, the near-collapse cyclic shear resistance (V_R) calculation that is provided in EC8-3 (equation A.3.3) is calculated for the examined wall and the results are compared with the analysis results as shown in Table 6.4. In addition, comparison is made with equations proposed by Fardis, Schetakis and Strepelias, (2013), and some design recommendations for the connections of the RC infill walls are proposed.

The analysis results reveal that the shear strength of the wall (with or without the bounding columns) is 2.3-3 times lower in relation to the shear resistance (V_R) calculated according to EC8-3 at the maximum base shear of the frame for the validated FE model as shown in Table 6.4. Additionally, as shown from the SERFIN experiment results in Chapter 3, the maximum total base shear of the frame, which includes the contribution of

the outer columns of the frame, is 1074kN that is also lower than the calculated shear resistance according to EC8-3, which includes only the contribution of the wall.

From the comparison in Table 6.4, it is shown that the EC8-3 equation overestimates the shear capacity of the wall when the wall is connected to the existing frame members through dowels and the EC8-3 equation may not be applied for such walls connected with the surrounding frame members through dowels, since it was calibrated for monolithic walls without dowels.

Table 6.4: Shear resistance of the wall according to EC8-3 and FE model shear strength of the wall

When the base shear is maximum	V_R (kN)	FE model shear force of the wall (kN)	FE model shear force of the wall (kN)	FE model shear force of the wall x V_R	FE model shear force of the wall x V_R
in the west direction	1628.74	553.3	725.83	**2.94**	**2.24**
in the east direction	1764.41	681.3	697.22	**2.59**	**2.53**

Table 6.5: Shear resistance of the wall according to (Fardis, Schetakis and Strepelias, 2013) and FE model shear strength of the wall

Vdi (kN)	FE model shear force of the wall (kN)	FE model shear force of the wall x Vdi
1396	725.83	**1.92**

Also, the shear force demand on the horizontal section through the bottom of the new RC wall (Vd,i) was calculated according to Fardis *et al.*, (2013) equation and it is compared with the FE model results in Table 6.5. This equation takes into consideration the number of dowels along the bottom side of the new web panel and the unfactored shear resistance of each of the two existing columns at the edge of the wall. As shown in Table 6.5, the estimated shear force demand at the base of the wall is 1.92 higher than the shear force

that was taken in the FE model. However, Vd,i is closer to the shear force at the base of the wall in the FE model compared to the values in Table 6.4. Also, Vd,i is closer to the total base shear force of the SERFIN experiment. This verifies that this equation is very close to the actual shear force that a new web panel connected with dowels along the sides of the new panel takes.

Moreover, the FE model results of dowels are compared with the equations of KANEPE (KANEPE, 2017). Specifically, according to KANEPE, the addition of RC infill walls in existing frames, requires ensuring the connection of the new RC infill wall with the existing bounding frame, so that the in-height flexural continuity of the new multi-storey wall is guaranteed. The analysis results showed that the in-height flexural continuity of the new multi-storey wall is also guaranteed with fewer dowels than the minimum that is suggested by KANEPE as discussed in section 6.1.8.

Comparison of calculated shear force that the dowels take according to KANEPE equations with the FE model results
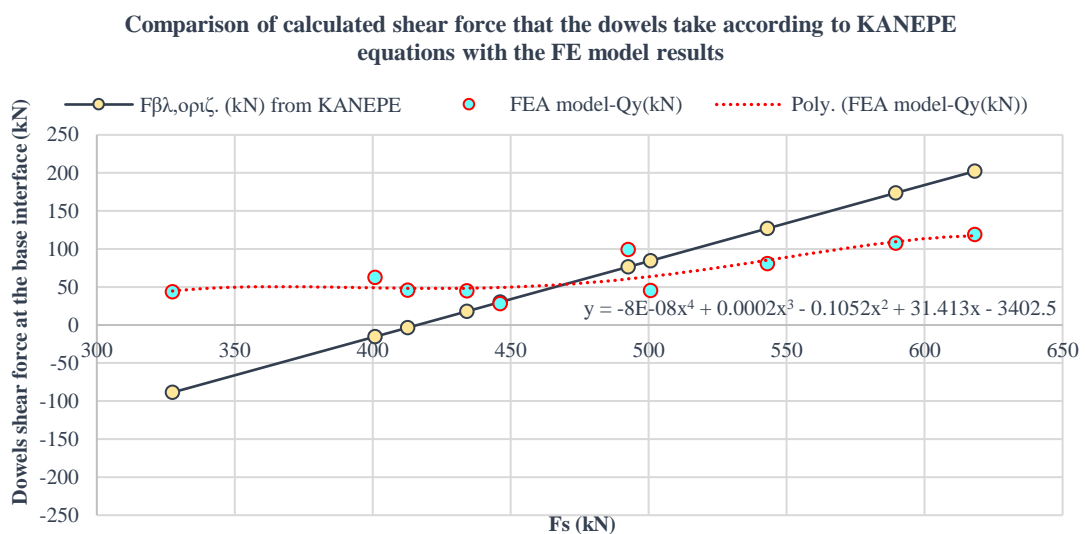
Figure 6.49: Maximum shear of dowels concerning the arrangement of dowels (d_s, mm)

The added shear to the frame (F_s) is calculated in KANEPE and a part of this force is taken by the diagonal strut (N_R) of the wall and the rest of the shear is undertaken by the dowels ($F_{\beta\lambda}$.) according to KANEPE. The calculation of F_s considers the total shear of the new wall (V_s) that is required from the earthquake and the shear strength of each bounding column (V_{Rc}). For the comparison that is made in this study, the shear strength of each bounding column was calculated according to EC8-3 and the total shear that the new wall takes is taken from the FE model analysis results for each case at the maximum base shear of the frame. Figure 6.49 displays the remaining shear force ($F_{\beta\lambda}$.) that the dowels

connecting the beams should take according to KANEPE and the shear force that the dowels take as taken from the FE model analysis results. As presented in Figure 6.49, the shear force that the dowels take according to KANEPE is a linear function related to the F_s and to the diagonal strut of the wall (as explained in KANEPE, 2017). Besides, it is illustrated that for F_s less than 400kN there is no shear left for the dowels to take (all the shear is taken by the diagonal strut of the wall). On the other hand, the analysis results show that the shear force that is taken by the dowels is less (1.6-1.9 times less) than one calculated by KANEPE for F_s higher than 500kN. Moreover, it is illustrated that the dowels take some of the shear force for smaller values of F_s even though the KANEPE calculated that the shear in these cases is taken by the diagonal strut.

Also, KANEPE suggests that the minimum quantity of dowels that should be provided along the perimeter is no less than 3Y16 per meter along the perimeter (8.2.1.3(β)(ν)). From the analysis results and the correlation of those in section 6.2.4, it is shown that the quantity of dowels that should be provided depends on the aim of the strengthening of each building and it could even be less than that. Added to that, regarding the KANEPE provisions, to ensure the reliable shear strength of the interface it is required to add a minimum percentage of longitudinal reinforcement on the interface, which is something to be studied further.

7 Conclusions

This study, among others, has proved that RC infills can be used to upgrade successfully structures that have been designed for gravity loads only. The numerical simulation of the experimental results of the SERFIN specimen has shown that the amount of reinforcement used in the experiment resulted in the monolithic behavior of the infill wall with the bounding frame. The parametric study, which was performed to complement the experimental results and investigate the effect of the reduction of the number of dowels starting from the number used in the experiment and going down to no dowels, has provided interesting results leading to some general conclusions.

As shown from the results of the parametric study, the fundamental frequency and the stiffness of the building is reduced with the reduction of the number of dowels. However, it is shown that the stiffness of the frame is not varying considerably for the first three case scenarios. This observation indicates that using 10 dowels (case 3) instead of 20 dowels (validated model) the initial stiffness is about the same. It is interesting to note that the stiffness considerably increased for cases 6 and 7 in which two dowels on columns and beams, and two dowels on beams are used, respectively, compared to case 8 in which there are no dowels. This demonstrates how important is the addition of dowels not just on beams but on columns as well and even more, it is shown how dominant is the addition of just two dowels even only on beams compared to a non-integral infill. The energy dissipation of the frame is not varying considerably for the five first case scenarios, while a more considerable reduction of the energy dissipation is observed for the sixth case scenario in comparison with the previous cases.

From the displacement results, it is concluded that the top-storey displacement of the frame is about the same in both directions for the first five case scenarios. The permanent deformation of the frame in one direction is obvious for the fifth and sixth case scenarios while this vanishes for the seventh and eighth one. From the waveform, the change of the fundamental characteristics of the frame is observed after the sixth case scenario. Also, the deformations for the eighth case scenario are considerably larger and the base shear force considerably lower than the previous case scenarios. This also indicated that it is beneficial to use even two dowels to connect the wall to the beams instead of having no dowels at all.

Regarding the base shear results, a general trend that is observed from the numerical parametric study is that the lower the number of dowels, the lower the base shear. It is also shown that the wall contributes the most to the base shear of the frame for all the case scenarios, except the last case scenario with no dowels. Nonetheless, even though the contribution to the shear resistance of the outer columns of the frames is relatively low, it is increased with the reduction of the number of dowels, especially in the last two cases. This indicates that the shear force at the base of the wall is transferred to the outer columns of the frame with the reduction of the number of dowels. Furthermore, it is shown that the frame members have not reached their shear strength in any of the cases, even though the outer columns of the frame reach shear values close to their capacity.

Generally, it can be concluded that the lower the number of dowels, the lower the base shear-force, the stiffness, and the energy dissipation of the building. However, it is shown that the global characteristics of the building are not varying considerably for the first five case scenarios (dowel spacing 5ds to 25ds). Also, it is shown that even with just two dowels connecting the bounding beams with the wall (seventh case scenario), not only their contribution to the total shear force is notable, but also their contribution to the stiffness of the frame is significant. In general, the overall behavior of the frame changes for the seventh case scenario with a significant decrease in base shear force, stiffness, and energy dissipation, and with an increase in top-storey displacement of the frame.

Regarding the local results of the dowels along the interface of the wall at the foundation, it is observed that the dowels of the first case scenario had the lowest axial forces in comparison with the other case scenarios since the infill wall behaves monolithically with the bounding frame. This results in an even distribution of the axial force of the dowels when the frame experiences its maximum base shear and top-storey displacement, in both directions. In the second and third case scenarios, the dowels reach higher axial forces and some of the dowels reached their yield strength capacity. It is also indicated that the lowest tensile and shear forces on dowels occur when the spacing is $5d_s$ as suggested in KANEPE, (2017). Then, the maximum tensile and shear forces are increased for spacing higher than 7.5ds and reach their highest values for the highest spacing of 25ds as shown in Figures 6.45 and 6.46. These correlation graphs indicate that if the aim is to keep the tensile and shear forces on dowels low, then the spacing of the dowels must be at a minimum of 5ds as proposed in KANEPE, (2017). Otherwise, for spacing of dowels

higher than 5ds, some dowels may reach their tensile strength while the maximum shear forces on dowels are about the same. The shear forces on dowels are significantly increased for spacing of the dowels higher than 15ds. So, 15ds could be recommended as a maximum arrangement of dowels in cases when an existing non-ductile frame is infilled for strengthening reasons.

Also, the position of the neutral axis of the wall including the bounding columns is in the middle for the first three case scenarios, thus, there is an even distribution of the axial force among the dowels for these cases. For the fourth and fifth case scenarios, the position of the neutral axis shifts closer to the edges of the wall, approaching the bounding columns, thus, more dowels are in tension, and more dowels yield. So, it is illustrated that the position of the neutral axis shifts closer to the edges of the wall with the reduction of the number of dowels which results for spacing larger than $15d_s$. Therefore, the larger the spacing of the dowels is, the more dowels are in tension and reach their yield.

The shear load is mainly distributed on dowels that are located on the tension side of the wall, which is opposite to the moving direction of the frame. Some of the dowels nearly reached their shear strength capacity when they were in tension, and as shown from the numerical results, the higher the spacing of the dowels is, the larger the length of the wall that is in tension and the more the dowels that are active in shear. Moreover, from the correlation of the axial and shear forces on dowels, it is observed that the spacing of dowels along the length of the wall (spacing) affects the interaction of the axial and shear force on a dowel since for the first two cases, when the spacing of the dowels is less than 10ds, the dowels with low tensile forces take low shear forces as well. On the other hand, when the spacing of the dowels is more than 10ds, the dowels with low tensile force reach high shear values.

Moreover, it is shown that the more the dowels that connect the wall to the bounding frame, the more is the moment demand at the base of the wall, due to the large number of dowels that increase the axial capacity at the base of the wall and hence its bending capacity. In addition, as it is shown from the local results of dowels, the moment demand at the base of the wall is higher at the maximum displacement of the frame rather than at its maximum base shear force. It is also shown that the moment demand at the base of the outer columns of the frame is higher when the frame is moving towards their direction, in which case the columns are in compression. However, the moment demand at the base

of the outer columns of the frame is about the same through the case scenarios. Furthermore, it is shown that the moment demand at the base of the wall is a third order polynomial function of the spacing of the dowels as shown in Figure 6.49, and that the moment demand at the base of the wall is obviously increased when the spacing of the dowels is less than 15ds.

From the results of this research, it can be concluded that the dowels provided to connect the new RC infill wall to the surrounding existing frame members, depends on the aim of the strengthening. More specifically, if the aim is to increase the shear capacity of the building, this can be achieved by the addition of closely spaced dowels, since as shown from the results, the larger the number of dowels is, the larger is the shear strength of the frame. Otherwise, if the goal is to increase the stiffness of the frame as much as possible, or to minimize the displacement of the frame, it seems that adding an area of dowels larger than 300mm² does not have a significant effect to these two quantities, as shown in Figures 6.40 and 6.42. Also, as shown in Figures 6.43 and 6.47, the moment demand at the base of the wall increases with the increase of the number of dowels, while there is a substantial decrease in the moment demand when the dowel spacing is larger than 10ds (cases 4 and 5). In the case that the aim is to provide the minimum possible dowels to the frame and at the same time to strengthen the building for such an earthquake event as the one examined, even the minimum provided dowels of 2Y20 (cases 6 and 7), which is less than the 3Y16 per meter along the perimeter that is suggested by KANEPE, increases the stiffness as well as the shear strength, and decreases significantly the displacement of the frame, relative to the one strengthened with a non-integral infill wall (case 8).

From the comparison in Table 6.4, it is shown that the EC8-3 equation overestimates the shear capacity of the wall when the wall is connected to the existing frame members through dowels and EC8-3 equation may not be applied for such walls connected with the surrounding frame members through dowels, since it was calibrated for monolithic walls without dowels.

Furthermore, the base shear force of the FE model wall and the SERFIN experiment was compared with the shear force demand (Vd,i) according to Fardis, Schetakis and Strepelias, (2013), which takes into consideration the number of dowels and the shear resistance of each of the two existing columns at the edge of the wall. It is shown that the estimated shear force demand at the base of the wall is 1.92 times higher than the shear

force at the base of the wall in the FE. However, the Vd,i is closer to the shear force at the base of the wall in the FE model and to the base shear force of the SERFIN experiment compared to the comparisons with the V_R from EC8-3, which is applied for monolithic walls.

Moreover, the analysis results illustrated that the in-height flexural continuity of the new multi-storey wall is also guaranteed with 2Y20 dowels than the minimum of 3Y16 that is suggested by KANEPE, (2017), which correspond to a smaller cross-sectional area. Also, the shear force, $F_{\beta\lambda}$, that the dowels connecting the beams to the wall should take according to KANEPE, (2017) and the shear force that the dowels take according to the FE model analysis, showed that KANEPE overestimates by 1.6-1.9 times the $F_{\beta\lambda}$ for higher than 500kN added shear to the frame (Figure 6.49). In addition, even though KANEPE calculates that when the added shear is lower than 413kN then it is all taken by the diagonal strut, it is illustrated in Figure 6.49 that the dowels take some of the shear force for smaller values of added shear.

These results complement the experimental results and show that the number of dowels used in the experimental study can be reduced, making the use of this method more cost-effective. From the analysis and correlation of results, it is shown that the quantity and spacing of dowels that should be provided depend on the aim of the strengthening of each building, and it could be less than the suggestions of KANEPE. Nevertheless, further studies should be performed to obtain a better understanding of this structural system that will allow the development of design guidelines as discussed in section 7.1.

7.1 Future work

As presented in this research, the numerical experiments tested the effectiveness of the reinforcement (dowels) between the old frame and the new wall. The parametric study results lead to some conclusions about the connection details and their interaction with the responses of RC infills that were missing from the literature. However, more investigations are necessary and can be done regarding the studied retrofitting method with the developed FE validated model for further research.

More specifically, the distribution of shear force to the frame members (joints, beams, columns) with the reduction of the number of dowels should be investigated further to draw some conclusions regarding the redistribution of the shear force in the case when the infill wall fails. Furthermore, from the results of this research work, it is indicated that it is beneficial (the stiffness of the frame is considerably increased) to use even two dowels to connect the wall to the beams instead of having no dowels at all. So, the introduction of minimally connected walls instead of monolithic walls to retrofit existing non-ductile RC frames should be studied further and maybe added as a proposal for the seismic strengthening of existing RC frames in EC8-3.

Furthermore, it is suggested to study experimentally smaller specimens in order to validate the results of the numerical experiments performed in this study. In addition, the minimum percentage of web reinforcement suggested by the KANEPE provisions, need to be studied further to draw some additional conclusions about the design and detailing of the new RC infill wall. Moreover, the effect of the diameter of dowels should be investigated, since in this research a constant dowel diameter was used. Also, the contribution of the interface in shear (friction and cohesion at the interface between the new RC wall and the existing bounding frame) and the correlation with the dowels contribution in shear should be studied further. Some other parameters that need further investigation are the embedment length and bond-slip of the dowels.

REFERENCES

American Concrete Institute (ACI), (2003) 'Bond and Development of Straight Reinforcing Bars in Tension (ACI-408R-03)', in. Farmington Hills, MI: ACI Committee 408.

American Concrete Institute (ACI), (1983) *Building code Requirements for Reinforced Concrete*.

Ahmet Murat Turk, Ugur Ersoy, G. O. (2006) 'Effect of introducing RC infill on seismic performance of damaged RC frames', *Structural Engineering and Mechanics*, 23(5), pp. 469–486.

Akin, J. E. (2005) *Finite Element Analysis with Error Estimators*. Butterworth-Heinemann (Materials & Mechanical).

Albanesi, T., Biondi, S., Candigliota, E., Le Maoult, A., Nuti, C., (2008) 'Seismic Full-Scale Tests on a 3D Infilled RC Frame'.

Altin, O. A. S. (2007) 'An experimental study on reinforced concrete partially infilled frames', *Engineering Structures*, 29(3), pp. 449–460. doi: 10.1016/j.engstruct.2006.05.011.

Altin, S., Ersoy, U. and Tamkut, T. (1992) 'Hysteretic response of reinforced-concrete infilled frames', *Journal of Structural Engineering*. American Society of Civil Engineers, 118(8), pp. 2133–2150.

American Society of Civil Engineers (2007) *Seismic rehabilitation of existing buildings*. Reston, VA.

Aoyama, H., Kato, D., Katsumata, H., Hosokawa, Y., (1984) 'Strenght and Behavior of Postcast Shear Walls for strengthening of existing Reinforced Concrete Buildings', *8WCEE*, pp. 485–492.

Baran, M. and Tankut, T. (2011) 'Experimental study on seismic strengthening of reinforced concrete frames by precast concrete panels', *ACI Structural Journal*. ACI, 108(2).

Bass, Robert A., Corrasquillo, Ramon L., J. J. O. (1985) *Interface Shear Capacity of Concrete Surfaces Used in Strengthening Structures*.

Benjamin, J. R. and Williams, H. A. (1958) 'Blast and Earthquake Resistant Design Data: Behavior of One-Story Reinforced Concrete Shear Walls Containing Openings*', in *ACI Journal Proceedings*. ACI.

Canbay, E., Ersoy, U. and Ozcebe, G. (2003) 'Contribution of reinforced concrete infills to seismic behavior of structural systems', *ACI Structural Journal*. ACI, 100(5).

CEN (2010) 'Assessment and retrofitting of buildings : Eurocode 8 : design of structures for earthquake reistance : Part 3 : Assessment and retrofitting of buildings / European Committee for Standardization ; editor Cyprus Organisation of Standardisation'. Brussels : European Committee for Standardization, c2010. Available at: https://vpn.cut.ac.cy/.

Choi, E., Chung, Y., Kim, Y., Kim, J., (2011) 'Monotonic and cyclic bond behavior of confined concrete using NiTiNb SMA wires', *Smart Materials and Structures*. IOP Publishing, 20(7), p. 75016.

Chrysostomou, C. Z. (1991) 'Effects of degrading infill walls on the nonlinear seismic response of two-dimensional steel frames', *Dissertation Abstracts International*, 51(12), p. 348.

Chrysostomou, C. Z., Poljansek, M.m Kyriakides, N., Taucer, F., Molina, F.J., (2013) 'Pseudo-dynamic tests on a full-scale four-storey reinforced concrete frame seismically retrofitted with reinforced concrete infilling', *Structural Engineering International: Journal of the International Association for Bridge and Structural Engineering (IABSE)*, 23(2), pp. 159–166. doi: 10.2749/101686613X13439149156831.

Chrysostomou, C. Z., Kyriakides, N., Poljansek, M., Taucer, F., Molina, F.J., (2014a) 'RC infilling of existing RC structures for seismic retrofitting', in *Geotechnical, Geological and Earthquake Engineering*, pp. 303–328. doi: 10.1007/978-3-319-00458-7_17.

Chrysostomou, C. Z., Kyriakides, N., Kotronis, P., Georgiou, E., (2014b) 'RC infilling of existing RC structures for seismic retrofitting', in *Second European Conference on Earthquake Engineering and Seismology*. Instabul.

Chrysostomou, C. Z., Kyriakides, N., Kotronis, P., Georgiou, E., (2016) 'Derivation of Fragility Curves for RC Frames Retrofitted with RC Infill Walls based on Full-Scale

Pseudodynamic Testing Results', in *ECCOMAS Congress 2016*. Crete, p. Paper 16727.

Chrysostomou, C. Z. and Asteris, P. G. (2012) 'On the in-plane properties and capacities of infilled frames', *Engineering Structures*, 41(0), pp. 385–402. doi: 10.1016/j.engstruct.2012.03.057.

Chrysostomou, C. Z. and Kyriakides, N. (2013a) 'Pseudo-Dynamic Tests on a Full-scale 4-storey RC Frame Seismically Retrofitted with RC Infilling'. Limassol, Cyprus: Cyprus University of Technology.

Chrysostomou, C. Z. and Kyriakides, N. (2013b) *Seismic Retrofitting of RC Frames with RC Infilling (SERFIN Project)*. doi: 10.2788/630.

Dhakal, R. P. and Maekawa, K. (2002) 'Path-dependent cyclic stress–strain relationship of reinforcing bar including buckling', *Engineering Structures*, 24(11), pp. 1383–1396. doi: http://dx.doi.org/10.1016/S0141-0296(02)00080-9.

DIANA FEA BV (2019) 'DIANA - Finite Element Analysis'. Delft: DIANA FEA BV.

Dionysis Biskinis, Michael N, Fardis, A. P.-A. (2016) 'Strength, stiffness and cyclic deformation capacity of RC frames converted into walls by infilling with RC', *Bull Earthquake Eng*, pp. 769–803. doi: 10.1007/s10518-015-9847-6.

E. W. Bennett, S. B. (1976) 'Strength of Beam-Column Connections With Dowel Reinforcement', *The Structural Engineer*, 54(4), pp. 133–139.

El-Ariss, B. (2007) 'Behavior of beams with dowel action', *Engineering Structures*, 29(6), pp. 899–903. doi: http://dx.doi.org/10.1016/j.engstruct.2006.07.008.

Eligehausen, R., Popov, E. P. and Bertero, V. V (1982) 'Local bond stress-slip relationships of deformed bars under generalized excitations'.

Ersoy, U. and Uzsoy, S. (1971) 'The behavior and strength of infilled frames', *Report No.MAG-205 TUBITAK, Ankara, Turkey*.

Fardis, M. N. (2009) *Seismic design, assessment and retrofitting of concrete buildings :based on EN-Eurocode 8, Geotechnical, geological, and earthquake engineering*. Dordrecht; New York: Springer.

Fardis, M. N., Schetakis, A. and Strepelias, E. (2013) 'RC buildings retrofitted by converting frame bays into RC walls', *Bulletin of Earthquake Engineering*. Affiliation:

Department of Civil Engineering, University of Patras, Patras, 26504, Greece; Correspondence Address: Fardis, M.N.; Department of Civil Engineering, University of Patras, Patras, 26504, Greece; email: fardis@upatras.gr, pp. 1–21. doi: 10.1007/s10518-013-9435-6.

Faur, A. and Mircea, C. (2012) 'Numerical Investigation of the Nonlinear Cyclic Behavior of Special Reinforcing Bars for Precast Concrete Frames with Hybrid Connections'. Citeseer.

FIB (2013) *fib Model Code for Concrete Structures 2010, 1st ed.*

Filippou, F. C., Popov, E. P. and Bertero, V. V. (1983) 'Effects of bond deterioration on hysteretic behavior of reinforced concrete joints'.

Fragiadakis, M., Pinho, R. and Antoniou, S. (2008) 'Modelling inelastic buckling of reinforcing bars under earthquake loading', *Computational Structural Dynamics and Earthquake Engineering: Structures and Infrastructures Book Series*. CRC Press, 2, p. 347.

Gan, Y. (2000) 'Bond Stress and Slip Modeling in Nonlinear Finite Element Analysis of Reinforced Concrete Structures'. University of Toronto.

Haroun, M.A, Elbahar, M. . (2002) *Testing of Column Bents Strengthened by Infill Walls*. Irvine.

Hayashi, T., Niwa, H. and Fukuhara, M. (1980) 'Strengthening Methods of the Existing Reinforced Concrete Buildings', in, pp. 89–96. Available at: http://www.scopus.com/inward/record.url?eid=2-s2.0-0019102805&partnerID=40&md5=e38c4f6f8121ee0f4c5c1289ad8202ac.

Higashi, T. E. Y., Ohkubo111, M. and Shimizu, Y. (1980) 'Experimental study on strengthening reinforced concrete structure by adding shear wall', in *Proceedings of the World Conference on Earthquake Engineering*, p. 173.

Ibrahim Erdem, Ugurhan Akyuz, Ugur Ersoy, G. O. (2006) 'An experimental study on two different strengthening techniques for RC frames', *Engineering Structures*, 28(13), pp. 1843–1851.

Jirsa, J. O. (1988) 'Behavior of epoxy-grouted dowels and bolts used for repair or strengthening of RC structures', in. Tokyo-Kyoto: Proceedings of Ninth Worls

Conference on Earthquake Engineering, p. VII 371-376.

Jirsa, J. O. and Kreger, M. E. (1989) 'Recent research on repair and strengthening of reinforced concrete structures', in *Seismic Engineering@ sResearch and Practice*. ASCE, pp. 679–688.

KANEPE (2012) 'Code for Intervention in Reinforced Concrete Buildings, Earthquake Planning and Protection Organization (OASP)'.

KANEPE (2017) 'Code for Intervention in Reinforced Concrete Buildings, Earthquake Plannig and Protection Organization (OASP)'.

Kaplan, H., Yilmaz, S., Cetinkaya, N., Atimtay, E., (2011) 'Seismic strengthening of RC structures with exterior shear walls', *Sadhana*. Springer, 36(1), pp. 17–34.

Kara, M. E. and Altin, S. (2006) 'Behavior of reinforced concrete frames with reinforced concrete partial infills', *ACI Structural Journal*, pp. 701–709. Available at: https://vpn.cut.ac.cy/.

Kato, D., Katsumata, H. and Aoyama, H. (1984) 'Effect of Wall Base Rotation on Behavior of Reinforced Concrete Frame-Wall Buildings', in *Proceedings of the Eighth World Conference on Earthquake Engineering, San-Francisco*.

Klingner, R. E. and Bertero, V. V. (1976) 'Infilled frames in earthquake-resistant construction'.

Kyriakides, N., Chrysostomou, C., Kotronis, P., Georgiou, E., Roussis, P., (2015) 'Numerical simulation of the experimental results of a RC frame retrofitted with RC Infill walls', *Earthquake and Structures*, 9(4), pp. 735–752. doi: 10.12989/eas.2015.9.4.735.

Loring A. Wyllie, J. (1988) 'Guidelines for Epoxy Grouted Dowels In Seismic Strengthening Projects', *Proceeding of Ninth World Conference on Earthquake Engineering, Tokyo-Kyoto, Japan*, pp. 499–504.

Luke. Philip C.C; Chon, Carlos; Jirsa, J. O. (1985) *Use of Epoxies for Grouting Reinforcing Bar Dowels in Concrete*.

Lundgren, K. (1999) *Three-dimensional modelling of bond in reinforced concrete theoretical model, experiments and applications*. Chalmers University of Technology.

Maekawa, Koichi, Okamura, H., Pinanmas, A. (2003) 'Nonlinear Mechanics of

Reinforced Concrete', *Spon Press*.

Magnusson J. (1997) *Bond and Anchorage of Deformed Bars in High-Strength Concrete*. Chalmers University of Technology.

Marcus H. (1951) 'Load Carrying capacity of Dowels at Transverse Pavement Joints', *Journal of the American Concrete Institute*, 48(2), pp. 169–184.

Martin, M. (2007) 'Nonlinear FE analysis of shear behaviour in reinforced concrete. Modelling of shear panel tests'. Chalmers University of Technology.

Menegotto, M. and Pinto, P. E. (1973) 'Method of Analysis for Cyclically Loaded RC Frames Including Changes in Geometry and Nonelastic Behaviour of Elements under Combined Normal Force and Bending', in *IABSE Congress Reports of the Working Commission Band13*.

Moehle, J. P. (2000) 'State of research on seismic retrofit of concrete building structures in the US', in *US-Japan symposium and workshop on seismic retrofit of concrete structures*.

Mohamed Mohamed Salah El-Din Darwish (2006) *Numerical Modeling of Infill RC Walls in Seismic Retrofit of RC Frames*.

Norbert Randl (2007) 'The Bearing Behaviour of Cast-in Shear Dowels', *Beton-und Stahbetonbau*. doi: 10.1002/best.200710103.

Ohki, K. and Bessho, S. (1980) 'Experimental Investigation on Aseismic Strengthening for existing reinforced concrete frames', pp. 517–524.

Papatheocharis, Theocharis, Perdikakis, Philip C., Moretti, M. L. (2019) 'Response of RC Frames Strengthened by RC Infill Walls: Experimental Study', *ASCE*.

Paulay. T., Park, R. and Phillips, M. H. (1974) 'Horizontal Construction Joints in Cast-in Place Reinforced Concrete', *ACI Special Publication SP-42 Shear in Reinforced Concrete*, II(S.), pp. 599–616.

Poljansek, M., Taucer, F., Molina, J., Chrysostomou, C.Z., Kyriakides, N., Kotronis, P., Kosmopoulos, A., (2014) *Seismic Retrofitting of RC Frames with RC Infilling (SERFIN Project)*. Publications Office of the European Union, Luxembourg. doi: 10.2788/630.

Qin, X. and Chouw, N. (2010) 'Experimental investigation of uplift effect on structures

in earthquakes', in *Proceedings, New Zealand society for earthquake engineering conference, Paper*.

R. Eligehausen, R. M. and J. F. S. (2006) '[3] Eligehausen et al 2006', in Ernst & Sohn GmbH & Co. KG. (ed.) *Anchorage in Concrete Construction*. First edit. Ernst & Sohn GmbH & Co. KG.

Radomir Folici, P. P. (2015) 'Seismic strengthening of buildings with RC walls', in *First scientific-applied conference with international participation reinforced concrete and masonry structures*.

Sinan Altin, Ozgur Anil, M. Emin Kara, Y. K. (2012) 'Comparison of Seismic Performance of RC Frames Strengthened with Four Different Techniques', *Advances in Structural Engineering*, 15(2), pp. 343–358. doi: 10.1260/1369-4332.15.2.343.

Sonuvar, M. O. (2001) 'Hysteretic response of reinforced concrete frames repaired by means of reinforced concrete infills', *A Doctor of Philosophy Thesis in Civil Engineering, Middle East Technical University, Ankara*.

Sonuvar, M. O., Ozcebe, G. and Ersoy, U. (2004) 'Rehabilitation of reinforced concrete frames with reinforced concrete infills', *ACI Structural Journal*. ACI, 101(4).

Strepelias, I., Fardis, M., Bousias, S., Palios, X., Biskinis, D., (2012) *RC Frames Infilled Ino RC Walls for Seismic Retrofitting: Design, Experimental Behaviour and Modelling*. Patra.

Sugano, S. (1981) 'Seismic strengthening of existing reinforced concrete buildings in Japan', *Bulletin of the New Zealand National Society for Earthquake Engineering*, 14(4).

Swati Roy Maitra, K. S. Reddy, and L. S. R. (2009) 'Load Transfer Charactesistics of Dowel Bar System in Jointed Concrete Pavement', *Transportation Engineering*. doi: 10.1061/(ASCE)TE.1943-5436.0000065.

Takase, Y. (2019) 'Testing and modeling of dowel action for a post-installed anchor subjected to combined shear force and tensile force', *Engineering Structures*. Elsevier, 195(May), pp. 551–558. doi: 10.1016/j.engstruct.2019.05.086.

Tepfers, R. and Olsson, P.-A. (1992) 'Ring test for evaluation of bond properties of reinforcing bars', in *Proceedings of the International Conference Bond in Concrete-From Research to Practice*, pp. 89–99.

Teymur, P., Yuksel, E. and Pala, S. (2008) 'Wet-mixed shotcrete walls to retrofit low ductile RC frames', in *Proceedings of the 14th world conference on earthquake engineering, Beijing, paper*.

Valluvan, R., Kreger, M. E. and Jirsa, J. O. (1993) 'Strengthening of column splices for seismic retrofit of nonductile reinforced concrete frames', *ACI Structural Journal*. ACI, 90(4).

Vecchio, Frank J, C. M. P. (1986) 'The modified compression field theory for reinforced concrete elements subjected to shear', *ACI Journal Proceedings*, 83(22), pp. 219–231.

Yanev Bojidar., M. H. D. (1979) 'Mathematical modelling of the seismic response of a one story steel frame with infilled partitions', *Earthquake engineering.*, 2, pp. 829–846.

Yoichi Higashi, T. E., Ohkubo111, M. and Shimizu, Y. (1980) 'Experimental study on strengthening reinforced concrete structure by adding shear wall', in *Proceedings of the World Conference on Earthquake Engineering*, p. 173.

Yu, W. (2006) *Inelastic Modeling of Reinforcing bars and Blind Analysis of the Beam Column Joints under Cyclic Loading*. European School for Advanced Studies in Reduction of Seismic Risk Rose School.